

AD-A096 560

COLORADO UNIV AT BOULDER DEPT OF ASTRO-GEOPHYSICS  
PLASMA WAVE TURBULENCE AND PARTICLE HEATING CAUSED BY ELECTRON --ETC(U)  
JAN 81 M V GOLDMAN

AFOSR-80-0022

F/G 4/1

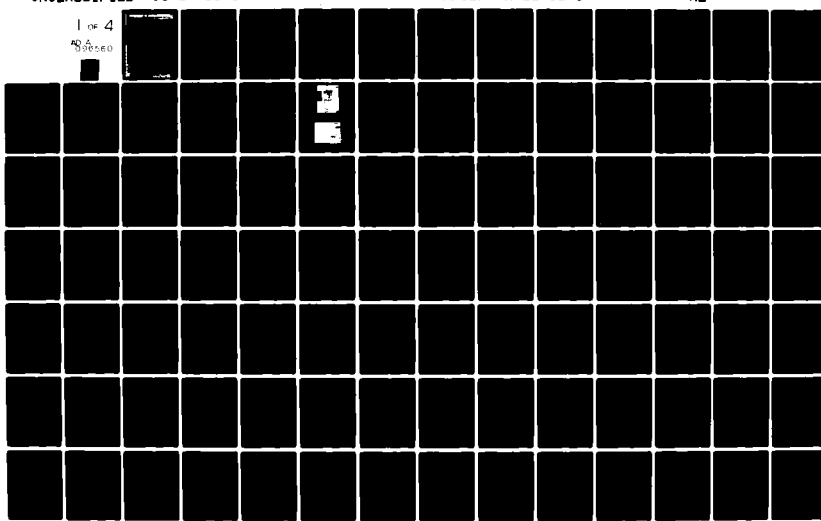
UNCLASSIFIED

CU-1533143

AFOSR-TR-81-0148

NL

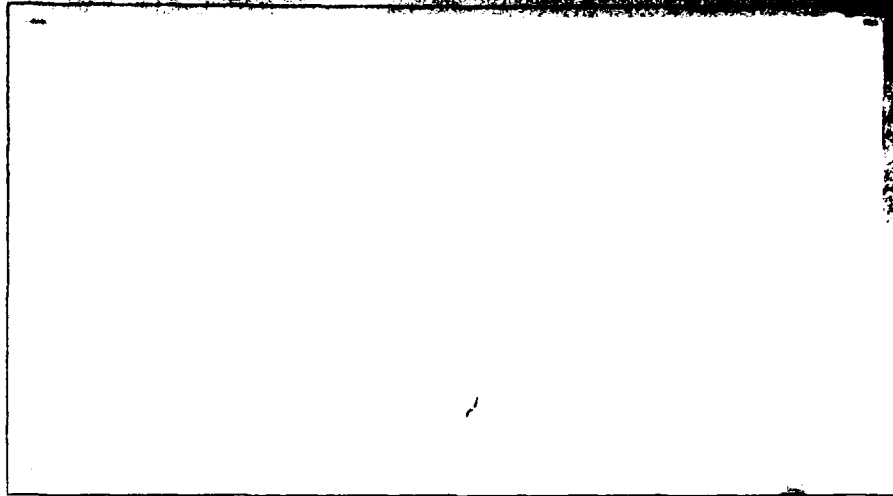
1 of 4  
4936560



AEOSR TR 81-0148

UNIVERSITY OF CALIFORNIA

AD A 096560



LEVEL

DTIC  
SELECTED

MAR 19 1981

F

010 10045

18

AFOSR TR-81-0148

19

LEVEL II

2

AIR FORCE OFFICE OF SCIENTIFIC RESEARCH

9 Interim Report, 1 Oct 1979 - 30 Sep 1980

6 Plasma Wave Turbulence and Particle Heating

Caused by Electron Beams, Radiation and Pinches.

10 Martin V. Goldman, Principal Investigator

15 AFOSR-80-0022

14 CU-1533143

DTIC  
ELECTED  
S MAR 19 1981  
D

F

Accession For	
NTIS GRA&I	
DTIC TAB	
Unannounced	
Justification	
By _____	
Distribution/	
Availability Codes	
Avail	and/or
Dist	Special
A	

11

Jan 81

12 350

AIR FORCE OFFICE OF SCIENTIFIC RESEARCH (AFOSR)  
NOTICE OF TECHNICAL REPORT  
This technical report has been reviewed and is  
approved for distribution to the public. AFAR 1.0-12 (7b).  
Distribution is unlimited.  
A. D. BLOD  
Technical Information Officer 088 46-511

SECURITY CLASSIFICATION OF THIS PAGE (Block 1)

~~UNCLASSIFIED~~

REPORT DOCUMENTATION PAGE		READ INSTRUCTIONS BEFORE COMPLETING FORM	
1. REPORT NUMBER	2. GOVT ACCESSION NO.	3. RECIPIENT'S CATALOG NUMBER	
<b>AFOSR-TR-81-0148 AD-A096560</b>			
4. TITLE (and Subtitle) PLASMA WAVE TURBULENCE AND PARTICLE HEATING CAUSED BY ELECTRON BEAMS, RADIATION AND PINCHES		5. TYPE OF REPORT & PERIOD COVERED Interim	
7. AUTHOR(s) Martin V Goldman		8. CONTRACT OR GRANT NUMBER AFOSR-80-0022 N	
9. PERFORMING ORGANIZATION NAME AND ADDRESS Department of Astro-Geophysics University of Colorado Boulder, CO 80309		10. EQUIPMENT FUNDING AREA & TIME IN MONTHS 61102F 23017A5	
11. CONTROLLING OFFICE NAME AND ADDRESS AFOSR/NP Bolling AFB Wash DC 20332		12. FUNDING DATE Jan 1981	
14. MONITORING AGENCY NAME & ADDRESS (if different from Controlling Office)		13. NUMBER OF PAGES 31	
16. DISTRIBUTION STATEMENT (of this Report)  Approved for public release; Distribution unlimited.		15. SECURITY CLASSIFICATION (Block 1) Unclassified 16. SECURITY CLASSIFICATION (Downgrade Schedule)	
17. DISTRIBUTION STATEMENT (of the abstract entered in Block 20, if different from Report)			
18. SUPPLEMENTARY NOTES			
19. KEY WORDS (Continue on reverse side if necessary and identify by block number)			
20. ABSTRACT (Continue on reverse side if necessary and identify by block number) This report covers research performed from 1 Oct 1979 thru 30 Sep 1980 on electromagnetic emissions from plasmas, plasma turbulence, the propagation of intense electromagnetic radiation in plasmas, on plasma diagnostics, and on experiments to accelerate ions and excite low frequency turbulence in laboratory plasmas.			

DD FORM 1 JAN 73 1473

UNCLASSIFIED

SECURITY CLASSIFICATION OF THIS PAGE (Block 1)

## TABLE OF CONTENTS

### List of Appendices

### Abstract

I.	Introduction .....	1
II.	Summary of Accomplishments .....	2
1.	Beam-Plasma Interaction and Electromagnetic Emission .....	2
2.	Propagation of Intense Microwaves .....	5
3.	Radiation Diagnostics .....	6
4.	Experimental Program .....	7
III.	Publications and Presentations During this Grant Period .....	15
1.	Publications .....	15
2.	Accepted for Publication .....	15
3.	Invited Papers .....	16
4.	Contributed Papers .....	16
5.	Conferences Organized .....	17
IV.	References .....	18
	Appendices	

## LIST OF APPENDICES

- A. "Radiation from a Strongly Turbulent Plasma:  
Application to Electron Beam-Excited Solar Emissions"  
M. V. Goldman, G. F. Reiter, and D. R. Nicholson  
Physics of Fluids, 23, 388-401 (1980)
- B. "Dimensionality and Dissipation in Langmuir Collapse"  
M. V. Goldman, K. Rypdal, and B. Hafizi  
Physics of Fluids, 23, 945-954 (1980)
- C. "Harmonic Emission from Adiabatically Collapsing  
Langmuir Solitons"  
B. Hafizi and M. V. Goldman  
Physics of Fluids, January 1981, in press
- D. "Langmuir Collapse in a Weak Magnetic Field"  
M. V. Goldman, J. C. Weatherall, and D. R. Nicholson  
Physics of Fluids, April 1981, in press
- E. "Nonlinear Langmuir Waves in a Weak Magnetic Field"  
J. C. Weatherall  
Ph.D. Thesis, University of Colorado, 1980
- F. "Breakup and Reconstitution of Langmuir Wavepackets"  
T. Tajima, M. V. Goldman, J. N. Leboeuf, and J. M. Dawson  
Physics of Fluids, January 1981, in press
- G. "Self-Focusing of Radio Waves in an Underdense Ionosphere"  
F. W. Perkins and M. V. Goldman  
Astrophysical Journal, in press
- H. "Inhomogeneous Effects in RIKE and Other Coherent  
Diagnostics"  
M. V. Goldman  
Research Memorandum, August 1980

## ABSTRACT

This interim report covers research performed from October 1, 1979 through September 30, 1980 on electron-beam excited plasma turbulence and electromagnetic emission, on propagation of intense electromagnetic radiation in the earth's ionosphere, on plasma diagnostics, and on experiments to accelerate ions and excite low frequency turbulence in the laboratory.

### I. Introduction

This interim report describes work performed under AFOSR grant #80-0022 during the period October 1, 1979 to September 30, 1980. The subject of research has been the theory of "Plasma Wave Turbulence and Particle Heating Caused by Electron Beams, Radiation, and Pinches." The period covered is the third stage of a comprehensive research program concerned with the nonlinear behavior of plasmas subjected to intensely energetic sources.

One of the significant developments in plasma physics over the past decade has been the theoretical and experimental progress made in our understanding of nonlinear plasma wave evolution in response to external sources: A wide variety of radiation sources such as lasers,<sup>1,2</sup> microwaves,<sup>3,4</sup> and radar,<sup>5,6</sup> and of electron beam sources, such as solar electron streams<sup>7,8</sup> and laboratory beams<sup>9</sup> can excite plasma wave instabilities in target plasmas. The waves saturate into a turbulent spectrum,<sup>10</sup> and may heat the plasma, accelerate plasma particles, and/or emit their own radiation. Such processes have been linked to inertial<sup>11</sup> and magnetic<sup>12</sup> controlled thermonuclear fusion schemes, radar communications in the earth's ionosphere, and Type III solar radio bursts.<sup>7,8</sup> The phenomena also bear heavily on certain fundamental questions of plasma turbulence, such as wave collapse in phase space, electric-field envelope-soliton evolution,<sup>13,14</sup> and the nature of the so-called "strong turbulence."<sup>13</sup>

Our research on pinches was completed over a year ago. The present report describes progress which has been made in the following areas:

1. Electron-beam excited plasma turbulence and electromagnetic emission;
2. Nonlinear propagation of intense microwaves in the ionosphere;
3. Radiation diagnostics of plasma turbulence;
4. Experiments to accelerate ions and excite low frequency turbulence in the laboratory.

## II. Summary of Accomplishments

### 1. Beam-Plasma Interaction and Electromagnetic Emission

Our earlier theoretical work concerning the effects of an electron beam on Langmuir waves and electromagnetic emission has now been published (Appendices A and B). An electron beam injects energy into a range of Langmuir modes (the injection range). When the intensity becomes high enough, wave-wave interactions transfer waves into an inertial range, and, eventually, a dissipative range in  $k$ -space. In the inertial range, the dominant effect appears to be spatial self-focusing of Langmuir wavepackets, leading to strong turbulence. The theory developed in Appendices A and B develops and confirms a picture in which electromagnetic emission at twice the plasma frequency emanates from the collapsing Langmuir wavepackets. The nature and intensity

of the emission depend on the details of the Langmuir wave turbulence. In the work of Appendix A the emission is assumed to come from the late (supersonic) stage of collapse, whereas in the later work of Appendix B, a more pronounced early (subsonic) evolution was found.

In the new work of Appendix C we find substantial electromagnetic emission in the early stage, an unexpected result. A three-dimensional model for collapse is proposed in which the electric field of the wavepacket has a spherically symmetric modulus and an asymmetric phase. The appropriate equations are solved numerically. Copious emission in the early stage comes about from Langmuir wave phase changes which enable two plasma waves to coalesce into an electromagnetic wave, with the proper kinematics (momentum and energy conservation). This paper has been accepted for publication in Physics of Fluids.

Appendices D and E represent new work concerning the effect of a background magnetic field on Langmuir collapse. Such a field usually accompanies and guides the electron beam. We have considered the case of a weak magnetic field (electron cyclotron frequency much less than electron plasma frequency). Even for such weak fields, important effects can occur. The transfer of energy out of the injection regime is slowed down, and the ions begin to play a more prominent role by taking up momentum. In addition, the real-space wavepackets are shaped into pancakes pierced by

magnetic field lines. An analytic theory for these effects is derived in Appendix D, in the form of a magnetic virial theorem. The behavior we have found will undoubtedly affect emission, but this has not yet been studied. The paper in Appendix D has been accepted for publication in Physics of Fluids. Appendix E is the Ph.D. thesis of James C. Weatherall who has been partially supported under this grant for the past few years. This thesis contains a comprehensive study of the effects of a magnetic field on collapse, and applications to the problem of Type III solar radio bursts.

Appendix F contains the results of research performed in collaboration with Prof. John Dawson's numerical group at U.C.L.A. We have carried out particle-in-cell simulations in two dimensions, for two particle species with a mass ratio of 5. The initial condition was a Gaussian Langmuir wavepacket of intensity and shape determined by the (prior) evolution of a beam instability. The subsequent evolution of this (undriven) wavepacket shows a recurrent behavior in which it breaks up and reconstitutes repeatedly over several cycles. This behavior seems consistent with recent theoretical work of Thyagaraja<sup>15</sup> of Culham Laboratories, who has shown that packets which do not collapse, must recur. It may have general implications for turbulence and for electromagnetic emission. This paper has been accepted for publication in Physics of Fluids.

Finally, we have performed research which is presently being organized for publication. Dr. G. Benford and his co-workers at the University of California at Irvine have just published experimental results<sup>16</sup> in which a relativistic electron beam of 50 kA current, incident on an unmagnetized laboratory plasma can produce up to megawatts of radiated power in the 20-100 Ghz frequency regime (corresponding to the local plasma frequency). The theoretical explanation<sup>16</sup> involves Langmuir turbulence of the type we are studying, but driven by more intense electron beams. Here the wavepackets were assumed to break up due to modulational instability, rather than the self-focus directly. Recently, we have used our two-dimensional numerical code for simulating this situation, and have found the hypothesized break-up to occur as expected.

## 2. Propagation of Intense Microwaves

This research has been motivated in part by the recent proposal<sup>17</sup> to orbit a geostationary satellite which would collect solar radiation and transmit energy to an earth-bound station via microwave radiation at 2.45 Ghz. Projected local intensities in the F-region of the ionosphere would be about  $25 \text{ mW/cm}^2$ . Our work on the propagation of this and longer wavelength radiation through the ionosphere is described in the paper in Appendix G, which has been accepted for publication in the Journal of Geophysical Research. We predict thermal self-focusing

instabilities to be excited in the E and F regions by such radiation. These instabilities have been observed<sup>18</sup> experimentally, recently, using a 10 Mhz ground-based radar, at times when the ionosphere peak plasma frequency is 7 Mhz, so there is no reflection. Our principal prediction for microwaves is that density striations as large as 10%, and intensity striations of up to 100% may be excited, with scale lengths of 100 meters.

Thermal self-focusing appears to be generic, and would affect the propagation of intense microwaves through most plasmas.

### 3. Radiation Diagnostics

Our collaboration with Dr. N. Peacock of Culham, on the development of the "Raman Induced Kerr Effect" (RIKE) as a radiation diagnostic of plasma collective behavior continues. As Appendix H, we have included a research memo to Dr. Peacock, in which the effects of density gradients are studied. It will be recalled that RIKE is a coherent process in which collective response of the plasma is evoked by the ponderomotive beat force between two radiation sources (e.g., lasers) and then detected by scatter off one of them. We have studied a parabolic density profile, and found under which conditions the spectral width of the probed collective mode is determined by intrinsic line width, and when it is determined by the profile gradient (see Table 1, pg. 27 of Appendix H). This work is continuing.

#### 4. Experimental Program

In the current contract period an experimental program was initiated. The proposed work for this year consisted of (i) the construction and development of a plasma device for obtaining long-lived wave-driven ion beam segments, and (ii) the initiation of a study of cross-field ion acceleration by waves in magnetized plasmas. Both tasks have been carried out on schedule. It should be noted that all costs for equipment, supplies, as well as salary for the senior (faculty) experimentalist, are not borne by AFOSR, which contributes only the salary of one Graduate Research Assistant towards the cost of the experimental program.

The goal of the program is to develop and enhance the efficiency of processes through which large-amplitude waves in plasmas are able to accelerate ions. The underlying principle was demonstrated in 1973: it was shown that ion-acoustic waves generated substantial internal ion beam segments in the stationary state. In contrast with the conventional pulsed beam generation techniques, this is a steady-state method with about 50% duty cycle, i.e., orders of magnitude more effective, although at present limited to low ion energies.

During this initial period we have constructed two types of facilities designed to overcome the main limitations on beam lifetime which were encountered in the original

experiment. These are: charge exchange and turbulence. Specifically, in the presence of a background gas, ions will charge-exchange with neutrals and effectively be removed from the beam. At the normal background pressures of  $10^{-4}$  Torr in Argon, the charge-exchange length was of order 20 cm, so that at the typical ion speed of order  $10^6$  cm sec $^{-1}$  a lifetime of only 20 sec could be expected. Secondly, the ion-beam segments were found to excite unstable off-axis ion acoustic waves in a broad spectrum. These waves in turn scattered ions out of the beam. We have assembled two sets of apparatus, designed to overcome each of these limitations, and enable further studies of the basic process.

A DP-type plasma device was constructed, in which charge exchange is reduced to a minimum through the use of confining magnets. DP plasmas are large-volume gas discharges in which primary electrons, generated by hot metallic filaments, are electrically accelerated and ionize a background gas through collisions. Conventionally, with cross sections in the range  $10^{-16}$  to  $10^{-18}$  cm $^2$  and gas densities of order  $10^{14}$  cm $^{-3}$  (filling pressures of 1 m Torr), the primary electron mean free path is of order  $10^2$  to  $10^3$  cm. It is therefore lost to the walls of laboratory-size machines after undergoing less than one ionizing collision on the average. By lining the walls of the machine with strong permanent magnets, say of 1 K Gauss, these primaries can be turned around without energy

loss and forced to traverse the background gas many times, increasing the ionization efficiency correspondingly.

Note that for 100 eV, the electron gyro-radius in a 1 KG field is less than  $10^{-1}$  cm, i.e., the trajectory bending is very effective.

With the aid of Prof. N. Hershkowitz of the University of Iowa, a foremost expert in devices of this type, who is spending the academic year 1980-81 with our group, we have assembled and tested such a machine. We are currently able to operate it at background pressures of  $10^{-5}$  Torr in Argon: at this pressure, the charge-exchange length is about 500 cm, longer than the device. That is, the ion beam life spans its motion across the machine. Large-amplitude waves have been launched, and experiments are proceeding on measurements of ion beam segments generated by these waves. The device (Figure 1) is fully instrumented with probes for measuring details of the wave structure. An ion energy analyzer probe for measuring the ion beam structure is being designed.

To decrease the limitation on ion beam lifetime due to turbulence, a novel scheme has been assembled and is being tested. It is based on the observation that, in unmagnetized plasmas, an ion beam can destabilize a broad spectrum of ion-acoustic waves, due to the fact that their dispersion relation is nearly straight. That is, the interaction condition that beam speed and wave phase speed be alike can be satisfied by many frequencies.

Conversely, in magnetized plasmas, only a narrow range of frequencies of waves is allowed. Thus the unstable spectrum is narrower, and can be expected to have a correspondingly limited effect on the ion beam. To test this effect, a magnetized plasma device has been assembled. It consists of a plasma column generated by microwave breakdown of a noble gas inside a solenoidal magnetic field of 1 K Gauss or higher. Ion-acoustic waves are launched by AC voltage applied to metal grids spanning the column. Probe instrumentation is in place, and the level of background noise in the machine has been reduced to the point where tests of the principle can be conducted. The assembly is shown in Figure 2.

The study of cross-field ion acceleration in a magnetized plasma was conducted using the Q-machine facility at the University of California, Irvine. In this instrument, similar in concept to the device described above, we destabilized ion waves propagating normally to the magnetic field (the Electrostatic Ion Cyclotron mode). These waves carry a strong electric field component in the direction of propagation, which pushes ions ahead of it and distorts the ion velocity distribution function correspondingly. Figure 3 shows the resulting perturbed velocity distribution function, containing an accelerated ion beam component with energy of about 1 eV, generated by waves with peak-to-peak potential variations of 1 V magnitude. The process is being studied experimentally and theoretically;

we propose to conduct similar studies in our machine as soon as the scheduled tests of turbulence mentioned above are completed. The principal advantage of our device lies in the fact that the Q-machine, although quieter, is limited to operation using alkali-metal plasmas or similar substances, in which the electron/ion temperature ratio is of order unity, whereas using noble gases we have temperature ratios of order 10 to  $10^2$ . Since the amplitude of driver ion waves is a strong function increasing with this ratio, we can launch much more intense waves, and correspondingly generate stronger and denser ion beams, than are possible in Q-machines.

In summary, during the contract period we have constructed our basic instrumentation, developed a new concept which may increase the efficiency of the basic process, and demonstrated for the first time the cross-field acceleration of ions in magnetized plasmas.

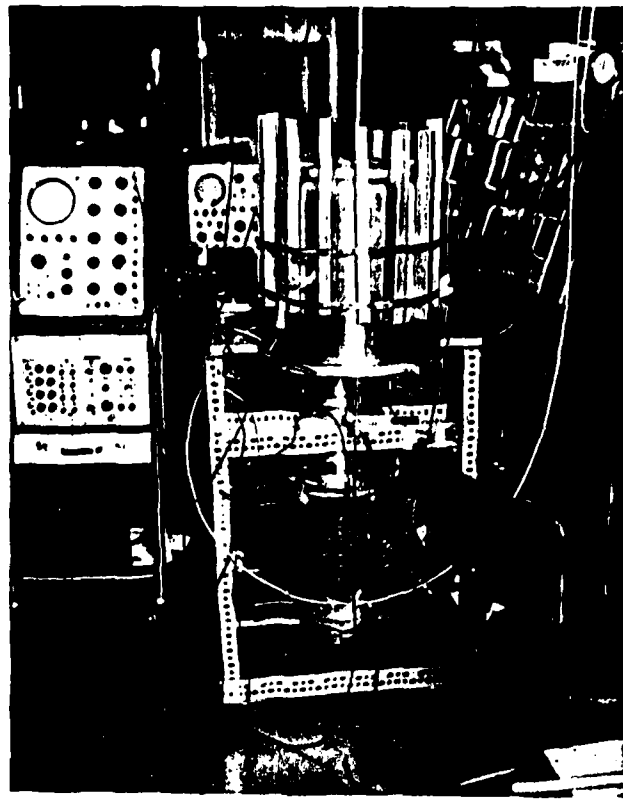


FIGURE 1  
DP PLASMA MACHINE ASSEMBLY

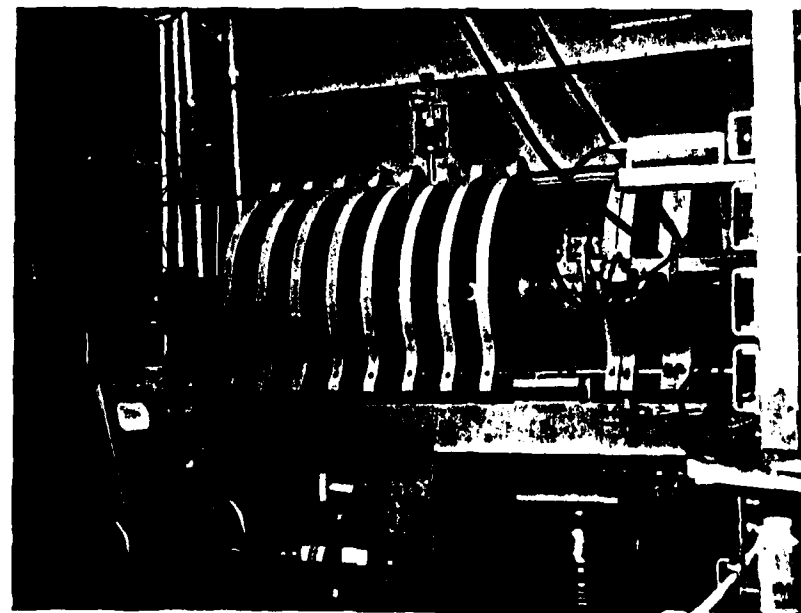


FIGURE 2  
MAGNETIZED PLASMA MACHINE ASSEMBLY

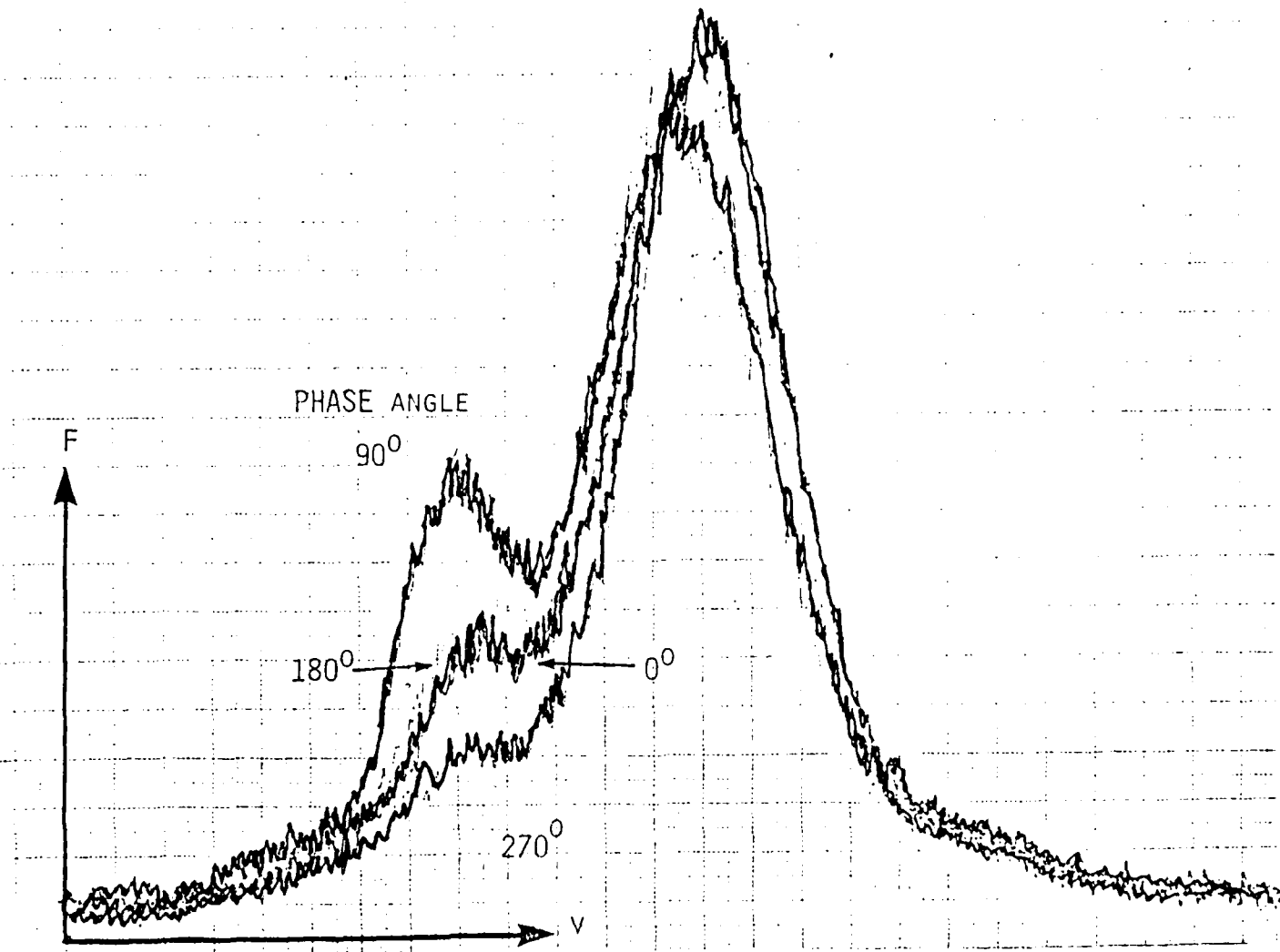


FIGURE 3

INSTANTANEOUS ION DISTRIBUTION

DURING A EICW CYCLE

RADIAL POSITION  $R = 1.2$  CM ; AZIMUTH  $0^0$

$V$  - VELOCITY ;  $F$  - ION VELOCITY DISTRIBUTION

### III. Publications and Presentations During this Grant Period

#### A. Publications

1. M. V. Goldman, G. F. Reiter, and D. R. Nicholson, "Radiation from a Strongly Turbulent Plasma: Application to Electron Beam-Excited Solar Emissions," *Phys. Fluids* 23, 388-401 (1980).
2. M. V. Goldman, K. Rypdal, and B. Hafizi, "Dimensionality and Dissipation in Langmuir Collapse," *Phys. Fluids* 23, 925-955 (1980).

#### B. Accepted for Publication

1. T. Tajima, M. V. Goldman, J. N. Leboef, and J. M. Dawson, "Breakup and Reconstitution of Langmuir Wavepackets," *Phys. Fluids Res. Note* 24, 182 (1981).
2. B. Hafizi and M. V. Goldman, "Harmonic Emission from Adiabatically Collapsing Langmuir Solitons," *Phys. Fluids* 24, 145 (1981).
3. F. W. Perkins and M. V. Goldman, "Self-Focusing of Radio Waves in an Underdense Ionosphere," *Journal of Geophysical Research*, in press (1981).
4. M. V. Goldman, J. C. Weatherall, and D. R. Nicholson, "Langmuir Collapse in a Weak Magnetic Field," *Phys. Fluids* 24, April (1980).
5. J. C. Weatherall, M. V. Goldman, and D. R. Nicholson, "Parametric Instabilities in Weakly Magnetized Plasma," *Astrophysical Journal*, in press (1981).

C. Invited Papers

1. M. V. Goldman, "Langmuir Collapse in Electron Beams of Solar Origin," invited seminar at the Department of Physics, University of California at Irvine, January 14, 1980.

2. M. V. Goldman, "Langmuir Collapse in Electron Beams of Solar Origin," invited talk at the Plasma Physics Division Meeting of the American Physical Society, November 1979, Boston, Massachusetts.

D. Contributed Papers

1. M. V. Goldman, B. Hafizi, and K. Rypdal, "Dimensionality and Langmuir Collapse, APS Meeting, Boston, Mass., November 1979.

2. W. T. Tajima, J. N. Leboef, J. M. Dawson, and M. V. Goldman, "Recursion of Langmuir Wavepackets," APS Meeting, Boston, Mass., November 1979.

3. M. V. Goldman, "Langmuir Collapse in Electron Beams of Solar Origin," APS Meeting, Boston, Mass., November 1979.

4. M. V. Goldman, G. F. Reiter, and D. R. Nicholson, "Type III Solar Emission and Langmuir Collapse," EOS 60 (46), November 1979, p. 932; AGU Meeting, Washington, D.C.

5. R. A. Stern, D. Hill, and N. Rynn, "Azimuthal Ion Ring Beam Generation in Unstable Magnetized Plasma," APS Meeting, Bull. Am. Phys. Soc. 25, 985 (1980).

6. K. L. Lam, R. W. Schumacher and R. A. Stern, "Ten Channel Optical Polychromator for Doppler Ion Temperature Measurements on the Dodecapole Surmac," Bull. Am. Phys. Soc. 25, 959 (1980).

7. R. A. Stern, D. N. Hill and N. Rynn, "Wave-Particle Interaction Studies," Bull. Am. Phys. Soc. 24, 1037 (1979).

E. Conference Organized

"Stochasticity vs. Coherence in Plasma Physics," Work-  
Shop at the Aspen Center for Physics, June 1980.

IV. References

1. S. Jackel, B. Perry, and M. Lubin, Phys. Rev. Lett. 37, 95 (1976).
2. M. J. Forrest, P. D. Morgan, N. J. Peacock, K. Kuriki, M. V. Goldman, and T. Rudolph, Phys. Rev. Lett. 37, 1681 (1976).
3. R. P. H. Chang, M. Porkolab, and B. Grek, Phys. Rev. Lett. 28, 206 (1972).
4. R. Stenzel and A. Y. Wong, Phys. Rev. Lett. 28, 274 (1972).
5. F. W. Perkins and P. K. Kaw, J. Geophys. Res. 76, 282 (1971).
6. H. C. Carlson, W. E. Gordon, and R. L. Showen, J. Geophys. Res. 77, 1242 (1972).
7. K. Papadopoulos, G. L. Goldstein, and R. Smith, Astrophys. J. 190, 1242 (1972).
8. S. Bardwell and M. V. Goldman, Astrophys. J. 209, 912 (1976).
9. A. Y. Wong and B. H. Quon, Phys. Rev. Lett. 28, 218 (1972).
10. D. F. DuBois and M. V. Goldman, Phys. Rev. Lett. 28, 218 (1972).
11. P. K. Kaw and J. M. Dawson, Phys. Fluids 12, 2585 (1969); D. W. Forslund, et al., Phys. Rev. Lett. 36, 35 (1975).
12. W. M. Hooke and S. Barnabei, Phys. Rev. Lett. 29, 1281 (1972).
13. V. E. Zakharov, Sov. Phys. JETP 35, 908 (1972).
14. G. J. Morales and Y. C. Lee, Phys. Fluids 19, 690 (1976).
15. A. Thyagaraja, "Recurrence, Dimensionality, and Catastrophic Behavior of Solutions of the Nonlinear Schroedinger Equation," submitted to Physics of Fluids, October 1980.
16. G. Benford, D. Tzach, K. Kato and D. F. Smith, Phys. Rev. Lett. 45, 1182 (1980).
17. P. E. Glaser, Physics Today, p. 30 (1977).
18. S. Basu, S. Basu, A. Johnson, J. A. Klobuchar, and C. M. Rush, Geophys. Res. Lett. 7, 609 (1980).

## APPENDIX A

A. "Radiation from a Strongly Turbulent Plasma:  
Application to Electron Beam-Excited Solar Emissions"

M. V. Goldman, G. F. Reiter, and D. R. Nicholson  
Physics of Fluids, 23, 388-401 (1980)

# Radiation from a strongly turbulent plasma: Application to electron beam-excited solar emissions

Martin V. Goldman

Department of Astro-Geophysics, University of Colorado, Boulder, Colorado 80309

George F. Reiter

Physics Department, Brookhaven National Laboratory, Upton, New York 11973

Dwight R. Nicholson

Department of Physics and Astronomy, University of Iowa, Iowa City, Iowa 52242  
(Received 4 May 1979; accepted 3 October 1979)

The emission of radiation at the plasma frequency and at twice the plasma frequency from beam-excited strong Langmuir turbulence, for the case of low-density high-velocity warm beams, is considered. Under these conditions, Langmuir wave packets undergo (direct) collapse in a time short compared with one  $e$  folding of a beam mode. The wave packet energy density threshold for collapse depends only on the beam temperature and velocity, not on the beam density. Upper and lower limits on the volume emissivity for harmonic emission from these collapsing wave packets are found. Within most of this range, the emissivity is large enough to account for observations of second harmonic radiation during type III solar radio wave bursts. The radiation at the fundamental is many orders of magnitude larger than predicted by weak turbulence theory.

## I. INTRODUCTION

In this paper we treat the emission of radiation from collapsing Langmuir wave packets excited by an electron beam of high velocity and low density. Emission rates at the plasma frequency  $\omega_p$  and the first harmonic  $2\omega_p$  are calculated for a nonmagnetic plasma with parameters appropriate to the solar wind plasma during so-called type III solar radio wave emission. The parameter space for Langmuir collapse and subsequent radiation is very rich, and many distinctly different phenomena can occur under different conditions. We believe the work of this paper deals with one of the simplest cases (possessing significant measured data), and probably has at least qualitative significance to other regimes of strong Langmuir turbulence.

The subject of type III solar radio-wave emission provides a unique arena for the interaction of modern nonlinear plasma physics with space physics. In this paper we shall show that conditions are commonly found in the solar wind, during type III bursts, when highly nonlinear evolution of electron plasma waves (Langmuir waves) can occur. This evolution can take the form of spatial "collapse"<sup>1,2</sup> of Langmuir wave packets of initially very low energy density. The collapse is essentially a nonlinear index-of-refraction effect, in which Langmuir waves are confined by the ponderomotive force, and intensify and steepen in an unstable manner which can only be stopped by eventual dissipation of energy into resonant electrons. A plasma in this condition is said to be "strongly turbulent."

The emission of electromagnetic waves from the collapsing Langmuir wave packets is estimated using various dynamical and statistical models. Most of these lead to favorable comparisons with recent observations by Gurnett and Anderson<sup>3</sup> at 1 AU (astronomical units).

We believe that previous attempts<sup>4</sup> at calculating this emission have been inconsistent (see Sec. VI).

One result of increasingly sophisticated and far-reaching experiments in space has been the establishment of a firmer foundation for the basic physics of type III bursts. There is now general agreement that an electron beam is launched during a flare event on the sun, and that as this beam propagates out in the solar wind along a magnetic field line, it excites Langmuir waves, which in turn produce radiation at the local plasma frequency and at its first harmonic. As the beam propagates from the sun to the earth and beyond, it encounters local plasma frequencies which progressively decrease by more than four orders of magnitude. The measured radiation shows this characteristic drop in frequency as a function of time. Spacecraft experiments on board satellites have detected the electron beam, Langmuir wave, and the emitted radiation, although the data on Langmuir waves have been rare, and difficult to obtain. A sketch of the events associated with a type III burst is depicted in Fig. 1. Measurements have been made from the earth-orbiting satellites (Ref. 5 and 6), IMP 6 and 8, and from the solar-orbiting satellites,<sup>7</sup> HELIOS 1 and 2.

Our concern in this paper is mainly with the emissivity measurements obtained by Gurnett and Anderson<sup>3</sup> at twice the local plasma frequency near HELIOS 1 (near 0.5 AU). In the strongest burst observed by them (31 March 1976, 18:10 U.T.), a radiation intensity of  $10^{-17} \text{ W m}^{-2} \text{ Hz}$  was measured. This leads to a volume emissivity (assuming isotropic emission) of<sup>8</sup>

$$J(2\omega_p) = 1.6 \cdot 10^{-11} \text{ ergs cm}^{-3} \text{ sec}^{-1} \text{ sr}^{-1}. \quad (1)$$

Langmuir waves were observed simultaneously, with an energy density (in units of the background particle en-

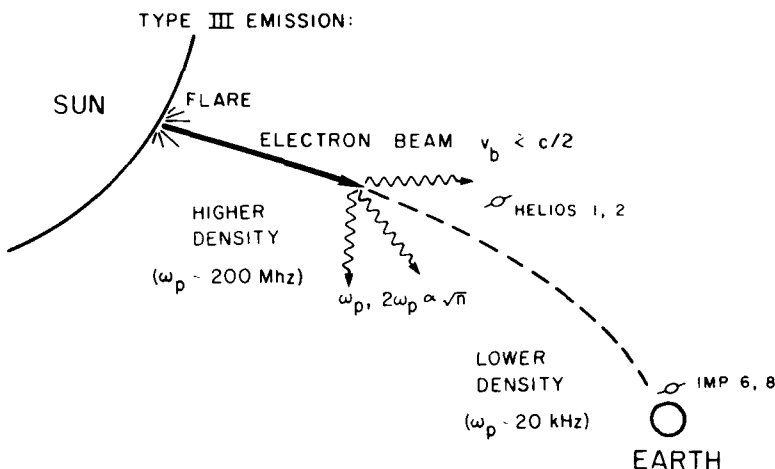


FIG. 1. Type III solar radio burst, showing an electron stream emanating from a flare and propagating to the earth along a magnetic field line. The radio wave emission is produced by beam-unstable Langmuir waves, and has been detected in space (by the indicated satellites) and on earth.

ergy density,  $nk_B T$ ) of

$$W = \langle |\mathcal{E}|^2 \rangle / 4\pi nk_B T \approx 1.4 \times 10^{-5}. \quad (2)$$

These Langmuir waves generally occurred as "spikes" with characteristic dimensions of 25–100 km or larger. (Structures of smaller size, such as the collapsing Langmuir wave packets discussed in this paper, would be too small to have been detected by the HELIOS spacecraft.) The background plasma parameters associated with these measurements were  $n_e = 42$  electrons per  $\text{cm}^3$  and  $k_B T_e = 10 \text{ eV}$  ( $T_e = 1.2 \times 10^5 \text{ K}$ ). We shall use these parameters in our calculations.

The plan of this paper will be as follows:

In Sec. II we shall treat the excitation of Langmuir waves by a typical electron beam associated with type III bursts and show how the beam determines the shape and spatial density of Langmuir wave packets up to the time at which their energy density begins to exceed the collapse threshold.

Section III is devoted to the subsequent collapse, and describes how a steady state is set up in which the beam acts as a source of energy density, and resonant wave-particle interaction (Landau damping) acts as a dissipative sink. Conditions for stabilizing the beam against quasi-linear plateau formation are also discussed here. The similarity solutions for collapsing wave packets in the adiabatic and supersonic regimes are presented.

In Sec. IV (and in the Appendix) we discuss the general problem of emission of electromagnetic waves by the nonlinear currents associated with Langmuir waves. It is shown that harmonic emission cannot be of lower order than quadrupole. Emission cannot occur from the beam-driven Langmuir waves without some form of nonlinear saturating wave interactions because of kinematical constraints. We estimate the harmonic and fundamental emission that occurs in the later stages of collapse by using similarity solutions and constants of the motion to approximate the Fourier transform of the emitting currents.

Calculation of the volume emissivity requires that we know (on the average) how many collapsing wave pack-

ets are present per unit volume. Models for this "density of collapsing packets" are developed in Sec. V, based on energy conservation in the steady-state power flow associated with Langmuir waves. The volume emissivity is calculated and compared with the measured value.

In Sec. VI we present detailed criticisms of other work on strong turbulence emissivity. In the Appendix we explain why the collapsing wave packets are mainly longitudinal.

## II. EXCITATION OF LANGMUIR WAVES BY THE BEAM

We shall assume a simple model of the electron beam and the background plasma. The beam will be assumed to be stationary, spatially homogeneous, and having a Gaussian distribution in velocity space centered around  $v_b \approx \frac{1}{2}c$ , with an isotropic half-width,  $\Delta v \approx \frac{1}{3}v_b$ :

$$f_b(v) = \frac{n_b \exp[-(v - v_b)^2/2\Delta v^2]}{(2\pi \Delta v^2)^{3/2}}, \quad v_b \approx \frac{c}{2}, \quad \frac{\Delta v_b}{v_b} \approx \frac{1}{3}. \quad (3)$$

The beam density will be taken to be no greater than  $10^{-6}$  times the background electron density  $n_e$ :

$$n_b/n_e \approx 10^{-6}. \quad (4)$$

The background plasma is assumed to be a Maxwellian with density  $n_e = 42$ , and temperature  $10 \text{ eV}$ , as in the experiments at  $\frac{1}{2}\text{AU}$  of Gurnett and Anderson.<sup>3</sup> This implies that  $n_e = 4.2 \times 10^{-5} \text{ cm}^{-3}$ , and  $v_e/v_b \approx 9 \times 10^{-3}$ , where  $v_e = (k_B T_e/m_e)^{1/2}$  is the electron thermal velocity associated with one degree of freedom.

We note that the assumption of a time-stationary beam is an approximation. Since the beam is injected with velocity dispersion at the site of a flare, the faster electrons will arrive downstream before the slower ones so that  $v_b$  (and possibly  $\Delta v$ ) are functions of time. The effects of this on the excited Langmuir waves were studied by Magelssen and Smith,<sup>4</sup> who took into account re-absorption of Langmuir waves by the beam, and determined that the beam could propagate over large distances. A relatively low level of Langmuir waves resulted ( $W \approx 10^{-4}$ ). However, the time scale for such effects is long compared with a collapse time, and we have ignored such space-time variations of the beam.

In this paper we show that Langmuir energy densities on the order of  $W \approx 10^{-4}$  are unstable against spatial collapse. These energy densities are a small fraction of the beam energy unless  $n_b/n_e$  is much smaller than  $10^{-6}$ . This justifies the neglect of the change in the beam due to homogeneous quasi-linear beam relaxation. Since the process of spatial collapse takes energy out of resonance with the beam, we can also view collapse as a potential mechanism for stabilizing the beam against plateau formation.

The beam distribution of Eq. (3) causes the growth of a  $k$ -space wave packet of Langmuir waves, centered around the wave vector  $\mathbf{k}_0$ , which satisfies the Cerenkov condition,

$$\mathbf{k}_0 \approx \omega_p \hat{v}_b / v_b, \quad (5a)$$

or

$$k_0 / k_D = v_e / v_b = 9 \times 10^{-3}. \quad (5b)$$

The resulting growth rate of resonant Langmuir waves is

$$\frac{\gamma_B}{\omega_p} = \left( \frac{\pi}{8} \right)^{1/2} \frac{n_b}{n_0} \left( \frac{v_b}{\Delta v} \right)^2 \frac{k_0^2}{k_{\perp}^2 + k_{\parallel}^2} Z \exp\left(-\frac{Z^2}{2}\right), \quad (6)$$

where

$$Z \equiv (v_b / \Delta v) (k_{\perp} - k_0) (k_{\parallel})^{-1}. \quad (7)$$

We note that the background magnetic field has been neglected in Eq. (6). This is completely justified, since the ratio of electron cyclotron frequency to plasma frequency is small (see Sec. VI).

The fastest growing Langmuir waves have  $k_{\perp} = 0$ , and  $k_{\parallel} = 0$ . We will determine the  $k$ -space shape of the Langmuir wave packet determined by Eq. (6). At a given time  $t$ , the wave energy system will have been amplified by the factor  $A(k) \equiv \exp[2\gamma_B(k)t]$ . We determine the half-widths by the condition  $A(\mathbf{k}_0 + \Delta\mathbf{k}) = A(\mathbf{k}_0)/2$ . The parallel and perpendicular half-widths are therefore obtained from the following equation:

$$\gamma_B(\mathbf{k}_0 \pm \Delta\mathbf{k}) / \gamma_B(\mathbf{k}_0) = 1 - \ln 2 / \ln A(\mathbf{k}_0). \quad (8)$$

Choosing  $A(k) = 2 \times 10^4$  (10  $e$  foldings) yields,

$$\frac{\Delta k_{\perp}}{k_0} = \left( \frac{\ln 2}{\ln 4} \right)^{1/2} \approx \frac{1}{4}, \quad (9a)$$

$$\frac{\Delta k_{\parallel}}{k_0} = \left( \frac{\ln 2}{\ln 4} \right)^{1/2} \frac{\Delta v}{v_b} \approx \frac{1}{4} \frac{\Delta v}{v_b}. \quad (9b)$$

We note that the perpendicular half-width  $\Delta k_{\perp}/k_0$  is determined entirely from the factor  $k_0^2/(k_{\parallel}^2 + k_{\perp}^2)$  in Eq. (6), while the parallel half-width  $\Delta k_{\parallel}/k_0$  is determined entirely from the factor  $Z \exp(-Z^2/2)$ . The shape of the  $k$ -space wave packet is therefore elongated in the perpendicular directions, producing a kind of pancake, as shown in the two-dimensional projection in Fig. 2.

This model assumes the amplification of spatially homogeneous noise, so that the convective nature of the beam instability is irrelevant. We also note, in this connection, that a typical excursion distance of a Langmuir wave packet in the perpendicular direction (during a collapse time) is 1 km, whereas the perpendicular spatial width of the electron beam has been measured<sup>5</sup>

to be at least 80 earth radii. This justifies the neglect of the finite spatial width of the beam in our treatment.

The phases of the Fourier modes in the beam-unstable Langmuir wave packet will be random, since we have assumed it is homogeneous white noise being amplified. This leads to a multitude of wave packets in real space, with mean spatial half-widths of  $\Delta r \approx (\Delta k)^{-1}$  and  $\Delta x \approx (\Delta k)^{-1}$ , as depicted in Fig. 2. For the parameters considered here, a typical real-space packet measures about 3 by 10 km. This would be too small a packet to be measured by current spacecraft techniques<sup>3</sup> at 1 AU. We shall assume the mean distance between wave packets to be on the order of this mean size.

This will constitute our picture of Langmuir waves while they are subject to beam growth, but before they have reached the critical intensity for nonlinear wave-wave interactions. We should remark, in passing, that the beam contribution to the dispersion relation of the Langmuir waves is negligible because  $n_b/n_e \gtrsim 10^{-6}$  [inequality (4)].

### III. LANGMUIR WAVE COLLAPSE

The electron beam creates the configuration of real-space Langmuir wave packets just described. The packets grow in time. When one of these packets is sufficiently intense, it can collapse "directly,"<sup>2</sup> in a time which is fast compared with one beam growth  $e$ -folding time. This process has recently been discussed at length by two of the present authors.<sup>2,4</sup>

#### A. Predictions of the virial theorem for initially adiabatic collapse

In brief, the threshold for collapse of a wave packet depends simply on its  $k$ -space widths (in the limit when its group velocity is less than sound speed, and assuming that its energy density is sufficiently less than the mass ratio). The critical energy density for an anisotropic wave packet is a slight generalization of the result in Ref. 2,

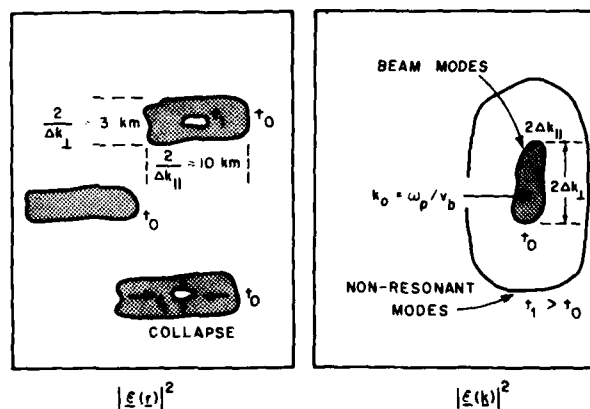


FIG. 2. Contours of constant Langmuir wave energy density in real and Fourier space, at an initial time  $t_0$ , and a later time  $t_1$  (after some real-space collapse has occurred). The initial Fourier-space wave packet consists of beam-unstable (resonant) modes, with random phases, centered about the wave vector  $\mathbf{k}_0 = \omega_p \hat{v}_b / v_b$ , forming a packet of size  $\Delta k_{\parallel}$  by  $\Delta k_{\perp}$ . In real space, this corresponds to packets of size 3 by 10 km.

$$W_{th} = 24 \{ [(\Delta k_x)^2 + (\Delta k_y)^2] / k_D^2 \}, \quad (10)$$

provided that

$$W \ll 16 m/M, \quad (11a)$$

and

$$k_0^2 / k_D^2 \ll (2/9)(m/M), \quad (11b)$$

where  $W$  is the energy density defined in Eq. (1),  $m/M$  is the electron-to-ion mass ratio,  $\Delta k$  is the  $k$ -space half-width of the packet, and  $k_D$  is the Debye wavenumber. The inequalities (11) are the conditions for adiabatic ions. In the later stages of collapse the ion inertia becomes important, and the inequalities (11) are strongly violated; however, the threshold condition (10) is justifiably adiabatic. From Eqs. (5) and (9) we have

$$\Delta k_x / k_D = 2.2 \times 10^{-3}, \quad \Delta k_y / k_D = 7.5 \times 10^{-4}. \quad (12)$$

The larger of these dominates in Eq. (10), and

$$W_{th} \approx 10^{-4}. \quad (13)$$

The adiabatic condition (11a) is then seen to be well-satisfied, but (11b) is only marginally satisfied. Nevertheless, numerical calculations<sup>9</sup> indicate the validity of this description under the present circumstances.

Next, we note that the energy  $W_{th}$  represents a small fraction of the energy density in the electron beam, when  $n_b/n_e \approx 10^{-6}$ . Under these circumstances

$$W_b = m n_b v_b^2 / n_e \Theta_e \approx 10^{-2}; \quad (14)$$

hence, the wave-wave interactions inherent in collapse occur before the wave-particle interactions governing homogeneous beam plateau formation. Since the wave energy of resonant modes never becomes comparable to the beam energy, the collapse process would seem to suppress quasi-linear plateau formation!

We also note that  $W_{th}$  is independent of the beam density  $n_b$ , whereas  $W_b$  decreases with  $n_b$ . Hence, for  $n_b/n_e$  significantly smaller than  $10^{-6}$ , it is likely that collapse will be prohibited because not enough energy is available in the beam to elevate the waves to threshold energy. Measurements indicate that  $10^{-6}$  is probably an upper limit for type III bursts.

These facts also help guarantee that the collapse time is shorter than a beam growth time. The collapse time predicted from virial theorem arguments<sup>2</sup> is

$$\omega_b t_v = 4[\sqrt{3} (\Delta k / k_D) (W - W_{th})^{1/2}]^{-1}. \quad (15)$$

(Near threshold, this is of the same order as the collapse time associated with similarity solutions.<sup>1</sup>) A typical value for  $t_v$  is about 0.1 sec, compared with about 1 sec for  $\gamma_b^{-1}$ . For  $n_b/n_e$  less than  $10^{-6}$  the beam instability will be even slower.

A model for steady state must go farther, and follow the power injected by the beam to its ultimate dissipation in the plasma. Our qualitative picture of this process is exhibited in Fig. 3. Here, the "state" of a Langmuir wave packet is characterized by two parameters: its energy density  $W$ , and the square of a characteristic spatial half-width  $\Delta x$  (in units of the Debye length). These two parameters form a kind of two-dimensional

phase space for Langmuir wave packets. Packets above the dashed line are subject to collapse, according to Eq. (10). Owing to the instability of the beam, a wave packet executes a trajectory in the phase space, as illustrated in Fig. 3. Packets of a size set by the beam parameters [Eq. (9)] grow until they exceed threshold. They then quickly collapse to smaller size and larger  $W$ . This collapse becomes supersonic when the adiabatic conditions (11) are violated. We assume that the collapse continues until  $\Delta x$  becomes on the order of about 5 Debye lengths, and that the collapse then ceases, with power flowing into electrons due to wave-particle interaction. The power balance this implies will be treated explicitly in Sec. V. We note from Fig. 3 that the packet size decreases by two orders of magnetic, and its energy density increases from  $10^{-4}$  at threshold, to order unity when Landau damping can occur.

In the adiabatic regime, above threshold, the Langmuir wave evolution should be accurately described<sup>2</sup> by the cubic nonlinear Schrödinger equation

$$i\partial_{\bar{t}} \bar{\mathcal{E}} + \frac{1}{2} \nabla^2 \bar{\mathcal{E}} + |\bar{\mathcal{E}}|^2 \bar{\mathcal{E}} = 0, \quad (16)$$

here,  $\bar{t} = \omega_b t / \sqrt{3}$ , and  $\bar{\mathcal{E}}$  is the dimensionless envelope of the plasma oscillations. The total real Langmuir wave field  $E_L$  is given in physical units in terms of the envelope  $\mathcal{E}$  as

$$E_L = \text{Re}[(32\pi n)^{1/2}(\theta_e + \theta_i)^{1/2} \bar{\mathcal{E}} \exp(-i\omega_b t)]. \quad (17)$$

In the early adiabatic stages of collapse, the evolution of a given initial wave packet can be described by virial theorem arguments.<sup>2</sup> In addition to the threshold  $W_t$ ,

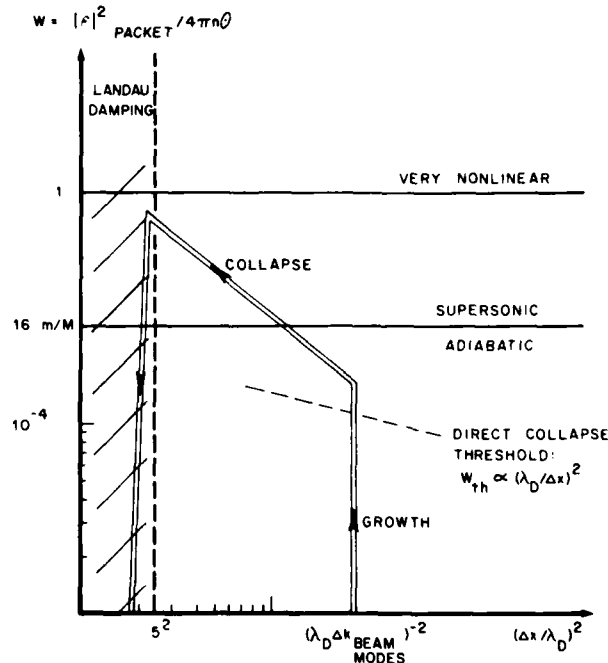


FIG. 3. Trajectory of the state of a collapsing wave packet, shown in a "phase" space, in which a packet is labeled by its square width,  $(\Delta x)^2 / \lambda_D^2$ , and its mean energy,  $W = \langle |\mathcal{E}|^2 \rangle / 4\pi n \theta$ . Energy is injected into packets of a width set by the beam instability. The collapse is initially adiabatic, then supersonic, and finally ends in wave-particle energy transfer.

[Eq. (10)] and the collapse time  $t_v$  [Eq. (15)], these arguments predict the dependence of the square width  $\langle \delta r^2 \rangle$  of the packet, on time,

$$\langle \delta r^2 \rangle = \langle \delta r^2 \rangle_0 (1 - t^2/t_v^2), \quad (18a)$$

and also the dependence of the energy density, if one assumes that the shape of the packet remains Gaussian

$$W(t) \propto \langle \delta r^2 \rangle^{-D/2}, \quad (18b)$$

where  $D$  is the number of spatial dimensions of Eq. (16).

### B. Adiabatic similarity solution

In the later stages of adiabatic collapse, it is likely that the packet has distorted in shape and has begun to approach the shape of the similarity solution.<sup>1</sup> The similarity solution is of the form

$$\tilde{\mathcal{E}} = (\bar{t}_a - \bar{t})^{-1/2} \mathbf{R}(\mathbf{u}), \quad (19a)$$

$$\mathbf{u} = \tilde{\mathbf{r}} / (\bar{t}_a - \bar{t})^{1/2}. \quad (19b)$$

When (19) is inserted into (16), an ordinary differential equation for  $\mathbf{R}$  results

$$\frac{1}{2} i (1 + \mathbf{u} \cdot \partial_{\mathbf{u}}) \mathbf{R} + \frac{1}{2} \partial_{\mathbf{u}}^2 \mathbf{R} + |\mathbf{R}|^2 \mathbf{R} = 0. \quad (19c)$$

We can arbitrarily set  $|\mathbf{R}|$  to be of order unity at its maximum. Then, we find that the collapse time of the adiabatic similarity solution is

$$\omega_p t_a = 8W^{-1}, \quad (20a)$$

where we have assumed the spatial average  $\langle |\tilde{\mathcal{E}}|^2 \rangle = \frac{1}{2} |\tilde{\mathcal{E}}_{\max}|^2$ . Note, this differs from the virial theorem prediction, although when  $W$  is several times  $W_{th}$ , they are numerically close. (In essence, the similarity solution does not "remember" initial scale lengths, such as  $\Delta k^{-1}$ .) From (19a) we also get a prediction from the similarity solution about how  $W$  varies with time

$$W_a(t) = W(0) / (\bar{t}_a - \bar{t}). \quad (20b)$$

This is in asymptotic agreement with (18b) only in two dimensions. Also, the half-width of the collapsing self-similar solution can be much narrower than  $\langle \delta r^2 \rangle$ .

### C. Supersonic similarity solution

As  $W$  increases, the collapse becomes supersonic, in the sense that the inequality (11a) is violated. At this time, the cubic nonlinear Schrödinger equation (16), no longer provides a correct description, and we must employ the so-called Zakharov<sup>2</sup> equations, which allow for ion inertial effects and electromagnetic dispersion.<sup>10</sup> These equations may be written as

$$(i\partial_{\tilde{t}} + \tilde{\nabla} \tilde{\nabla} \cdot + \frac{c^2}{3v_{th}^2} \tilde{\nabla} \times \tilde{\nabla} \times - \frac{\tilde{n}}{2}) \tilde{\mathcal{E}} = 0, \quad (21a)$$

$$(\partial_{\tilde{t}}^2 - \beta \tilde{\nabla}^2) \tilde{n} = \tilde{\nabla}^2 |\tilde{\mathcal{E}}|^2, \quad (21b)$$

where  $\tilde{n}$  is the ion density fluctuation, and the dimensionless units are<sup>10</sup>

$$\tilde{t} = \frac{2}{3} \frac{m}{M} \omega_p t, \quad \tilde{\mathbf{r}} = \frac{2}{3} \left( \frac{m}{M} \right)^{1/2} \mathbf{r} k_D, \quad (22)$$

$$\tilde{n} = \frac{3}{2} \frac{M}{m} \frac{\delta n}{n_0}, \quad \beta = 1 + \frac{\gamma_1 \theta_1}{\theta_p},$$

where  $m/M$  is the electron-to-ion mass ratio, and  $\gamma_1$  is the usual ratio of ion specific heats. The real electric field of the Langmuir waves in physical units in terms of the dimensionless envelope  $\tilde{\mathcal{E}}$  is

$$\mathbf{E}_L = \text{Re}[(m/M)^{1/2} (32\pi n_0/3)^{1/2} \tilde{\mathcal{E}} \exp(-i\omega_p t)]. \quad (23)$$

in the extreme supersonic limit, only the  $\partial_{\tilde{t}}^2$  term need be retained on the left side of Eq. (21b). Equations (21) then have a well-known three-dimensional (supersonic) similarity solution,<sup>10,11</sup> given by

$$\tilde{\mathcal{E}} = (\bar{t}_s - \bar{t})^{-1} \mathbf{R}(\mathbf{u}), \quad \mathbf{u} = \tilde{\mathbf{r}} / (\bar{t}_s - \bar{t})^{2/3}, \quad (24)$$

$$\tilde{n} = (\bar{t}_s - \bar{t})^{-4/3} \eta(\mathbf{u}),$$

where  $t_s$  is the supersonic collapse time, and  $|\mathbf{R}|$  is again chosen to have a maximum equal to unity. This implies that the time for supersonic collapse is given (in real units) by

$$\omega_p t_s = [(m/31) W_{s0}]^{-1/2}, \quad (25a)$$

where  $W_{s0}$  is the value of  $\tilde{\mathcal{E}}_{\max}^2 / 8\pi n_0$  at the time supersonic collapse begins. If the supersonic stage follows an initially adiabatic collapse, as we are assuming here, we can roughly take  $W_{s0} \approx 16 m/M$  [from (11a)], so that

$$\omega_p t_s = (3/16)^{1/2} (M/m). \quad (25b)$$

We shall use these similarity solutions later to calculate the emission from collapsing Langmuir waves. There is numerical evidence that certain initial field configurations relax into similarity solutions,<sup>10-12</sup> but the analytical foundations for why this is so remain largely unknown. It is also useful to note that the dimensionless dispersion collapse time  $\bar{t}_s$  is simply  $(12)^{-1/2}$ .

In summary, the role of Langmuir collapse is indicated in the energy flow diagram in Fig. 4. Most of the electron stream energy remains intact during its propagation from the sun. A small fraction of this energy [see Eqs. (10) and (14)] goes into Langmuir waves due to the bump-on-tail instability. Some of the resulting Langmuir wave packets collapse due to nonlinear wave interactions. During the collapse, a small fraction of the Langmuir energy is radiated away, mainly at  $2\omega_p$ . However, most of the Langmuir energy is eventually dissipated by coupling to electrons and ions in the late stages of collapse, which we do not treat explicitly in this paper.

It is important to note that a strong conversion of the Langmuir waves into (transversely polarized) radiation is not expected, because the parameter  $c^2/3v_p^2$  is much greater than one, and the early fields are entirely longitudinal. This matter is discussed in some detail in the Appendix. In the next section we treat the conversion into radiation by familiar techniques for given current distributions, and obtain expressions for the emission from a single collapsing Langmuir wave packet.

### IV. EMISSIVITY OF RADIATION FROM LANGMUIR WAVE PACKETS

The transverse nonlinear currents,  $\mathbf{J}^T$ , associated with (longitudinal) Langmuir waves can lead to emission of radiation at  $2\omega_p$  and at  $\omega_p$ . We assume a model of

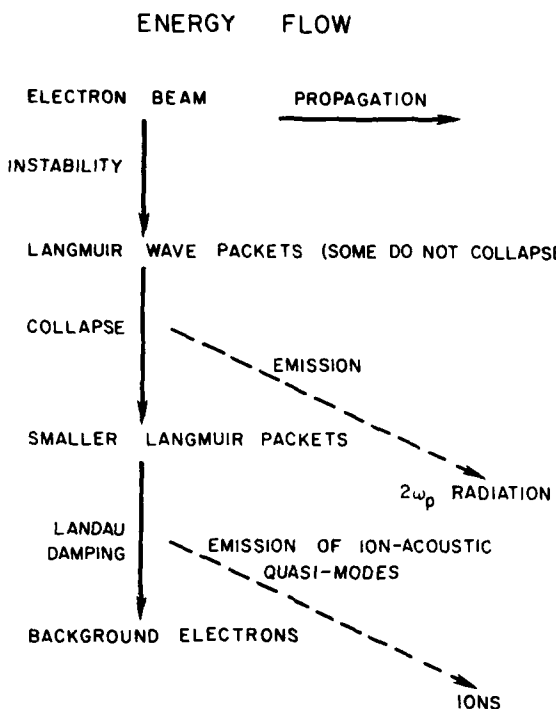
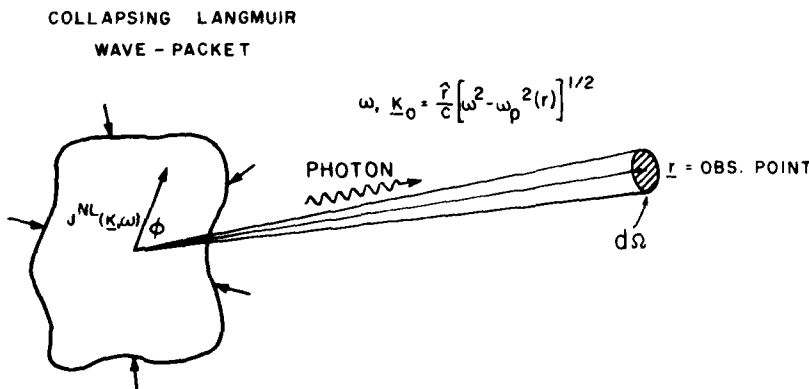


FIG. 4. Energy flow during a type III solar radio burst. Most of the energy remains in the beam. A smaller fraction goes into beam-unstable Langmuir waves, some of which collapse. A small fraction of the Langmuir energy goes into radiation. When a packet has collapsed to a size of several Debye lengths it surrenders its energy to electrons and ions.

independent emissions associated with the current of each of an assembly of Langmuir wave packets. The emissivity of a given wave packet is then a simple function of the nonlinear current  $\mathbf{j}^n$ . By standard techniques, we find

$$\frac{dP}{d\Omega} = \frac{cr^2}{4\pi} \frac{1}{T} \int_0^T dt \mathbf{E} \times \mathbf{B} = \frac{r}{4\pi c^2 T} \int_{-\infty}^{\infty} \frac{d\omega}{2\pi} \omega K |\mathbf{j}^n(\mathbf{K}, \omega)|^2 \sin^2 \phi, \quad (26)$$

where  $\mathbf{r}$  is a position vector from the current distribution to an observation point in the radiation zone, the wave vector  $\mathbf{K}$  is defined as  $\mathbf{K} = (\mathbf{r}/c)[\omega^2 - \omega_p^2(\mathbf{r})]^{1/2}$ , and



$\phi$  is the angle between  $\mathbf{j}^n(\mathbf{K}, \omega)$  and  $\hat{\mathbf{r}}$ . Equation (26) takes into account the fact that the observation point is imbedded in the plasma with a local plasma frequency  $\omega_p(\mathbf{r})$  which varies on the scale of an AU.

The geometry is illustrated in Fig. 5. Note, the factor  $\sin^2 \phi$  guarantees that only the transverse component of the current contributes to the emission. The time average is over a time  $T$  which is long compared with the dominant frequency  $\omega_0$  ( $T$  may be set equal to the collapse time).

We are interested in nonlinear currents centered about a dominant frequency  $\omega_0$

$$\mathbf{j}^n(\mathbf{r}, t) = \frac{1}{2} \mathbf{j}^n(\mathbf{r}, t) \exp(-i\omega_0 t) + c.c., \quad (27)$$

where the time dependence of the envelope  $\mathbf{j}^n(\mathbf{r}, t)$  is slow on the scale of  $\omega_0^{-1}$ . Making use of this slowness, Eq. (26) can be expressed in terms of the envelope current as

$$\frac{dP}{d\Omega} \approx \frac{K_0 \omega_0 \sin^2 \phi_0}{8\pi c^2} \frac{1}{T} \int_0^T dt |\mathbf{j}^n(\mathbf{K}_0, t)|^2, \quad (28a)$$

where

$$\mathbf{K}_0 = \hat{\mathbf{r}}/c [\omega_0^2 - \omega_p^2(\mathbf{r})]^{1/2}, \quad (28b)$$

is the principal wave vector of the emitted radiation, and  $\omega_p(\mathbf{r})$  is the plasma frequency at the observation point. Also,  $\phi_0$  is the angle between  $\hat{\mathbf{r}}$  and  $\mathbf{j}^n(\mathbf{K}_0, \omega=0)$ .

We now need to develop expressions for the appropriate nonlinear currents. These currents arise from the beating of first- or second-order electron density fluctuations with the velocity of electrons oscillating in the Langmuir field.

The current which gives rise to emission at the plasma frequency is third order in the Langmuir field

$$4\pi \theta_p J_{\omega_p}^n(\mathbf{r}, t) = \omega_p^2 (\delta n_2 / n_0) \mathbf{E}_L, \quad (29)$$

where  $\delta n_2$  is the density driven by the ponderomotive force in Eq. (21b), and hence second order<sup>13</sup> in the Langmuir field  $\mathbf{E}_L$ . The relationship between  $\delta n_2$  and the dimensionless  $n$  is given in Eq. (22). We note that, although  $\mathbf{E}_L$  is entirely longitudinal, the product  $\delta n_2 \mathbf{E}_L$  has a transverse component, in general. Also note that in the adiabatic limit  $\delta n_2$  reduces simply to  $-|\vec{E}|^2$  [see Eq. (16)].

FIG. 5. Emission from a single collapsing Langmuir wave packet. Photons of frequency  $\omega$  and wave vector  $\mathbf{K}_0$  are radiated into the solid angle  $d\Omega$  about the observation point  $\mathbf{r}$ . Note this observation point is embedded in the plasma [with local plasma frequency  $\omega_p(\mathbf{r})$ ].

The current at  $2\omega_p$  is second order in the Langmuir field  $\mathbf{E}_L$

$$4\pi\partial_t J_{2\omega_p}^{nl}(\mathbf{r}, t) = \omega_p^2 (2\delta n_1/n_0) \mathbf{E}_L. \quad (30a)$$

Here,  $\delta n_1$  is the first-order density of electrons oscillating at the plasma frequency. (The factor 2 arises because the emission frequency is  $2\omega_p$ .) An expression for  $\delta n_1$  follows immediately from Poisson's equation for the Langmuir field  $\mathbf{E}_L$ ,

$$n_1 = -\nabla \cdot \mathbf{E}_L / 4\pi e. \quad (30b)$$

### A. Emission at $2\omega_p$

It is easy to prove that there can be no dipole emission at  $2\omega_p$ . The standard multipole expansion for  $\mathbf{j}^{nl}(\mathbf{K}, t)$  is generated by writing the spatial Fourier transform of the current in terms of the Kronecker delta  $\delta_{lm} = \nabla_m \cdot \nabla_l$ :

$$\mathbf{j}^{nl}(\mathbf{K}, t) = \int d^3 \mathbf{r} (\nabla_m \cdot \mathbf{r}) \mathbf{j}_m^{nl}(\mathbf{r}, t) \exp(-i\mathbf{K} \cdot \mathbf{r}). \quad (31)$$

In the dipole approximation,  $\mathbf{K} \cdot \mathbf{r}$  is set equal to zero. After an integration by parts and application of the continuity equation, this yields  $\mathbf{j}^{nl}(\mathbf{K}, t) \approx -i\omega_0 \mathbf{d}$ , where  $\mathbf{d}$  is the dipole moment of the nonlinear charge density distribution. Hence, whenever the spatial integral of  $\mathbf{j}^{nl}(\mathbf{r}, t)$  vanishes, there is no dipole emission. We can show that this is the case for harmonic emission by using Eqs. (30) for the nonlinear current  $\mathbf{j}_{2\omega_p}^{nl}$ . If  $\mathbf{E}_L = \text{Re}[\mathcal{E} \exp(-i\omega_p t)]$ , then  $\mathbf{j}_{2\omega_p}^{nl} = \text{Re}[\mathbf{j}_{2\omega_p}^{nl} \exp(-2i\omega_p t)]$ , where the envelope,  $\mathbf{j}_{2\omega_p}^{nl}(\mathbf{r})$  is proportional to  $(\nabla \cdot \mathcal{E}) \mathcal{E}$ , from Eq. (30). Since  $\mathcal{E}$  is predominantly curl-free (see the Appendix), there follows the vector identity

$$\mathbf{j}_{2\omega_p}^{nl}(\mathbf{r}, t) = \frac{-ie/m}{4\pi\omega_p} \nabla_i \left( \mathcal{E}_i \mathcal{E}_i - \frac{\delta_{11} \mathcal{E} \cdot \mathcal{E}}{2} \right). \quad (32)$$

Hence,  $\int d^3 \mathbf{r} \mathbf{j}_{2\omega_p}^{nl}$  vanishes, by the divergence theorem, and there is no dipole emission at  $2\omega_p$ .

To find the emissivity for harmonic emission in terms of the field  $\mathcal{E}$  of a Langmuir wave packet, take the spatial Fourier transform of the current given in (32). Upon integrating by parts

$$\mathbf{j}_{2\omega_p}^{nl}(\mathbf{K}_0, t) = \frac{-eK_{0i}}{4\pi\omega_p m} \int d^3 \mathbf{r} \exp(-i\mathbf{K}_0 \cdot \mathbf{r}) \left( \mathcal{E}_i \mathcal{E}_m - \frac{\delta_{11} \mathcal{E} \cdot \mathcal{E}}{2} \right). \quad (33)$$

For simplicity, let us assume that the Langmuir field direction remains essentially parallel to  $\mathbf{k}_0$  during collapse. We write

$$\mathcal{E}(\mathbf{r}, t) = \hat{k}_0 A \exp(i\theta/2), \quad (34)$$

where the (real) scalar amplitude  $A$ , and phase  $\theta$ , depend on space and time. From Eq. (33), we find

$$\mathbf{j}_{2\omega_p} = \frac{e(\mathbf{K}_0/2 - \mathbf{K}_0 \cdot \hat{k}_0 \hat{k}_0)}{4\pi\omega_p m} \int d^3 \mathbf{r} \exp[i(\mathbf{K}_0 \cdot \mathbf{r} - \theta)] A^2, \quad (35)$$

The magnitude of the emission depends in detail upon the space-time evolution of  $A(\mathbf{r}, t)$  and  $\theta(\mathbf{r}, t)$ . We shall assume that  $A^2$  collapses, and that  $\theta$  starts out as  $2\mathbf{k}_0 \cdot \mathbf{r}$  and does not evolve pathologically.

We note parenthetically, however, some recent evidence<sup>12</sup> that the nonlinear behavior may consist of periodic breakup and reconstitution, rather than collapse, due to ponderomotive effects in the phase. Since no theoretical understanding yet exists concerning the competition of such behavior with collapse, it is not taken into account in the present paper. We assume here that collapse continues down to scale lengths of several Debye lengths.

In the very early phases of collapse there cannot be substantial emission because of the momentum mismatch,  $\mathbf{K}_0 - 2\mathbf{k}_0$ , in the phase factor in the integrand of Eq. (35). There is strong phase mixing, as we shall soon show. As  $A^2$  collapses more and more, the phase mixing becomes less important. By the time the collapse has become supersonic ( $W > 16 m/M$ ), emission can occur.

The amount of emission depends sensitively on the shape of  $A^2$ , as supersonic collapse proceeds to still smaller scales. There have been no calculations of the three-dimensional evolution of  $A^2$  and  $\theta$  predicted by Zakharov equations. Model equations studied by Budneva *et al.*<sup>11</sup> suggest that a small collapsing core breaks away from an initially Gaussian packet, leaving the (essentially) Gaussian corona behind. The core eventually tends toward the form of a similarity solution to the equations.

We shall estimate the current in two different ways. First, we shall assume that the entire Gaussian corona collapses. This will lead to an upper bound on the emissivity. Then, we shall assume that only the (much smaller) core collapses, and tends toward a supersonic similarity solution. This will give less emission. The actual emissivity probably lies between the two limits.

In order to present a coherent discussion of the various spatial scales, we introduce the following definitions: Define  $L_{n+1}(t)$  as the half-widths of  $A^2$

$$A^2(z = L_n, r = 0) \quad A^2(z = 0, r = L_1) \equiv \frac{1}{2} A^2(0, 0), \quad (36a)$$

and  $l_{n+1}$  as the scale lengths of the phase

$$l_{n+1} = |\theta| / \nabla_{n+1} \theta. \quad (36b)$$

We now discuss the implications of the time dependence of  $L(t)$  and  $l(t)$  for the size of the current,  $\mathbf{j}_{2\omega_p}$ , in Eq. (35). We begin with the time  $t = 0$  at which the beam-amplified Langmuir wave packets begin their collapse.

#### 1. Onset of collapse ( $t=0$ )

Initially, the packet moves at a phase velocity equal to the beam velocity, so the phase is

$$\theta = 2\mathbf{k}_0 \cdot \mathbf{r}, \quad |l| = (2k_0)^{-1}, \quad l_1 = 0. \quad (37a)$$

The half-widths  $L_n$  and  $L_1$  correspond to the half-widths of the initial packet defined by Eqs. (9) and (12)

$$L_n(0) = (\Delta k_n)^{-1}, \quad L_1(0) = (\Delta k_1)^{-1}. \quad (37b)$$

If we assume that  $A^2$  is Gaussian, the integral for  $\mathbf{j}_{2\omega_p}$  can be performed. It is proportional to

$$\mathbf{j}_{2\omega_p} \propto \exp[-(K_0 - 2k_0)^2 L_n^2 / 4], \quad (37c)$$

which is vanishingly small. This result corresponds to

the well-known fact that beam-driven Langmuir wave packets cannot emit type III radiation at  $2\omega_p$  in the absence of nonlinear (or other) interactions which broaden their  $k$ -space widths. This is because momentum conservation demands that the photon wave vector  $\mathbf{K}_0$  be equal to the sum of two Langmuir wave vectors  $\mathbf{k}_{01}$  and  $\mathbf{k}_{02}$ , which lie within the packet. Since  $K_0 = \sqrt{3}\omega_p/c$  [by (28b)] and  $k_0 = \omega_p/v_b$  [by (5a)], we see that this is not possible for beams with speeds  $v_b$  of order  $\frac{1}{2}c$  or smaller. The situation is illustrated in Fig. 6. Essentially, the wave packet is too narrow in  $k$  space to contain Langmuir wave vectors  $\mathbf{k}_{01}$  and  $\mathbf{k}_{02}$  sufficiently smaller in magnitude than  $\mathbf{k}_0$  to add up to  $\mathbf{K}_0$ . The mathematical expression of this is that the exponent  $-(K_0 - 2k_0)^2 L_n^2/4$  in Eq. (37c) is initially a large negative number.

However, as the packet collapses,  $(K_0 - 2k_0)^2 L_n^2/4$  tends to zero. The reduction factor  $\exp^{-(K_0 - 2k_0)^2 L_n^2/4}$  is no longer effective, and the time  $L_n$  has become small enough for the following condition to be satisfied:

$$L_n(t)k_0 \approx 1, \quad (38)$$

for no phase mixing (here, we have used the fact that  $K_0$  is of order  $k_0$ , and assumed that  $L_n$  does not get much smaller than  $L_n$ ). By this time, the packet has broadened<sup>2,9</sup> sufficiently in  $k$  space, so that it contains pairs of wave vectors [such as  $\mathbf{k}_1$  and  $\mathbf{k}_2$  in Fig. 6(b)] which properly sum to  $\mathbf{K}_0$ . Put in another way, the phase factor in the integrand of Eq. (35) is no longer effective in phase-mixing the integral by the time inequality (38) is

#### LANGMUIR PACKETS IN $k$ -SPACE

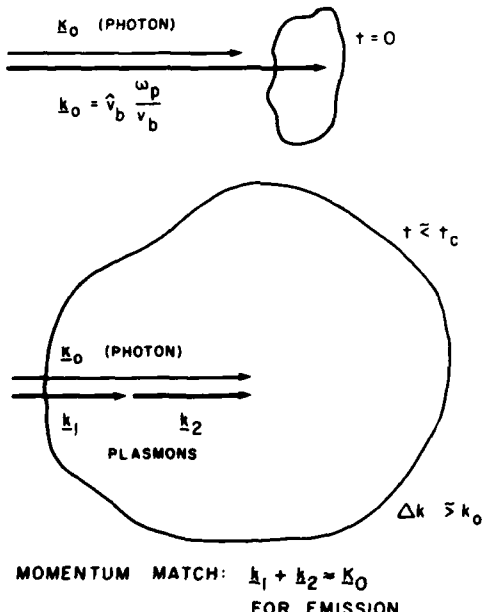


FIG. 6. Momentum conservation requirements for emission of harmonic radiation (at  $2\omega_p$ ) by a wave packet. Initially, the packet is centered around  $\mathbf{k}_0$ , and is too small to contain two plasmon wave vectors which sum to the photon wave vector  $\mathbf{K}_0$ . After some collapse, the packet has enlarged in  $k$  space, and contains enough plasmon pairs of the proper momentum to conserve.

satisfied.

To proceed further, we need models of the time dependence of  $L_n$ . The most optimistic of these assumes a collapsing Gaussian corona. This leads to an upper bound on the emissivity.

#### 2. Coronal collapse model

In the adiabatic stage we can use the scaling implied by the virial theorem [see Eqs. (18)]

$$L_{n,1} \sim (\Delta k_{n,1})^{-1} (1 - t^2/t_{V}^2)^{1/2}. \quad (39)$$

We also assume that  $\theta = 2\mathbf{k}_0 \cdot \mathbf{r}$ . This is acceptable in the adiabatic stage as long as  $L_{n,1} k_0 \ll 1$ , since plasmon momentum is conserved.<sup>2</sup> Another conserved quantity is the plasmon number,<sup>1,2</sup>

$$N \equiv \int d^3r A^2 = \text{const.} \quad (40)$$

Equations (39) and (40), taken together with the assumption of a Gaussian shape, give us the time dependence of the space-averaged energy density  $W(t)$  [see also Eq. (18b):]

$$W(t) = \frac{W(0)}{(1 - t^2/t_{V}^2)^{3/2}}. \quad (41)$$

For phase mixing to disappear, Eq. (38) must be satisfied. Using the expression for  $L_n$  in Eq. (39), this gives the time  $t_n$  at which a collapsed corona begins to emit harmonic radiation

$$(1 - t_n^2/t_{V}^2)^{1/2} \approx \Delta k_n/k_0 = 1/12. \quad (42)$$

However, at this time, according to Eq. (41), the energy density  $W(t_n)$  will have increased by three orders of magnitude, and the collapse will be well into the supersonic regime. If the entire corona collapses enough for phase mixing to be negligible, then the current in Eq. (35) becomes proportional to the plasmon number  $N$  in Eq. (40). Since  $N$  is an invariant of the Zakharov equations (21), it is conserved even in the supersonic stage of collapse. We can therefore find an upper bound on  $j_{2\omega_p}$  by using  $N$  to evaluate the integral during the supersonic regime.  $N$  can be evaluated from the initial Gaussian conditions

$$N = \mathcal{E}_0^2 \pi^{3/2} (\Delta k_n)^{-1} (\Delta k_n)^{-2} \cdot 192 \pi^{5/2} \frac{h \theta}{k_D^3} \frac{k_D}{\Delta k} \frac{W(t=0)}{W_{th}}. \quad (43)$$

Using this as the value for the integral in Eq. (35) and inserting into the emissivity formula (28a) yields an upper bound for the emissivity during the supersonic stage of collapse

$$\left. \frac{dP}{d\Omega} \right|_{2\omega_p}^{\max} = 108 \sqrt{3} \pi \sin^2 \phi_0 \times \left( \frac{k_D}{\Delta k_n} \right)^2 \left( \frac{W}{W_{th}} \right)^2 \left[ \left( \frac{V_e}{c} \right)^5 \frac{h}{k_D^3} \omega_p \theta \right]. \quad (44a)$$

The angular factor is

$$\sin^2 \phi_0 = 1 - [2(\hat{\mathbf{k}}_0 \cdot \hat{\mathbf{K}}_0)^2 - 1]^2. \quad (44b)$$

This factor has its largest value (of unity) when the radiation comes out in a  $45^\circ$  cone about the beam direc-

tion, which is in agreement with the known<sup>14</sup> coupling of radiation at  $2\omega_b$  to two Langmuir waves in parametric instability theory.

We note, in passing, that the maximum total energy radiated, according to Eq. (44), is  $10^{-3}$  times the total energy in the Langmuir packet. Hence, it is indeed valid to ignore the effect of radiation losses on the collapse process (see Fig. 4).

### 3. Core collapse; similarity solutions

A very different picture emerges if we assume that the collapsing packet quickly assumes the form of a similarity solution. In the adiabatic stage, the packet width of a similarity solution,  $L_s$ , can be considerably smaller than that of a Gaussian corona [Eq. (39)]. Budneva *et al.*<sup>11</sup> have studied the adiabatic collapse of a spherically symmetric scalar field obeying a cubic nonlinear Schrödinger equation [the scalar version of our Eq. (16)]. The corona of an initially Gaussian packet substantially above threshold was observed to remain essentially stationary, while a narrowly spiked core collapsed and approached the form of a similarity solution. A repetition of these calculations near threshold also seems to show self-similarity. Under such conditions we might expect much less emission.

The width of an adiabatic similarity solution is obtained, roughly, by setting  $u = 1$  in Eq. (19b). Then, the half-widths,  $L_s^{\text{ss}}$  and  $L_1^{\text{ss}}$ , of the adiabatic similarity solutions are

$$L_s^{\text{ss}} \approx L_1^{\text{ss}} \approx (\Delta k_1)^{-1} (W_{\text{th}}/W)^{1/2} (1 - t/t_a)^{1/2}. \quad (45a)$$

Note, the half-widths are independent of  $\Delta k_1$ , since  $W_{\text{th}} \approx 24(\Delta k_1)^2/k_b^2$ . In effect, the similarity shape is independent of the initial shape, and is narrower, particularly when  $W \gg W_{\text{th}}$ . However, in our case,  $W$  is only slightly greater than  $W_{\text{th}}$ , so that the half-width  $L_s^{\text{ss}}$  appears to be proportional to  $(\Delta k_1)^{-1}$ . This is much smaller than the parallel half-width of the initial Gaussian packet,  $L_0^0 = (\Delta k_0)^{-1}$ . The presumption is that a narrow spike is superposed over the broad Gaussian corona. Pereira and Sudan<sup>15</sup> have shown that initially anisotropic two-dimensional packets tend to become more isotropic as collapse gets underway, so the scaling of  $L_s^{\text{ss}} \approx L_1^{\text{ss}}$  is not surprising. We must note, however, that Eq. (45a) has no validity until collapse is well underway.

The scaling of the energy density of an adiabatic similarity solution with time is given from Eq. (19a)

$$W(t) = \frac{W(0)}{(1 - t/t_a)}. \quad (45b)$$

Comparing (45a) with (45b), we see that, in three dimensions, the half-width volume decreases at a faster rate than the energy density increases, hence,

$$\int_C d^3r A^2 \propto \left(1 - \frac{t}{t_a}\right)^{1/2}, \quad (45c)$$

where  $C$  indicates integration over the core. The contribution of the core to the  $N$  invariant is therefore small. (Phase mixing may still be expected at larger  $r$ , due to  $K_0$  and the self-similar phases.) We now

calculate the (smaller) emission from the similarity core.

From Eqs. (45a) and (38), we find the time  $t_1$  at which the collapsed core can begin to contribute to the current,  $j_{2\omega_b}$ , without substantial phase mixing

$$(1 - t_1^2/t_a^2)^{1/2} \approx \Delta k_1/k_0 \approx 1/4. \quad (45d)$$

According to (45b), the energy will have increased by a factor of 16 at this time, and the collapse will shortly enter the supersonic stage. We shall assume that all the emission occurs in the supersonic stage, since by then a supersonic core of similarity form may have had time to develop.

The half-widths  $L_{s,1}^{\text{ss}}$  of a supersonic similarity solution are obtained from Eqs. (22)–(24) by setting  $u = 1$ :

$$L_{s,1}^{\text{ss}} \approx L_1^{\text{ss}} \approx \left(1 - \frac{t}{t_s}\right)^{2/3} \left[ \frac{2}{3} (12)^{1/3} \left( \frac{m}{M} \right)^{1/2} k_D \right]^{-1}, \quad (46a)$$

where  $t = 0$  is now the onset time for the supersonic stage of collapse, and  $W = 16 m/M$ . (We note that  $\int_C d^3r A^2$  is small but invariant in the supersonic stage.) At  $t = 0$ , the phase-mixing criterion (38) yields  $k_0 L_s^{\text{ss}} = 0.3$ , so that the current  $j_{2\omega_b}$  can be evaluated with the phase factor in the integrand of Eq. (35) ignored. The result for the current may be written as,

$$j_{2\omega_b} = -\frac{9\omega_b^2}{ck_D^4} \left( \frac{3}{4\pi} u \Theta \frac{M}{m} \right)^{1/2} I_2, \quad (46b)$$

where

$$I_2 = \hat{K}_{01} \int d^3u \left( R_1 R_m - \frac{\delta_{1m} R \cdot R}{2} \right), \quad (46c)$$

and  $R$  is the similarity field, defined in Eq. (24). As discussed beneath that equation,  $R$  has a maximum value equal to one. Its half-width is also of order unity, so we expect  $I_2$  to be of order unity as well. The emissivity that follows from this current is found [via Eq. (28a)] to be

$$\frac{dP}{d\Omega} \bigg|_{2\omega_b} \approx \frac{3^5 \sqrt{3}}{64\pi^2} \frac{M}{m} \left[ \left( \frac{V_c}{c} \right)^2 \frac{u}{k_b} \omega_b \Omega \right], \quad (47)$$

where we have approximated  $I_2 \approx 1$ . This estimate gives substantially less emission than that of the coronal collapse model, Eq. (44), because the core is so much smaller than the corona. For the parameters we have been considering,  $|dP/d\Omega|_{2\omega_b}^{\text{max}}$  is about  $10^{-6}$  times smaller than  $|dP/d\Omega|_{2\omega_b}^{\text{max}}$ .

There is a clear need, here, for numerical work to determine the time-dependent shape of a three-dimensional collapsing packet, under type III conditions. Unfortunately, the Zakharov equations should not be solved in fewer than three dimensions, because the  $N$  integral of a truncated similarity solution only goes to zero with time in three dimensions [cf. Eq. (45c)]. One cannot use spherical or even cylindrical symmetry, because such symmetries require zero field at the origin,<sup>11</sup> due to the vector nature of the envelope. A full three-dimensional numerical solution of the vector Zakharov equations is prohibitively expensive at this time. However, some insight has been gained by further studies of model equations for a scalar envelope, such

as that of Budneva *et al.*<sup>11</sup> In particular, we have found narrow cores in packets close to threshold in recent<sup>16</sup> numerical work using Budneva's model, which suggest that the emissivity may lie closer to the lower estimate of Eq. (47).

## B. Emission at the fundamental

The treatment of emission of radiation at frequencies close to the plasma frequency is somewhat more challenging. We must have approximate frequency matching between the Langmuir waves and the radiation:  $\omega_p^2 + c^2 k_0^2 = \omega^2 + 3r_e^2 k_0^2$ . This means that the wavenumber  $k_0$  of the fundamental is much smaller than the wavenumber  $k_0$  of the Langmuir waves.  $|K_0| = \sqrt{3}r_e k_0$ ,  $c \ll k_0$ , as long as  $r_e c \sim 1$  (see the Appendix). In order to conserve momentum, one requires either dynamical ions or strong spatial inhomogeneity. In the present calculation we ignore background plasma inhomogeneity, so we do not allow local or global density gradients to absorb the extra momentum. In the conventional discussions of fundamental emission it is usually assumed that ions or ion-acoustic waves take up the required momentum. The corresponding "weak" turbulence process involves the scattering of a Langmuir wave (plasmon) off ions and its transformation into a photon:  $l \rightarrow i + l$ . This may even occur as a stimulated process (instability).

We shall make the case here that fundamental emission can also occur in "strong" turbulence, i.e., from collapsing Langmuir wave packets. It is clear that emission cannot occur in the subsonic stage of collapse, because the ions are adiabatic, and momentum cannot be conserved. However, fundamental emission can occur in the supersonic stage when the ions are dynamic.

(An argument has been advanced that a collapsing wave packet cannot emit radiation at  $\omega_p$  because the associated density cavity "traps" it. This argument is specious because the wavelength of such radiation is much longer than the characteristic size of the cavity. The emission occurs from this packet as a whole, in a manner analogous to the radiation by an antenna. This is stated mathematically in the Appendix.)

The current which governs the fundamental emission is given by Eq. (29). The Fourier transform of its envelope is

$$J_{\omega_p}(K_0, t) = \frac{i\omega_p}{4\pi} \int d^3r \exp(-iK_0 \cdot r) \frac{\delta n_2(r, t)}{n_0} \mathcal{E}_L(r, t). \quad (48)$$

In the adiabatic stage of collapse,  $\delta n_2$  is proportional to  $-|\mathcal{E}|^2$ . The dominant phase in the integral is then in  $\exp(-iK_0 \cdot r)$  which arises from  $\mathcal{E}_L(r, t)$ . This causes the integral to phase mix to zero [see Eq. (35)], so that there is indeed no emission in the adiabatic stage.

In the supersonic stage, the prediction from the supersonic similarity solutions (21)–(25) is that

$$J_{\omega_p}(K_0, t) = \frac{i\omega_p}{k_D} (12)^{1/6} \frac{3}{\sqrt{2}} \left( \frac{3n_0}{4\pi} \right)^{1/2} \frac{t}{(t - t/t_s)^{1/3}} I_1, \quad (49a)$$

where

$$I_1 \approx \int d^3u \eta(u) R(u), \quad (49b)$$

and the dimensionless density and field supersonic similarity solutions  $\eta$  and  $R$  are defined in Eq. (24). We have omitted the phase factor  $\exp(iK_0 \cdot r)$ , which is always of order unity. In the absence of phase mixing, we expect the magnitude of  $I_1$  to be of order unity. The current is then inserted into the emissivity formula (28). The time-averaging interval  $T$  is chosen to be  $t_s$ , the collapse time. The result may be written as

$$\frac{dP}{d\Omega} \Big|_{\omega_p}^{ss} = \frac{3^4 \sqrt{3} (12)^{1/3}}{64\pi^2} \frac{k_0}{k_D} |I_1|^2 \left[ \left( \frac{r_e}{c} \right)^3 \frac{n\theta\omega_p}{k_D^3} \right]. \quad (50)$$

It is of interest to compare this with the similarity solution prediction of emission at the harmonic [Eq. (47)]:

$$\frac{dP/d\Omega \Big|_{2\omega_p}^{ss}}{dP/d\Omega \Big|_{\omega_p}^{ss}} \approx \frac{k_0}{k_D} \frac{c^2}{r_e^2} \frac{m}{M}. \quad (51a)$$

The large factor  $c^2/r_e^2$  in Eq. (51a) arises because the harmonic emission is quadrupole, whereas the fundamental emission is dipole. The small factors  $k_0/k_D$  and  $m/M$  correspond, respectively, to the smallness of the wavenumber and the higher-order field dependence in the fundamental emission.

The ratio on the right side of Eq. (51a) is about 0.2 for our parameters, indicating almost as much fundamental as harmonic emission from a single collapsing packet in its supersonic phase, provided that the similarity form is justified. It is also of interest to compare this value with the value obtained from weak turbulence theory. The weak turbulence estimate<sup>17</sup> depends upon the assumed distribution of  $\langle E_k^2 \rangle$ . Taking the ratio of the result predicted by (50) to the weak turbulence result gives

$$\frac{dP/d\Omega \Big|_{\omega_p}^{ss}}{dP/d\Omega \Big|_{\omega_p}^{wt}} = \beta N \frac{m}{M} \frac{c}{r_e}, \quad (51b)$$

where  $\beta$  depends upon the assumed form of the distribution of wave energy, and can vary by three orders of magnitude with assumptions that Smith<sup>17</sup> takes to be reasonable. We will take  $\beta = 1$ . Here,  $N$  is the number of particles in a Debye cube;  $N = 10^{10}$  for the plasma we are considering. The numerical value of the ratio in (51b) is therefore approximately 10<sup>9</sup>. The enormous enhancement over the weak turbulence result is readily understandable. The weak turbulence processes require a spontaneous fluctuation in the ion density on a scale of the Debye length. In order that the longitudinal fluctuations can scatter into transverse fluctuations, these have amplitude for occurring that decreases as  $1/N$ . The collapsing wave packet makes its own density fluctuation, and thus this factor is absent. To be more precise, the power radiated depends upon

$$\frac{dP}{d\Omega} \approx \int \left\langle \frac{\delta n(0)}{n_0} \mathbf{E}(0) \cdot \frac{\delta n(r)}{n_0} \mathbf{E}(r) \right\rangle d^3r.$$

The weak turbulence assumption is that the correlation function can be factored. Since  $\langle \mathbf{E}(0) \cdot \mathbf{E}(r) \rangle$  will only be significant over distances the order of  $\lambda_D$ , this is roughly

$$\frac{dP}{d\Omega} \propto W \int_{|r| < \lambda_D} \left\langle \frac{\delta n(0)}{n_0} \frac{\delta n(r)}{n_0} \right\rangle d^3 r.$$

If

$$\delta \tilde{N} = \int_{|r| < \lambda_D} d^3 r \delta n(r),$$

then

$$\frac{dP}{d\Omega} \propto W \lambda_D^3 \left\langle \frac{\delta \tilde{N}}{N} \frac{\delta \tilde{N}}{N} \right\rangle,$$

and by the central limit theorem  $\langle \delta \tilde{N} \delta \tilde{N} \rangle \propto N$ . Consequently,  $dP/d\Omega \propto W \lambda_D^3 N$ . In the strong turbulence case,  $\delta n$  is driven by  $\mathbf{E}$  and is not statistically independent, so there is no factor of  $N$  in the expression for the power radiated, resulting in many orders of magnitude more emission.

In fact, fundamental emission is observed for bursts which are interpreted to originate near the sun, with intensities which are comparable to the harmonic intensities from the same burst.<sup>18</sup> This is essentially inexplicable from the weak turbulence viewpoint, which fails by many orders of magnitude to predict sufficient radiation in the fundamental. The collapse mechanism discussed here needs to be modified to treat the situation near the sun, but the argument given here is quite general and suggests that strong turbulence effects can provide an explanation for the observed radiation.

At  $\frac{1}{2}$  AU there has been no observation of fundamental radiation, which, in view of the relatively large amplitudes predicted by (51b) is apparently inconsistent with the similarity solution predication. This may be due to refraction by random inhomogeneities in the background plasma density which could have the effect that only radiation emitted at the location of maximum density would be able to escape. Inasmuch as the pulse of radiation emitted by the soliton has a frequency spread of only about  $10^{-4} \omega_p$ , inhomogeneities of the order of only  $\delta n/n_0 = 10^{-4}$  would have a profound effect.<sup>19</sup> We note that a uniform gradient on a scale smaller than or comparable to the random inhomogeneities would eliminate the self-trapping.

## V. DENSITY OF COLLAPSING PACKETS AND VOLUME EMISSIVITY

Thus far, we have only found expressions for the emission from a single collapsing wave packet. We must now go farther, and estimate the number density of collapsing packets (in the various stages of collapse), in order to calculate the volume emissivity and make comparisons with measurements.

Our model for steady state was described beneath Eq. (15), and is summarized in Fig. 3. Langmuir wave packets receive energy from the beam, collapse, and finally surrender their energy to particles via wave-particle interactions. The wave packets in real space fill the volume occupied by the beam. Their "discreteness" arises from the interference of beam-amplified random-phase Langmuir noise. We may define a wave packet roughly by finding the spatial mean value  $|\mathcal{E}(\mathbf{r})|^2$  over some large volume, and letting the packets con-

sist of the simply connected volume in which  $|\mathcal{E}(\mathbf{r})|^2 = \langle \mathcal{E}(\mathbf{r}) \rangle^2$ . The packets will be distributed in terms of energy and in terms of spatial widths. At a given instant, some will be growing (due to the beam), some will be in various stages of collapse, and some will be dissipating their energy into electrons. In the ensemble or space average sense a steady state or quasi-steady state is assumed to exist.

The instantaneous rate of work performed by the beam on the waves is

$$P_{in} = \int \frac{d^3 k}{(2\pi)^3} \gamma_e(\mathbf{k}) |\mathcal{E}_k|^2 \approx \gamma_e \int_R \frac{d^3 k}{(2\pi)^3} |\mathcal{E}_k|^2, \quad (52)$$

where  $\gamma_e(\mathbf{k})$  is the growth rate of Langmuir waves in resonance with the beam [Eqs. (6) and (7)],  $\gamma_e$  is the peak growth rate, and  $R$  indicates integration over resonant modes only. The modes in resonance with the beam are those lying in the phase space volume centered about  $\mathbf{k}_0$ , within the bounds of the beam-determined widths,  $\Delta k_\parallel$  and  $\Delta k_\perp$ , as in Fig. 2 [see, also, Eqs. (9)]. In real space, those wave packets which are well into collapse will not have appreciable Fourier components in the resonance region. In order to estimate  $P_{in}$  we next need to consider how the packet and energy densities are related.

The packet densities are related to the total Fourier energy spectrum by

$$\int \frac{d^3 k}{(2\pi)^3} |\mathcal{E}_k|^2 = \int d^3 r |\mathcal{E}(\mathbf{r})|^2 \approx V \sum_i n_i U_i, \quad (53)$$

where

$$U_i = \int_{\mathbf{r}_i} |\mathcal{E}(\mathbf{r})|^2 d^3 r \quad (54)$$

is the energy in one packet (denoted by the subscript  $i$ ) and  $n_i$  is the density of packets with given energy  $U_i$ . We expect most of the total energy to reside in packets which satisfy or almost satisfy the condition for collapse. These packets will all be clustered about a critical value,  $U_0$ , with a density  $n_0$ . We then have approximately,

$$\int \frac{d^3 k}{(2\pi)^3} |\mathcal{E}_k|^2 \approx V n_0 U_0. \quad (55)$$

The mean spacing of these packets is assumed to be on the order of their volume, which is determined by the beam. This "close-packing" assumption tells us that  $n_0$  is on the order of the inverse volume of a packet, or

$$n_0 \approx \frac{1}{V} [(\Delta k_\parallel)(\Delta k_\perp)^2], \quad (56)$$

where  $\Delta k_\parallel$  and  $\Delta k_\perp$  are the half-widths given by Eqs. (9).

The average resonant mode energy depends on which of two distinct packet-evolution scenarios occurs:

In the first case, the number of packets which remain slightly below the collapse threshold during one collapse time is much greater than the number collapsing. This might be expected on the grounds that the collapse time is much less than  $\gamma_e^{-1}$ , so, at any given time, there are still a large number of wave packets below the critical  $W$  contributing to the beam power input in Eq. (52).

A second possibility is that there is a quasi-periodic behavior in time with period on the order of  $\gamma_e^{-1}$ , in which there is cyclical resonant mode depletion. Resonant mode energy builds up during the growth phase, creating a majority of energy-contributing packets on the verge of collapse. They all collapse together quickly, causing a severe depletion of resonant mode energy for a time on the order of  $\gamma_e^{-1}$ . During this time, amplification of noise (and perhaps residual fragments of packets) occurs, and the process repeats. A long-term time average gives a resonant mode energy equal to some small fraction  $F$  of the total mode energy given in (55).

In either case, the average input power is [from Eq. (52) and (55)],

$$P_{in} \approx \gamma_e F n_0 V U_0, \quad (57)$$

where  $F \approx 1$  according to the first scenario, and  $F \ll 1$  in the second. It is not easy to decide between these scenarios on the basis of existing theory or numerical simulation,<sup>9</sup> so we shall leave  $F$  undetermined, for the moment. (The problem with numerical simulation is that the "box" size would have to be chosen large enough to contain a statistically significant distribution of wave packets. This seems to be prohibitively costly at present.)

The spatial density  $n_c$  of collapsing packets can be estimated by equating  $P_{in}$  to the rate of energy flow  $P_c$  where,

$$P_c \approx (1/\tau_c) n_c V U_0. \quad (58)$$

Here  $\tau_c$  is the appropriate collapse time. Equating (57) and (58),

$$n_c \approx \gamma_e \tau_c (F n_0). \quad (59)$$

The density of adiabatic collapsing packets is then obtained by letting  $\tau_c$  equal the adiabatic collapse time  $\tau_a$  given in Eq. (20a)

$$n_{ad} = (\gamma_e / \omega_p) (8/W) (F n_0); \quad (60)$$

and the density of supersonic collapsing packets is obtained by letting  $\tau_c$  equal the supersonic collapse time  $\tau_s$  given in Eq. (25b)

$$n_{ss} = \frac{\gamma_e}{\omega_p} \frac{\sqrt{3}}{4} \frac{M}{m} (F n_0). \quad (61)$$

We can use Eq. (61) to calculate the volume emissivity:

If we combine Eqs. (44), (61), and (56), we obtain an upper bound on the volume emissivity for emission at  $2\omega_p$ :

$$\begin{aligned} J_{2\omega_p} &= n_{ss} \left. \frac{dP}{d\Omega} \right|_{2\omega_p}^{\max} \\ &= \frac{3\pi}{8} F \frac{\gamma_e}{\omega_p} \frac{M}{m} \left( \frac{\Delta k_s}{k_D} \right)^2 \left( \frac{k_D}{\Delta k_n} \right) \left( \frac{W}{W_{th}} \right)^2 \left( \frac{r_e}{c} \right)^5 n \omega_p \theta. \end{aligned} \quad (62)$$

We evaluate this for the following parameters:

$$\begin{aligned} n_e &= 40 \text{ cm}^{-3}, \quad \theta_e = 10 \text{ eV}, \\ n_p/n_e &= 10^{-6}, \quad \Delta n_b/n_b = 1/3, \quad W = 2W_{th}, \end{aligned}$$

and  $\Delta k_s$  and  $\Delta k_n$  as given by Eqs. (12). The maximum growth rate is taken [from Eq. (6)] to be

$$\frac{\gamma_e^{\max}}{\omega_p} = \left( \frac{\pi}{8c} \right)^{1/2} \frac{n_b}{n_0} \left( \frac{r_b}{\Delta r_b} \right)^2.$$

The resulting evaluation gives

$$J_{2\omega_p} = 2 \times 10^{-17} F \text{ ergs cm}^{-3} \text{ sec}^{-1} \text{ sr}^{-1}. \quad (63)$$

This is to be compared with the measured value in Eq. (1), which gives  $2 \times 10^{-24}$ . The upper bound provided by the theory when  $F$  is larger than  $10^{-6}$  is adequate to make collapsing-packet emission an attractive candidate to account for observed radiation at twice the plasma frequency.

Even if the collapse quickly approached similarity form, so that the core emissivity, Eq. (47), were more appropriate than the coronal emissivity, Eq. (44), the volume emissivity with  $F$  of order unity would still be consistent with the observed emission. However, as we discussed below Eq. (47), no one has demonstrated that three-dimensional Langmuir packets just above threshold will quickly converge to the form of similarity solutions. We note further that only the most pessimistic assumption of core emissivity and cyclical resonant mode depletion ( $F \ll 1$ ) leads to a theoretical volume emissivity below the observed levels.

As an important side issue, it is worth pointing out once more that either of our statistical models ( $F=1$ , or  $F \ll 1$ ) is consistent with the absence of quasi-linear beam plateau formation. This is because the wave energy density of beam-resonant modes can never greatly exceed the collapse threshold, which is well below the beam energy density [see Eqs. (13) and (14), and the discussion which follows].

## VI. CONTRAST WITH PREVIOUS THEORETICAL WORK

We wish to point out the main differences between the theory proposed here and an earlier attempt at treating emission from stable solitons, due to Papadopoulos and Freund.<sup>4</sup>

A central difference hinges on the role that the magnetic field plays in the evolution of the solitons. Papadopoulos and Freund assert that the effect of the magnetic field is to produce stable, that is, not collapsing, essentially one-dimensional solitons. This argument relies, in part, on their claim that the magnetic field plays an important role in the linear stage of beam-mode growth and distorts the real-space wave packets into one-dimensional "pancakes." We assert that the magnetic field is irrelevant in shaping the beam-mode packets for the ratio of  $\omega_c/\omega_p \approx 10^{-2}$  at 0.45 AU.

The argument that Papadopoulos and Freund rely on is stated more explicitly in Smith *et al.*,<sup>20</sup> where they claim that the angular spread in wave vector space of the growing modes excited by the two-stream instability is less than  $1^\circ$  for  $\omega_c/\omega_p \approx 10^{-2}$ . This conclusion is erroneous, and based on an incorrect application of a standard formula for the growth rate of the unstable modes in the presence of a magnetic field.<sup>21</sup>

$$\gamma \propto [K_0^2 + K_1^2] g(K_1^2 R_B^2),$$

where  $R_B = \Delta V_B / \omega_c$  and

$$g(a) = e^{1/2} \sum_{l=0}^{\infty} e^{-a} I_l(a) \exp\left[-\frac{1}{2}\left(1 + \frac{l}{K_0 R_B}\right)^2\right],$$

where  $I_l(a)$  is the Bessel function. Papadopoulos and Freund claim that the growth rate is only significant when  $K_0 R_B \sim 1$ , basing their claim on the approximation of  $g(a)$  by the term with  $l=0$ . This approximation is totally unjustified for larger  $a$ , however, since  $K_0 R_B = (V/V_B) (\omega_c / \omega_p) \approx 10$ , and approximately 20 terms need to be kept in the series. If one does this, one finds that  $g(0) = 1$ ,  $g(a) = 0.9989$ , i.e., the dispersion relation is extremely insensitive to  $K_0 R_B$  for these values of  $K_0 R_B$ . Furthermore, it should be noted that in the limit of vanishing field,  $K_0 R_B \rightarrow \infty$ , all terms in the series must be summed. Papadopoulos and Freund's result is obtained by taking the strong field limit of the dispersion relation, and then applying it for weak fields.

Their argument that the solitons are stable is based on the assertion that they are essentially one dimensional. Since the assertion is false, there is no evidence which suggests that they are indeed stable. We note that Petviashvili<sup>22</sup> has argued that there are indeed static localized solutions of the equations one obtains by including the magnetic field in the linear part of the equation of motion (A2). It is not clear whether such solutions really exist (since he relied on a numerical solution of the equation to prove existence), or if they are stable. In any case, the linear and transverse dimensions of these entities will bear no relation to the dimensions of the packets formed by the modes that grow in the presence of the beam, and we think that they will play no role in the problem.

A second major difference lies in the relationship between the linear growth rate of the unstable beam modes and the average level of energy in the plasma oscillations  $W$ . The picture of Papadopoulos and Freund<sup>4</sup> is that the energy is transferred out of the beam modes by the modulational instability, acting uniformly throughout the plasma. By an argument that they think reasonable, they then conclude that  $\gamma_B \propto \gamma_{nl}$  is the condition for a steady state.  $\gamma_{nl}$  has the same dependence on the parameters of the problem as  $1/\tau_c$ , where  $\tau_c$  is the collapse time of the solitons, and in this way they obtain  $\gamma_B \propto W$ ,  $W \propto m/M$ , or  $\gamma_B \propto (m/M)^{1/2} W^{1/2}$ ,  $W > m/M$ .

Our picture is that the transfer of energy is due to the direct collapse of wave packets, which occurs when the energy in the unstable modes has grown so that  $W \gtrsim (\Delta K)^2$ ;  $W$  is fixed by the velocity spread, not the intensity of the beam. The collapse does not occur throughout all space, and, in fact, the density of collapsing packets,  $n_c$ , can be computed from an energy balance equation

$$\gamma_B W = (1/\tau_c) (W L_c^3) n_c,$$

as long as  $\gamma_B \ll 1/\tau_c$ ,  $n_c \ll 1/L_c^3$ . When  $\gamma_B \gg 1/\tau_c$ , the collapsing solitons are closely packed, and the physical situation is similar to the picture that Papadopoulos and Freund propose in that  $n_c$  would remain at  $1/L_c^3$ .

as  $\gamma_B$  increased, and  $\gamma_B \gg 1/\tau_c$ . However, this regime is inappropriate for the type III parameters, in which the ratio of beam to background density  $n_b / n_c$  is never expected to exceed  $10^{-6}$ , so that  $\gamma_B \ll (1/10)(1/\tau_c)$ . As shown by Goldman and Nicholson<sup>2</sup> direct collapse is the dominant energy transfer mechanism in this regime, not the modulational instability.

## VII. CONCLUSIONS

In conclusion, we believe the models we have developed in this paper for electromagnetic wave emission from collapsing Langmuir wave packets, give the best possible state-of-the-art estimates for such emission. Reasonable models give predictions which are well above the volume emissivity observed during type III bursts, Eq. (1). Further numerical work on the dynamical and statistical details of collapse would be highly desirable, but the need for working in three dimensions may make the cost prohibitive [see discussion below Eq. (47)]. Further theoretical work is also necessary, particularly in the refinement of our statistical assumptions.

## ACKNOWLEDGMENTS

One of us (M.V.G.) would like to thank the Guggenheim Foundation for a Fellowship held during part of this research, and also to acknowledge helpful conversations with R. Hellwarth, V. Zakharov, F. Tappert, C. Kennel, D. Smith, and D. F. DuBois. This work was also supported by the National Science Foundation, Atmospheric Research Section under ATM 76-14275, and by the Air Force Office of Scientific Research (M.V.G. and G.F.R.) under Contract F49620-76-C-0005. The work of one of us (D.N.) was also supported by the Solar Terrestrial Research Program, Division of Atmospheric Sciences, National Science Foundation, ATM78-22487 and by U. S. Department of Energy Grant No. EY-76-5-02-2059. We thank the National Center for Atmospheric Research, supported by the National Science Foundation, for computer time used in this study.

## APPENDIX: DERIVATION OF EQUATIONS FOR TRANSVERSE AND LONGITUDINAL FIELDS

We want to show that if  $c' \ll c \ll \tau_c^{-1}$ , then a consistent solution of the equations of motion for a plasma can be obtained in the form

$$\delta = \delta_0 + \delta_1 / (c')^2,$$

where  $\delta_0 = -\nabla \phi$  and  $|\delta_0| \sim |\delta_1|$ . The field  $\delta$  is always predominantly longitudinal. The longitudinal part  $\delta_0$  satisfies a modified form of the Zakharov equations, and  $\delta_1$  is the radiation field. We begin with Eqs. (21), with all tildas omitted from dimensionless quantities

$$i \frac{\partial \delta}{\partial t} - c'^2 \nabla \times \nabla \times \delta + \nabla (\nabla \cdot \delta) = \frac{\eta}{2} \delta, \quad (A1)$$

$$(\delta_t^2 - \beta^2 \nabla^2) \eta = \nabla^2 |\delta|^2, \quad (A2)$$

where  $c' = c / \sqrt{3} \tau_c$ , and will be assumed  $\ll 1$ . If we make the ansatz  $\delta = \delta_0 + \delta_1 / c'^2$ ,  $\delta_0 = -\nabla \phi$ , we find, to lowest order in  $1/c'^2$ :

$$i \frac{\partial \mathcal{E}_0}{\partial t} - \nabla \times \nabla \times \mathcal{E}_1 + \nabla (\nabla \cdot \mathcal{E}_0) = \frac{\eta}{2} \mathcal{E}_0, \quad (A3)$$

$$i \frac{\partial (\nabla \times \mathcal{E}_1)}{\partial t} - c'^2 \nabla^2 (\nabla \times \mathcal{E}_1) = c'^2 \nabla \times \left( \frac{\eta}{2} \mathcal{E}_0 \right), \quad (A4)$$

$$\frac{\partial^2 \eta}{\partial t^2} - \beta \nabla^2 \eta = \nabla^2 |\mathcal{E}_0|^2. \quad (A5)$$

We Fourier transform (A4) for the transverse field  $\mathcal{E}_1$  in time and invert the resulting Helmholtz equation:

$$\nabla \times \mathcal{E}_{1,\omega} = \frac{1}{4\pi} \int \frac{\exp(iK|r-r'|)}{|r-r'|} \nabla \times \left( \frac{\eta}{2} \mathcal{E}_0 \right)_\omega d^3 r', \quad (A6)$$

$$K \equiv \omega/(c'^2).$$

Integrating (A6) by parts and substituting in (A3), we have

$$K^2 \mathcal{E}_{0,\omega} + \frac{1}{4\pi} \nabla \times \nabla \times \int \frac{\exp(iK|r-r'|)}{|r-r'|} \times \left[ \frac{\eta}{2} \mathcal{E}_0(r') \right]_\omega d^3 r' + \nabla (\nabla \cdot \mathcal{E}_{0,\omega}) = \left( \frac{\eta}{2} \mathcal{E}_0 \right)_\omega. \quad (A7)$$

Consider fundamental emission (near the plasma frequency  $\omega_p$ ). If we set  $K=0$  in the integral on the left side of (A7) it is just the transverse part of the current ( $\eta \mathcal{E}_0/2$ ). Since for any vector field,  $\mathbf{A}(r,t) = \mathbf{A}_l(r,t) + \mathbf{A}_t(r,t)$ , where  $l$  and  $t$  designate the longitudinal and transverse parts of the vector, we find that  $\mathcal{E}_0$  satisfies the equation

$$i \frac{\partial \mathcal{E}_0}{\partial t} + \nabla (\nabla \cdot \mathcal{E}_0) = \left( \frac{\eta}{2} \mathcal{E}_0 \right)_l, \quad (A8)$$

the corrections due to finite values of  $K$  being of order  $1/c'$ . Equations (A8) and the divergence of (A1) imply that

$$i \frac{\partial}{\partial t} \nabla \cdot \mathcal{E}_1 + \nabla^2 (\nabla \cdot \mathcal{E}_1) = 0, \quad (A9)$$

and hence if  $\nabla \cdot \mathcal{E}_1 = 0$ , initially [or at least  $\mathcal{O}(1/c')$ ] it will be zero for all time, and the solution of (A6) can be taken to be

$$\mathcal{E}_{1,\omega} = -\frac{1}{4\pi} \int \frac{\exp(iK|r-r'|)}{|r-r'|} \left( \frac{\eta}{2} \mathcal{E}_0(r') \right)_{T,\omega} d^3 r'. \quad (A10)$$

The problem therefore breaks up into two parts: the solution of the equations of motion for the longitudinal field (A8) determined entirely by the longitudinal part of the current ( $\delta n/n_0$ )  $\mathcal{E}_0$ , and the radiation produced by that field, determined by the transverse part of the current (A10). The emissivity formula (28a) which we have used can be derived from (A10).

The supersonic similarity solutions and plasmon number invariant arguments we have employed for the field  $\mathcal{E}$  are based on the field equation (A1). Since we have just demonstrated that the transverse part of  $\mathcal{E}$  is of order  $(c')^2$  times smaller than the longitudinal part, our solutions can also be regarded as satisfying (A8).

We note that if second harmonic terms are included in the current, these will have a negligible effect on the motion of  $\mathcal{E}_0$ . The radiation due to these terms is calculated from (A10) with the appropriate current, and  $K = (3/2)^{1/2}(1/c)$ .

- <sup>1</sup>V. E. Zakharov, *Zh. Eksp. Teor. Fiz.* **62**, 1745 (1972) [Sov. Phys.-JETP **35**, 908 (1972)].
- <sup>2</sup>M. V. Goldman and D. R. Nicholson, *Phys. Rev. Lett.* **41**, 406 (1978).
- <sup>3</sup>D. A. Gurnett and R. R. Anderson, *Science* **194**, 1159 (1976); *J. Geophys. Res.* **82**, 632 (1977).
- <sup>4</sup>K. Papadopoulos and H. P. Freund, *Geophys. Res. Lett.* **5**, 881 (1978).
- <sup>5</sup>D. A. Gurnett and L. A. Frank, *Solar Phys.* **45**, 477 (1975).
- <sup>6</sup>R. J. Fitzpatrick, L. D. Evans, and R. P. Lin, *Solar Phys.* **46**, 437 (1976).
- <sup>7</sup>D. F. Smith and D. R. Nicholson, in *Wave Instabilities in Space Plasmas*, edited by P. J. Palmadesso and K. Papadopoulos (Reidel, Dordrecht, 1980).
- <sup>8</sup>G. R. Magelssen and D. F. Smith, *Solar Phys.* **55**, 211 (1977).
- <sup>9</sup>D. R. Nicholson, M. V. Goldman, P. Hoyng, and J. C. Weatherall, *Astrophys. J.* **223**, 605 (1978).
- <sup>10</sup>V. E. Zakharov, A. F. Mastryukov, and V. S. Synakh, *Fiz. Plazmy* **1**, 614 (1975) [Sov. J. Plasma Phys. **1**, 339 (1975)].
- <sup>11</sup>O. B. Budneva, V. E. Zakharov, and V. S. Synakh, *Fiz. Plazmy* **1**, 606 (1975) [Sov. J. Plasma Phys. **1**, 335 (1975)].
- <sup>12</sup>A. A. Galeev, R. Z. Sagdeev, Y. S. Sigov, V. P. Shapiro, and V. I. Shevchenko, *Fiz. Plazmy* **1**, 10 (1975) [Sov. J. Plasma Phys. **1**, 5 (1975)].
- <sup>13</sup>T. Tajima, J. LeBoeuf, J. M. Dawson, and M. V. Goldman (to be published).
- <sup>14</sup>M. V. Goldman, *Ann. Phys. (N. Y.)* **38**, 117 (1966); see p. 154.
- <sup>15</sup>M. V. Goldman, K. Rypdal, and B. Hafizi (to be published).
- <sup>16</sup>N. Pereira, R. Sudan, and J. Denavit, *Phys. Fluids* **20**, 936 (1977).
- <sup>17</sup>D. F. Smith, *Adv. Astron. Astrophys.* **7**, 147 (1970).
- <sup>18</sup>D. F. Smith, *Space Sci. Rev.* **16**, 91 (1974).
- <sup>19</sup>D. F. Smith and D. Sime (to be published).
- <sup>20</sup>R. A. Smith, M. L. Goldstein, and K. Papadopoulos, *Astrophys. J.* (to be published).
- <sup>21</sup>A. I. Akhiezer, I. A. Akhiezer, R. V. Polovin, A. G. Sitenko, and K. N. Stepanov, *Plasma Electrodynamics* (Pergamon, New York, 1975).
- <sup>22</sup>V. I. Petviashvili, *Fiz. Plazmy* **1**, 15 (1975) [Sov. J. Plasma Phys. **1**, 28 (1975)].

## APPENDIX B

B. "Dimensionality and Dissipation in Langmuir Collapse"  
M. V. Goldman, K. Rypdal, and B. Hafizi  
Physics of Fluids, 23, 945-954 (1980)

# Dimensionality and dissipation in Langmuir collapse

Martin V. Goldman, K. Rypdal,<sup>a)</sup> and B. Hafizi

Department of Astro-Geophysics, University of Colorado, Boulder, Colorado 80309  
(Received 7 September 1979; accepted 15 February 1980)

The nonlinear Schrödinger equation provides a model for Langmuir evolution at low energy density and wavenumber. This equation is studied using virial theorem techniques. Stationary solitons and pulsating solitons (related to "breathers") are found in one dimension, as well as collapsing packets in two or more dimensions. Initial wave-packet collapse thresholds and times are found, with and without constant collisional damping. In three dimensions, a narrow collapsing core is observed to break away from an initial Gaussian packet and become asymptotically self-similar with time.

## I. INTRODUCTION

It was Zakharov<sup>1</sup> who first pointed out the relevance of optical self-focusing phenomena to the nonlinear behavior of large amplitude Langmuir waves. Whether the waves are electromagnetic or electrostatic is of little consequence. The associated ponderomotive force pushes electrons out of a spatial region, and they drag the ions along. The lowered density creates a higher index of refraction in which rays undergo total internal refraction and can be trapped if the nonlinearity is strong enough. In one dimension, this nonlinearity can exactly balance the linear dispersion (diffraction) of a wave packet, leading to the formation of an envelope soliton. In two or more dimensions, nonlinear refraction can permanently exceed dispersion. When this occurs, a stationary balance is impossible and the packet collapses spatially. The collapse threshold can occur at initial Langmuir energy densities which are still many orders of magnitude smaller than the background electron energy density; so, simple nonlinear models are expected to provide a good description of the early stages of collapse.

In the so-called Zakharov equations,<sup>1,2</sup> the (slow time) electron density in the Langmuir wave equation is allowed to be nonlinear. Quasi-neutrality is assumed, and the (ion or electron) density obeys a second, ion-acoustic wave equation with a source term proportional to the ponderomotive force of the Langmuir waves.<sup>3</sup> These coupled equations have been used extensively<sup>2-5</sup> to describe Langmuir collapse. They provide the dynamical basis for what is often called "strong" Langmuir turbulence.

In the early stages of collapse, at low wave energy densities, the time-dependent (inertial) term in the ion density equations is negligible. The ions are then adiabatic, and the density is proportional to the negative of the ponderomotive force. Under these conditions, the envelope approximation to the Langmuir wave equation leads to a Schrödinger equation with cubic nonlinearity.

This paper is concerned with the effects of spatial dimensionality and collisional damping on solutions to the nonlinear Schrödinger equation for a vector field

envelope  $\delta$ . Goldman and Nicholson have recently shown<sup>6</sup> that the nonlinear Schrödinger equation provides a good model for the early nonlinear evolution of certain beam-excited Langmuir wave instabilities. When the beam growth rate is slow compared with the nonlinear (collapse) time scale, the role of the beam is essentially only to determine the shape of a "linear" Langmuir wave packet, which is then used as an initial value for the undriven nonlinear Schrödinger equation. Under these conditions, virial theorem techniques<sup>1</sup> have been used to find the threshold and collapse time of two-dimensional<sup>6</sup> Langmuir packets. Two-dimensional theory and numerical analyses<sup>4,6</sup> show that such direct adiabatic collapse is very likely to play an important role in the saturation of beam instabilities at very low beam densities. An important example is furnished by the solar-generated electron beams responsible for type III radio bursts.<sup>4</sup>

One of the purposes of the present paper is to show how the assumption of near-Gaussian spatial behavior of the Langmuir field leads to a closure approximation in the virial theory. With this approximation, we are able to estimate the threshold and find an upper bound for the collapse time of three-dimensional Langmuir packets. Additional numerical work, based not on the virial theorem but on the Schrödinger equation for a spherically symmetric scalar field, shows a self-similar collapsing core developing out of an initial three-dimensional wave packet close to threshold.

In one dimension, the virial theorem with closure approximation leads to very simple predictions of pulsating solitons which are consistent with the results of detailed numerical solutions<sup>7</sup> based on inverse scattering theory. The pulsating solitons have amplitudes slightly higher than for the corresponding stationary ( $\text{sech } x$ ) solitons. They are closely related to "breathers," which are strictly periodic bound states of two solitons. The one-dimensional nonlinear Schrödinger equation has been used extensively<sup>8,9</sup> as a model for nonlinear behavior of deep water waves. The recurrence observed by Yuen and Ferguson<sup>8</sup> in this connection may be closely related to pulsating solitons and breathers.

Other observations in the present paper have to do with the competition between modulational instabilities and collapse, and with comparisons between the virial theorem and similarity solutions. A number of these observations are based on similar phenomena in nonlinear optics,<sup>10</sup> in which a laser beam undergoes total

<sup>a)</sup> Present address: Institute of Mathematical and Physical Sciences, University of Tromsø, Norway.

self-focusing at moderate intensities, and at higher intensities break-up into filaments.

We have derived a virial theorem for the nonlinear Schrödinger equation with constant damping included. In two dimensions, this results in a dissipative threshold for direct collapse, enabling us to predict the role of collisional damping in Langmuir collapse.

The plan of this paper is as follows: In Sec. II we treat the nonlinear Schrödinger equation using general virial theorem arguments. In Sec. III we explore the evolution of initial Gaussian wave packets in one, two, and three dimensions. Section IV is devoted to the effects of damping on collapse. Section V deals with self-similar behavior, both in general, and for the special case of three-dimensional spherically symmetric collapse of a scalar field. In the Appendix we study the conditions of validity for the nonlinear Schrödinger equation model of Langmuir collapse (i.e., the adiabatic ion and electrostatic field approximations).

## II. CONSERVATION LAWS AND VIRIAL THEOREMS

The most general way to derive conservation laws for field equations is to exploit the invariance properties of the corresponding Lagrangian. The Lagrangian density for Zakharov's equations (see the Appendix) is given by Gibbons *et al.*<sup>11</sup> In the limit of electrostatic waves and adiabatic ions, their expression reduces to

$$\mathcal{L} = \frac{1}{2}i(\mathcal{E}_m^* \dot{\mathcal{E}}_m - \mathcal{E}_m \dot{\mathcal{E}}_m^*) - \frac{1}{2}(\nabla_m \mathcal{E}_m)(\nabla_i \mathcal{E}_i^*) + \frac{1}{2}(\mathcal{E}_m \mathcal{E}_m^*)^2. \quad (1)$$

(We employ the usual summation convention over repeated indices.) From the Euler-Lagrange equations

$$\frac{\partial}{\partial t} \frac{\delta \mathcal{L}}{\delta \mathcal{E}_m^*} = \frac{\delta \mathcal{L}}{\delta \mathcal{E}_m^*}, \quad (2)$$

the nonlinear Schrödinger equation follows

$$i\dot{\mathcal{E}} + \frac{1}{2}\nabla^2 \mathcal{E} + |\mathcal{E}|^2 \mathcal{E} = 0. \quad (3)$$

Here, we have used the variational derivative of the Lagrangian  $\mathcal{L} \equiv \int \mathcal{L} d^D r$ ,

$$\frac{\delta \mathcal{L}}{\delta \mathcal{E}_m^*} = \frac{\partial \mathcal{L}}{\partial \mathcal{E}_m^*} - \nabla_i \frac{\partial \mathcal{L}}{\partial (\nabla_i \mathcal{E}_m^*)}. \quad (4)$$

Note that we have treated  $\mathcal{E}_m$  and  $\mathcal{E}_m^*$  as independent generalized coordinates. Variation with respect to  $\mathcal{E}_m$  gives the complex conjugate nonlinear Schrödinger equation. The relation between the dimensionless units employed here and the physical units is given by  $t = \omega_p t$ ,  $\mathbf{r} = k_D \mathbf{r} / \sqrt{3}$ , and  $|\mathcal{E}|^2 = |\mathcal{E}|^2 / [32\pi n_0(\theta_e + \theta_i)]$ . The electron plasma frequency is  $\omega_p$ , the Debye wavenumber is  $k_D$ , the background plasma density is  $n_0$ , and the electron and ion temperatures in energy units are  $\theta_e$  and  $\theta_i$ .  $\mathcal{E}$  is the envelope of the electric field,  $\mathcal{E}(\mathbf{r}, t) = \text{Re}[\mathcal{E} \exp(-i\omega_p t)]$ .

The conservation laws for plasmon number, energy, and momentum follow generally from Noether's theorem<sup>12</sup> and the invariance of the Lagrangian under a gauge transformation  $\mathcal{E} \rightarrow \mathcal{E} \exp(i\phi)$ , under translation in time, and under translation in space, respectively. Alternatively, they can be obtained directly. Continuity of plasmon number density,  $|\mathcal{E}(\mathbf{r})|^2$ , follows directly by multiplying the nonlinear Schrödinger equation with  $\mathcal{E}^*$

and subtracting the complex conjugate, giving the continuity equation

$$\frac{\partial |\mathcal{E}|^2}{\partial t} + \nabla \cdot \mathbf{g} = 0, \quad (5)$$

where  $\mathbf{g}$  is the plasmon current density

$$\mathbf{g}_i = (1/2i)(\mathcal{E}_m^* \nabla_i \mathcal{E}_m - \mathcal{E}_m \nabla_i \mathcal{E}_m^*). \quad (6)$$

Energy and momentum conservation can be derived from the following  $(D+1)$ -dimensional energy-momentum tensor

$$T_{\mu\nu} = \frac{-\partial \mathcal{L}}{\partial(\partial \mathcal{E}_i / \partial x_\mu)} \frac{\partial \mathcal{E}_i}{\partial x_\nu} - \frac{\partial \mathcal{L}}{\partial(\partial \mathcal{E}_i^* / \partial x_\mu)} \frac{\partial \mathcal{E}_i^*}{\partial x_\nu} + \mathcal{L} \delta_{\mu\nu}, \quad (7)$$

where the indices  $\mu$  and  $\nu$  can assume values  $0, 1, \dots, D$ , and  $x_0 \equiv t$ ,  $(x_1, \dots, x_D) \equiv \mathbf{r}$ .

From the Euler-Lagrange equations (2), and the fact that  $\mathcal{L}$  does not depend explicitly on time and space (translational invariance), we easily verify that

$$\nabla_\mu T_{\mu\nu} = 0, \quad \mu, \nu = 0, 1, \dots, D. \quad (8)$$

This is a set of  $(D+1)$  continuity equations, one for energy

$$\frac{\partial \mathcal{K}}{\partial t} + \nabla \cdot \mathbf{Q} = 0, \quad (9)$$

where the energy (Hamiltonian) density  $\mathcal{K}$  and the energy flux vector  $\mathbf{Q}$  are defined as

$$\mathcal{K} \equiv -T_{00} = \frac{1}{2}[\nabla_m \mathcal{E}_m)(\nabla_i \mathcal{E}_i^*) - (\mathcal{E}_m \mathcal{E}_m^*)^2], \quad (10)$$

$$Q_\mu = -T_{\mu 0} = -\text{Re}(\nabla_m \mathcal{E}_m^* \mathcal{E}_\mu), \quad \mu = 1, \dots, D, \quad (11)$$

and one equation for each momentum component

$$\frac{\partial \mathcal{P}_\nu}{\partial t} + \nabla_\mu T_{\mu\nu} = 0, \quad \mu, \nu = 1, \dots, D, \quad (12)$$

where the momentum density  $\mathcal{P}_\nu$  and the stress tensor  $T_{\mu\nu}$  are defined as

$$\mathcal{P}_\nu = T_{0\nu} = (1/2i)(\mathcal{E}_i^* \nabla_\nu \mathcal{E}_i - \mathcal{E}_i \nabla_\nu \mathcal{E}_i^*), \quad \nu = 1, \dots, D \quad (13)$$

$$T_{\mu\nu} = \text{Re}(\nabla_\mu \mathcal{E}_i^* \nabla_\nu \mathcal{E}_i) + \mathcal{L} \delta_{\mu\nu}, \quad \mu, \nu = 1, \dots, D. \quad (14a)$$

Note that the momentum density  $\mathcal{P}_\nu$  is here identical to the current density  $\mathbf{g}_\nu$  in Eq. (6). The time derivatives in  $\mathcal{L}$  can be eliminated by means of the nonlinear Schrödinger equation (3); and by applying the relation  $\nabla \nabla \cdot \mathbf{g} \approx \nabla^2 \mathcal{E}$  (valid for electrostatic fields; see the Appendix), we find

$$\mathcal{L} \approx -\frac{1}{2} [|\mathcal{E}|^4 + \nabla \cdot \text{Re}(\mathcal{E}^* \nabla \cdot \mathcal{E})], \quad (15)$$

which inserted in Eq. (14) gives  $T_{\mu\nu}$  in the simple form of Goldman and Nicholson<sup>6</sup>:

$$T_{ij} = \text{Re}[(\nabla \cdot \mathcal{E}) \nabla_i \mathcal{E}_j^*] - \frac{1}{2} \delta_{ij} [|\mathcal{E}|^4 + \nabla \cdot (\text{Re} \mathcal{E}^* \nabla \cdot \mathcal{E})]. \quad (14b)$$

The three continuity equations can be integrated to yield the following conserved quantities, assuming localized fields:  $N = \int |\mathcal{E}|^2 d^D r$ ,  $H = \int \mathcal{K} d^D r$ , and  $P = \int \mathcal{P} d^D r$ . They can also be used to explore the particle-like behavior of a wave packet by defining the average of any quantity using the normalized plasmon number density  $|\mathcal{E}|^2/N$  as a weighting function

$$\langle f(\mathbf{r}) \rangle = \int \left( \frac{|\mathcal{E}|^2}{N} \right) f(\mathbf{r}) d^D r.$$

If we multiply Eq. (5) by  $\mathbf{r}$  and integrate by parts, we find the Ehrenfest theorem for the velocity of the centroid coordinate of the wave packet

$$\partial_t \langle \mathbf{r} \rangle = \mathbf{S}/N = \mathbf{P}/N = \text{const.} \quad (16)$$

Similarly, by Eqs. (5) and (12), and again using  $\mathbf{S} = \mathbf{P}$ , we can prove the following virial theorem for the time evolution of the mean-square spatial deviation  $\langle \delta r^2 \rangle$

$$\equiv \int (|\mathcal{E}|^2/N) |\mathbf{r} - \langle \mathbf{r} \rangle|^2 d^D r:$$

$$\partial_t^2 \langle \delta r^2 \rangle = 2 \left[ \frac{1}{N} \int T_{11} d^D r - \left( \frac{\mathbf{S}}{N} \right)^2 \right]. \quad (17)$$

From Eq. (14) we find  $T_{11} = 2K + \frac{1}{2}(2-D)|\mathcal{E}|^2 + (D/2)\nabla \cdot (\text{Re} \mathcal{E}^* \nabla \cdot \mathcal{E})$ , which, inserted in Eq. (17), gives

$$\partial_t^2 \langle \delta r^2 \rangle = 2A + (2-D)\langle |\mathcal{E}|^2 \rangle, \quad (18a)$$

where

$$A \equiv 2H/N - S^2/N^2 \quad (18b)$$

is a constant of motion. By integrating twice in time, we get

$$\langle \delta r^2 \rangle = At^2 + Bt + C + (2-D) \int_0^t dt' \int_0^{t'} dt'' \langle |\mathcal{E}|^2 \rangle, \quad (19)$$

where  $B \equiv \partial_t \langle \delta r^2 \rangle|_{t=0}$  and  $C \equiv \langle \delta r^2 \rangle|_{t=0}$ . This is the result of Goldman and Nicholson.<sup>6</sup> If the number of spatial dimensions  $D \geq 2$  and the conserved quantity  $A < 0$ , it follows that  $\langle \delta r^2 \rangle$  will collapse to zero in a finite time. This general result is based on the assumption of adiabatic ions and electrostatic fields, both of which are eventually violated when  $\langle \delta r^2 \rangle$  becomes sufficiently small (see the Appendix).

Thus, in the late stages of the collapse, the collapson may radiate ion-acoustic waves as well as electromagnetic waves. If these effects are not sufficient to stop the collapse, it will finally be stabilized by Landau-damping when  $\langle \delta r^2 \rangle^{1/2}$  becomes of the same order of magnitude as the Debye length  $\lambda_D$ . (We believe wave-particle interactions to be the dominant stabilization mechanism.) The useful form of the virial theorem for the nonlinear Schrödinger equation depends on the identity  $\mathbf{S} = \mathbf{P}$ . This identity is not satisfied by the more general Zakharov's equations. Hence, a useful virial theorem that can describe the late stages of a collapse has not been derived. At the present time, the most fruitful approaches to these problems seem to be numerical integration of Zakharov's equations and particle simulations.

### III. GAUSSIAN PACKETS

#### A. Threshold and collapse time

We treat an initial Langmuir wave packet of the form

$$\mathcal{E}(\mathbf{r}, t=0) = -\nabla [\phi_0 \exp(-\Delta k^2 r^2/D) \exp(i\mathbf{k}_0 \cdot \mathbf{r})], \quad (20a)$$

where we assume that the  $k$ -space width of the packet,  $\Delta k$ , is much less than the wavenumber  $k_0$ :

$$\epsilon = \Delta k/k_0 \ll 1. \quad (20b)$$

(In the Appendix we shall see that  $\epsilon \ll 1$  is the condition

for neglecting electromagnetic effects.) We note several features of this initial wave packet: It is purely electrostatic, since it is the gradient of a potential. As long as  $\Delta k \ll k_0$ , the field  $\mathcal{E}$  points essentially in the  $\mathbf{k}_0$  direction and has a maximum value

$$\mathcal{E}_0 \equiv |\mathcal{E}_{\max}(t=0)| \approx k_0 \phi_0, \quad (20c)$$

where  $\phi_0$  is assumed to be real and constant. If we evaluate the mean packet momentum density  $S/N$ , we find

$$S/N = k_0 [1 + \Theta(\epsilon^2)]. \quad (21)$$

The factor  $D$  in the exponent of Eq. (20a) is equal to the number of spatial dimensions considered. It is included to assure that  $\Delta k^2$  is indeed the correct measure of the  $k$ -space width of the packet. To justify this interpretation, we note that the Fourier transform of (20a), (with  $D$  in the exponent), leads to the correct  $k$ -space width measure, namely,

$$N^{-1} \int |\mathcal{E}_k|^2 |\mathbf{k} - \mathbf{k}_0|^2 \frac{d^D k}{(2\pi)^D} \approx (\Delta k)^2, \quad (22)$$

after using the inequality  $\Delta k \ll k_0$ .

The physical quantities and invariants defined in Sec. II can be evaluated for the initial field of Eq. (20), and expressed entirely in terms of  $\mathcal{E}_0$ ,  $\Delta k$ ,  $k_0$ , and  $D$ . For example, to zero order in  $\epsilon$ ,

$$N \approx \mathcal{E}_0^2 (D\pi/2\Delta k^2)^{D/2}, \quad (23)$$

$$\langle \delta r^2 \rangle_0 \approx (D/2\Delta k)^2, \quad (24)$$

$$\langle |\mathcal{E}|^2 \rangle \approx \mathcal{E}_0^2/2^{D/2}. \quad (25)$$

The invariant  $A$ , defined in Eq. (18b), is

$$A \equiv \frac{2H}{N} - \left| \frac{\mathbf{S}}{N} \right|^2 = \Delta k^2 - \frac{\mathcal{E}_0^2}{2^{D/2}}. \quad (26)$$

The threshold for collapse for  $D=2$  (two dimensions) is  $A < 0$ . This is also an upper bound on the three-dimensional threshold:

$$\mathcal{E}_0^2|_{\text{th}} = 2^{D/2} \Delta k^2. \quad (27)$$

For our Gaussian initial packet, the integration constants  $B$  and  $C$  in Eq. (19) are easily evaluated. We find  $B=0$ , and  $C=(D/2)^3/\Delta k^2$ . From Eqs. (19) and (26) the time  $t_c$  follows

$$t_c = |C/A|^{1/2} = D/2\Delta k^2(P-1)^{1/2}. \quad (28)$$

This is the virial theorem prediction of the collapse time for  $D=2$ , and an upper bound on the collapse time for  $D=3$ . The quantity  $P$  is defined as

$$P \equiv \mathcal{E}_0^2/2^{D/2} \Delta k^2. \quad (29)$$

When  $D=2$ ,  $P$  is the ratio of field energy to threshold energy. We shall use  $P$  in our treatment for arbitrary  $D$ , although its interpretation as wave to threshold energy holds only for  $D=2$ .

#### B. Gaussian approximation

In general, as a packet develops nonlinearly, it does not preserve its Gaussian shape. If  $P$  is much greater than one, the packet may be unstable against "breaking-up" into smaller packets (modulational instability).

ity<sup>13</sup>). One-dimensional "breathers" may have many spatial oscillations when  $P \gg 1$ .

In three dimensions, even very close to threshold, self-similar behavior<sup>2</sup> develops asymptotically as the collapse proceeds. Using a scalar nonlinear Schrödinger equation, Budneva *et al.*<sup>2</sup> have shown that an initial three-dimensional Gaussian packet with  $P \gg 1$  soon develops such a feature. In Sec. V we show that such a feature also develops when  $P \gtrsim 1$  (near threshold). A quickly collapsing core of similarity form rises at the center of the packet. This core becomes singular, and its width goes to zero for nonzero  $\langle \delta r^2 \rangle$ . However, the threshold for collapse and the early time behavior of  $\langle \delta r^2 \rangle$  are well described by the virial theorem methods we are about to describe.

Assuming that the packet remains approximately Gaussian, a closure scheme for Eqs. (18) may be formulated with  $D=1$  or  $D=3$ . The problem is with the quantity  $\langle |\delta|^2 \rangle$ , which is *not* an invariant. We shall make the (Gaussian) approximation that

$$\langle |\delta|^2 \rangle = QN\langle \delta r^2 \rangle^{-D/2}, \quad (30a)$$

where  $Q$  is assumed constant. We may evaluate  $Q$  at  $t=0$ , using Eqs. (23)–(25). To zero order in  $\epsilon$ , the result is

$$Q = (D/4\pi)^{D/2}. \quad (30b)$$

Inserting Eqs. (30) into the time-evolution equation (19) for  $\langle \delta r^2 \rangle$  enables it to be integrated by potential theory methods. A first integral is

$$\dot{\xi}^2/2 + V(\xi) = E, \quad \xi = \langle \delta r^2 \rangle. \quad (31a)$$

Here,  $E$  is an arbitrary integration variable, and the potential  $V(\xi)$  is given by

$$V(\xi) = -2A\xi - 2NQ\xi^{(1-D/2)}. \quad (31b)$$

Equations (31) are convenient for studying effects of dimensionality on the evolution of solitary wave packets. Calculations of characteristic times, such as pulsation and collapse times, are easier if we express the potential in terms of the normalized coordinate  $\eta \equiv \xi/\xi_{t=0}$ , where  $\xi_{t=0} = (D/2\Delta k)^2$  is the initial mean-square spatial width of the wave packet

$$V = (D^2/2)[(P-1)\eta - P\eta^{1-D/2}]. \quad (32)$$

Note that the potential for the initial packet ( $\eta=1$ ) is  $V(\xi_{t=0}) = -D^2/2$  and, hence, it is independent of the initial parameters. We study the implications of the potential of Eq. (32) for various cases:

**D=1.** For  $A < 0$ , ( $P > 1$ ), the potential has the concave shape of Fig. 1. For a Gaussian packet the potential has a minimum at  $\eta_0 \equiv \frac{1}{4}(1-P^{-1})^{-2}$  and a zero point at  $\eta_1 \equiv (1-P^{-1})^{-2}$ . This allows bounded, oscillating solutions about the equilibrium point  $\eta_0$ . For  $P=2$  we find that  $\eta_0 = 1$ , which is the initial coordinate, thus giving the stationary equilibrium solution corresponding to the well-known nonlinear Schrödinger equation soliton  $\delta = \alpha \operatorname{sech}(\alpha x) \exp(i\alpha^2 t/2)$ . Since  $\eta_1 > 1$  for all  $P > 1$ , and  $\eta_1 \rightarrow 1$  as  $P \rightarrow \infty$ , it is clear that full collapse never occurs. For sufficiently large  $P$  the oscillations about  $\eta_0$  will be so large that the minimum  $\eta$  will be

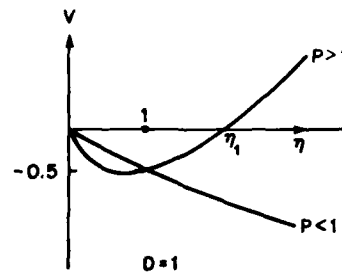


FIG. 1. Pseudo-potential  $V(\eta)$  for  $D=1$  ( $\eta = \langle \delta r^2 \rangle / \langle \delta r^2 \rangle_0$ ).

below the limits of validity of the nonlinear Schrödinger equation as given in the Appendix.

Assuming that  $(P-2)$  is sufficiently small, our theory gives pulsating solutions corresponding to the bound states near the bottom of the potential well in Fig. 1.  $\langle \delta x^2 \rangle$  oscillates periodically, and, by the invariance of  $\int dx |\delta|^2$ , so does  $|\delta|_{\max}^2$ .

This behavior appears to be related to certain numerical solutions obtained by Satsuma and Yajima,<sup>7</sup> who apply the inverse scattering method to solve for the time evolution of an initial wave packet of form

$$\delta(x, 0) = a \operatorname{sech} x. \quad (33)$$

When  $a = 1 + \epsilon$ , and  $\epsilon \ll 1$ , they also observe oscillations in  $|\delta|_{\max}^2$ , but these oscillations slowly relax, presumably due to "continuum" radiation of Langmuir waves. We do not observe such damping of the oscillations, probably because continuum radiation is excluded by the assumption of localized fields in the spatially Gaussian closure approximation.

The validity of our treatment of periodic pulsations of one single wave packet requires that the packet not break up due to secondary instabilities in a time shorter than the period. The possibility of such a break-up is not accounted for in our Gaussian model. The period is obtained by integrating Eq. (31) using Eq. (32),

$$\tau = F(P) / |\delta_0|^2, \quad (34a)$$

where the function  $F(P)$  is defined by the integral

$$F(P) \equiv \pm \frac{P}{\sqrt{2}} \int_{\eta_1}^1 \frac{d\eta}{[P\eta^{1/2} - (P-1)\eta - 1]^{1/2}}. \quad (34b)$$

Here,  $\eta_1$  is the turning point. The positive sign is for  $P > 2$ , ( $\eta_1 < 1$ ), the negative sign for  $P > 2(\eta_1 > 1)$ .  $F(P)$  is plotted in Fig. 2. The period predicted by our Eqs. (34) is in good agreement with the numerical results exhibited in Fig. 2 of Ref. 7. As  $P \rightarrow 1$ , the period goes to infinity.

The growth rate of secondary instabilities such as modulational instability and parametric decay<sup>13</sup> is  $\gamma_s \sim |\delta_0|^2$ . If we let  $f = \gamma_s t_s$  be the number of  $e$  folding needed for the noise to grow to nonlinear levels, we get

$$\tau / t_s = F(P) / f.$$

The value of  $f$  depends on the noise level from which the unstable waves are amplified, however, even very conservative estimates give  $f \gtrsim 10$ . This means that

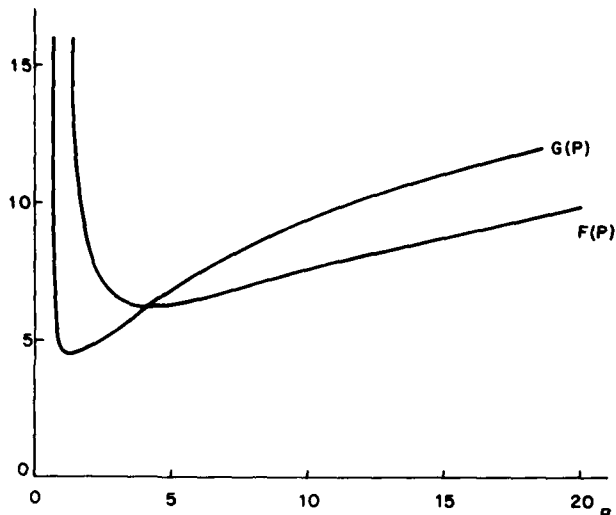


FIG. 2. Functions  $F(P)$  and  $G(P)$  versus  $P$ .

breathing and break-up times are of the same order of magnitude for  $2 < P \leq 10^2$ . Break-up instabilities are effective only if the packet size is larger than the shortest unstable wavelength:  $\langle \delta r^2 \rangle^{1/2} = 1/(2\Delta k) > \lambda_s = \pi/|\mathcal{E}_0|$  or, equivalently,  $P \geq 2\sqrt{2\pi^2} \approx 28$ . If this threshold is exceeded, the wave packet will break up into smaller packets on a time scale of the same order as the pulsation period. We do not expect our theory to apply under these conditions.

A different way to view one-dimensional break-up behavior when  $P \gg 2$  is provided by the work of Satsuma and Yajima.<sup>7</sup> They also studied initial packets of the form given in Eq. (33) for  $\alpha = 1, 2, 3$  (see their Fig. 1). The case  $\alpha = 1$  corresponds to the usual single soliton, but  $\alpha = 2$  and 3 correspond to breathers, which are exactly periodic pulsating bound states of two or three solitons. The case  $\alpha = 3$ , in particular, shows markedly non-Gaussian behavior, as the packet splits into two and three narrower packets in the course of its periodic behavior. (Similar behavior was also observed by Yuen and Ferguson,<sup>8</sup> in what they call "complex" recurrence.) If we set the area under our Gaussian packet equal to the area under their sech $\chi$  packet, we obtain a relation between our  $P$  and their  $\alpha$

$$P = \pi\alpha^2/\sqrt{2}. \quad (35)$$

From this we see that  $\alpha = 1$  corresponds to  $P \approx 2$  in the single soliton result. The case  $\alpha = 2$  corresponds to  $P \approx 9$ , which is a somewhat lower bound for validity than found from consideration of modulational instabilities.

For  $P < 1$  ( $A > 0$ ), the potential in Fig. 1 is monotonically decreasing for all  $\eta > 0$ , so that any localized wave packet will disperse spatially with time. Break-up, recurrence, or collapse will never occur.

$D = 2$ . In this case, the term containing  $\langle |\mathcal{E}|^2 \rangle$  vanishes, and no approximation is necessary in the virial theorem. The potential  $V(\xi)$  is linear with slope  $-2A$ , giving collapse for  $A < 0$ , and spatial dispersion for  $A > 0$ . Threshold for collapse and collapse time are

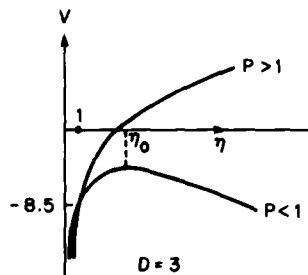


FIG. 3. Pseudo-potential  $V(\eta)$  for  $D=3$  ( $\eta = \langle \delta r^2 \rangle / \langle \delta r^2 \rangle_0$ ).

given by Eqs. (27) and (28), respectively.

$D=3$  (see Fig. 3). The potential for  $A < 0$  grows monotonically from minus infinity at  $\xi = 0$ , approaching the straight line  $-2A\xi$  as  $\xi \rightarrow \infty$ . Consequently, collapse occurs for all initial wave packets, and an upper bound for the collapse time is found by considering collapse along the linear potential  $-2A\xi$ . This gives the expression of Eq. (27). The convex shaped potential appearing for  $A > 0$  has an unstable equilibrium for  $\eta_0 = [2(P^2 - 1)]^{-1/3}$ . Collapse for a Gaussian wave packet occurs when  $\eta_0 > 1$ , or

$$P > \frac{2}{3}. \quad (36)$$

The threshold condition  $P > 1$  for  $D = 2$  corresponds to the threshold condition  $\mathcal{E}_0^2 > 2\Delta k^2$ , while Eq. (36) for  $D = 3$  requires  $\mathcal{E}_0^2 > (2^{5/2}/3)\Delta k^2$ . This means that the threshold is slightly lower in three dimensions.

The virial theorem prediction for the collapse time, valid for all  $P > \frac{2}{3}$ , is easily obtained by integration of Eq. (31),

$$t_c = G(P)/|\mathcal{E}_0|^2, \quad (37)$$

where  $G(P)$  is defined by the integral

$$G(P) = \frac{3P}{\sqrt{2}} \int_0^1 \frac{d\eta}{[P\eta^{-1/2} - (P-1)\eta - 1]^{1/2}}, \quad (38)$$

which is plotted in Fig. 2.

The collapse time predicted by (37) is an upper limit. We shall see in Sec. V that a self-similar core can collapse faster than  $\langle \delta r^2 \rangle$ .

The threshold condition for break-up, that the packet size is larger than the smallest unstable wavelength, now becomes  $P > \sqrt{2}(\pi/3)^2 \approx 1.6$ , while the ratio

$$t_c/t_s = G(P)/f, \quad (39)$$

is smaller than unity only for  $0.7 < P \leq 10$ . Hence for large  $P$  ( $P > 10$ ), a wave packet should break up into smaller packets before it has had time to collapse. If the smaller packets have  $P$  in the range where  $t_c/t_s < 1$ , they will collapse. This succession of break-up and collapse has been referred to as indirect collapse.<sup>6</sup>

Similar phenomena are well known in nonlinear optics.<sup>9</sup> A nonlinear laser beam with  $P > 1$  breaks up into intense filaments, whereas when  $P$  is closer to one, the beam self-focuses as a whole.

#### IV. EFFECT OF DAMPING ON TWO-DIMENSIONAL COLLAPSE

We next introduce a local damping term in the form  $i\gamma\delta$  on the left side of the nonlinear Schrödinger equation (3). The conservation laws, based on the integrals of Eqs. (5), (9), and (12) are modified in the following manner:

$$(\partial_t + 2\gamma)N = 0 \quad \text{or} \quad N = N_0 \exp(-2\gamma t). \quad (40)$$

Since there is no driver, the plasmon number decreases exponentially with time. The momentum behaves the same way

$$(\partial_t + 2\gamma)P = 0 \quad \text{or} \quad P = S = S_0 \exp(-2\gamma t); \quad (41)$$

however, the energy  $H$  has a more subtle evolution equation

$$(\partial_t + 2\gamma)H = \gamma N \langle |\delta|^2 \rangle. \quad (42)$$

An initially negative  $H$  may become positive if the effective source on the right side is large enough. Sufficiently large dissipation causes the nonlinear refraction term ( $\propto |\delta|^4$ ) in  $H$  to decrease faster than the dispersion term ( $\propto |\nabla \cdot \delta|^2$ ). Hence,  $H$  and  $A$  eventually change from negative to positive, and collapse stops. The virial theorem takes the form (for  $D=2$ )

$$(\partial_t + 2\gamma)^2 \langle \delta r^2 \rangle = 2A. \quad (43)$$

Assuming an approximately Gaussian wave packet, Eqs. (30) imply that  $\langle |\delta|^2 \rangle = (D^2/\pi 2^3)^{D/2} \langle \delta r^2 \rangle^{-D/2} N_0 \exp(-2\gamma t)$ , which can be inserted in Eq. (42). We restrict our treatment to the case  $D=2$  for which Eq. (42) may be written in the form

$$\partial_t A = (\gamma/\pi) (N_0/\langle \delta r^2 \rangle) \exp(-2\gamma t). \quad (44)$$

In Eqs. (43) and (44) we make the following substitutions

$$\tau = t/t_c, \quad \nu = \gamma t_c, \quad (45)$$

$$x(\tau) = \frac{\exp(2\nu\tau)}{2t_c(P\nu)^{1/2}} \langle \delta r^2 \rangle, \quad y(\tau) = \frac{t_c A}{(P\nu)^{1/2}}, \quad (46)$$

where  $t_c$  is the collapse time of Eq. (28). The resulting equations are

$$\partial_\tau^2 x = y \exp(2\nu\tau), \quad \partial_\tau y = x^{-1}, \quad (47)$$

with initial conditions

$$x(0) = 1/2\alpha^{1/2}, \quad x'(0) = \nu\alpha^{-1/2}, \quad (48a)$$

$$y(0) = -\alpha^{-1/2}, \quad \alpha = \nu/(1 - P^{-1}). \quad (48b)$$

This initial-value problem has been solved numerically for various values of  $P$  and  $\alpha$ . For a given  $P$ , there exists a critical value  $\alpha_c(P)$ . For  $\alpha < \alpha_c$ , the packet collapses completely. For  $\alpha \geq \alpha_c$ , the variable  $x$  defined in Eq. (46) decays to a minimum,  $x_{\min}$ , and then increases. The packet size  $\langle \delta r^2 \rangle$  asymptotically approaches a constant, due to the balance between linear dissipation and linear dispersion. This can be seen from Eqs. (47). As  $x \rightarrow \infty$ ,  $y$  goes to a constant, and  $x$  approaches  $\exp(2\nu t)$ . From the definition of  $x$ , this implies that  $\langle \delta r^2 \rangle$  approaches a constant. From Eq. (43), we see that  $\langle \delta r^2 \rangle \sim A/2\gamma^2$ . In the asymptotic limit, only linear dispersion contributes to  $H$ , so  $A \sim \langle \delta r^2 \rangle^{-1}$  [see Eq. (28), for example], and, consequently,  $\lim_{t \rightarrow \infty} \langle \delta r^2 \rangle$

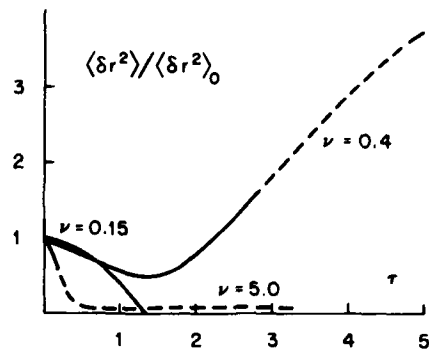


FIG. 4.  $\langle \delta r^2 \rangle / \langle \delta r^2 \rangle_0$  versus time  $\tau$  for  $\nu = 0.15$ , 0.4, and 5.0. Curves are dotted for times when  $N$  has damped by more than one order of magnitude.

$\sim \gamma^{-1}$ . This may be of little interest, however, because  $|\delta|^2$  has damped to a small value by this time and the packet is linear. In Fig. 4 we show some typical curves of  $\langle \delta r^2 \rangle$  versus time, for various values of the damping. Each curve is shown as a dashed line after the plasmon number  $N$  has decreased by one order of magnitude.

In Fig. 5 the quantity  $\beta \equiv x_{\min}/x(0)$  has been plotted versus  $\alpha$  for various  $P$  values. These plots show that collapse is stabilized for  $\alpha > \alpha_c \approx \frac{1}{3}$ . Thus, we have noncollapsing solutions for  $\gamma > \gamma_c$ , where the critical damping rate  $\gamma_c$  is given by

$$\gamma_c \approx (1 - P^{-1})/(3t_c). \quad (49)$$

If the collapse proceeds too far before stabilization occurs, the nonlinear Schrödinger equation breaks down and results based on the virial theorem are not reliable. Initial wave packet conditions for which the nonlinear Schrödinger equation remains valid throughout the nonlinear evolution are given in the Appendix.

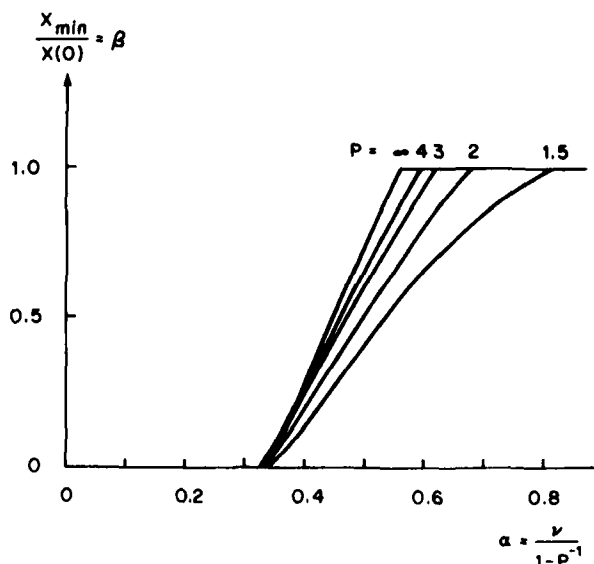


FIG. 5.  $\beta = x_{\min}/x(0)$  plotted versus  $\alpha$  for  $P = 1.5$ , 2, 3, 5, and  $\infty$ .

## V. SELF-SIMILAR BEHAVIOR

### A. Scaling laws

By making the self-similar substitution<sup>1,2</sup>

$$\mathbf{g} = (t_c - t)^{-1/2} \mathbf{R}(\mathbf{u}), \quad \mathbf{u} = (t_c - t)^{-1/2} \mathbf{r} \quad (50)$$

in Eq. (3), we get rid of the time dependence

$$\frac{1}{2} i (1 + \mathbf{u} \cdot \partial_{\mathbf{u}}) \mathbf{R} + \frac{1}{2} \partial_{\mathbf{u}}^2 \mathbf{R} + |\mathbf{R}|^2 \mathbf{R} = 0. \quad (51)$$

At collapse threshold the nonlinear pressure term must balance the dispersion term; hence, for the ratio of field energy to threshold energy we get

$$P \sim \left| \frac{|\mathbf{R}|^2 \mathbf{R}}{\frac{1}{2} \partial_{\mathbf{u}}^2 \mathbf{R}} \right| \sim (R_{\max} \Delta u)^2, \quad (52)$$

where  $\Delta u$  is the half-width of the function  $\mathbf{R}(\mathbf{u})$ . Assuming that the first term in Eq. (51) is of the same order of magnitude as the nonlinear term (which is obviously true for  $P \gg 1$ ), we find that  $R_{\max} = \Theta(1)$ . From Eq. (50), it then follows that

$$t_c = \Theta(|\mathbf{g}_0|^{-2}). \quad (53)$$

This always turns out to be a faster time than the predicted by virial theory (an example will be given).

The self-similar solution in Eq. (50) has some peculiar properties which might tend to obscure its relation to arbitrary initial-value problems. For example, its  $N$  invariant is infinite in three dimensions (although not in two). To see this, we note first that Eq. (50) implies

$$N = (t_c - t)^{1/2} \int d^3 u |\mathbf{R}(\mathbf{u})|^2. \quad (54)$$

However, in the limit of large  $u$ , the last two terms in Eq. (51) are negligible, and  $R \propto u^{-1}$ . Hence, the integral in (54) diverges. Indeed, this must be the case, in order for  $N$  to be time independent. However, in any initial-value problem of physical interest,  $N$  is always finite. What role can self-similar solutions play in arbitrary initial-value problems? This question is addressed next.

### B. Numerical studies of three-dimensional collapse

We support our discussion with numerical solutions of a scalar nonlinear Schrödinger equation in spherical symmetry

$$i \frac{\partial \psi}{\partial t} + \frac{1}{2r^2} \frac{\partial}{\partial r} \left( r^2 \frac{\partial \psi}{\partial r} \right) + |\psi|^2 \psi = 0, \quad (55)$$

with boundary conditions

$$\left( \frac{\partial \psi}{\partial r} \right)_{r=0} = \psi_{r \rightarrow \infty} = 0.$$

This equation follows from the vectorial nonlinear Schrödinger equation (3) under certain conditions. Assume that the electric field envelope  $\mathbf{E}$  has a rapidly oscillating spatial phase factor  $\exp(i\mathbf{k}_0 \cdot \mathbf{r})$ , where  $\mathbf{k}_0$  is much larger than the  $k$ -space width  $\Delta k$  of the spatial envelope. Under this assumption the electric field can be represented in terms of a scalar function  $\phi(\mathbf{r}', t)$ :

$$\mathbf{E}(\mathbf{r}', t) = \nabla[\phi(\mathbf{r}', t)/k_0] \approx i\phi(\mathbf{r}', t)\hat{\mathbf{k}}_0. \quad (56)$$

This immediately gives a scalar nonlinear Schrödinger equation in  $\phi$ , but it is not spherically symmetric be-

cause  $\phi(\mathbf{r}', t)$  still contains the nonsymmetric phase factor. This means that the wave packet has a nonzero momentum,  $\mathbf{P}' = N'\mathbf{k}_0$ . However, the momentum can be removed by the following gauge-frame transformation:

$$\phi(\mathbf{r}', t) = \psi(\mathbf{r}, t) \exp(-ik_0^2 t/2 + i\mathbf{k}_0 \cdot \mathbf{r}'), \quad (57)$$

$$\mathbf{r} = \mathbf{r}' - \mathbf{k}_0 t, \quad (58)$$

under which the nonlinear Schrödinger equation and the constants of motion  $N$  and  $A$  [see Eq. (18b)] are invariant. The momentum transforms as

$$\mathbf{P} = \mathbf{P}' - N'\mathbf{k}_0 = 0,$$

so that  $\psi(\mathbf{r}, t)$  does not contain the phase factor  $\exp(i\mathbf{k}_0 \cdot \mathbf{r})$ , and it is possible to impose spherical symmetry to obtain Eq. (55).

Equation (55) was solved by Budnev et al. for an initial Gaussian shape corresponding to  $P = 8.5$  (threshold is  $P = \frac{2}{3}$ ). We solve it for several  $P$  values, both below and above threshold, and the results can be summed up as follows: For all  $P > \frac{2}{3}$  a collapsing "core" develops whose collapse time is less than one-half of the collapse time derived from the virial theorem under the Gaussian approximation.

However, the collapse threshold condition,  $P = \frac{2}{3}$ , obtained from the virial theorem with the Gaussian closure approximation provides a surprisingly good criterion for core collapse. When  $P < \frac{2}{3}$ , the corona disperses ( $\langle \delta r^2 \rangle$  grows monotonically), in agreement with virial theorem predictions. Just below threshold, however, we have the situation of a collapsing core co-existing with a dispersing corona, indicating that core and corona can behave independently of each other.

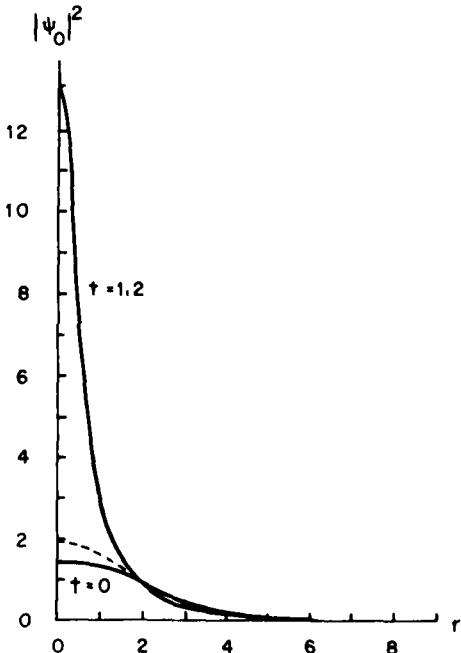


FIG. 6. Initial Gaussian ( $t = 0$ ), and nearly collapsed solution with a core of similarity form ( $t = 1.2$ ). Dotted curve is the solution at  $t = 1.2$  in the Gaussian approximation.

In Fig. 6 we illustrate a solution to Eq. (55) (the factor  $\frac{1}{2}$  in the dispersion term has been scaled away, by stretching  $r$  by a factor  $\sqrt{2}$ , in order to correspond to the equation of Budneva *et al.*). Figure 6 shows the build-up of the core for  $P = \frac{4}{3}$  (two times threshold). The intensity is displayed at time  $t = 1.2$ . The dotted curve shows the corresponding shape if the packet has remained of Gaussian shape and collapsed in accordance with virial theorem arguments. The steepness of the core is of much less consequence when we recall that moments and invariants are weighted by  $r^2$  when three-dimensional integrations are performed.

For example, at early times, the virial theorem prediction of width  $\langle \delta r^2 \rangle$  is well satisfied. If we assume that

$$|1 - \langle \delta r^2 \rangle / \langle \delta r^2 \rangle_0| \ll 1,$$

then the virial result, Eq. (31), may be integrated analytically to yield

$$\langle \delta r^2 \rangle \approx \langle \delta r^2 \rangle_0 (1 - at^2), \quad a = (\frac{3}{2}P - 1)(\delta_0^4/18P^2). \quad (59)$$

This curve is plotted in Fig. 7 for  $P = \frac{4}{3}$  ( $\delta_0^2 = 2.39$ ). Superimposed on it are the results for  $\langle \delta r^2 \rangle$  obtained by spatial integration of the numerical solutions to (55), at various times. By the time  $t = 1.2$  (corresponding to Fig. 6), the non-Gaussian character of the core is causing the numerically determined  $\langle \delta r^2 \rangle$  values to fall about 1% below the virial theorem predictions. This

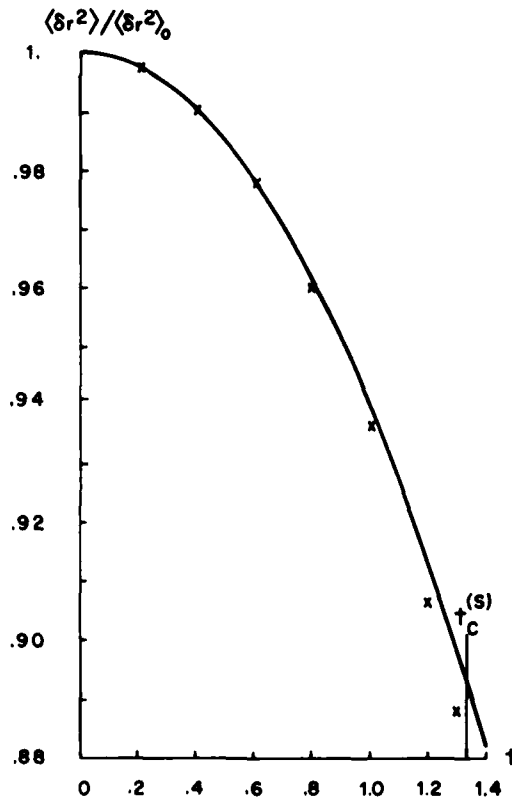


FIG. 7. Spherically symmetric numerical determination of  $\langle \delta r^2 \rangle$  (x marks) as a function of time, versus virial theorem prediction (solid curve—see Eq. (59)), for the case  $P = \frac{4}{3}$ .  $t_c^{(s)} = 1.3265$ .

happens because Eq. (59) was obtained by assuming  $Q$  is constant and equal to the value given in Eq. (30b). In the actual numerical solution,  $Q$  has increased by a factor of 2 by the time  $t = 1.2$ , and it is this non-Gaussianity which is causing the slight lowering of the  $\langle \delta r^2 \rangle$  points.

The virial theorem prediction for the collapse time [Eq. (37)] gives  $t \approx 3.2$ . However, the collapse of the core is seen to occur at  $t \approx 1.33$ , by arguments we shall advance shortly. At this time  $\langle \delta r^2 \rangle$  is nonzero and comes from a tail which remains even when the core has gone singular. This time is indicated on Fig. 7 as  $t_c^{(s)}$ . The significance of the virial theorem predictions of  $\langle \delta r^2 \rangle$  beyond  $t_c^{(s)}$  are not clear. The nature of the problem will be summarized later.

In Fig. 8 we verify that the field is self-similar at  $r = 0$ , and determine the collapse time by extrapolation. According to the scalar-field version of Eq. (50), if the field is self-similar at the origin, then  $\psi(0, t) = R(0)(t_c - t)^{-1/2}$ . Hence, in Fig. 8, we have plotted  $|\psi(0, t)|^{-2}$  versus time and have found the expected straight line, with  $|\psi(0, t_c)|^{-2} = 0$  at  $t_c^{(s)} = 1.3265$ .

Of more interest is the question of the spatial extent of the self-similarity. Consider the field at two times  $t_1$  and  $t_2$ , such that  $t_1 < t_2 < t_c^{(s)}$ . If the field is self-similar at  $t_1$ , with respect to the later time  $t_2$ , then it must have the form  $\psi_{ss}(r, t_1)$  which is related to  $\psi(r, t_2)$  by

$$\psi_{ss}(r, t_1) = \alpha_{21} \psi(r/\alpha_{21}, t_2), \quad \alpha_{21} \equiv \left( \frac{t_c^{(s)} - t_2}{t_c^{(s)} - t_1} \right)^{1/2}. \quad (60)$$

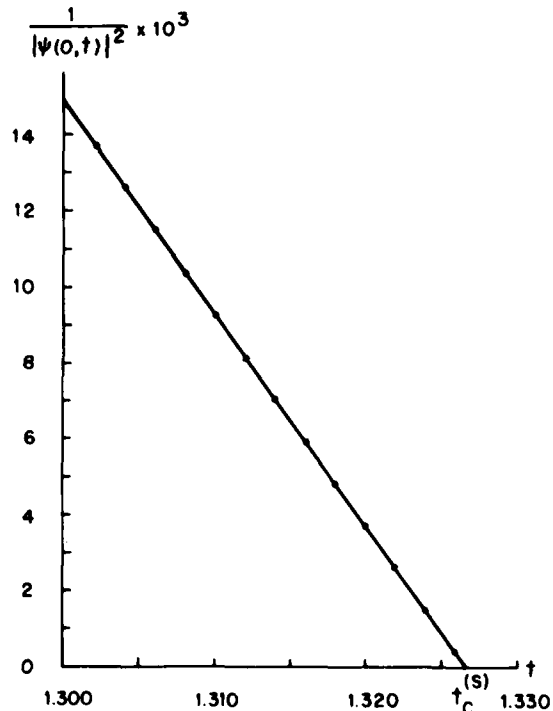


FIG. 8.  $|\psi(0, t)|^{-2}$  versus time, showing self-similar approach to singularity in  $|\psi(0, t)|^2$  at  $r = 0$ , and  $t_c^{(s)} = 1.3265$ .

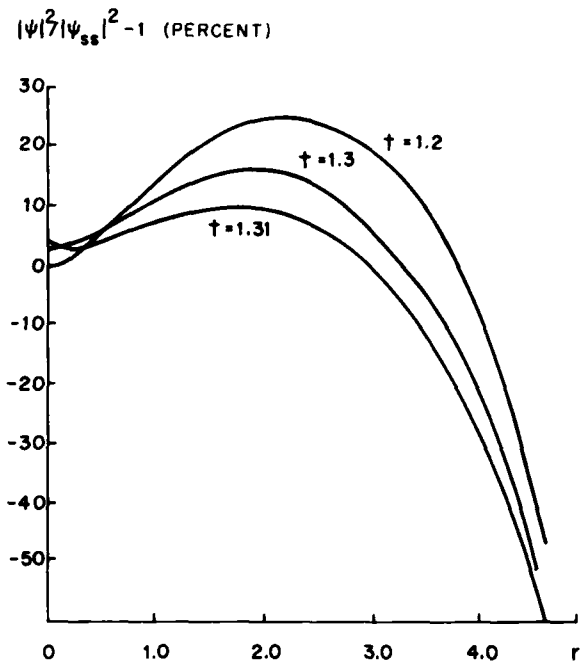


FIG. 9.  $|\psi|^2/|\psi_{ss}|^2 - 1$  as a function of  $r$  at  $t = 1.2, 1.3$ , and  $1.31$ . This exhibits the relative percentage difference between  $|\psi|^2$  and  $|\psi_{ss}|^2$ . The latter is reconstituted from  $|\psi(t=1.3220)|^2$ , under the assumption of self-similarity.

In Fig. 9 we have plotted the quantities

$$|\psi|^2/|\psi_{ss}|^2 - 1,$$

for  $t_2 = 1.3220$  and three different values of the earlier time  $t_1$ . This represents the percent difference between  $|\psi|^2$  and the self-similar solution, as a function of radius, for the three earlier times. At times later than 1.30,  $|\psi|^2$  is self-similar to within 15% up to radii of about  $r = 3.7$ . At these times the half-width of the peak occurs at  $r < 0.5$ , so a relatively long self-similar tail is observed.

How much of a contribution to the "number invariant,"  $N$ , is made by the self-similar part of the solution? To answer this question in Fig. 10 we have plotted the volume integral of  $|\psi|^2$  up to radius  $r$ , as a function of  $r$ ,

$$N_r(t) = 4\pi \int_0^r dr r^2 |\psi(r, t)|^2, \quad (61)$$

at the initial time and at two later times. Note,  $N_r$  is the plasmon number invariant,  $N$ , here equal to about 14. The arrows on the curves at  $t = 1.2$  and at  $1.31$  indicate the radius at which  $|\psi|^2$  deviates from self-similarity by  $\pm 25\%$ . We note that about half of  $N$  comes from the self-similar portion of the solution. The dots indicate the radius at which the half-maximum in  $|\psi|^2$  occurs for each time. Most of the contribution of the self-similar portion of  $|\psi|^2$  to  $N$  comes from the tail rather than the peak. As the collapse proceeds, the self-similar peak makes a vanishingly small contribution to  $N$ , while the self-similar tail makes an increasing contribution.

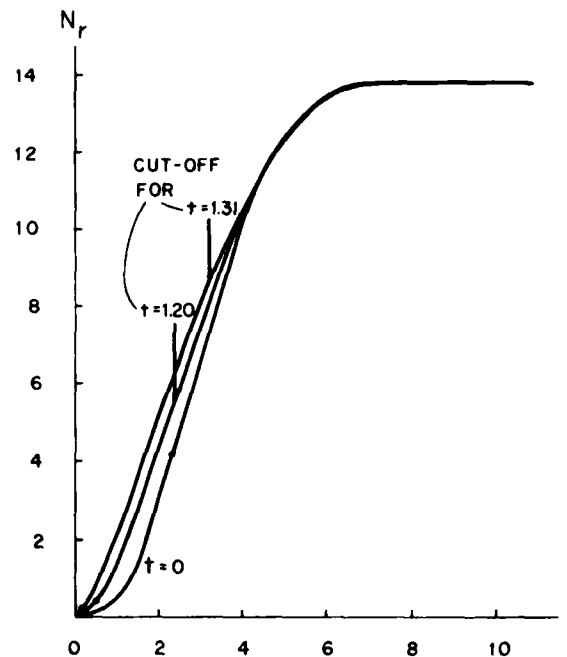


FIG. 10.  $N_r = 4\pi \int_0^r dr r^2 |\psi|^2$  as a function of  $r$  for  $t = 0, 1.2$ , and  $1.31$ . The radii at which  $|\psi|^2$  is equal to its half-maximum are shown on each curve as a dot. The cutoff points for deviation from self-similarity by more than 25% are shown by arrows.

The important issue of what happens to the entire tail (and to  $\langle \delta r^2 \rangle$ ), after the three-dimensional collapse of the central peak at time  $t_c^{(s)}$ , cannot be resolved within the context of the present theory. A proper resolution should take into account the inevitable break-down of the Schrödinger equation and the need for more physical processes. In the Langmuir wave application, this means the inclusion of a dynamic ion response and, possibly, energy transfer to electrons. The criteria for neglect of these physical effects are described in the Appendix.

We note that the non-Gaussian character of collapse appears to be a three-dimensional phenomenon. In two dimensions, even the self-similar solutions appear more Gaussian, and are not associated with an infinite  $N$  invariant. Our results on pulsating solitons in one dimension and on the effects of dissipation in two-dimensional collapse should not be affected by the non-Gaussian character of three-dimensional collapse.

#### ACKNOWLEDGMENTS

One of us (M.V.G.), would like to thank the Guggenheim Foundation for a Fellowship held during part of this research, and also to acknowledge helpful conversations with G. Reiter, D. Nicholson, F. Tappert, and H. H. Chen. This work was supported by the National Science Foundation, Atmospheric Sciences Section, and by the Air Force Office of Scientific Research. The work of one of us (K.R.) was also supported by the Institute of Mathematical and Physical Sciences, University of Tromsø, Norway. We thank the National Center

for Atmospheric Research, supported by the National Science Foundation, for computer time used in this study.

## APPENDIX

Here, we briefly review the plasma physics conditions which must be satisfied for the validity of the cubic Schrödinger equation (3). We begin with a more general set of equations, the Zakharov equations, which have been used extensively<sup>14</sup> to describe nonlinear Langmuir and electromagnetic wave evolution

$$i\dot{\mathcal{E}} + \frac{1}{2}\nabla\nabla\cdot\mathcal{E} - (C^2/2)\nabla\mathbf{x}\cdot\nabla\mathbf{x}\cdot\mathcal{E} - \delta n\mathcal{E} = 0, \quad (A1)$$

$$(C_s^2\theta_t^2 - \nabla^2)\delta n = \nabla^2|\mathcal{E}|^2. \quad (A2)$$

The units are the same as described after Eq. (3); in addition,  $\delta n$  is the low frequency electron (or ion) density response, in units of  $2n_0$ , where  $n_0$  is the average background density. The parameters  $C$  and  $C_s$  are, respectively, the speed of light and the ion-acoustic sound speed, in units of  $\sqrt{3}v_s$ , where  $v_s$  is the electron thermal speed ( $\theta_e/m_e$ )<sup>1/2</sup>. There are five conditions for the validity of the Zakharov equations (A1) and (A2):

- (i)  $(k/k_D)|\mathcal{E}| \ll 1$  (dipole approximation);
- (ii)  $\omega_s \ll \omega_e$  (slow-fast time separation);
- (iii) neglect of wave-particle interactions ( $k/k_D \ll 1$ ,  $\theta_e \gg \theta_i$ );
- (iv) quasi-neutrality;
- (v) linear ion response to ponderomotive force ( $\delta n \ll n_0$ ).

We shall be concerned mainly with the conditions for two further approximations, which lead to the cubic Schrödinger equation. These are, respectively, the electrostatic approximation ( $\nabla\cdot\mathcal{E} = 0$ ) and the adiabatic ion approximation  $|C_s^2\theta_t^2\mathcal{E}| \ll |\nabla^2\mathcal{E}|$  in Eq. (A2).

We begin by assuming the electrostatic approximation, and then show that this approximation can be well satisfied in the adiabatic limit, provided that the packet also satisfies certain criteria in  $k$  space.

With  $\nabla\cdot\mathcal{E} = 0$ , it follows that  $\nabla\nabla\cdot\mathcal{E} = \nabla^2\mathcal{E}$ , in Eq. (A1). In the adiabatic limit, the first term on the left side of (A2) is neglected in comparison with the second term. For localized fields, (A2) then integrates to  $\delta n = -|\mathcal{E}|^2$ , and (A1) becomes the cubic Schrödinger equation. An *a posteriori* examination of the terms on the left side of (A2) then gives us the necessary inequality for the adiabatic limit

$$|C_s^2\theta_t^2|\mathcal{E}|^2 \ll |\nabla^2|\mathcal{E}|^2|. \quad (A3)$$

From Eqs. (5) and (12), and the identity of current and momentum densities for the Schrödinger equations, we find

$$\theta_t^2|\mathcal{E}|^2 = \nabla_t\nabla_t T_{11}. \quad (A4)$$

The stress tensor is given by Eq. (14b). It may be re-written in a useful form by expressing the field in terms of an amplitude and phase:

$$\mathcal{E} = \mathbf{A} \exp(i\theta), \quad \mathbf{A}, \theta \text{ real.} \quad (A5)$$

Then

$$T_{11} = (\nabla\cdot\mathbf{A})(\nabla_t\mathbf{A}_t) + \mathbf{u}\cdot\mathbf{A}\mathbf{u}_t\mathbf{A}_t - (\delta_{11}/2)[\mathbf{A}^4 + \nabla\cdot(\mathbf{A}\nabla\cdot\mathbf{A})], \quad (A6)$$

where

$$\mathbf{u} \equiv \nabla\theta \quad (A7)$$

corresponds to the packet velocity [note, with the help of (A5), the current density (6) may be rewritten as  $\mathbf{S} = \mathbf{u}|\mathcal{E}|^2$ ]. In order to reduce the inequality (A3) still further, we consider a wave packet which is centered about wave vector  $\mathbf{k}_0$  and has a  $k$ -space width  $\Delta k$ :

$$\mathbf{A} \sim \mathbf{A}_0 \exp(-r^2\Delta k^2), \quad \mathbf{u} = \mathbf{k}_0. \quad (A8)$$

From (A6) we see that the various terms in the stress tensor are then of the orders

$$T = \Theta[(\Delta k)^2\mathbf{A}^2] + \Theta(k_0^2\mathbf{A}^2) + \Theta(\mathbf{A}^4) + \Theta[(\Delta k)^2\mathbf{A}^2]. \quad (A9)$$

Hence, (A3) and (A4) yield the following inequality for the adiabatic limit

$$\Theta[(\Delta k)^2] + \Theta(k_0^2) + \Theta(|\mathbf{A}|^2) \ll C_s^2 = r(m/M), \quad (A10)$$

where  $r = (1/3)(1 + \gamma_i\theta_e/\theta_s)$  and  $\gamma_i$  is the usual ratio of ion specific heats. The condition on the wavenumbers means essentially that the packet velocities (or group velocity, in the limit  $\Delta k \ll k_0$ ) must be much less than sound speed, so that the ions can follow the packet spatial translation. The condition on the amplitude,  $|\mathbf{A}|$ , means that the collapse speed of the packet must also be much less than sound speed. Both conditions are theoretically met, for example, in the case of the type III solar radio emission.<sup>6,15</sup>

It is also useful to examine the adiabaticity criterion (A3) for the case of self-similar solutions of form (40). Once again, if  $(R)_{\max}$  and  $(\theta_i R)_{\max}$  are considered to be of order unity, the adiabaticity condition (A3) becomes  $|\mathcal{E}|^2_{\max} \ll C_s^2$ , for nontranslating similarity solutions.

Next, we show that the condition for electrostatic approximation in the adiabatic limit is merely

$$\Delta k \ll k_0, \quad (A11)$$

for the electrostatic approximation. Here, we imagine an initially pure electrostatic packet (such as may arise from a beam instability, for example<sup>6,15</sup>), centered around the wave vector  $\mathbf{k}_0$ . As the packet collapses, its effective  $k$ -space width,  $\Delta k$ , increases. As long as  $\Delta k$  remains much less than  $k_0$ , the term  $C^2\nabla\mathbf{x}\cdot\nabla\mathbf{x}\cdot\mathcal{E}/2$  on the left of Eq. (A1) may be ignored.

The demonstration consists of two parts. First we require that the transverse part of  $\mathcal{E}$  be much smaller than the longitudinal part. This has been shown in Refs. 2 and 15, where  $|\mathcal{E}_t|/|\mathcal{E}_z|$  is shown to be of order  $C^{-2}$ . Given  $|\mathcal{E}_z| \gg |\mathcal{E}_t|$ , we may take the longitudinal and transverse parts of (A1) and write them approximately as

$$i\dot{\mathcal{E}}_z + \frac{1}{2}\nabla^2\mathcal{E}_z - (\delta n\mathcal{E}_z)_z = 0, \quad (A12)$$

$$i\dot{\mathcal{E}}_t + \frac{1}{2}C^2\nabla^2\mathcal{E}_t - (\delta n\mathcal{E}_t)_t = 0. \quad (A13)$$

Note that if we can demonstrate  $|\delta n\mathcal{E}_z|_z \ll |\delta n\mathcal{E}_t|_t$ , it will then follow that the third term in (A12) can be written approximately as  $(\delta n\mathcal{E}_z)_z + (\delta n\mathcal{E}_t)_t = \delta n\mathcal{E}_{zz}$ , and

the resulting equation is equivalent to (A1), in the electrostatic approximation. The condition  $|\delta n \mathcal{E}_1| \ll |\delta n \mathcal{E}_1|_1$ , with  $\delta n \approx -|\mathcal{E}_1|^2$  (adiabatic approximation), may be written as

$$\left| \int d^3r' \frac{\nabla' \times \nabla' \times (|\mathcal{E}_1|^2 \mathcal{E}_1)}{|\mathbf{r} - \mathbf{r}'|} \right| \ll \left| \int d^3r' \frac{\nabla' \nabla' \cdot |\mathcal{E}_1|^2 \mathcal{E}_1}{|\mathbf{r} - \mathbf{r}'|} \right|. \quad (\text{A14})$$

Next, take  $\mathbf{E}_1$  to be of the form  $\mathcal{E}_1 = \mathbf{A}_0 \exp(-r^2 \Delta k^2) \times \exp(i \mathbf{k}_0 \cdot \mathbf{r})$ , as in (A5) and (A8). Then, since  $\nabla' \times \mathcal{E}_1(\mathbf{r}') = 0$ , the left side is of order  $\Delta k/k_0$  smaller than the right side, when  $\Delta k \ll k_0$ . This demonstrates that  $\Delta k \ll k_0$  is indeed the condition for the electrostatic approximation, in the adiabatic limit. Together with the inequality (A10), this defines the conditions for converting the Zakharov equations (A1) and (A2) into the cubic Schrödinger equation (3). However, we note that these conditions are based on spatially Gaussian packets. If collapse has proceeded sufficiently into the self-similar regime, these estimates may have to be modified.

<sup>1</sup>V. E. Zakharov, Zh. Eksp. Teor. Fiz. **62**, 1745 (1972) [Sov. Phys. JETP **35**, 908 (1972)].

- <sup>2</sup>V. E. Zakharov, A. F. Mastryukov, and V. S. Synakh, Fiz. Plazmy **1**, 614 (1975) [Sov. J. Plasma Phys. **1**, 339 (1975)]; P. B. Budneva, V. E. Zakharov, and V. S. Synakh, Fiz. Plazmy **1**, 606 (1975) [Sov. J. Plasma Phys. **1**, 335 (1975)].
- <sup>3</sup>A. A. Galeev, R. Z. Sagdeev, Y. S. Sigov, V. P. Shapiro, and V. I. Shevchenko, Fiz. Plazmy **1**, 10 (1975) [Sov. J. Plasma Phys. **1**, 5 (1975)].
- <sup>4</sup>D. R. Nicholson, M. V. Goldman, P. Hoyng, and J. C. Weatherall, Astrophys. J. **223**, 605 (1978).
- <sup>5</sup>N. Pereira, R. Sudan, and J. Denavit, Phys. Fluids **20**, 936 (1977).
- <sup>6</sup>M. V. Goldman and D. R. Nicholson, Phys. Rev. Lett. **41**, 406 (1978).
- <sup>7</sup>J. Satsuma and N. Yajima, Prog. Theor. Phys. Suppl. **55**, 284 (1974).
- <sup>8</sup>H. C. Yuen and W. E. Ferguson, Phys. Fluids **21**, 1275 (1978).
- <sup>9</sup>H. C. Yuen and B. M. Lake, Phys. Fluids **18**, 958 (1975).
- <sup>10</sup>B. R. Suydam, IEEE J. Quantum Electron. **11**, 225 (1975); A. J. Campillo, S. L. Shapiro, and B. R. Suydam, Appl. Phys. Lett. **23**, 628 (1973).
- <sup>11</sup>J. Gibbons, S. G. Thornhill, M. J. Wordrop, and D. Ter Harr, J. Plasma Phys. **17**, 153 (1977).
- <sup>12</sup>I. M. Gelfand and S. F. Fomin, *Calculations of Variations* (Prentice-Hall, Englewood Cliffs, N. J., 1963).
- <sup>13</sup>S. Bardwell and M. V. Goldman, Astrophys. J. **209**, 912 (1976).
- <sup>14</sup>E. A. Kuznetsov, Zh. Eksp. Teor. Fiz. **66**, 2037 (1974) [Sov. Phys. -JETP **39**, 1003 (1974)].
- <sup>15</sup>M. V. Goldman, G. Reiter, and D. Nicholson, Phys. Fluids **23**, 388 (1980).

## APPENDIX C

C. "Harmonic Emission from Adiabatically Collapsing  
Langmuir Solitons"  
B. Hafizi and M. V. Goldman  
Physics of Fluids, January 1981, in press

Harmonic emission from adiabatically collapsing  
Langmuir solitons

Bahman Hafizi and Martin V. Goldman

Department of Astro-Geophysics, University of Colorado,  
Boulder, Colorado 80309

(Received May 1980)

Numerical studies of radiation at  $2\omega_p$  from a Langmuir envelope collapsing adiabatically in three dimensions show the emissivity is higher than expected. A volume emissivity obtained from an approximate density of collapsing packets leads to favorable comparisons with measurements of type III solar radio bursts.

CU 1039  
Submitted to Physics of Fluids

## I. INTRODUCTION

It is now believed that a type III solar radio burst is associated with an electron beam launched into the solar wind during a solar flare, leading to electromagnetic emission at the fundamental and harmonics of the local plasma frequency. Gurnett and Anderson<sup>1</sup> have measured the volume emissivity of harmonic emission at 1/2 A.U.

Recently, Goldman *et al.*<sup>2</sup> proposed a model for the emission based on the following scenario. An energetic beam of electrons launched into the solar wind excites Langmuir Waves. Computations<sup>3</sup> indicate that a Langmuir wave packet grows up to a point where the spatially averaged energy density  $W$  (normalized to the thermal energy) in the packet exceeds the threshold,  $W_{th}$ , for direct collapse.<sup>4,5</sup> The collapse time is infinite at threshold and decreases rapidly as  $W$  increases above  $W_{th}$ .<sup>5</sup> It is found that typically a packet continues to grow in strength up to about twice the threshold energy density before there is noticeable evidence of spatial collapse (and broadening in wave vector space). Once the packet becomes broad enough in  $k$ -space, it should be kinematically possible to couple two Langmuir waves into a photon at twice the local plasma frequency.

The physics of Langmuir collapse is described by the Zakharov equations.<sup>4</sup> The general solution of these equations is unknown. However, it is known that they possess certain invariants.<sup>4,5,6</sup> It is also known<sup>4,7,8</sup> that in some cases the solutions approach

a self-similar form over a region of space. There are two distinct stages of early collapse, the subsonic or adiabatic stage (described by a cubic Schrödinger equation), and the supersonic stage. In the subsonic stage the ions respond to the ponderomotive force adiabatically, while, in the supersonic stage, ion inertia plays an important role.

In Ref. 2, using the plasmon number invariant, an upper bound, and using a supersonic self-similar solution, a much lower estimate of the emissivity of a bunch of collapsing packets was obtained. It was argued that most of the harmonic emission would occur in the supersonic stage.

In the present work we examine the adiabatic stage numerically. We find that an adiabatically collapsing wave packet can lead to emission in the subsonic stage which is significantly higher than was thought possible. Due to subtle stationary phase effects, this can occur for packets whose width  $\Delta k$  is still smaller than  $p/v_{beam}$ . With reasonable choices for the number density of collapsing wave packets, we find levels of emission consistent with the experimental estimate<sup>1</sup> for the volume emissivity.

## II. EMISSIVITY OF A LANGMUIR WAVE PACKET

The emissivity is given by

$$\frac{dP}{d\Omega} = \frac{cr^2}{4\pi} \lim_{T \rightarrow \infty} \frac{1}{T} \int_{-T/2}^{T/2} dt E \cdot B ,$$

where  $c$  is the speed of light,  $E(B)$  is the electric (magnetic)

field, and  $r$  is the distance between the point of observation (where  $\mathbf{E} \times \mathbf{B}$  is evaluated) and the origin. In terms of the current,  $\mathbf{j}_{2\omega_p}$ , at twice the (local) plasma frequency,  $\omega_p$ , the emissivity is,

$$\frac{dp}{d\Omega} = \frac{\hat{r}}{4\pi c^2} \lim_{T \rightarrow \infty} \frac{1}{T} \int_{-\infty}^{\infty} \frac{d\omega}{2\pi} \omega k |j_{2\omega_p}(K\hat{r}, \omega)|^2 \sin^2 \theta , \quad (1)$$

where  $\hat{r}$  is the unit vector directed towards the point of observation,  $\omega$  is the frequency variable in the temporal Fourier transform of the current,  $K = [\omega^2 - \omega_p^2(r)]^{1/2}/c$ , and  $\theta$  is the angle between  $j_{2\omega_p}(K\hat{r}, \omega)$  and  $\hat{r}$ , i.e.,

$$\sin \theta = |\hat{j}_{2\omega_p}(K\hat{r}, \omega) \times \hat{r}| .$$

We now make use of Zakharov's fundamental simplification<sup>4</sup> by expressing the current as a slowly varying envelope  $j_{2\omega_p}$  and a rapidly oscillating phase:

$$j_{2\omega_p}(K\hat{r}, \omega_0) = \frac{1}{2} j_{2\omega_p} e^{-i\omega_0 t} + c.c. ,$$

where  $\omega_0$  is the photon frequency. The emissivity can then be expressed as<sup>2</sup>

$$\frac{dp}{d\Omega} \approx \frac{K_0 \omega_0 \sin^2 \theta_0}{8\pi c^2} \lim_{T \rightarrow \infty} \frac{1}{T} \int_{-T/2}^{T/2} dt |j_{2\omega_p}(K_0 \hat{r}, t)|^2 , \quad (2)$$

where Eq. (1) has been simplified by taking an "average" angle  $\theta_0$ , wavenumber  $K_0$ , and frequency  $\omega_0$  out of the integral, where

$$K_0 = [\omega_0^2 - \omega_p^2(r)]^{1/2}/c . \quad (3)$$

This procedure should be valid as long as the direction of  $\hat{J}_{2\omega_p}(\hat{K}\hat{r}, \omega)$  does not vary significantly over values of the integrand in Eq. (1) for which  $|\hat{J}_{2\omega_p}|^2$  is large.

### III. DYNAMICS OF A LANGMUIR WAVE PACKET

We describe the nonlinear wave packet by a Schrödinger equation with cubic nonlinearity<sup>2</sup>:

$$\left( i\partial_t + \frac{3T_e}{2m_e\omega_p} \nabla'^2 + \frac{e^2}{8m_e\omega_p \bar{T}} |\tilde{E}|^2 \right) \tilde{E} = 0 ,$$

where  $\nabla' \equiv \partial/\partial \tilde{r}'$ ;  $\bar{T} \equiv \gamma_e T_e + \gamma_i T_i$ ;  $T_e(T_i)$  is the electron (ion) temperature, with  $\gamma_e(\gamma_i)$  being the associated adiabaticity index;  $m_e$ ,  $e$  are the mass and charge of the electron, respectively;  $\tilde{E}$  is the envelope of the electric field  $\tilde{E}$ :

$$\tilde{E}(\tilde{r}', t) = \frac{1}{2} \tilde{E}(\tilde{r}', t) e^{-i\omega_p t} + c.c.$$

Under the following substitutions,

$$\tilde{E} \rightarrow (32\pi n_e \bar{T})^{\frac{1}{2}} \tilde{E} ,$$

$$t \rightarrow \omega_p t , \quad (4)$$

$$\tilde{r}' \rightarrow \sqrt{3} \lambda_D \tilde{r}' ,$$

where  $n_e$  is the background number density and  $\lambda_D = (T_e/4\pi n_e e^2)^{\frac{1}{2}}$  is the Debye length, the dimensionless form of Schrödinger's equation is obtained:

$$(i\partial_t + \frac{1}{2}\nabla^2 + |\mathbf{E}|^2)_{\mathbf{E}} = 0. \quad (5)$$

We note that the use of the Schrödinger equation is valid only in the subsonic stage where the ions are adiabatic.<sup>4,5</sup> In the Appendix this is justified for the time scale over which we calculate the emissivity.

The electrostatic field envelope,  $E$ , can be written as

$$\mathbf{E}(\mathbf{r}, t) = -\nabla [i\psi(\mathbf{r}, t)e^{i\mathbf{k}_0 \cdot \mathbf{r}} / k_0]. \quad (6)$$

Here,  $\mathbf{k}_0 = \omega_p \hat{\mathbf{v}}_b / v_b$  is the wave vector of the most unstable beam mode. At  $t = 0$ ,  $\psi(\mathbf{r}, t=0)$  is a real function which is localized around  $\mathbf{r} = 0$  and has spatial widths parallel and perpendicular to  $\mathbf{k}_0$ . These initial widths are set by the  $\mathbf{k}$ -space contours of the beam instability.<sup>2</sup> Roughly,  $|\nabla_{\parallel} \psi| \approx \Delta k_{\parallel} |\psi|$  and  $|\nabla_{\perp} \psi| \approx \Delta k_{\perp} |\psi|$  where  $\Delta k_{\parallel}$  and  $\Delta k_{\perp}$  are the parallel and perpendicular widths associated<sup>2</sup> with the beam instability.

Initially,  $\Delta k_{\parallel, \perp} \ll k_0$ .

Our central approximation will be to take  $\psi$  to be spherically symmetric at the initial and later times, so there will only be a symmetric width measure which changes with time. Throughout the calculation the inequality  $|\nabla \psi| \ll k_0 |\psi|$  will be satisfied, so the wave packet will remain relatively narrow in  $\mathbf{k}$ -space. This enables us to write Eq. (6) approximately as

$$\mathbf{E}(\mathbf{r}', t) \approx \hat{\mathbf{k}}_0 \psi(\mathbf{r}', t) e^{i\mathbf{k}_0 \cdot \mathbf{r}'} . \quad (6')$$

This field still has the phase factor,  $\exp(i\mathbf{k}_0 \cdot \mathbf{r}')$ , and is thus not spherically symmetric. However, the momentum  $\mathbf{k}_0$  can

be transformed away by the following gauge-frame transformation<sup>7</sup>

$$\begin{aligned}\psi(\tilde{r}', t) &= \phi(r, t) \exp(-ik_o^2 t/2), \\ \tilde{r} &= \tilde{r}' - k_o t.\end{aligned}\quad (7)$$

Using Eqs. (5)-(7) we find that the spherically symmetric scalar,  $\phi(r, t)$  satisfies,

$$(i\partial_t + \frac{1}{2}\nabla^2 + |\phi|^2)\phi = 0. \quad (8)$$

We have studied this equation in Ref. 7. It was shown there that the condition for the electrostatic approximation is

$$|\nabla\psi| \ll |k_o\psi|,$$

which is well satisfied for most times of interest. This differs substantially from the so-called head-on approximation often made<sup>8</sup> to calculate harmonic emission. In addition, conditions were found for the adiabatic approximation. These can be expressed as

$$|\phi|^2, k_o^2 \ll m/M.$$

In the Appendix we shall consider the validity of these inequalities for the parameters of the present calculation.

In terms of  $\phi$ , the current density  $j_{2\omega_p}$  can be written as [see Eq. (33) of Ref. 2]:

$$j_{2\omega_p}(\mathbf{k}_o \hat{r}, t) = \frac{-3\sqrt{8}\omega_p \lambda_D^2 \bar{T}}{\pi e} \mathbf{k}_o \left( \frac{\hat{r}}{2} - \hat{r} \cdot \hat{\mathbf{k}}_o \hat{\mathbf{k}}_o \right) \exp(-i\mathbf{k}_o \cdot \mathbf{k}_o \hat{r})$$

$$\int d^3r \phi^2(r) \exp[-i(\mathbf{k}_o \hat{r} - 2\mathbf{k}_o) \cdot \hat{r}] .$$

The angular part of the integral can be easily evaluated, leading to

$$|j_{2\omega_p}(\mathbf{k}_o \hat{r}, t)|^2 = \left[ \frac{\sqrt{24} \cdot 6\bar{T}\omega_p \lambda_D^2}{e(19-8\sqrt{3}\mu)^2} \right]^2 \left| \int_0^\infty r \phi^2 \sin(sr) dr \right|^2 , \quad (9)$$

where

$$s = |\mathbf{k}_o \hat{r} - 2\mathbf{k}_o| = \sqrt{3} \frac{v_{th}}{c} (19-8\sqrt{3}\mu)^{\frac{1}{2}} ,$$

$$\mu \equiv \hat{\mathbf{k}}_o \cdot \hat{r} . \quad (10)$$

The quantity  $s$  is the momentum mismatch between the harmonic photon and two plasmons. Also,  $v_{th}$  is the electron thermal speed. Use has been made of the fact that for emission at twice the local plasma frequency, Eq. (3) gives  $\mathbf{k}_o = \sqrt{3}(\omega_p/c)$ ; moreover  $|\mathbf{k}_o| = 2(\omega_p/c)$ . [Note that in Eq. (10) the dimensionless forms of  $\mathbf{k}_o$  and  $\mathbf{k}_o$  appear in accord with Eq. (4).]

Substituting Eq. (9) for the modulus-square of the  $2\omega_p$ -current into Eq. (2), we have the following expression for the emissivity of a single wave packet:

$$\frac{dp}{d\Omega} = \hat{r} \sin^2 \theta_o \frac{\sqrt{6}(6\bar{T})^2 \mathbf{k}_o \omega_o}{\pi(19-8\sqrt{3}\mu)e^2} \left( \frac{v_{th}}{c} \right)^2 v_{th} \lim_{T \rightarrow \infty} \frac{1}{T} \int_{-T/2}^{T/2} dt \left| \int_0^\infty dr r \phi^2 \sin(sr) \right|^2 . \quad (11)$$

## IV. NUMERICS AND SCALING

Equation (8) is solved in the Hilbert space of  $\phi$  by an implicit finite difference method in spherical geometry. The following invariants can easily be derived from this equation<sup>6,9</sup>:

$$\begin{aligned} I_1 &= \int_0^\infty |\phi|^2 r^2 dr , \\ I_2 &= \int_0^\infty (|\partial_r \phi|^2 - |\phi|^4) dr , \end{aligned} \quad (12)$$

where  $I_1$  is proportional to the boson number and  $I_2$  is proportional to the Hamiltonian. The accuracy and stability of the numerical scheme is checked by the (semi-) invariance of the discrete forms of the functionals  $I_1$  and  $I_2$  on the Hilbert space.

The computations are started by choosing a Gaussian for the initial potential:

$$\phi(r, t=0) = \phi_0 \exp(-2r^2/\ell^2) . \quad (13)$$

For the particular mesh size chosen, we take  $\ell = 5.66$ . From Eq. (9b) of Ref. 2, and the parallel half-width of the packet is found to be

$$\frac{\Delta k_{||}}{k_0} = \frac{1}{4} \frac{\Delta v_b}{v_b} ,$$

[Eq. (9b), Ref. 2], where  $v_b$  is the beam speed and  $\Delta v_b$  the spread in this speed. From the values quoted in Ref. 2 we find

$$\frac{\Delta k_{||}}{k_D} \equiv \frac{\Delta k_{||}}{1/\lambda_D} = \frac{1}{4} \frac{\Delta v_b}{v_b} \cdot \frac{k_o}{k_D} \approx \frac{3}{4} \times 10^{-3} .$$

Note that the Schrödinger equation (5) is invariant under a stretching of  $r'$  by a factor  $A$ , provided the time,  $t$ , is stretched by  $A^2$ , and  $E$  is reduced by  $A$ . With  $A = 300$ , our choice of  $\ell = 5.66$  can be made to correspond to the above value of  $\Delta k_{||}$ . We therefore arrive at the following approximate scaling from type III values (subscript "III") to computational values (subscript "c"):

$$\begin{aligned} (\phi)_{III} &= (300)^{-1} (\phi)_c , \\ (t)_{III} &= (300)^2 (t)_c , \\ (r)_{III} &= 300 (r)_c . \end{aligned} \tag{14}$$

We choose  $(\phi_o)_c$  to be 1.18, corresponding to an average energy density,  $(W)_c$ , at twice the threshold value.<sup>2,7</sup> Using the scaling of Eq. (14) this leads to a value for  $(W)_{III} \approx 10^{-4}$ , which is in agreement with the value used in Ref. 2. Further, from Eqs. (4), (10), and (14) we find that

$$(S)_c = 300 (S)_{III} = 300 \sqrt{3} \cdot \frac{v_{th}}{c} (19 - 8\sqrt{3})^{\frac{1}{2}} . \tag{15}$$

With  $(v_{th}/c) \approx 4.5 \times 10^{-3}$  in Eq. (15),  $S$  is sufficiently large for all  $\phi$  that the spatial integral in Eq. (11) is seen to be practically zero for an initial  $\phi$  of the form of Eq. (13). Thus, the scaling implied by  $\Delta k_{||}$  [Eq. (9b) of Ref. 2] leads to a negligible emissivity initially. The interesting feature that emerges from our computations is that the modulus and phase of  $\phi$  change sufficiently in the subsonic regime to enable substantial emission to occur.

## V. RESULTS AND DISCUSSION

Figures 1(a) and 1(b) show the time development of the emissivity of a single packet, i.e., the expression given in Eq. (11) before performing a time-average. The emission grows in an approximately exponential manner for most of the time development of the packet, reaching a maximum and decreasing thereafter until the collapse point. In this calculation  $\theta_0$  has been taken as  $45^\circ$  [see the remark following Eq. (2)] and  $\mu = \hat{k}_0 \cdot \hat{r}$  has been taken as  $\sqrt{3}/2$  ( $\hat{k}_0$  making an angle of  $30^\circ$  with  $\hat{r}$ ).

We note the emissivity climbs from an initially negligible value to a peak many orders of magnitude larger, and then begins to decay. The peak occurs at  $0.994 t_c$ , where  $t_c$  is the adiabatic collapse time. To understand this behavior, we note that  $dP/d\Omega$  in Eq. (11) is proportional to the absolute square of the following integral over  $\phi^2$ :

$$I \equiv \int_0^\infty dr r \phi^2 \sin Sr . \quad (16)$$

Let us now write  $\phi = A e^{i\alpha}$ , where  $A(r)$  is a real modulus, and  $\alpha(r)$  a real phase, and both are spherically symmetric. The integrand will be largest around the peak of  $rA^2$ , provided the phase factors  $e^{i(2\alpha \pm Sr)}$  do not produce severe phase mixing.

For our initial  $\phi$  of Gaussian form,  $\alpha$  is zero and the quantity  $rA^2 \propto r e^{-2r^2/\ell^2}$  peaks at  $r_A = 2$ , and has a width of  $\Delta r_A \approx 2$ . However,  $\sin Sr$  oscillates with a half wavelength  $\pi/S \approx 0.5$ . Hence, there is strong phase-mixing of the emissivity. This corresponds physically to the failure to conserve momentum in the coalescence of two plasmons to produce a photon.

At later times, the packet has collapsed considerably, so that  $rA^2$  can peak at smaller  $r$ -values with a smaller half-width, which is therefore less susceptible to phase mixing. In Figure 2(a), we have plotted  $A^2$  as a function of  $r$  at  $t = 0$  and at  $t = 1.312$ . The half-width of  $A^2$  has decreased by a factor of 6. In addition, the quantity  $rA^2$  now peaks at  $r_A = 0.25$  with a half-width  $\Delta r_A \approx 0.25$ . This peak and half-width coincide with the peak and half-width of the first maximum of  $\sin rS$ , which would seem to indicate reduced phase mixing. However, effects associated with the phase  $\alpha$  of the field are also beginning to come into play at this time. A region of stationary phase in the integrand of Eq. (16) corresponds to a range of points where  $|S \pm (\partial\alpha/\partial r)|$  becomes significantly smaller than  $S$ . Such a region of stationary phase is beginning to occur at  $t = 1.312$ , and is seen to overlap the peak of  $rA^2$ . This also contributes to the reduction of phase mixing. The normalized gradient of  $\alpha$ ,  $(\partial\alpha/\partial r)/S$  is plotted as a function

of  $r$  in Fig. 2(b) for the time  $t = 1.312$ , and is seen to reach a maximum absolute value of about 1/2.

The phase,  $\alpha$ , is also responsible for the eventual reduction of emissivity at later times. In Fig. 3, we have plotted  $(\partial\alpha/\partial r)/S$  as a function of  $r$  at the later time  $t = 1.324$ , corresponding to a reduced emissivity [see Fig. 1(b)]. The emissivity is reduced at this time because of the positive and negative oscillations in the gradient of  $\alpha$  which once more lead to phase mixing. The reduction can also be viewed as a cancellation of the integrals over  $e^{i(2\alpha+Sr)}$  and  $e^{+i(2\alpha-Sr)}$ , which have slightly different narrow regions of stationary phase.

A word is in order concerning the physical significance of the phase  $\alpha$ . The momentum density carried by the Langmuir field is<sup>7</sup>  $p \equiv (1/2i)(E_i^* \nabla E_i - E_i \nabla E_i^*)$ . In our case, this reduces to,

$$p = [k_0 + \nabla \alpha(r)] |E|^2.$$

Hence,  $\nabla \alpha$  is a local plasmon momentum, which arises from the nonlinear dynamics of collapse, and adds to  $k_0 = \omega_p v_b / v_b$ . (We should bear in mind, however, that average plasmon momentum is conserved<sup>7</sup> and equal to  $k_0$  in the adiabatic stage of collapse so  $\langle \nabla \alpha \rangle \equiv \int d^3r |E|^2 \nabla \alpha / \int d^3r |E|^2 = 0$ .) The momentum conservation in the coalescence of two plasmons to produce a photon thus becomes  $2k_0 - K_0 - 2\nabla \alpha \approx 0$ , which is essentially the stationary phase condition in the integral in Eq. (16). As the square modulus  $A^2$  narrows spatially, the failure of this phase matching condition is less serious. The gradient of  $A$  is  $|\nabla A/A|$ , which we may identify as a spread of wavenumbers,  $\Delta k$ . Its maximum

value of  $\Delta k : (\Delta r_A)^{-1}$  becomes broader as real space collapse progresses (as  $\Delta r_A$  tends to zero). At  $t = 0$ , we find  $\Delta k/k_o \approx 10\%$ , whereas at time  $t = 1.316$ ,  $\Delta k/k_o \approx 60\%$ . Thus, stationary phase becomes less important as collapse proceeds. The exception is the late stages, in which the phase oscillates rapidly, causing the resumption of phase mixing.

It is important to note the role of coherent phase in this calculation. Past estimates<sup>8</sup> of the emissivity rely on the random phase approximation and assumptions about the relative-size of the average plasmon momentum,  $k_o$ , and the photon momentum,  $K_o$ . For example, in the head-on approximation,<sup>8</sup> the plasmon momentum  $k_o$  is assumed to be  $\gg K_o$ . No such assumptions are made here, and in fact the plasma wave momentum is not  $\gg K_o$ . The coherence of each collapsing packet is taken into account, although the contributions from different packets are incoherent with respect to each other. Statistical assumptions underly only our treatment of the density of collapsing packets, which yields the volume emissivity.

In order to compute the volume emissivity we need to know the density of collapsing packets  $n_c$  in the beam. We just quote the estimate made in Ref. 2:

$$n_c = \gamma_g \tau_c F n_o ,$$

[Eq. (59), Ref. 2], where  $\gamma_g$  is the beam growth rate,  $\tau_c$  is the collapse time,  $n_o$  is the density of wave packets, given by

$$n_o \approx \Delta k_{\parallel} (\Delta k_{\perp})^2 / 8 ,$$

[Eq. (56), Ref. 2] in terms of the parallel,  $\Delta k_{||}$ , and perpendicular,  $\Delta k_{\perp}$ , width of a single packet, and  $F$  is a dimensionless unknown parameter in our model that essentially measures the fraction of energy transferred from the beam to collapsing packets.

To work out the time-averaging implied in Eq. (11) we follow Ref. 2 and compute the fractional time the emissivity is within a half-width of its peak value. From Fig. 1 this fraction is roughly .025/1.325. Thus, we write,

$$\left\langle \frac{dP}{d\Omega} \right\rangle_{\text{time}} \approx \frac{0.025}{1.325} \times 0.16 = 0.003 \text{ ergs s}^{-1} \text{ ster}^{-1} ,$$

and obtain for the time-average volume emissivity the following result:

$$\begin{aligned} \mathcal{J}_{2\omega_p} &= n_e \langle dP/d\Omega \rangle , \\ &= \frac{\gamma q}{8} \tau_c F \Delta k_{||} (\Delta k_{\perp})^2 \times 0.003 , \\ &= \frac{1}{8} \left( \frac{\pi}{8e} \right)^{\frac{1}{2}} \frac{n_b}{n_e} \left( \frac{v_b}{\Delta v_b} \right)^2 \times 1.3265 \times 300 \times F \\ &\quad \times \frac{1}{4} \frac{\Delta v_b}{v_b} \cdot \frac{\omega_p}{v_b} \cdot \left( \frac{1}{4} \right)^2 \left( \frac{\omega_p}{v_b} \right)^2 \times 0.003 , \end{aligned}$$

where  $1.3265 \times 300/\omega_p$  is the numerically determined<sup>8</sup> collapse time,

$$\frac{\gamma q}{\omega_p} = \left( \frac{\pi}{8e} \right)^{\frac{1}{2}} \frac{n_b}{n_e} \left( \frac{v_b}{\Delta v_b} \right)^2 ,$$

following Eq. (62) of Ref. 2;  $n_c$  is the background density,

$40 \text{ cm}^{-3}$ ,  $n_b$  is the beam density,  $10^{-6} n_e$ ,  $v_b$  and  $\Delta v_b$  are the beam speed and spread in speed, with  $\Delta v_b/v_b \approx 1/3$ ,

$$\Delta k_{\perp}/k_o \approx 1/4 ,$$

Eq. (9a), Ref. 2, and

$$\Delta k_{\parallel}/k_o = (1/4)(\Delta v_b/v_b) ,$$

Eq. (9b), Ref. 2. The quantity  $F$  is a factor (described in Ref. 2) which relates to the depletion of beam modes according to two different evolution scenarios. The final answer for the volume emissivity is therefore

$$J_{2\omega_p} \approx 1 \times 10^{-20} F \text{ ergs cm}^{-3} \text{ s}^{-1} \text{ ster}^{-1} . \quad (15)$$

This is compared with the measured<sup>1</sup> value of  $2 \times 10^{-23}$  [see also Eq. (1) of Ref. 2]. We see that in order to reconcile the two values,  $F$  has to be around  $10^{-3}$ . Considering the arguments presented in Ref. 2 concerning the magnitude of  $F$ , we see that a value of  $10^{-3}$  is not unreasonable.

## VI. CONCLUSION

Our calculations for a group of collapsing Langmuir wave packets account quite reasonably for the observed emissivity associated with type III solar radio bursts. These results are encouraging enough to merit further elaboration; in particular, there is a clear need for a better estimate of the density of "collapsons."

**ACKNOWLEDGMENTS**

This work was supported by the Atmospheric Sciences Section of the National Science Foundation under Grants ATM 76-14275 and 7916837 to the University of Colorado. The work of M. V. Goldman was also supported by the Air Force Office of Scientific Research through Contract #AFF49620-76-C-0005 and Grant 80-0022, also awarded to the University of Colorado.

## REFERENCES

1. D. A. Gurnett and R. R. Anderson, *Science* 194, 1159 (1976);  
*J. Geophys. Res.* 82, 632 (1977).
2. M. V. Goldman, G. F. Reiter and D. R. Nicholson, *Phys. Fluids* 23, 388 (1980)..
3. D. R. Nicholson, M. V. Goldman, P. Hoyng, J. C. Weatherall, *Astrophys. J.* 223, 605 (1978).
4. V. E. Zakharov, *Zh. Eksp. Teor. Fiz.* 62, 1745 (1972) [Sov. *Phys.-JETP* 35, 908 (1972)].
5. M. V. Goldman and D. R. Nicholson, *Phys. Rev. Lett.* 41, 406 (1978).
6. J. Gibbons, S. G. Thornhill, M. J. Wordrop and D. ter Haar, *J. Plasma Phys.* 17, 153 (1977).
7. M. V. Goldman, K. Rypdal, and B. Hafizi, *Phys. Fluids* 23, in press.
8. D. B. Melrose and J. E. Stenhouse, *Astron. Astrophys.* 73, 151 (1979).
9. P. B. Budneva, V. E. Zakharov and V. S. Synakh, *Fiz. Plazmy* 1, 606 (1975) [Sov. *J. Plasma Phys.* 1, 335 (1975)].

APPENDIX: VALIDITY OF ADIABATIC AND ELECTROSTATIC APPROXIMATIONS

Our calculations have been based on the cubic Schrödinger equation, (5). The validity of this equation requires that the wave field be predominately electrostatic, and the low frequency (ion) motions be adiabatic. The conditions for both approximations are set forth in the Appendix of Ref. 7.

For the waves to be electrostatic, we must satisfy

$$\Delta k/k_o \ll 1 ,$$

where  $\Delta k \approx |\nabla|\phi|/\phi|$  is a measure of the gradient of  $\phi$ . Our wave packets satisfy this criterion up until the very latest times of  $t = 1.324$ , where  $\Delta k/k_o \approx 60\%$ .

The adiabatic ion approximation requires that

$$k_o^2 , |E|^2 < m/M = 5.4 \times 10^{-4} .$$

The condition on  $k_o$  means that the mean wave packet group velocity is slow enough for the ions to follow the ambipolar field adiabatically. Since  $k_o = 10^{-2}$  in our calculations, it is always satisfied. The second condition essentially requires that the collapse speed remain subsonic. Taking into account the scaling of  $\phi$  in Eq. (14), we may rewrite this condition as

$$|\phi_c|^2 \ll 50 .$$

This condition breaks down at  $r = 0$  near the time of peak emissivity at  $t = 1.312$ . However, only the peak of  $r|\phi_c|^2$  is

significant for the emissivity in Eq. (16). At this peak, we find from Fig. 2 that  $|\phi_c|^2$  is of order 50, so the adiabatic approximation is marginal. At later times, it would appear to be violated. However, we have found the emissivity to go down at these times [see Fig. 1(b)], so our calculation probably does not overestimate the emissivity.

## FIGURE CAPTIONS

FIG. 1. Temporal development of emissivity from a collapsing wave packet. Note the logarithmic scale in (a) for the early stage, and the linear scale in (b), close to the collapse time. The scale on the time axis is in  $\omega_p^{-1}$  and the computational scaling [see Eqs. (14) in text]. Collapse time is 1.3265.

FIG. 2. (a) Square modulus of Langmuir field,  $|\phi|^2$  as a function of  $r$  at  $t = 0$  and at  $t = 1.32$ . Note the Gaussian at  $t = 0$  appears flat because of limited range of  $r$  plotted. (b) Gradient of intrinsic phase of Langmuir envelope in units of momentum mismatch  $S$ , as a function of  $r$ , for  $t = 1.312$ .

FIG. 3. Gradient of intrinsic phase of Langmuir envelope in units of momentum mismatch  $S$ , as a function of  $r$  for  $t = 1.324$ .

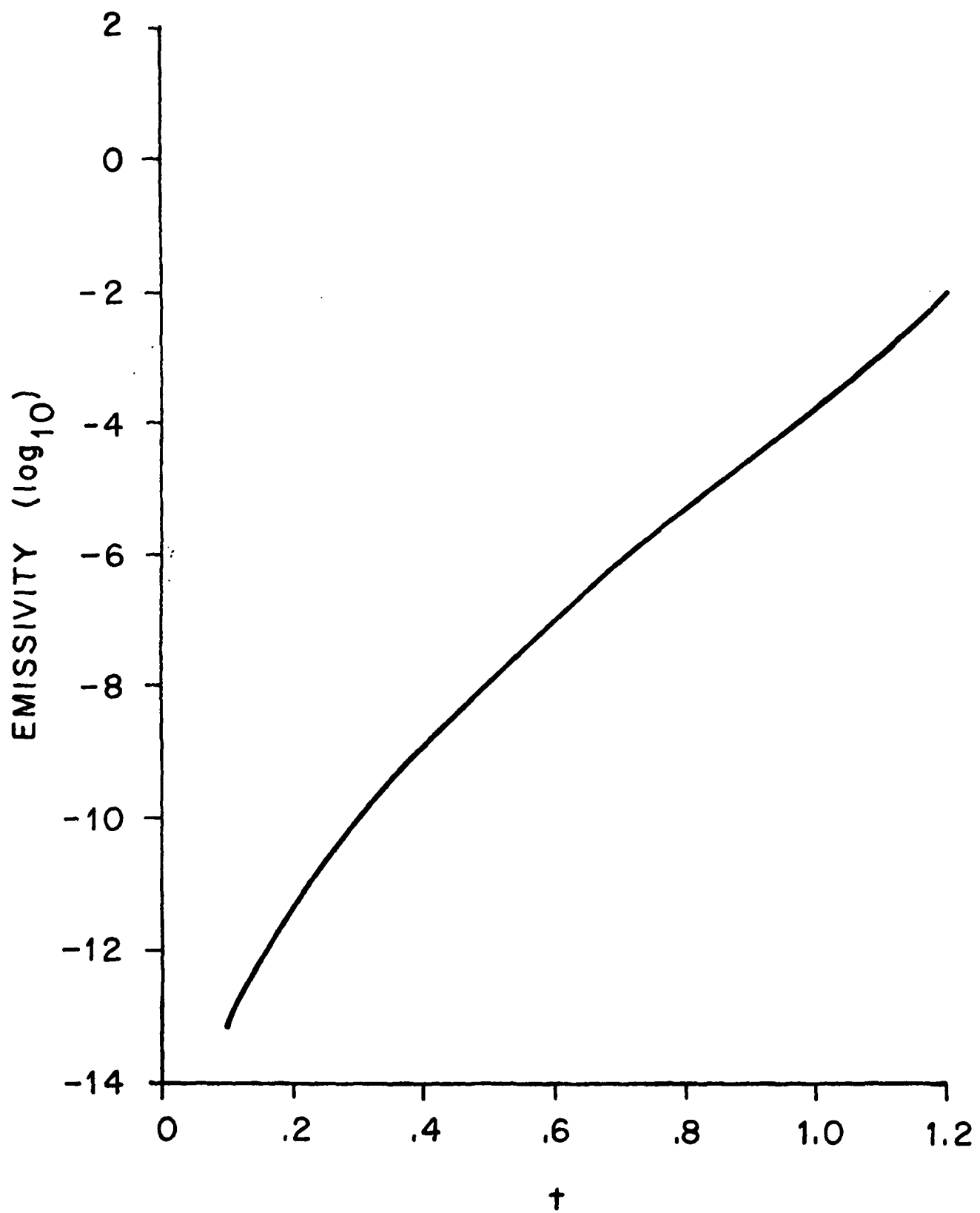


FIGURE 1(a)

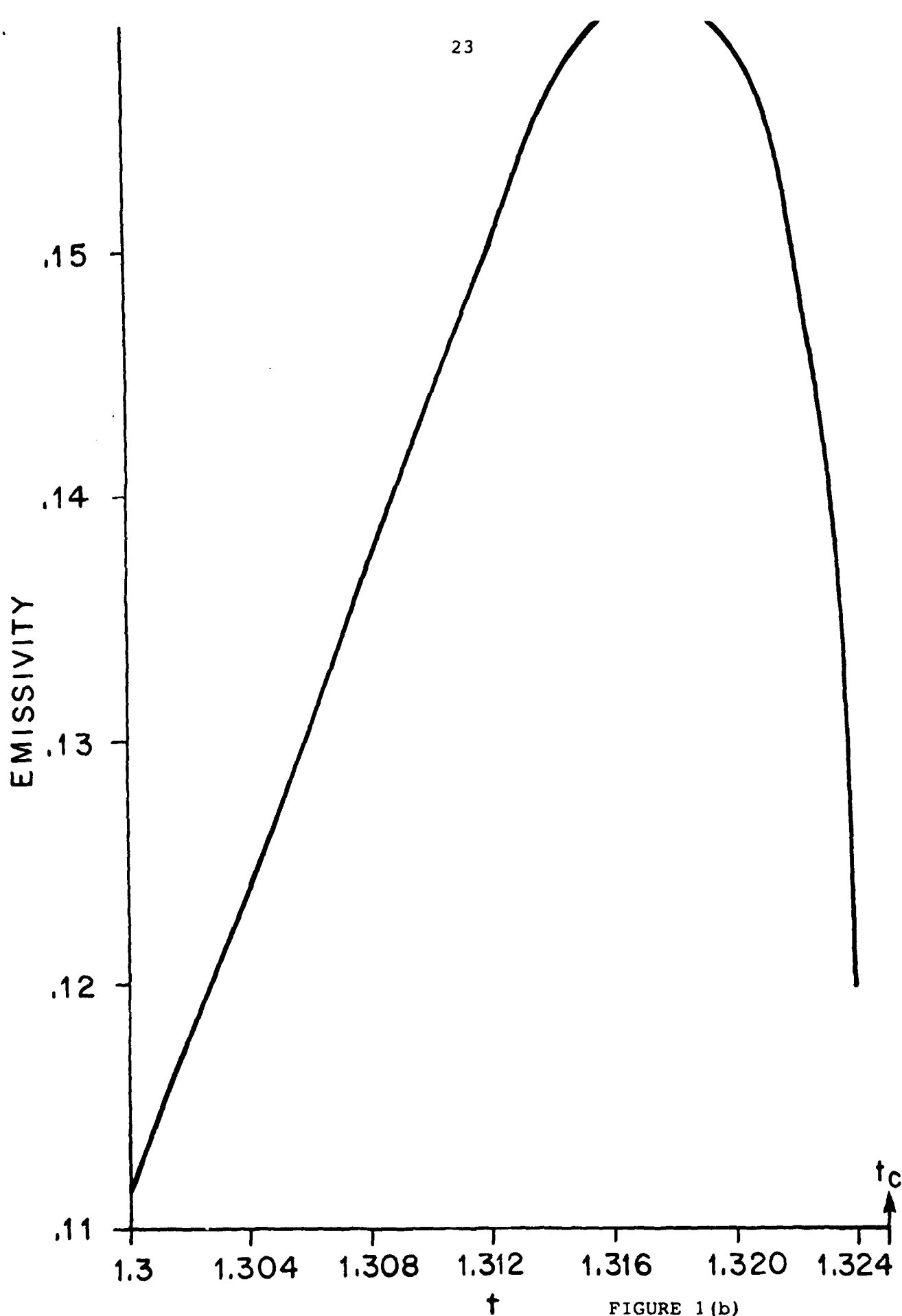


FIGURE 1 (b)

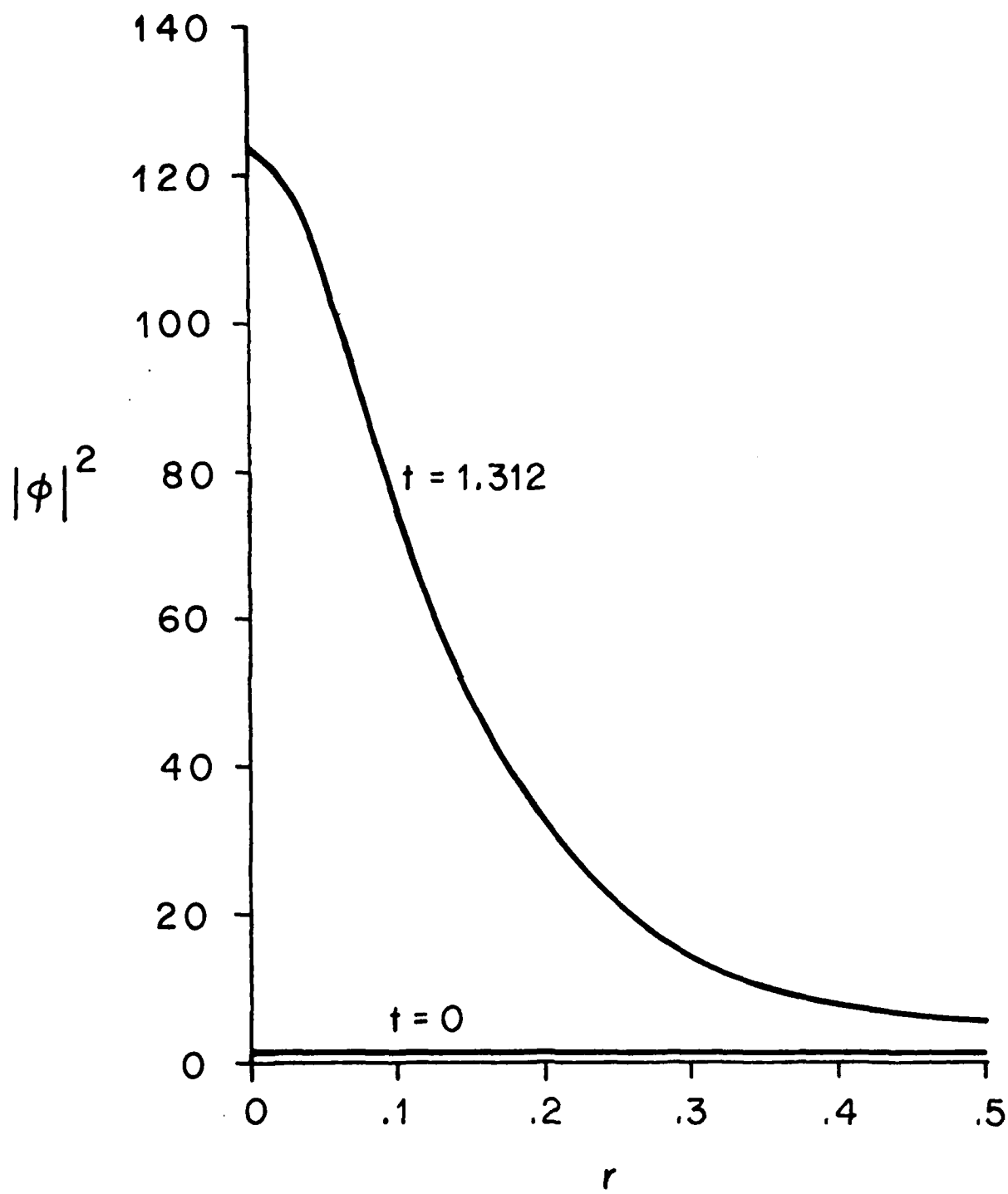


FIGURE 2(a)

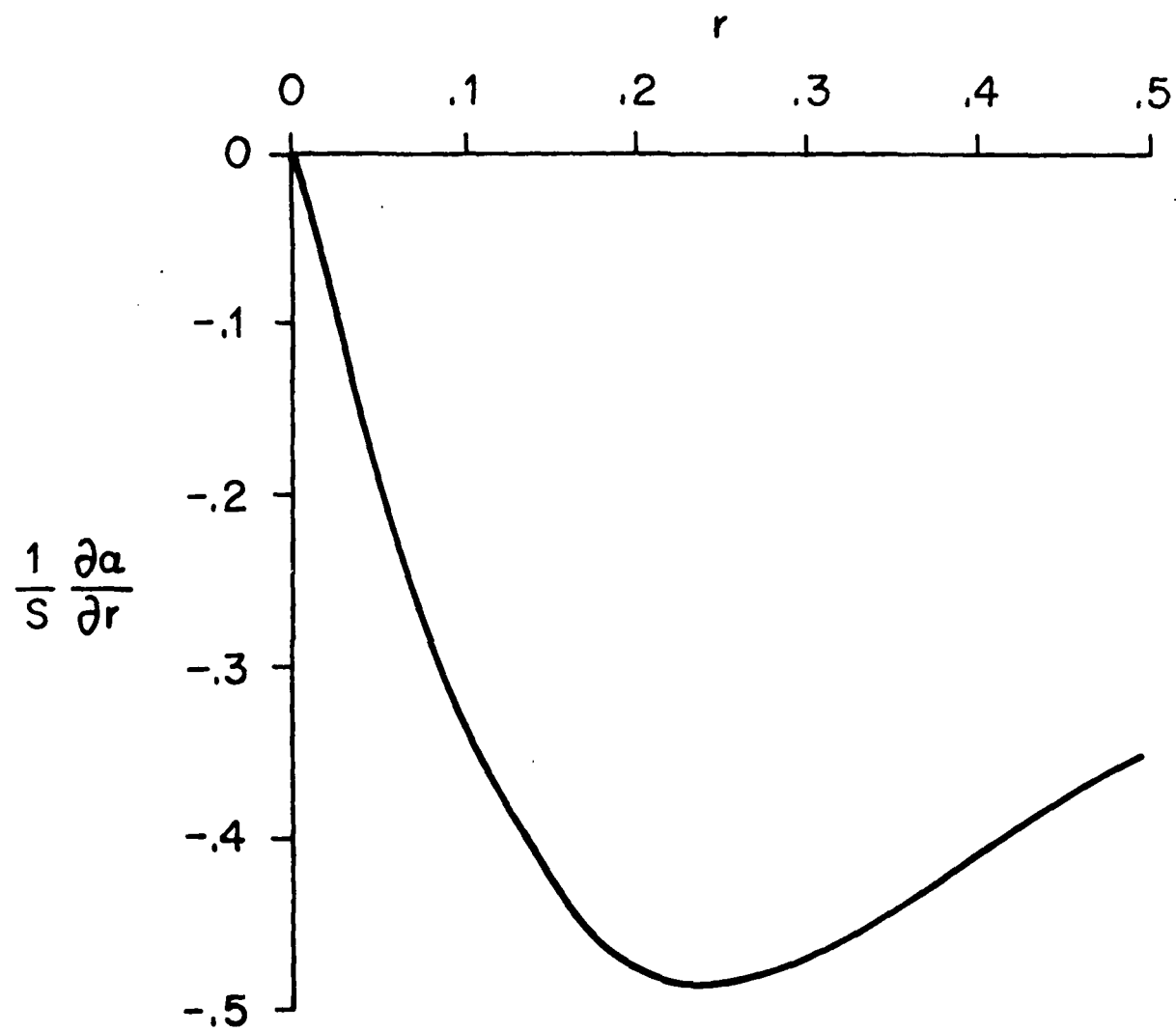


FIGURE 2 (b)

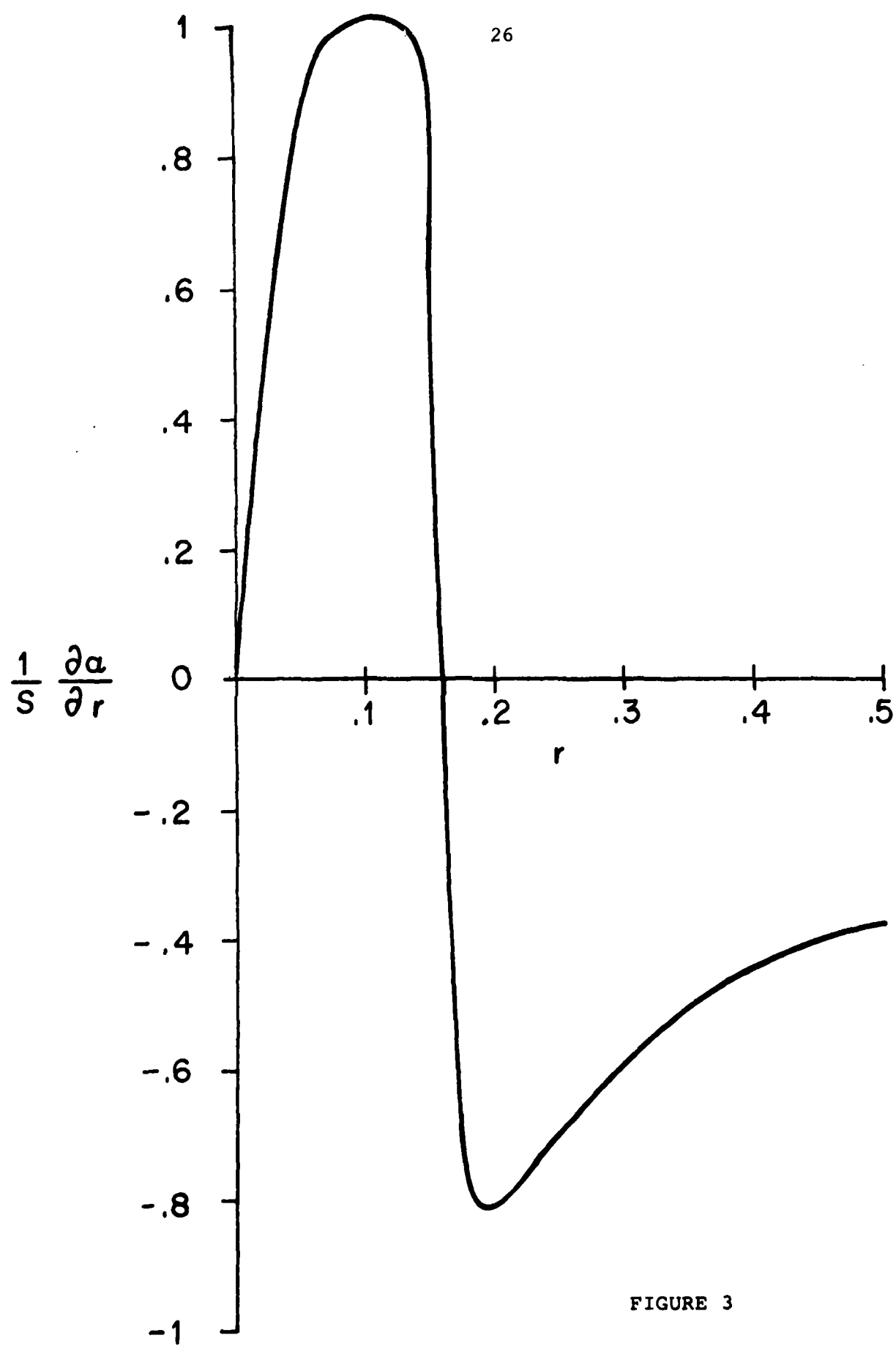


FIGURE 3

## APPENDIX D

D. "Langmuir Collapse in a Weak Magnetic Field"  
M. V. Goldman, J. C. Weatherall, and D. R. Nicholson  
Physics of Fluids, April 1981, in press

Langmuir Collapse in a Weak Magnetic Field

Martin V. Goldman, James C. Weatherall

Department of Astro-Geophysics, University of Colorado,  
Boulder, Colorado 80309

and

Dwight R. Nicholson

Department of Physics and Astronomy, University of Iowa,  
Iowa City, Iowa 52242

March 1980

ABSTRACT

With magnetic fields that are not too weak, Langmuir collapse times can be prolonged and the packet geometry significantly distorted.

Submitted to Physical Review Letters

CU #1037

Within the last few years, there have been great theoretical strides in the understanding of "self-focusing" mechanisms for the nonlinear saturation of certain Langmuir wave instabilities.<sup>1-5</sup> In particular, it has been shown<sup>4</sup> for a class of weak "bump-on-tail" instabilities that direct spatial collapse can occur, due to the self-ponderomotive force of intense Langmuir wave packets. This may have important implications for Type III solar radio bursts,<sup>4,5</sup> for the radar-modified ionosphere,<sup>6</sup> and for laboratory and space beam-plasma systems. Undriven Langmuir collapse cannot occur in fewer than two dimensions, so numerical simulation study is difficult. The relevance of one-dimensional simulations has not been established.

In physical problems a weak background magnetic field is often present, pointing parallel to the propagation direction of the driven Langmuir wave packet. Linear stability analyses have recently been performed<sup>7,8</sup> for monochromatic Langmuir waves in the presence of a weak magnetic field.

There has been little or no work on the effects of a magnetic field on collapse outside the Soviet Union. One theory<sup>6</sup> claims to have found stable pancake-shaped Langmuir solitons pumped by radio waves in the ionosphere, in the presence of the geomagnetic field. Other studies<sup>6,9,10</sup> have shown Langmuir collapse in magnetic fields, but only for special symmetries and in parameter regimes apparently unrelated to experiment. Our work differs from these in terms of parameter regime, geometry, phenomena observed, and physical explanation.

First, we shall demonstrate numerically that weak magnetic fields can significantly prolong the time for collapse of a broad-band Langmuir wave packet, and alter its geometry into a more dipolar form, but cannot render it one-dimensional. Second, we prove analytically a magnetic virial theorem which gives sufficient conditions for collapse, and helps explain its retardation. Third, we demonstrate that measured mean solar magnetic fields do not affect the Langmuir collapse associated with Type III bursts at 0.5 A.U. Fluctuations in the magnetic field would have to be an order of magnitude larger than the mean to have significant consequences for collapse.

The Langmuir field envelope,  $\underline{E}$ , obeys a generalized nonlinear Schrödinger equation:

$$i\partial_t \underline{E} + \frac{1}{2} \nabla \cdot \underline{E} - \frac{C^2}{2} \nabla \times \nabla \times \underline{E} - \frac{\Omega^2}{2} \underline{P} \cdot \underline{E} - \delta n \underline{E} = 0. \quad (1)$$

Here, the units of time are  $\omega_p^{-1}$ , length is measured in units of  $\sqrt{3}$  times the Debye length,  $|\underline{E}|^2$  has the units of  $64\pi n\theta$ , where  $\theta$  is the common electron and ion temperature, and  $C^2 \equiv c^2/3v_e^2 \gg 1$ ,  $\Omega^2 \equiv \omega_{ce}^2/\omega_p^2 \ll 1$ . The magnetic dispersive term,  $(-\Omega^2/2)(\underline{P} \cdot \underline{E})$ , arises from an expansion in the magnetic field. The operator  $P_{ij} = \delta_{ij} - \hat{b}_i \hat{b}_j$  projects out vector components perpendicular to the magnetic field direction,  $\hat{b}$ . In the linear limit, Eq. (1) gives the quasilongitudinal dispersion relation for an oblique Langmuir-wave envelope:

$$\omega = \frac{k^2}{2} + \frac{\Omega^2}{2} \sin^2 \theta, \quad (2a)$$

Here,  $\theta$  is the angle between  $\underline{k}$  and  $\hat{\underline{b}}$ . The condition for neglect of the transverse part of the field is

$$\Omega^2 \sin^2 \theta \ll C^2 k^2 , \quad (2b)$$

which we shall assume is well-satisfied. Physical driving terms, such as growth due to a beam, have been omitted from Eq. (1) on the grounds that the driving time scale is slower than the nonlinear time scales.<sup>4</sup>

The density deviation,  $\delta n$ , is in units of  $2n_0$ , where  $n_0$  is the average background density. It obeys a hydrodynamic equation driven by ponderomotive force:

$$(C_s^{-2} \partial_t^2 + \hat{v} \partial_t - \nabla^2) \delta n = v^2 |E|^2 . \quad (3)$$

Here  $C_s$  is the ion acoustic speed, in units of  $\sqrt{3\theta/m_e}$ , and  $\hat{v}$  is an operator representing the effect of Landau damping of ion acoustic waves in an equal temperature plasma. We have also briefly studied<sup>7</sup> magnetic field contributions to equation (3), but find no effect on the nonlinear evolution of a broadband packet (only a small volume in  $k$ -space is affected).

Our numerical work assumes  $\underline{E} = -\nabla\phi$ , and generates solutions to Eq. (3), together with the divergence of Eq. (1), namely,

$$i \partial_t \nabla^2 \phi + \frac{1}{2} v^4 - \frac{v^2}{2} \underline{v} \cdot \underline{P} \cdot \underline{v} \phi - \underline{v} \cdot (\delta n \underline{v} \phi) = 0 . \quad (4)$$

In  $k$ -space we take an initial packet of randomly phased modes with a shape characteristic of a prior, slow bump-on-tail instability.<sup>5</sup> In real space this appears as an initial pattern

of wave packets oriented along the beam direction (see Fig. 1a). The initial energy density of the packet is  $W \equiv 16\langle|E|^2\rangle = 5.6 \times 10^{-4}$ , and it is centered about a  $k$ -space wavenumber of  $k_o = 0.011 k_D$ . The parallel and perpendicular widths are  $\Delta k_{\perp} = 0.25 k_o$ ,  $\Delta k_{\parallel} = 0.17 k_o$ . These are parameters thought to be associated with type III solar radio bursts. In the absence of a magnetic field,  $W$  exceeds the threshold<sup>4,5</sup> for adiabatic collapse,  $\sim 24[(\Delta k_{\perp})^2 + (\Delta k_{\parallel})^2]$ , and the packets collapse, as shown in Fig. 1b.

Next, with the same initial conditions, we introduce a small magnetic field in the  $k_o$ -direction, such that  $\Omega = 0.1$ . This is sufficient to make the magnetic dispersion in Eq. (2) exceed the thermal dispersion. The collapse is slowed down by a factor 5, as shown in Figs. 1c and 1d. The packets now tend toward a pancake shape, but are not one-dimensional.

Neither the slowdown nor the pancake shape is found when  $\Omega = 0.01$ , which is an experimentally found<sup>11</sup> upper bound on the mean solar magnetic field at 0.5 A.U.

We shall argue that the effect of the small magnetic field when  $\Omega = 0.1$  is to retard direct adiabatic collapse, allowing induced scattering of Langmuir waves off (dynamic) ions<sup>7,12</sup> to occur. For our parameters, the scattered waves are in the forward direction,<sup>13</sup> with wavenumber on the order of  $k_o/3$ . The evidence for this is shown in the  $k$ -space picture in Fig. 1f for the  $\Omega = 0.1$  case, compared to Fig. 1e in the non-magnetic case,  $\Omega = 0$ . The geometry and time-scale for the

configuration shown in Fig. 1f are similar to what we obtain for a monochromatic initial packet, with  $B$  set equal to zero (not shown here). For a monochromatic initial packet, direct collapse cannot occur, because there is no ponderomotive force, and the linear induced scatter instability dominates at early times. This enables a fairly positive identification of Fig. 1f as resulting from induced scatter off ions. Such scatter is principally in the B-direction. A more one-dimensional configuration in  $k$ -space results, followed by collapse.

In Fig. 2 we plot, as a function of  $\tau$ , the time for the peak energy density in a collapsing packet to increase by a factor of ten. Significant slowing requires  $\Omega \geq 0.1$ .

We now offer a theoretical explanation for why the direct collapse is slowed down by almost an order of magnitude when  $\Omega = 0.1$ . The results shown in Fig. 1 all occur in the regime of adiabatic ions, where Eq. (3) reduces to,

$$\delta n = -|E|^2 . \quad (5)$$

We now derive a virial theorem for Eqs. (4) and (5) (with  $E = -\Gamma\phi$ ). Such theorems are based on continuity and conservation laws for Eq. (4). To generate these laws we first require the Lagrangian density,

$$L = \frac{i}{2} (\dot{\phi}^* \nabla^2 \phi - \dot{\phi} \nabla^2 \phi^*) - \frac{1}{2} |\nabla^2 \phi|^2 - \frac{\Omega^2}{2} (\nabla \phi \cdot \underline{P} \cdot \nabla \phi^*) + \frac{1}{2} |\nabla \phi|^4 . \quad (6)$$

This Lagrangian density depends on  $\dot{\phi}$ ,  $\nabla\phi$ ,  $\nabla^2\phi$ , and their complex conjugates. The dependence on  $\nabla^2\phi$  requires a generalization of Lagrange's equation.<sup>15</sup> Hence, the equation of motion [Eq. (4)] is obtained from  $\partial_t^L \dot{\phi}^* + \nabla \cdot L \nabla \phi^* - \left[ (\partial^2 / \partial x_i^2) [\partial L / \partial (\partial^2 \phi^* / \partial x_i^2)] \right] = 0$ , where a subscript of  $L$  indicates differentiation with respect to that variable.

From the Lagrangian density we derive<sup>15,16</sup> a momentum equation

$$\partial_t p + \nabla \cdot T = 0, \quad (7)$$

where the momentum density is  $p = (\underline{E}_L^* \cdot \nabla \underline{E}_L - \underline{E}_L \cdot \nabla \underline{E}_L^*) / 2i$ , with  $\underline{E}_L \equiv -\nabla\phi$ . The stress tensor for a Lagrangian with higher order derivatives is<sup>15,16</sup>:

$$T_{ij} = \frac{\delta_{ij}^L}{2} - \phi_j^* \partial_i \phi - \left[ \phi_{ij}^* - \partial_j \frac{\partial}{\partial x_i} \right] \frac{\partial L}{\partial (\partial^2 \phi^* / \partial x_i^2)}$$

+ complex conjugate.

A subscript  $i$  on  $\phi$  or  $\phi^*$  indicates a derivative with respect to  $x_i$ , and there is no sum over  $i$ .

The total momentum,  $\underline{P} = \int d\underline{x} p$  is conserved for fields which fall to zero fast enough at infinity in the (unbounded) plasma.

Another conserved quantity is

$$H \equiv \frac{1}{2} \int d\underline{x} [|\nabla \cdot \underline{E}_L|^2 - |\underline{E}_L|^4] + H_B, \quad (8a)$$

where

$$H_B \equiv \frac{\Omega^2}{2} \int d\underline{r} |\underline{E}_L \cdot \underline{P}|^2 . \quad (8b)$$

In Eq. (8a) both the magnetic and thermal dispersion terms work in opposition to the nonlinear refraction,  $|\underline{E}_L|^4$ .

The final equation needed to generate a virial theorem is obtained from Eq. (1) rather than Eq. (4). For an initially longitudinal wave packet, the transverse part of the field,  $\underline{E}_T$ , will remain small as long as inequality (2b) is satisfied, and as long as  $\Delta k \ll k_0$ . Then  $|\underline{E}_T| = O(|\underline{E}_L|/c^2) \ll |\underline{E}_L|$ . We take the scalar product of Eq. (1) with  $\underline{E}_L^*$  and subtract the complex conjugate to obtain the approximate result,

$$\partial_t |\underline{E}_L|^2 + \nabla \cdot \underline{P} = 0 . \quad (9)$$

From Eqs. (7) and (9) we derive a virial theorem<sup>4</sup> for the mean packet width,  $\langle \delta r^2 \rangle \equiv \int d\underline{r} \delta r^2 |\underline{E}_L|^2 / N$ , where  $N \equiv \int d\underline{r} |\underline{E}_L|^2$  is the conserved quantity which follows from (9). The virial theorem involves the trace of the stress tensor.<sup>4</sup> The result is:

$$\partial_t^2 \langle \delta r^2 \rangle = 2A - 2 \frac{H_B}{N} + (2-D) \langle |\underline{E}_L|^2 \rangle , \quad (10a)$$

$$A \equiv \frac{2H}{N} - \left( \frac{P}{N} \right)^2 . \quad (10b)$$

Here  $D$  is the dimensionality of coordinate space. Hence, we derive a sufficient condition for adiabatic collapse:  $A < 0$  for  $D \geq 2$ .

For a stationary two-dimensional Gaussian wave packet,

$$E_L = i \left( \frac{E_0}{k_0} \right) \exp \left[ ik_0 x - \frac{\Delta k_{||}^2 x^2}{2} - \frac{\Delta k_{\perp}^2 y^2}{2} \right] ,$$

and

$$A = \frac{3}{2} \left[ \frac{\Delta k_{||}^2}{k_D^2} + \frac{\Delta k_{\perp}^2}{k_D^2} + \frac{\Omega^2 \Delta k_{\perp}^2}{3k_0^2} - \frac{W}{24} \right] . \quad (11)$$

For the case  $\Omega = 0.1$ , Eq. (11) yields  $A = 3 \times 10^{-4}$ . At  $t = 0$ ,  $H_B/N$  is the same order of magnitude as  $A$ , so the initial value of the right side of (10a) is  $A - H_B/N = -2 \times 10^{-5}$ . Numerical integrations during our  $\Omega = 0.1$  run for times prior to the pile-up of mode energy at  $k_0/3$  (Fig. 1f) show that  $H_B$  decreases by about a factor of 2. This is ample to inhibit collapse by changing the sign of  $A - H_B/N$ . In the next stage, momentum is lost to ions, and Eq. (5) is violated, so our virial theorem does not apply, and  $A$  is not invariant. By the time exhibited in Fig. 1f, there is very little magnetic dispersion, and the thermal dispersion is also reduced. The new value of  $A - H_B/N$  is negative, and adiabatic collapse begins.

Our results for Langmuir collapse in a weak magnetic field could be significant for ionospheric modification (where  $\Omega = 0.25$ ) and for the effect of intense solar magnetic field fluctuations on type III emission. When collapse times are prolonged sufficiently, they may exceed characteristic times for driving. This, in turn, could lead to higher levels of strong plasma turbulence and more

dramatic physical effects, such as electromagnetic emission. The altered packet shapes would also be expected to affect the pattern of electromagnetic emission and its polarization characteristics.

We would like to acknowledge important conversations with A. Barut and G. Dulk. This work was supported by the Atmospheric Research Section, National Science Foundation, Grant No. ATM 76-14275, and by the Air Force Office of Scientific Research (M.V.G. and J.C.W. only), Grant No. F49620-76-C-0005. One of us (D.R.N.) was also supported by the Atmospheric Research Section, National Science Foundation, Grant Nos. ATM 76-22487 and ATM 79-18778, and by S.U.D.O.E. Grant No. EY-76-5-02-2059.

## REFERENCES

1. V. E. Zakharov, *Zh. Eksp. Teor. Fiz.* 62, 1745 (1972) [Sov. Phys. JETP 35, 908 (1972)].
2. R. N. Sudan, in "Proceedings of the 6th European Conference on Controlled Fusion and Plasma Physics, Moscow" (Joint Institute for Nuclear Research, Moscow, USSR, 1973), Vol. 2, p. 185.
3. N. R. Pereira, R. N. Sudan, and J. Denavit, *Phys. Fluids* 20, 936 (1977).
4. M. V. Goldman, and D. R. Nicholson, *Phys. Rev. Lett.* 41, 406 (1978).
5. M. V. Goldman, G. F. Reiter, and D. R. Nicholson, *Phys. Fluids* 23, (1980).
6. V. I. Petviashvili, *Fiz. Plazmy* 2, 450 (1976) [Sov. J. Plasma Phys. 2, 247 (1977)].
7. J. C. Weatherall, M. V. Goldman, and D. R. Nicholson, "Parametric Instabilities in Weakly Magnetized Plasmas," accepted for publication in Astrophysical Journal (1980).
8. H. P. Freund and K. Papadopoulos, *Phys. Fluids* 23, 139 (1980).
9. V. V. Krasnosel'skikh and V. I. Sotnikov, *Fiz. Plazmy* 3, 872 (1977) [Sov. J. Plasma Phys. 3, 491 (1978)].
10. A. S. Lipatov, *Pis'ma Zh. Eksp. Teor. Fiz.* 26, 516 (1977) [Sov. Phys. JETP 26, 337 (1977)].
11. G. A. Dulk and D. J. McLean, *Solar Phys.* 57, 279 (1978).
12. D. R. Nicholson and M. V. Goldman, *Phys. Fluids* 21, 1766 (1978).
13. D. R. Nicholson, M. V. Goldman, P. Hoyng, and J. C. Weatherall, *Astrophys. J.* 223, 605 (1978).

14. M. V. Goldman, K. Rypdal, and R. Hafizi, "Dimensionality and Dissipation in Langmuir Collapse," to be published in *Phys. Fluids* (1980).
15. A. Barut and G. H. Mullen, *Ann. Phys.* 20, 203 (1962).
16. L. D. Landau and E. M. Lifshitz, Classical Theory of Fields, 3rd Ed. (Addison Wesley, 1971), p. 77.

Figure Captions

Fig. 1. In Figs. a, b, c, and d we plot contours of equal Langmuir field modulus in real space. The spacing in the  $64 \times 64$  grid is four times finer in x than in y. Contours 1, 2, and 3 correspond to  $W = 7.3 \times 10^{-4}$ ,  $2.9 \times 10^{-3}$ , and  $6.5 \times 10^{-3}$ . Figure 1a is at  $t = 0$ . Figure 1b is at  $t = 0.76 \times 10^5$  with  $B = 0$ . Figures 1c and 1d represent the evolution from 1a (at times  $t = 3.6 \times 10^5$  and  $4.1 \times 10^5$ ) for the case  $\omega_{ce}/\omega_{pe} = 0.1$ . Figures 1e and 1f show field contours in k-space, for the nonmagnetic case (1e) and the magnetic case (1f) at times corresponding to Figs. 1b and 1d, respectively.

Fig. 2. Time for central energy density in collapsing wave-packet to reach ten times initial value.

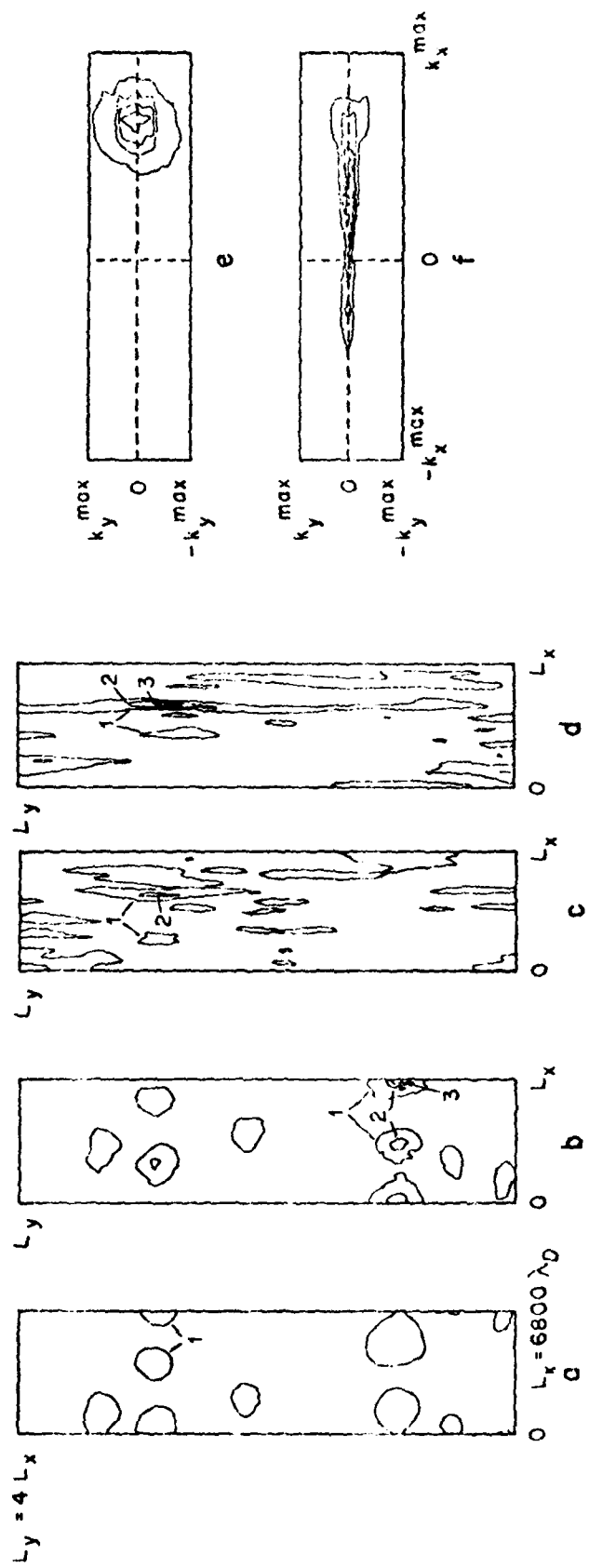


Figure 1

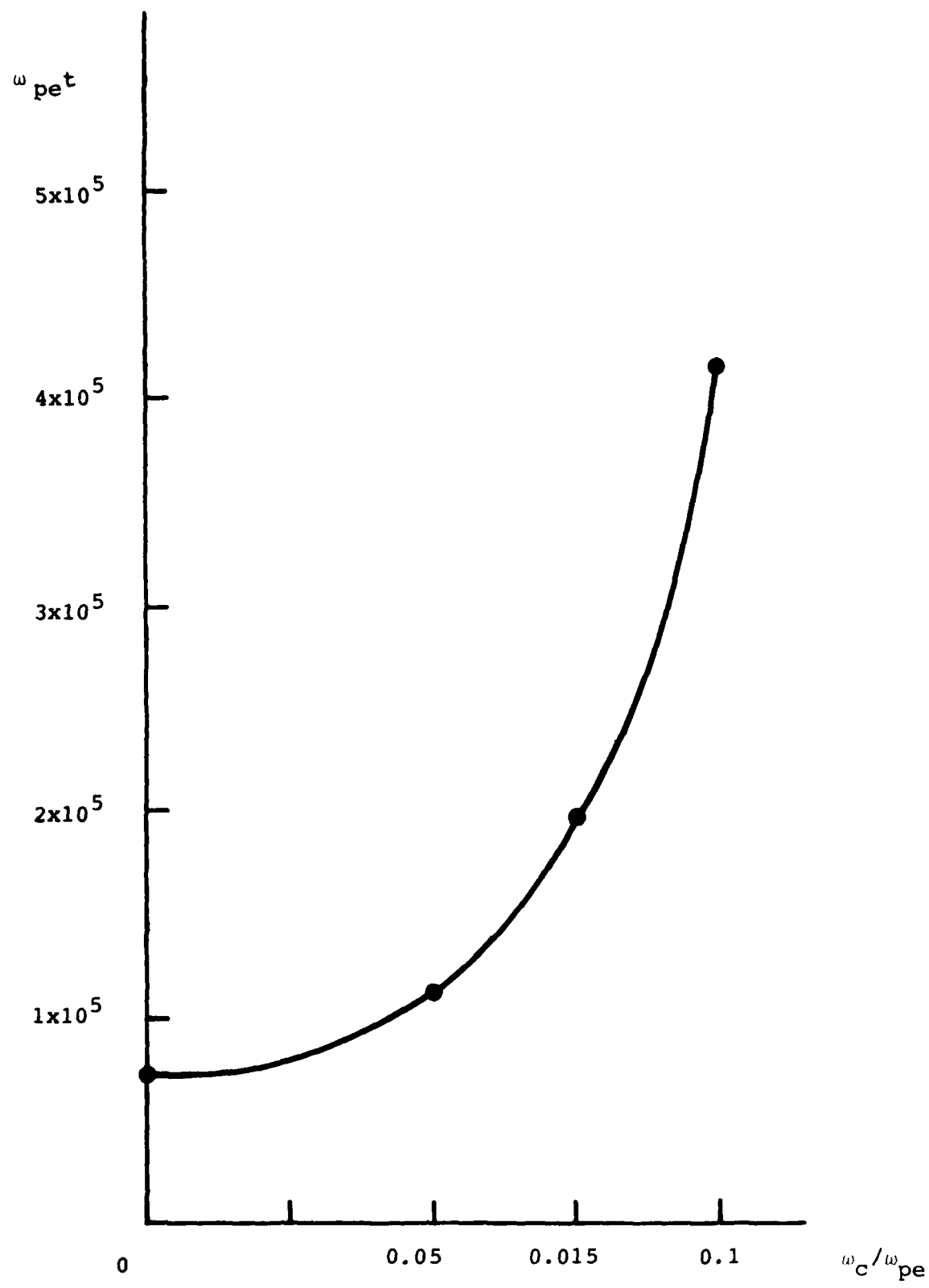


Figure 2

APPENDIX E

E. "Nonlinear Langmuir Waves in a Weak Magnetic Field"  
J. C. Weatherall  
Ph.D. Thesis, University of Colorado, 1980

NONLINEAR LANGMUIR WAVES IN A WEAK MAGNETIC FIELD

by

James Christopher Weatherall

B.S., California Institute of Technology, 1975

A thesis submitted to the Faculty of the Graduate  
School of the University of Colorado in partial  
fulfillment of the requirements for the degree of

Doctor of Philosophy

Department of Astro-Geophysics

1980

This Thesis for the Doctor of Philosophy Degree by  
James Christopher Weatherall  
has been approved for the  
Department of  
Astro-Geophysics  
by

Martin V. Goldman  
Martin V. Goldman

George A. Dulk  
George A. Dulk

Date 12/4/90

AD-A096 560

COLORADO UNIV AT BOULDER DEPT OF ASTRO-GEOPHYSICS  
PLASMA WAVE TURBULENCE AND PARTICLE HEATING CAUSED BY ELECTRON --ETC(U)  
JAN 81 M V GOLDMAN

F/6 4/1

AFOSR-80-0022

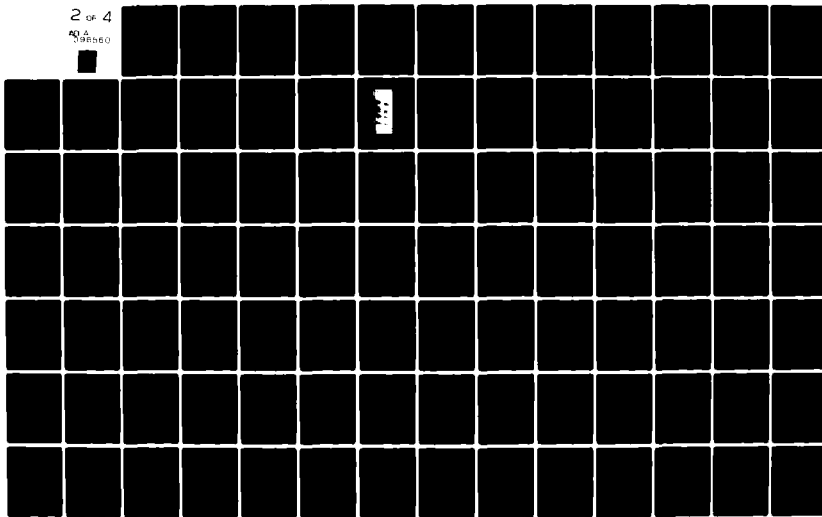
UNCLASSIFIED

CU-1533143

AFOSR-TR-81-0148

NL

2 OF 4  
AFOSR-80-0022



Weatherall, James Christopher (Ph.D., Astro-Geophysics)

Nonlinear Langmuir Waves in a Weak Magnetic Field

Thesis directed by Professor Martin V. Goldman

Large amplitude Langmuir waves are known to experience a variety of nonlinear effects: they can couple to other modes in the plasma to excite parametric instabilities; they can also self-focus to form localized regions of intense electrostatic fields. This thesis studies the effect of a weak magnetic field on both of these processes.

First, a set of coupled equations between the envelope electric field and the plasma density are derived with careful treatment of the magnetic field. When the electron cyclotron frequency is less than the plasma frequency, the dominant nonlinearities do not involve the magnetic field. However, the magnetic field does increase the dispersion of the Langmuir waves and prevents density perturbations directly transverse to the field.

Numerical calculations show that when the magnetic dispersion exceeds the thermal dispersion of Langmuir waves generated by parametric instability, the wave vectors of these waves shift to smaller perpendicular wavenumbers. This shift preserves the frequency matching in the wave interaction, and does not change the

growth rate. Instabilities directly across the magnetic field and perpendicular to the pump wave, such as might occur for the oscillating two-stream instability, are suppressed by very small fields.

When intense wavepackets of Langmuir waves can experience direct collapse, the magnetic field causes two interesting effects: the collapsing wavepackets assume a pancake-shaped geometry; and the collapse takes a longer time. These effects occur when the magnetic dispersion competes with the nonlinear self-focusing. A virial theorem and a broadband perturbation theory help to explain this behavior.

We find that magnetic effects may have some relevance in the theory of Type III solar radio bursts. In computer simulations of Langmuir wave turbulence during a Type III burst at one-half the distance between the sun and the earth, we observe some changes in the wave behavior when a realistic background magnetic field is added. For a magnetic field several times larger than the average measured field, there are significant effects on the shape of wavepackets and on the turbulent wave energy levels. As a consequence, the properties of the radio emission, such as the amplitude, directivity, and polarization, may be different than given by an unmagnetized theory.

This abstract is approved as to form and content. I  
recommend its publication.

Signed Mark V. Fiedl  
Faculty member in charge of thesis

## TABLE OF CONTENTS

CHAPTER	PAGE
I. INTRODUCTION . . . . .	1
Solar Plasma Physics . . . . .	3
Solar Radio Bursts . . . . .	8
The Type III Burst . . . . .	11
Theory of Type III Bursts . . . . .	14
Preview and Motivation of Present	
Work . . . . .	17
II. WAVES AND WAVE INTERACTIONS . . . . .	27
Langmuir Waves in a Magnetic Field .	29
Ion-Acoustic Waves in a Magnetic	
Field . . . . .	33
Wave-Wave Interaction . . . . .	36
Derivation of Nonlinear Wave	
Equations . . . . .	37
Nonlinear High Frequency	
Equation . . . . .	42
Low Frequency Waves . . . . .	43
Nonlinear Low Frequency Equation	50
Summary of Nonlinear Equations . . .	51
Numerical Simulation . . . . .	54

CHAPTER	PAGE
III. LINEAR AND NONLINEAR LANGMUIR WAVEPACKETS . . .	56
Linear Dispersion . . . . .	56
Nonlinear Instability . . . . .	68
Summary of Magnetic Effects . . . . .	79
IV. PARAMETRIC INSTABILITY . . . . .	80
Instability Geometries in the Type	
III Problem . . . . .	84
Magnetic Effects . . . . .	97
Broadband Effects . . . . .	107
Summary . . . . .	114
V. PLASMA WAVE COLLAPSE . . . . .	116
Simulation of Type III Wave Processes .	120
Scenario for Magnetic Collapse . . . . .	132
The Virial Theorem . . . . .	134
Perturbative Collapse Theory . . . . .	141
Modulational Theory . . . . .	146
Collapse Theory . . . . .	147
Summary . . . . .	153
VI. CONCLUSION . . . . .	155
BIBLIOGRAPHY . . . . .	158

## LIST OF FIGURES

FIGURE	PAGE
1. Spectrograph of a Type III Burst . . . . .	10
2. Radioheliograph Contours of Brightness Temperature of a Type III Burst . . . . .	13
3. Model of Beam Emission of Langmuir Waves in k-Space . . . . .	18
4. Coordinate System in $k$ , $B_0$ Plane . . . . .	31
5. Dispersion Relation for Waves with $B_0 \neq 0$ . .	34
6. Three-Wave Momentum Matching Condition . . . .	48
7. Initial Linear Gaussian Wavepacket . . . . .	63
8. Electric Field Contours of Wavepacket after $T = 7700$ Plasma Periods with no Magnetic Field . . . . .	65
9. Electric Field Contours of Wavepacket in a Magnetic Field (a) After $T = 1100$ Plasma Periods . . . . .	66
(b) After $T = 3300$ Plasma Periods . . . . .	67
10. One-Dimensional Soliton . . . . .	71
11. Unperturbed Soliton after $T = 22,000$ Plasma Periods . . . . .	72
12. Soliton after $T = 11,000$ Plasma Periods after Being Perturbed in the Longitudinal Direction.	74

FIGURE	PAGE
13. Soliton after Being Perturbed in the Transverse Direction	
(a) After $T = 6,600$ Plasma Periods . . . . .	75
(b) After $T = 8,800$ Plasma Periods . . . . .	76
14. Soliton in a Magnetic Field after Being Perturbed in the Transverse Direction	
(a) After $T = 8,800$ Plasma Periods . . . . .	77
(b) After $T = 11,000$ Plasma Periods . . . . .	78
15. Parametric Growth Rates in $k$ -space for Langmuir Waves Excited by a Pump Wave at $k_o = 0.01 k_{De}$	
(a) $W_o = 10^{-4}$ . . . . .	91
(b) $W_o = 10^{-3}$ . . . . .	92
(c) $W_o = 3 \times 10^{-3}$ . . . . .	93
(d) $W_o = 10^{-2}$ . . . . .	94
16. Solution of Dispersion Relation in the Unmagnetized Case $k_o = 0.05 k_{De}$ , $W_o = 3 \times 10^{-4}$ .	101
17. Solution of Dispersion Relation in the Weakly Magnetized Case: $\omega_{ce} = 0.1 \omega_{pe}$ . . . . .	103
18. Electric field Amplitude in $k$ -space for a Broadband Pump: $k_o = 0.05 k_{De}$ , $W_o = 3 \times 10^{-4}$	
(a) $T = 0$ . . . . .	109
(b) After $T = 33,000$ Plasma Periods . . . . .	110
(c) After $T = 52,800$ Plasma Periods . . . . .	113

FIGURE	PAGE
19. Simulation of Type III Burst at 0.5 A.U. with a Growing Broadband Pump, and No Magnetic Field. Real Space Electric Field Contours . . . . .	122
20. Simulation of Type III Burst at 0.5 A.U. with a Magnetic Field, $\omega_{ce} = 0.01 \omega_{pe}$ . Real Space Electric Field Contours . . . . .	123
21. Simulation of Type III Burst at 0.5 A.U. with a Magnetic Field, $\omega_{ce} = 0.05 \omega_{pe}$ . Real Space Electric Field Contours . . . . .	124
22. Pump Electrostatic Energy vs. Time During Type III Simulations . . . . .	126
23. Total Electrostatic Energy vs. Time During Type III Simulations . . . . .	127
24. Electric Field in k-space During Type III Simulations with $\omega_{ce} = 0$ . . . . .	129
25. Electric Field in k-space During Type III Simulation with $\omega_{ce} = 0.01 \omega_{pe}$ . . . . .	130
26. Electric Field in k-space During Type III Simulation with $\omega_{ce} = 0.05 \omega_{pe}$ . . . . .	131
27. Time for Central Energy Density in Collapsing Wavepacket to Reach Ten Times Initial Value for Various Magnetic Field Strengths . . . . .	139
28. Pump Modes for Broadband Perturbation Theory .	142

## LIST OF TABLES

TABLE	PAGE
1. Coronal Temperature, Density, and Magnetic Field at Different Heights . . . . .	5
2. Important Parameters in the Type III Problem for Different Heights in the Corona . . . . .	21
3. Sample of Magnetized Waves and Their Coupling Through Density Perturbations with Langmuir Waves . . . . .	45
4. Numerically Determined Properties of Parametric Instability for $k_o = 0.01 k_{De}$ and Various Values of Pump Energy . . . . .	95
5. $2H_B/N$ During Adiabatic Collapse . . . . .	138
6. Wavenumber Matched Transitions . . . . .	148
7. Effect of Frequency Mismatch on Amplitude Growth of Collapse Modes . . . . .	151

## CHAPTER I

### INTRODUCTION

Waves of all types exhibit fascinating and varied behavior at large amplitudes. Of particular interest to solar and plasma physicists is the Langmuir wave, which is a charge density wave in a plasma. Theory shows that at large amplitudes these waves can couple to other plasma modes or can self-focus to form very intense regions of electrostatic fields. These so-called turbulent processes are central to the production of radio emission from plasmas and to the stability of beams of charged particles. Usually the theories assume isotropic plasmas, despite the fact that in physical situations where such phenomena are of interest, a magnetic field is often present. The main intent of this thesis is to demonstrate that even a small magnetic field can have dramatic effects on the nonlinear behavior of Langmuir waves.

In nature, intense Langmuir waves are thought to occur during Type III solar radio bursts. Spacecraft experiments at one-half the distance from the sun to the earth (Gurnett and Anderson, 1976 and 1977) and at

the earth's orbit (Lin, private communication, 1979) have shown that in conjunction with the emission of radio waves at the plasma frequency and at twice the plasma frequency, regions of intense localized electrostatic fields occur. This is presumed to be Langmuir turbulence generated by a high velocity electron stream emitted from the sun at the onset of the burst, and the radiation is due to the interaction of the Langmuir waves with the plasma.

This subject is also relevant to other problems in which plasma turbulence plays a role. For example, in ionospheric modification, when Langmuir waves are generated by intense radar waves, a rather strong magnetic field is present. Also, laboratory experiments (Benford, private communication, 1979) show that radiation emitted when a particle beam passes through the plasma is decreased when a small magnetic field is introduced. This is evidence that the magnetic field does have important effects on wave processes.

The principal application of this thesis will concern the nonlinear behavior of Langmuir waves during Type III bursts. In addressing this problem, we solve a general set of wave equations in two dimensions by computer. The wave-wave processes we study include the induced scatter off ions (Kaplan and Tsytovich, 1968), modulational instability (Nishikawa, 1968; Papadopoulos,

Goldstein, and Smith, 1974; and Bardwell and Goldman, 1976), and plasma wave collapse (Zakharov, 1972; Goldman and Nicholson, 1978). These interactions encompass both weak and strong turbulent effects.

In order to appreciate the relationship of these theoretical problems to real solar phenomena, we will present a brief review of solar physics (Pasachoff, 1977) and solar radio astronomy (Kundu, 1965).

#### Solar Plasma Physics

The solar atmosphere consists of three regions. The processes we will study involving Langmuir waves occur in the solar corona. Below the corona is the photosphere and the chromosphere. The photosphere is the visible surface of the sun. Most of the radiation from the sun escapes from a layer of gas only 200 km thick at the base of the photosphere, which is  $6.96 \times 10^5$  km (1 solar radius,  $R_\odot$ ) from the sun's center. The chromosphere is a region between the photosphere and the corona extending roughly 10,000 km ( $1.003 R_\odot$ ) above the surface, and is studied at H $\alpha$  wavelengths with narrow band filters. The characteristic temperature of the chromosphere is about three times higher than the effective temperature of the photosphere, which is 5700 °K. This increase in temperature, as well as the heating

in the corona, is attributed to the dissipation of wave energy. The transition from the chromosphere to the corona is abrupt. The temperature rises from about  $10^4$  to  $10^6$  K, and the density falls by about a factor of 100. The corona is optically thin, so most of the observed radiation is due to photospheric light scattered by electrons and dust. The corona which is not normally visible because it is fainter than the daytime sky, can be seen during a total solar eclipse, by special telescopes (coronagraphs) in exceptionally clear skies, or by spacecraft above the atmosphere. The average density of the solar corona varies with height, but the temperature remains roughly constant. The corona is continuously expanding into interplanetary space. The so-called solar wind sweeps by the earth at  $215 R_\odot$ , with a characteristic velocity of  $450 \text{ km s}^{-1}$ . All of our calculations are in a reference frame at rest with respect to the solar wind motion.

The physical parameters in the solar corona are summarized in Table 1 (Allen, 1976; Newkirk, 1967; Dulk and McLean, 1978). The electron density,  $n_e$ , is determined (Billings, 1966) from white light and radio noise scattering data, and directly by spacecraft measurement. The density varies by about a factor of two during the solar cycle and coronal streamers are typically overdense by factors of 2 at  $2 R_\odot$ , and 10 at  $10 R_\odot$  and beyond.

TABLE 1  
 CORONAL TEMPERATURE, DENSITY, AND MAGNETIC  
 FIELD AT DIFFERENT HEIGHTS

$r/R_O$	$T (10^6 K)$	$n_e (cm^{-3})$	$B_O (G)$
1.1	1.0	$2 \times 10^8$	10
1.2	1.2	$8 \times 10^7$	3
1.5	1.7	$2 \times 10^7$	1
2.0	1.8	$3 \times 10^6$	0.3
3.0	1.7	$5 \times 10^5$	0.2
5.0	1.4	$8 \times 10^4$	0.06
10	1.1	$1 \times 10^4$	0.01
20	0.8	$2 \times 10^3$	$3 \times 10^{-3}$
100	0.2	30	$1 \times 10^{-4}$
215	0.2	5	$3 \times 10^{-5}$

The temperature is determined (Billings, 1966) in a variety of ways, including atomic ionization data, spectral line profiles, decay times of radio bursts, radar reflection, and in situ measurements by spacecraft. The magnetic field strength is known (Dulk and McLean, 1978) from in situ measurements between 0.5 and 5 A.U., which may be extrapolated to the surface until about  $2 R_\odot$ , where closed magnetic structures begin to occur. Other estimates involve extrapolation from photospheric data, Zeeman splitting, and measurements of the intensity, polarization, and motion of radio sources in the corona.

Beyond these general characteristics of the solar atmosphere, there are often active regions which exhibit variable activity characterized by sunspots and filaments. Sunspots are the result of very intense magnetic fields (thousands of gauss), and appear dark because they are relatively cool (4500 K). Sunspots form in groups, generally containing two major spots of opposite polarity and many small spots. The filaments are cool gaseous formations extending 20,000 to 500,000 km into the corona. They are observed as bright arches or prominences on the sun's limb. Prominences can be stable for 200 to 300 days when they occur away from sunspot groups, but loop prominences following flares last for only a few hours.

Flares are very violent events, sometimes releasing as much as  $10^{31}$  ergs in energy over a period of only twenty minutes. Flares occur in active regions with very strong and rapidly evolving magnetic fields, and seem to involve the release of energy by the reconnection of magnetic field lines. Flares are usually observed as a brightening in H $\alpha$ , but can sometimes be seen in white light. They also produce intense ultraviolet and X-ray radiation which affects long range communication on earth by increasing the ionization of the ionosphere. Energetic particles which reach the earth about a day later cause disturbances in the magnetosphere and produce aurorae and other solar-terrestrial phenomena. Also, during a flare the observed brightness temperatures at radio wavelengths can increase a thousand times over quiet levels.

Although only a small fraction of the flare energy,  $\sim 10^{24}$  ergs, is released at meter wavelength radiation, observation at radio wavelengths provides much information about the temperature and density structure of the corona. Beyond their importance in understanding eruptive solar phenomena, radio bursts are of general interest in the understanding of nonlinear processes occurring in plasmas.

### Solar Radio Bursts

The discovery of radio emission from the sun was made in 1942 by Hey, and strong meter wavelength emission from the sun was first associated with a large solar flare by Appleton and Hey in 1946. These observations marked the beginnings of solar radio astronomy (see Kundu, 1965; Wild and Smerd, 1963; and Wild and Smerd, 1972, for reviews and extensive references).

The radio emission from the sun can be separated into a number of components (Allen, 1976). First, there is the thermal radio emission from the quiet sun. There is also a slowly varying emission associated with sunspots. Finally, there are rapidly changing phenomena, associated with sunspots and flares, which are classified into the burst types I, II, III, IV, and V. These can be observed as noise storms (Type I bursts), as complicated outbursts containing Type II, III, IV, and V bursts or emission, or as isolated Type III and V bursts.

The Type I bursts are broadband enhancement of the continuous solar radiation during which hundreds of short, narrow band bursts occur every hour. Type I bursts can last for days, and are present 10% of the time at solar maximum. They occur in active regions near sunspots, and are sometimes, but not always, initiated by a solar flare.

Type II bursts are more rare, occurring about every 50 hours near sunspot maximum. They appear about 5 or

20 minutes after the start of a large flare, and last for about 10 minutes. The distinguishing feature of Type II bursts is a systematic drift from high to low frequency at a rate of about  $1 \text{ Mc s}^{-1}$ .

Type III bursts are fairly common, with three per hour occurring during solar maximum. Individual bursts last for only ten seconds, but occur in groups of ten or so (see Figure 1). They occur near the start of either a large or small flare. The important characteristic of a Type III burst is a rapid drift from high to low frequency, at a rate of  $20 \text{ Mc s}^{-1}$ . There is also a type U burst, which is a variant of a Type III burst in which the frequency drift reverses direction, and drifts back toward higher frequencies.

Type IV and V bursts are continuous radiation following a flare. The Type IV is rare, and usually starts after a Type II burst, although not all Type II bursts are followed by a Type IV burst. The Type IV is a smooth, often featureless emission, over a very broad band from centimeter to decameter waves, lasting from 10 minutes to a few hours. The Type V is a similar continuum event which follows about 10% of Type III bursts.

Various mechanisms have been proposed to describe the many components of radio emission (see Wild and Smerd, 1963 and 1972). Bremsstrahlung is responsible

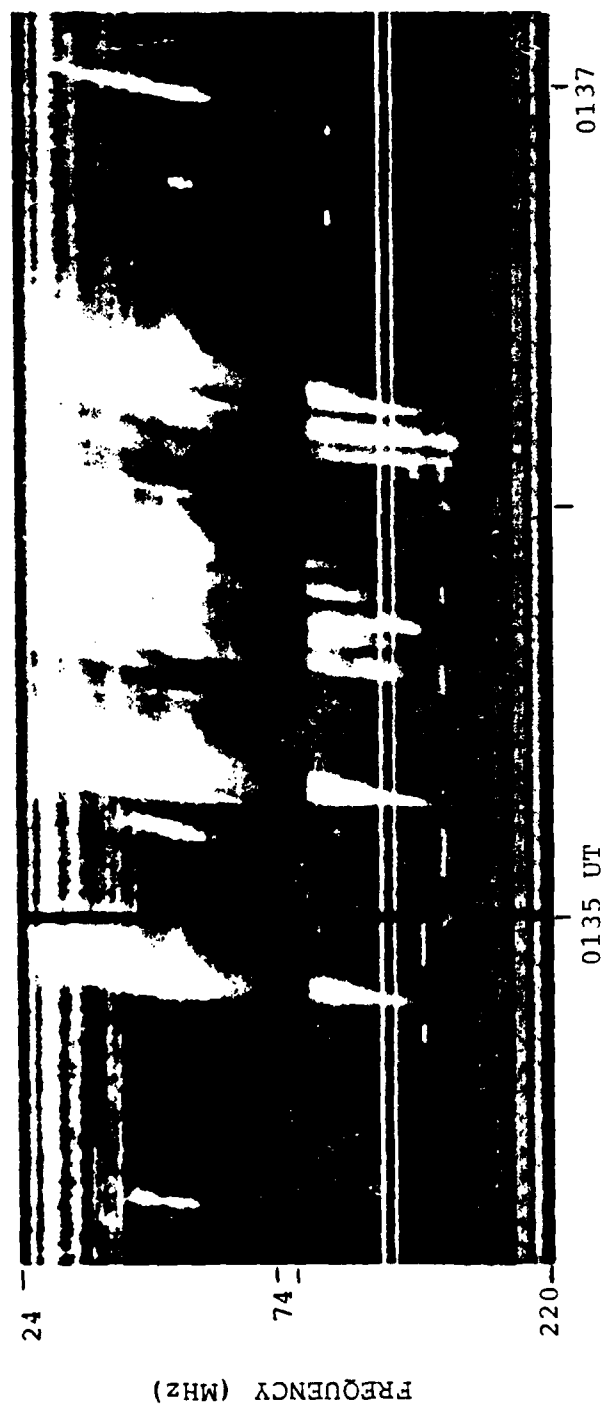


FIGURE 1. Spectrograph of Type III bursts occurring 1978 April 10, 0134 UT.  
(Courtesy of G. Dulk.)

for the quiet sun emission and the slowly varying component, and may be important for bursts on centimeter wavelength scales for which the corona is optically thick. Gyro-synchroton radiation from energetic electrons spiraling in magnetic fields can account for continuum bursts. Radiation from plasma waves is the cause of Type II and Type III bursts, and perhaps some continuum storms also. The excitation of plasma waves in Type II bursts is attributed to a magnetosonic shock wave, and in Type III bursts, a high velocity electron stream.

The study of radio bursts, in particular, the Type III bursts, has stimulated the development of new plasma theory for the description of nonlinear wave phenomena. There are many problems posed by the conversion of plasma waves into radio emission and the behavior of plasma waves at high amplitudes.

#### The Type III Burst

The explanation of Type III bursts as due to plasma oscillations was proposed by Wild in 1950. The typical spectra of a Type III burst (as in Figure 1) shows the rapid drift from high to low frequencies, and the appearance of identical spectral structures instantaneously at two frequencies. The drift can be attributed to the propagation of the source of plasma waves outward

through the corona into regions of lower electron density, and slower plasma oscillation. This requires a source traveling from 1/6 to 1/2 the speed of light, such as a particle beam ejected by a flare. This beam can generate plasma waves by a well-known instability (see, for example, Mikhailovskii, 1974; or Melrose, 1977). The appearance of the double structures is evidence of emission at the fundamental plasma frequency, and its harmonic at twice the plasma frequency.

Modern observations are consistent with this picture. High resolution radio heliograph pictures show the position of different frequency emission at different characteristic heights (see Figure 2). In addition, satellites have detected the plasma oscillations directly (Gurnett and Anderson, 1976 and 1977). These plasma oscillations are observed as narrow band spiky electrostatic noise near the local electron plasma frequency. The oscillations are confined to small regions of space, with typical dimensions of 10 km (Smith and Nicholson, 1979; Lin, 1979). Satellites also detect high energy particles and electromagnetic emission (Fitzenreiter, Evans, and Lin, 1976). The particles are electrons with energies from a few to several hundred kiloelectron volts (Lin, Evans, and Fainberg, 1973). The number of electrons in the stream,  $n_b$ , is small compared with the background density,  $n_o$ ,  $n_b/n_o \approx 10^{-6}$  (Smith and Nicholson, 1979; Lin, 1979).

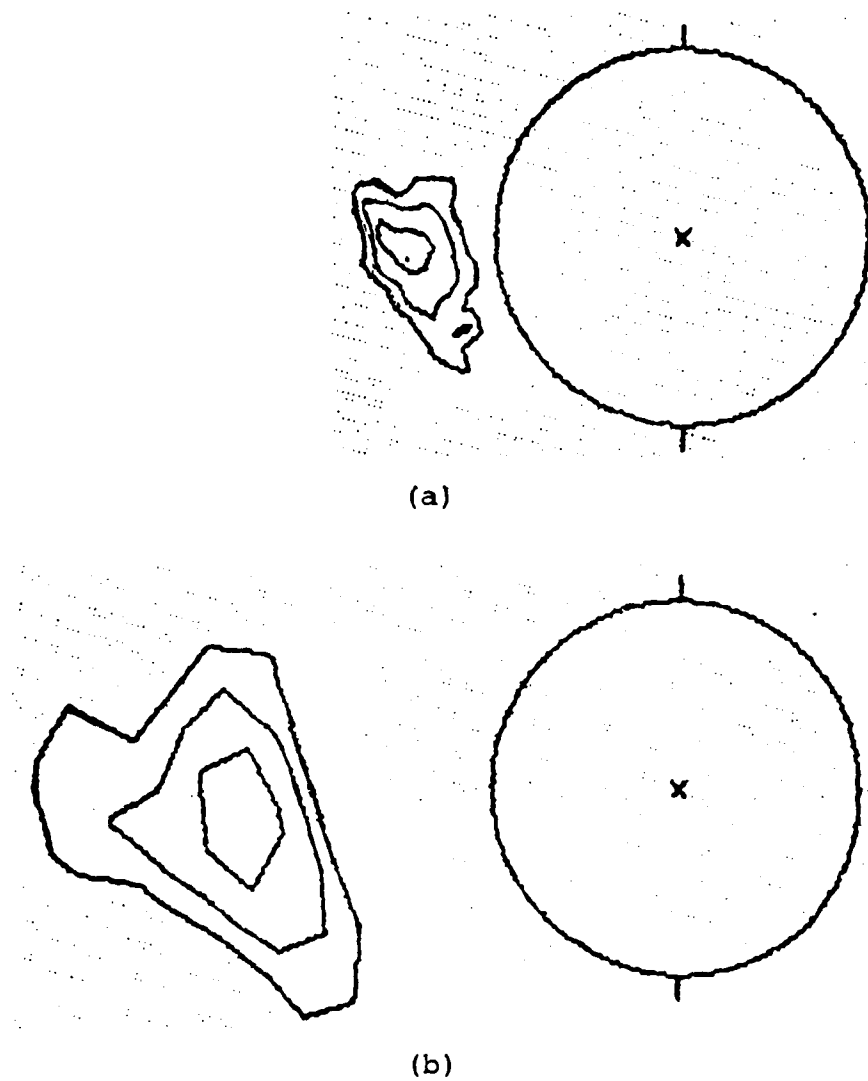


FIGURE 2. Radioheliograph contours of brightness temperature for Type III bursts, 1980 April 27, at 0228 UT; (a) at 160 MHz, and (b) at 43 MHz. Contours indicate relative temperature. (Courtesy of R. Stewart.)

The appearance of the electron stream is simultaneous with the observation of radio emission, but the plasma wave turbulence occurs nearly 20 minutes later (Lin, 1979).

#### Theory of Type III Bursts

The areas of theoretical interest in Type III bursts can be identified as the propagation of the electron stream, the plasma wave generation, and the radiation (for recent review of these topics, see Nicholson and Smith, 1979). There are two useful approaches to these problems. One is a quasilinear theory, which treats the interaction of the particles and waves, but ignores the interaction between waves. The other is to ignore changes in the particle distribution function, but include wave-wave interactions in a reasonably complete way. A complete analysis in more than one dimension including both wave-particle and wave-wave processes is desirable, but difficult, and is not really justified until the steady-state characteristics of plasma turbulence are better understood.

The quasilinear calculation assumes that the exciting stream is sufficiently weak and broad in velocity that quasilinear relaxation is the dominant effect (Smith, 1974). Ordinary quasilinear theory predicts that the electron stream will rapidly lose its energy to waves, and will not propagate away from the

sun (Sturrock, 1964). However, when inhomogeneity in time and space is allowed, almost all the wave energy is reabsorbed by the stream (Ryutov and Sagdeev, 1970; Takakura and Shibahashi, 1976; Takakura, 1977). As a result, the stream can propagate for several A.U. Magelssen and Smith (1977) performed a numerical calculation for Type III parameters over the entire distance from the sun to the earth. Their results are consistent with electron observations at the earth. However, the electrostatic field amplitudes they find are large enough so that wave-wave interaction is possible.

The theory for wave-wave interaction is based on equations derived by Zakharov (1972). Applied to the Type III problem, this theory ignores the time dependence of the electron beam distribution function due to quasilinear relaxation and velocity dispersion in the beam. This can be justified when the nonlinear wave time scales are short. Papadopoulos, Goldstein, and Smith (1974) showed that Langmuir waves in Type III bursts could drive the oscillating two-stream instability at wave energies lower than given by quasilinear theory. This work was extended by Hubbard and Joyce (1976), Galeev, Sagdeev, Sigov, Shapiro, and Shevchenko (1975), Smith, Goldstein, and Papadopoulos (1979), and Rowland and Papadopoulos (1977). All of these works are in one dimension along the stream direction. The importance of the second

spatial dimension was pointed out by Bardwell and Goldman (1976), who showed that for a monochromatic pump wave the oscillating two-stream instability could occur in a direction perpendicular to the stream direction. The two-dimensional work of Bardwell and Goldman was extended by Nicholson, Goldman, Hoyng, and Weatherall (1978), who used the plasma wave distribution given by the quasilinear calculations (Magelssen and Smith, 1977) as an initial condition in a numerical simulation of the wave equations. They found that immediate soliton collapse occurred in two spatial dimensions, and the collapse is independent of and proceeds faster than any associated parametric instability. The collapse takes almost all of the wave energy out of resonance with the beam. Thus, in principle, wave turbulence effects may play an important role in the stream propagation.

The basic processes for transforming plasma waves into electromagnetic radiation was first described by Ginzburg and Zheleznyakov (1958), and further studied by Tsytovich (1970), Melrose (1974), and Smith (1970). One process involves the scattering of plasma waves ( $p$ ) on charge clouds surrounding thermal ions ( $i$ ), resulting in the emission of a photon ( $t$ ) near the plasma frequency  $\omega_{pe}$ :

$$p + i \rightarrow t(\omega_{pe}) . \quad (1)$$

The process for second harmonic emission is the coalescence of two plasma waves to generate a photon at twice the plasma frequency:

$$p + p' \rightarrow t(2\omega_{pe}) . \quad (2)$$

It has been shown that the Type III radiation can be explained by the observed plasma wave levels by this theory (Smith, 1977). However, the theory of Type III emission will not be complete until the effect on radiation of strong Langmuir turbulence, such as soliton collapse, is understood. This is the subject of much current work (Brejzman and Pekker, 1978; Papadopoulos and Freund, 1978; Goldman, Reiter, and Nicholson, 1980).

#### Preview and Motivation of Present Work

We have seen that the central aspect of the Type III problem is the nonlinear evolution of Langmuir waves driven by an electron beam. In this work, we consider the effect of a weak magnetic field on two-dimensional wave processes. We use a very simple model as in Nicholson, et al. (1978), in which waves driven by the beam are represented by a finite number of growing wave modes in  $k$ -space with a finite wavenumber and bandwidth (see Figure 3). We will ignore particle-wave interactions beyond this beam instability, but will allow the beam waves to interact with other Langmuir waves.

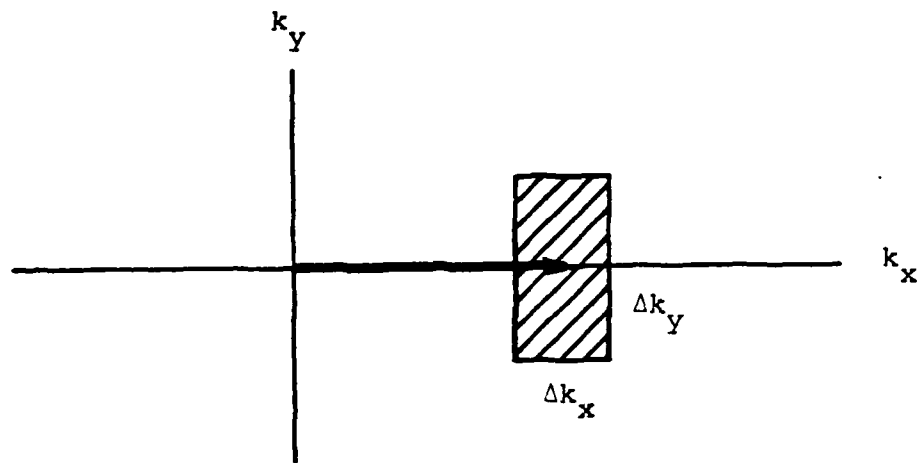


FIGURE 3. Model of beam emission of Langmuir waves in  $k$ -space. Shaded region represents growing wave modes.

The basic nonlinear wave interactions included are due to the ponderomotive force, which tends to expel charged particles from regions of large electric fields, and an index of refraction effect from variations in plasma density which tends to focus the waves.

The linear growth of the modes interacting with the beam is described by the warm beam growth rate (Melrose, 1977)

$$\gamma = \omega_R \frac{n_b}{n_o} \sqrt{\frac{\pi}{8}} \left( \frac{\omega_R^2}{k^2 \Delta v_b^2} \right) y_s e^{-y_s^2/2},$$

$$y_s = \frac{\omega - k \cdot v_b}{\sqrt{2} k \Delta v_b}, \quad (3)$$

where  $\omega_R$  is near the plasma frequency;  $n_b/n_o \sim 10^{-6}$  is the ratio of the beam to background electron density;  $k$  is the wavenumber of the wave;  $v_b \sim \frac{1}{2}c$  is the mean velocity of the beam; and  $\Delta v_b \sim \frac{1}{4} v_b$  is the spread in beam velocity. The maximum growth rate occurs along the beam direction and, for these parameters, has the value  $\gamma/\omega_R \sim 10^{-6}$ . The fastest growing wave has the wavenumber  $k_o$  given by

$$k_o \lambda_{De} = \frac{\omega_R}{v_b - \Delta v_b} \lambda_{De} = 3.5 \times 10^{-5} T^{\frac{1}{2}}, \quad (4)$$

where  $T$  is measured in K. The Debye length,  $\lambda_{De}$ , is given by

$$\lambda_{De} = 6.9 T^{\frac{1}{2}} n^{-\frac{1}{2}} \text{ cm}. \quad (5)$$

The Debye length and the resonant wave vectors, derived from the temperatures and densities in Table 1, are given for various heights in the corona in Table 2.

Although  $k_o$  is the fastest growing wave, there will be a finite band of growing waves near  $k_o$  which will have significant growth rates. The spread in wavenumber parallel to  $k_o$  is due to the dispersion in velocity of the beam. However, even for a one-dimensional beam, there is a spread in wavenumber perpendicular to  $k_o$  also, because of the angular dependence in Equation (3).

These widths, roughly estimated from Equation (3), are  $\Delta k_{||} \sim 1/10 k_o$ ;  $\Delta k_{\perp} \sim 1/4 k_o$ . These estimates motivate the choice of  $\gamma/\omega_{pe}$ ,  $k_o$ , and  $\Delta k$  in future numerical simulations.

Most theories of wave-wave effects on Type III bursts have disregarded the magnetic field. The magnetic field is generally ignored in the context of Langmuir waves when the electron cyclotron frequency is small compared with the plasma frequency. The electron cyclotron frequency is given by

$$\omega_{ce} = 1.76 \times 10^7 B \text{ rad s}^{-1}, \quad (6)$$

(B is in gauss) and the plasma frequency is found from

$$\omega_{pe} = 5.64 \times 10^4 n_e^{1/3} \text{ rad s}^{-1} \quad (7)$$

( $n_e$ , the number density of electrons, measured in  $\text{cm}^{-3}$ ).

TABLE 2  
 IMPORTANT PARAMETERS IN THE TYPE III PROBLEM  
 FOR DIFFERENT HEIGHTS IN THE CORONA

$r/R_O$	$\lambda_{De}$ (cm)	$\omega_{ce}$ ( $s^{-1}$ )	$\omega_{pe}$ ( $s^{-1}$ )	$k_O \lambda_{De}$	$\frac{\omega_{ce}}{\omega_{pe}}$
1.2	.84	$5 \times 10^7$	$5 \times 10^8$	.04	.1
2.0	5	$5 \times 10^6$	$1 \times 10^8$	.05	.05
10	70	$2 \times 10^5$	$6 \times 10^6$	.04	.03
20	430	$5 \times 10^4$	$3 \times 10^6$	.03	.02
100	550	$2 \times 10^3$	$3 \times 10^5$	.015	.01
215	1400	$5 \times 10^2$	$1 \times 10^5$	.015	.005

Using the data from Table 1 for the solar corona, we can calculate the values of  $\omega_{ce}$  and  $\omega_{pe}$  for various heights in the corona. The results, given in Table 2, show that for the average values of density and magnetic fields in the solar corona, the cyclotron frequency is much less than the plasma frequency.

Are these values for  $\omega_{ce}$ , derived from the average condition of the magnetic field, appropriate for the environment of the Type III burst? To answer this question, one must consider the possible magnetic fields created by the electron beam. It turns out that when the background electron plasma density exceeds that of the beam ( $n_b \ll n_o$ ), a reverse current appears which tends to cancel the magnetic field induced by the beam (Lawson, 1977; Levine, Vitkovitsky, Hammer, and Andrews, 1971; Hammer and Rostoker, 1970; and Cox and Bennett, 1970). Furthermore, the return current is contained within the same volume as the beam when the time for a signal to cross the beam of dimension  $b$  at the speed of light takes longer than the response time of the plasma. When collisions are ignored, this response time is  $\sim \omega_{pe}^{-1}$ . Therefore, the magnetic field is neutralized when  $n_b/n_o \ll 1$  and  $\omega_{pe} b/c \gg 1$ . These conditions are well realized for Type III bursts. This conclusion is supported by measurements of the polarization of the radio emission from the burst (Kai, 1970). If the magnetic

field were not weak, the extraordinary component of the radiation would be filtered out no matter what the emission mechanism, and the burst would be strongly polarized. Strong polarization is not observed in the Type III emission. On the average, the fundamental radiation is 35% circularly polarized and the harmonic radiation is 11% polarized (Dulk and Suzuki, 1980). The magnetic field strength derived from these polarization data give values of the magnetic field which are consistent with the average coronal magnetic field structure described in Table 1.

Although the cyclotron frequency is much less than the plasma frequency, magnetic field effects should still be considered. For many wave interactions, it is the dispersion of the Langmuir waves which is important, and in the solar corona, the magnetic dispersion can be large enough to compete with the thermal dispersion. Therefore, even though the magnetic field appears in the basic nonlinear equations as a perturbation, as we show in Chapter 2, the effects on wave interactions must not be ignored. This thesis examines this topic in detail.

In the third chapter we show how the magnetic field can affect the dispersive behavior of linear wavepackets and the nonlinear stability of large amplitude wavepackets. The two examples illustrate many important points which are explored in the later chapters. They

show that the linear and nonlinear wave behavior is very different; that it is important to include at least two spatial dimensions in the treatment of nonlinear effects because one-dimensional solutions (solitons) are unstable in more dimensions; and that even small magnetic fields can produce significant effects on waves and wave interactions.

These ideas are applied in the fourth chapter to Type III bursts and parametric instabilities. This chapter contains a review of current wave theories as they apply to the Type III problem, and examines critically the relevancy of one-dimensional treatments. In particular, the effects of wave amplitude, the magnetic field, and finite bandwidth on parametric instabilities is considered.

The most interesting effects of the magnetic field are seen in Chapter V, in which we study the evolution of the initial wave geometry given in Figure 3. Depending upon the values of the central wavenumber,  $k_o$ , the bandwidths,  $\Delta k$ , and the wave energy  $W$ , the real space wave-packets produced by the beam can evolve in a number of ways. If  $k_o$  is such that the wavepacket is traveling slowly relative to the ion wave speed, the ponderomotive effects can resonate strongly to expel plasma, and refract waves into the regions of reduced plasma density. For small  $W$ , however, this effect cannot overcome the

dispersive nature of the wavepacket. For stronger  $W$ , the self-focusing can overcome dispersion, and the wavepacket contracts or collapses (Goldman and Nicholson, 1978). For even larger  $W$ , intense modulational instability breaks up the wavepacket, and many collapsons form.

For wavepackets in Type III bursts, the Langmuir group speed is such that for distances from the sun greater than  $\sim 10 R_{\odot}$ , direct collapse can occur. For distances closer than  $\sim 10 R_{\odot}$ , the ponderomotive effect cannot resonate strongly with the wavepackets. In this case, parametric instability (induced scattering off ions) occurs, producing a new initial condition, and subsequent collapse (Nicholson and Goldman, 1978).

With a magnetic field, the collapse still occurs. As a result of the magnetic field, collapsing wavepackets become pancake-shaped, with the largest dimension transverse to the field, and the collapse is delayed. This can have several consequences in the Type III problem. The different wave configuration can affect the emission and polarization of radio emission, and the lengthened collapse time can allow the beam to interact longer with the waves in the plasma. A computer simulation shows that this results in higher levels of electrostatic energy. An analytic theory is presented which is

successful in describing the new wave configuration and the slowing of the nonlinear processes.

## CHAPTER II

### WAVES AND WAVE INTERACTIONS

There are three simple linear waves in an unmagnetized two-component plasma; an electromagnetic wave, a plasma wave, and an ion-sound wave (Krall and Trivelpiece, 1973; Jackson, 1975; Chen 1974). These waves have the following dispersion relations:

$$\omega^2 = \omega_{pe}^2 + c^2 k^2 ,$$

$$\omega^2 = \omega_{pe}^2 + 3v_e^2 k^2 ,$$

$$\omega^2 = k^2 c_s^2 ;$$

(8)

$\omega$  is the wave frequency,  $k$  is the wavenumber, and  $c$  is the speed of light. The plasma frequency,  $\omega_{pe} = (4\pi e^2 n_o / m_e)^{1/2}$ , is the frequency of free oscillation of electrons in a plasma ( $e$  is the electron charge,  $m_e$  the electron mass, and  $n_o$  the number density of electrons). The sound speed is  $c_s = [(T_e + T_i) / m_i]^{1/2}$ , where  $m_i$  is the ion mass, and  $T_e$  and  $T_i$  the electron and ion temperatures. The electron thermal speed is  $v_e = (T_e / m_e)^{1/2}$ .

Two kinds of plasma motions occur in these waves. When the wave is high frequency ( $\omega \gg kv_e$ ), the electrons, because of their lesser mass, are easily displaced relative to the ions. This separation of charge causes an electric field which tends to restore the electrons to their equilibrium position. This oscillation occurs near the plasma frequency. At lower frequencies ( $\omega \ll kv_e$ ), however, a quasi-neutral fluid displacement takes place. Since the two kinds of motion are associated with complementary frequency ranges, two distinct time scales naturally occur. On the high frequency time scale, there are the plasma and electromagnetic waves. The ion-acoustic wave is low frequency.

In a magnetic field,  $B_0$ , cyclotron motion is also possible. However, because the cyclotron frequencies,  $\omega_{ce} = eB_0/m_e c$  for electrons and  $\omega_{ci} = eB_0/m_i c$  for ions, can be assumed to be much less than the plasma frequency in the solar corona, these motions are also distinct from the high frequency motion.

Before deriving the nonlinear equations, we will examine the linear properties of two waves, the oblique Langmuir wave and the ion-acoustic wave, which will turn out to be the relevant waves in this problem. The Langmuir wave is of special interest because it can be driven to large amplitude by a plasma beam, such as a stream of electrons from a solar burst, while the electromagnetic

mode has a phase velocity greater than the speed of light, so cannot resonate with a beam. And we will see later that the ion sound wave interacts nonlinearly more strongly with the high frequency wave field than do any of the magnetic low frequency modes.

#### Langmuir Waves in a Magnetic Field

The Langmuir wave is an electrostatic plasma wave with an electric field  $\underline{\mathcal{E}}$  parallel to the direction of propagation,  $\hat{\underline{k}}$ . We want to know how a magnetic field will affect its frequency and polarization.

The general wave equation for  $\underline{\mathcal{E}}$  in the case of no external field is found (Jackson, 1975) from Maxwell's equations and linearized fluid momentum and continuity equations:

$$\frac{\partial^2 \underline{\mathcal{E}}}{\partial t^2} + \omega_{pe}^2 \underline{\mathcal{E}} - 3v_e^2 \underline{\nabla}(\underline{\nabla} \cdot \underline{\mathcal{E}}) + c^2 \underline{\nabla} \times \underline{\nabla} \times \underline{\mathcal{E}} = 0 . \quad (9)$$

We can include the effect of a small magnetic field as a perturbation in the momentum equation when the frequency of the wave ( $\sim \omega_{pe}$ ) is greater than the magnetic gyration frequency; i.e.,  $\omega_{pe} \gg \omega_{ce}$ . The result is the following wave equation (Goldman, Weatherall, and Nicholson, 1980):

$$\begin{aligned} \frac{\partial^2 \underline{\mathcal{E}}}{\partial t^2} + \omega_{pe}^2 \underline{\mathcal{E}} - 3v_e^2 \underline{\nabla}(\underline{\nabla} \cdot \underline{\mathcal{E}}) + c^2 \underline{\nabla} \times \underline{\nabla} \times \underline{\mathcal{E}} - \underline{\mathcal{E}} \times \underline{\omega}_{ce} \\ - (\underline{\mathcal{E}} \times \underline{\omega}_{ce}) \times \underline{\omega}_{ce} = 0 , \end{aligned} \quad (10)$$

where the vector  $\omega_{ce}$  is in the direction of the magnetic field,  $\omega_{ce} = \omega_{ce} \hat{b}$ .

This equation may be solved with the usual matrix methods to find normal modes. The change in the Langmuir wave natural frequency which is of order  $\omega_{ce}^2$  is

$$\omega^2 - \omega_{pe}^2 - 3k^2 v_e^2 = \omega_{ce}^2 \sin^2 \theta , \quad (11)$$

when  $\omega_{pe}^2 \ll c^2 k^2$ , and  $\theta$  is the angle between  $\underline{k}$  and  $\underline{B}_0$ .

If we write the electric field as the real part of  $eE \exp(i\omega_0 t)$ , the polarization vector  $\underline{e}$  is

$$\underline{e} = \begin{pmatrix} \sin \theta \\ 0 \\ \cos \theta \end{pmatrix} + \frac{i\omega_{ce} \omega_{pe}}{k^2 c^2} \sin \theta \begin{pmatrix} 0 \\ 1 \\ 0 \end{pmatrix} + \frac{1}{2} \frac{\omega_{ce}^2}{k^2 c^2} \begin{pmatrix} -\sin \theta \\ 0 \\ \cos \theta \end{pmatrix} \quad (12)$$

in a coordinate system with  $\underline{B}_0$  in the  $\hat{z}$ -direction and  $\underline{k}$  in the  $x$ - $z$  plane (see Figure 4). The first term is a vector in the direction of  $\underline{k}$ . The other two vectors, containing the transverse components of the field, will be small when

$$\omega_{pe} \omega_{ce} \ll k^2 c^2 . \quad (13)$$

If we ignore the transverse parts of the field, however, we can make errors of order  $\omega_{ce}/\omega_{pe}$  in the wave equation. This is because in the  $c^2 \nabla \times \nabla \times \underline{E}$  term, the electric field is multiplied by an enormous factor. We

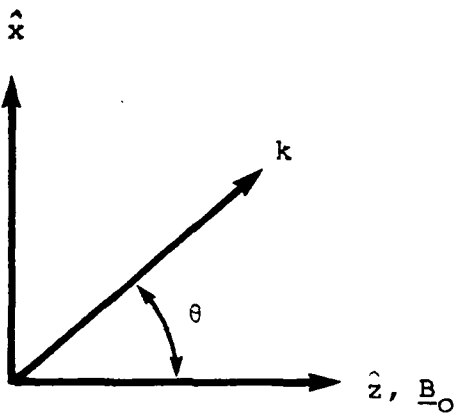


FIGURE 4. Coordinate system with magnetic field  $\underline{B}_0$  in  $\hat{z}$  direction.  $\theta$  is the angle between wave vector  $\underline{k}$  and  $\underline{B}_0$ .

see by substituting the vector electric field into this term that

$$c^2 \nabla \times \nabla \times \underline{e} = i\omega_{pe} \omega_{ce} \begin{pmatrix} 0 \\ 1 \\ 0 \end{pmatrix} + \omega_{ce}^2 \sin\theta \cos\theta \begin{pmatrix} \cos\theta \\ 0 \\ -\sin\theta \end{pmatrix}. \quad (14)$$

Actually, such terms due to the transverse part of the field cancel or combine with other magnetic terms in the equation:

$$\begin{aligned} i\omega_{pe} \omega_{ce} \times \underline{e} &= -i\omega_{pe} \omega_{ce} \begin{pmatrix} 0 \\ 1 \\ 0 \end{pmatrix} + 0 \left( \frac{\omega_{pe}^2}{c^2 k^2} \right) \omega_{ce}^2 \\ \omega_{ce} \times \omega_{ce} \times \underline{e} &= -\omega_{ce}^2 \begin{pmatrix} \sin\theta \\ 0 \\ 0 \end{pmatrix} + 0 \left( \frac{\omega_{pe}^2}{c^2 k^2} \frac{\omega_{ce}}{\omega_{pe}} \right) \omega_{ce}^2. \end{aligned} \quad (15)$$

After use of the polarization information (equivalent to diagonalizing the wave matrix), the wave equation becomes

$$\frac{\partial^2}{\partial t^2} \underline{\xi} = -\omega_{pe}^2 \underline{\xi} + 3v_e^2 \nabla \cdot \underline{\xi} - \sin^2\theta \omega_{ce}^2 \underline{\xi}. \quad (16)$$

With this equation, the longitudinal approximation will cause only small errors of order  $\omega_{ce} \omega_{pe} / k^2 c^2$ . The term  $\underline{\xi} \sin^2\theta$  represents the inverse Fourier transform of  $\underline{\xi}(\underline{k}) k_x^2 / k^2$ , and is conveniently evaluated in  $k$ -space.

### Ion-Acoustic Waves in a Magnetic Field

The low frequency electrostatic ion-acoustic wave is described by the wave equation (Krall and Trivelpiece, 1973) for the quasineutral density perturbation,  $\delta n$

$$\frac{\partial^2}{\partial t^2} \delta n - c_s^2 \nabla^2 \delta n = 0. \quad (17)$$

In the solar corona, the slowly varying wave time scale,  $\omega^{-1}$ , is such that (Nicholson, et al., 1978)

$$\omega_{ce} \gg \omega \gg \omega_{ci}. \quad (18)$$

This means that we should add the effect of magnetized electrons, while leaving the ions unmagnetized, to the fluid theory of ion-acoustic waves. Using the electron and ion continuity equation, the unmagnetized ion momentum equation, the electron momentum equation with the magnetic force, and the assumptions of quasi-neutrality and electrostatic fields, we obtain the dispersion relation (Nicholson, et al., 1978):

$$\omega^2 = k^2 c_s^2 + \frac{\omega_{ce} \omega_{ci}}{1 - \frac{k_z^2}{k_x^2} \left( \frac{\omega_{ce}}{\omega^2} - 1 \right)}, \quad (19)$$

$\hat{k}_z$  is parallel to  $\underline{B}_0$ , as shown in Figure 4.

The dispersion relation has two branches, which are plotted as a function of angle  $\theta$  in Figure 5. At  $\theta = 0$  ( $\underline{k}$  parallel to  $\underline{B}_0$ ), the two branches can be identified

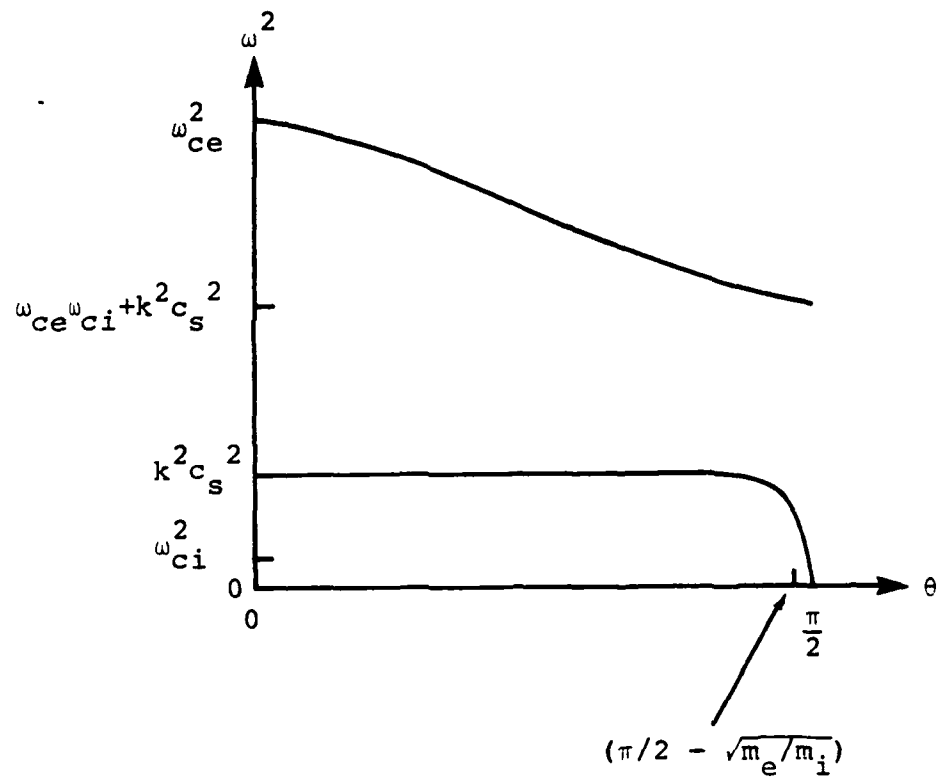


FIGURE 5. Electrostatic waves with  $B_0 \neq 0$ .  $\omega^2$  vs.  $\theta$  holding the magnitude of  $k$  fixed.

with an electron cyclotron wave and the well-known ion-acoustic wave along the magnetic field (Jackson, 1975). As the angle increases toward  $\theta = \pi/2$  ( $\mathbf{k}$  perpendicular to  $\mathbf{B}_0$ ), the cyclotron branch evolves toward the lower hybrid resonance, while the ion-acoustic branch shows a substantial change only in a narrow region near  $\theta = \pi/2$  of width  $\sim \sqrt{m_e/m_i}$ . This leads us to conclude that the wave equation for ion-acoustic density perturbations is the same as with no magnetic field, except for the wave vectors directly perpendicular to the magnetic field.

These properties of the sound wave in a magnetic field can be explained by a simple physical model in which the motion of electrons is restricted to the direction of the magnetic field like "beads on a wire." This assumption does not change the fact that the electric field must be in the direction of the pressure gradient, and the resulting wave equation has the same form as in the unmagnetized case. But in order for the motion of the electrons, which is now strictly in the direction of the magnetic field, to be uninhibited by electron inertia, we require that  $\omega \ll k_z v_e$ . This gives us the condition

$$\frac{k_z}{k} \gg \sqrt{\frac{m_e}{m_i}} . \quad (20)$$

There are many low frequency modes which exist when the plasma is magnetized besides this one. We will

investigate these in the context of their interaction with nonlinear Langmuir waves in a later section.

### Wave-Wave Interaction

Although the above linear waves occur on different time scales, we can deduce several ways by which the high frequency electric field and low frequency density might be coupled together. First, suppose that the Langmuir electric field envelope is slowly varying. If the displacement  $x_{osc} = qE/m\omega^2$  of an electron in an oscillating electric field,  $\xi = E \cos \omega t$ , is much smaller than the length scale,  $L$ , of the inhomogeneity, then we can treat the inhomogeneity as a perturbation. The net effect is that over many oscillations, the electrons feel a force away from regions of larger electric field amplitudes:

$$m\ddot{x} = -\frac{\partial}{\partial x} V_p = -\frac{\partial}{\partial x} \frac{1}{4} \frac{q^2 E^2}{m\omega_0^2} . \quad (21)$$

This is the ponderomotive force, and  $V_p$  is the ponderomotive potential. Although the force on ions is  $m_e/m_i$  smaller, the ions will be displaced also because of electrical forces caused by the departure of the electrons. The result is a decrease of the fluid density in regions of large electric field.

The density irregularities can also affect the high frequency wave. From the Langmuir dispersion relation,

we can see that the phase velocity of the Langmuir waves depends upon the electron density:

$$\frac{\omega}{k} \sim \frac{\omega_{pe}}{k} \propto n^{\frac{1}{2}}. \quad (22)$$

This will cause the plasma waves to be refracted into the regions of lower density. Together, these two nonlinear effects are known to result in plasma instability. The particular contribution of this work is to include a magnetic field in the study of the nonlinear behavior. Before proceeding further, we will derive the nonlinear coupled equations.

#### Derivation of Nonlinear Wave Equations

If there are two distinct time scales, we can separate the fluid and field quantities into two parts. For example, the low frequency (slow time scale) component of the fluid density  $n$  is found by averaging over the period of the high frequency motions:

$$n_L = \bar{n} = \frac{\omega}{2\pi} \int_0^{2\pi/\omega} n \, dt. \quad (23)$$

The part averaged out is fluctuating at the high frequency:

$$n_H = n - n_L. \quad (24)$$

If the averaging is to be useful,  $n_L$  must not change

significantly during the period of the fast motions.

Let the characteristic time for change in  $n_L$  be called  $T$ . Then the requirement for separable time scales is

$$\frac{1}{\omega T} \ll 1 . \quad (25)$$

The high and low frequency variables are defined in this way:

$$n^e = n_L^e + n_H^e , \quad n^i = n_L^i + n_H^i ,$$

$$\underline{v}^e = \underline{v}_L^e + \underline{v}_H^e , \quad \underline{v}^i = \underline{v}_L^i + \underline{v}_H^i ,$$

$$\underline{B} = \underline{B}_L , \quad \underline{\mathcal{E}} = \underline{\mathcal{E}}_H + \underline{\mathcal{E}}_L . \quad (26)$$

Notice that  $\underline{B}_L$  includes the background magnetic field,  $\underline{B}_0$ , and the background density,  $n_0$ , is contained in  $n_L$ . Because the high frequency wave is electrostatic, there is no  $\underline{B}_H$  term. The high frequency oscillation can be factored out of the high frequency electric field by writing it

$$\underline{\mathcal{E}}_H = \underline{E} e^{-i\omega_p e t} + \underline{E}^* e^{i\omega_p e t} . \quad (27)$$

$\underline{E}$  is called the "envelope" of the field. The superscripts  $e$  and  $i$  refer to the two plasma species, electrons and ions. When no superscript appears on the fluid quantities  $n$ ,  $\underline{v}$ ,  $q$ , or  $m$  (density, velocity, charge, or mass),

it is understood that the equation may be written for either electrons or ions.

By time averaging, an equation containing two time scale quantities may be separated into two equations, one which is high frequency, and one which is low frequency. We will analyze the fluid continuity and momentum equations in this way. When the forces acting in the fluid are electric, magnetic, and pressure, the fluid equations are

$$\frac{\partial n}{\partial t} + \nabla \cdot n \underline{v} = 0 ,$$

$$n \frac{\partial \underline{v}}{\partial t} + n \underline{v} \cdot \nabla \underline{v} = \frac{nq}{m} \underline{E} + \frac{nq}{mc} \underline{v} \times \underline{B} - \gamma v_s^2 \nabla n \quad (28)$$

where  $\gamma$  is an adiabatic index, and  $v_s$  is the thermal velocity.

Each variable contains a high and low frequency part, so many components are involved in a product such as  $n \underline{v}$ :

$$n \underline{v} = n_H \underline{v}_H + n_L \underline{v}_L + n_H \underline{v}_L + n_L \underline{v}_H . \quad (29)$$

The low frequency quantity which survives the time average over the high frequency period is  $n_L \underline{v}_L$ . The high frequency quantity which oscillates at  $\omega$  is  $n_H \underline{v}_L + n_L \underline{v}_H$ .

The fluid equations (for electrons or ions), after separating the time scales and eliminating terms which are of order  $1/\omega T$  or  $x_{osc}/L$ , are

1) high frequency:

$$\begin{aligned} \frac{\partial n_H}{\partial t} + \nabla \cdot n_L \underline{v}_H &= 0, \\ n_L \frac{\partial}{\partial t} \underline{v}_H - n_L \frac{q}{m} \underline{\mathcal{E}}_H - 3v_s^2 \nabla n_H + \frac{n_L q}{mc} (\underline{v}_H \times \underline{B}_L) \\ &+ \frac{n_H q}{m} \underline{\mathcal{E}}_L = 0; \end{aligned} \quad (30)$$

2) low frequency:

$$\begin{aligned} \frac{\partial n_L}{\partial t} + \nabla \cdot n_L \underline{v}_L &= 0, \\ n_L \frac{\partial}{\partial t} \underline{v}_L + n_L \underline{v}_L \cdot \nabla \underline{v}_L + n_L \underline{v}_H \cdot \nabla \underline{v}_H - n_L \frac{q}{m} \underline{\mathcal{E}}_L \\ &+ v_s^2 \nabla n_L - \frac{q}{mc} n_L \underline{v}_L \times \underline{B}_L = 0. \end{aligned} \quad (31)$$

The nonlinear term in the low frequency momentum equation is the ponderomotive force:

$$m_e n_L e \frac{\underline{v}_H \cdot \nabla \underline{v}_H e}{n_0} = n_0 \frac{q^2 |\underline{E}|^2}{m \omega_{pe}^2}. \quad (32)$$

We can identify several nonlinear forces in (30) which affect the high frequency motion of the electrons:

$$\delta n (q/m) \underline{\mathcal{E}}_H, \quad (33)$$

$$\underline{\mathcal{E}}_L (n_H q/m), \quad (34)$$

$$\text{and } n_L (q/m) \underline{v}_H / c \times \delta \underline{B}_L; \quad (35)$$

$\delta n$ ,  $\delta \underline{E}_L$ , and  $\delta \underline{B}_L$  are fluctuations due to the low frequency wave. If  $n_o$  and  $\underline{B}_o$  are the constant density and magnetic field, then  $n_L = n_o + \delta n$  and  $\underline{B}_L = \underline{B}_o + \delta \underline{B}_L$ .

The dominant nonlinearity in the high frequency equation will depend on the character of the low frequency wave. For example, the ion-acoustic wave has density fluctuations, but because it is electrostatic, there is no magnetic field associated with it. In this case, the pressure term is largest, because the magnetic term is zero, and the electric term is of order  $1/L^2 k_{De}^2$  when compared with the pressure. On the other hand, the Alfvén wave has no density fluctuations associated with it. Now the magnetic term is largest, the pressure term is zero, and the electric term is again small, of order  $1/\omega T$ . So the various low frequency waves will have different nonlinear effects.

Notwithstanding the above remarks, the only nonlinear term that we are going to keep is the pressure term. The reasoning is that we are not interested in all of the nonlinearities caused by all of the low frequency wave modes, only the largest one. The important low frequency fluctuation will be the one which has the strongest influence on the high frequency wave. So we ask the following question: if the plasma has large low frequency density fluctuations,  $\delta n/n_o$ , large magnetic fluctuations,  $|\delta \underline{B}_L|/|\underline{B}_o|$ , and large electric fluctuations,

$|\underline{\mathcal{E}}_L|/|\underline{\mathcal{E}}_H|$ , which will the high frequency wave couple to strongest?

To answer this question, we first take the ratio of the magnetic nonlinearity (35) to the density term (33):

$$\frac{|\delta B_L|/|B_0|}{\delta n/n_0} \frac{\omega_{ce}}{\omega_{pe}} . \quad (36)$$

If there is a nonlinear wave which has large density fluctuations,  $\delta n/n_0 \sim 1$ , and another nonlinear wave which has large magnetic fluctuations,  $|\delta B_L|/|B_0| \sim 1$ , the density perturbation causes the larger nonlinearity in the high frequency equation since  $\omega_{ce}/\omega_{pe} \ll 1$ . We can similarly compare the electric field term (34) to the density term (33) to form the ratio

$$\frac{|\delta \underline{\mathcal{E}}_L|/|\underline{\mathcal{E}}_H|}{\delta n/n_0} \frac{x_{osc}}{L} . \quad (37)$$

This also will be small since  $x_{osc}/L \ll 1$ . Therefore, we will limit our attention to waves which have large density fluctuations, and ignore the electric and magnetic fluctuations.

#### Nonlinear High Frequency Equation

Keeping only the pressure nonlinearity, the high frequency equations are identical with the linear ones except that  $n_0$  is replaced with  $n = n_0 + \delta n$ . The derivation proceeds as in the linear example, except that  $\omega_{pe}^2$  is

now  $4\pi e^2/m_e (n_0 + \delta n)$ . The nonlinear high frequency equation is

$$\begin{aligned} \frac{\partial^2}{\partial t^2} \underline{\mathcal{E}} + \frac{4\pi e^2 n_0}{m_e} \underline{\mathcal{E}} + 3v_e^2 \nabla \cdot \underline{\mathcal{E}} + \sin^2 \theta \omega_{ce}^2 \underline{\mathcal{E}} \\ = - \frac{4\pi e^2}{m_e} \delta n \underline{\mathcal{E}} . \end{aligned} \quad (38)$$

Actually, we are more interested in the slowly varying behavior of the envelope field. This can be easily obtained by factoring out the common multiples of  $\exp(-i\omega_{pe}t)$  from the high frequency equation. Notice that the term containing time derivatives is

$$\begin{aligned} \frac{\partial^2}{\partial t^2} \underline{E} e^{-i\omega_{pe}t} = \left( \frac{\partial^2}{\partial t^2} \underline{E} - 2i\omega_{pe} \frac{\partial}{\partial t} \underline{E} - \omega_{pe}^2 \underline{E} \right) \\ \cdot e^{-i\omega_{pe}t} . \end{aligned} \quad (39)$$

The term  $-\omega_{pe} \underline{E}$  cancels with  $4\pi e^2 n_0/m_e \underline{E}$ . Because the envelope is slowly varying,  $\partial^2/\partial t^2 \underline{E}$  can be ignored compared with  $\omega_{pe}^2/\partial t \underline{E}$ . The resulting equation for the envelope field is then:

$$2i\omega_{pe} \frac{\partial}{\partial t} \underline{E} + 3v_e^2 \nabla \cdot \underline{E} - \omega_{ce}^2 \sin^2 \theta \underline{E} = \frac{4\pi e^2}{m_e} \delta n \underline{E} . \quad (40)$$

### Low Frequency Waves

The introduction of the background magnetic field produces a rich set of low frequency normal modes (Stix,

1963). Some can be described from the linearized versions of the low frequency fluid equations. Others need a more elaborate kinetic theory derivation. A partial list of these modes and their frequency of oscillation is in Table 3.

We have argued that the most important source of nonlinearity in the high frequency equation is due to the low frequency density perturbations. If we Fourier analyze these density perturbations, the largest amplitudes of  $\delta n(\omega, \underline{k})$  might be expected to be when  $\omega$  is near some natural frequency of the plasma,  $\omega^\sigma(\underline{k})$ . Therefore, we solve for the density perturbations which are resonant with each of the normal modes, and see if any mode has exceptionally large amplitude.

The low frequency electron density perturbation may be derived by first using the wave equation (including the nonlinear currents) to find the amplitude of the electric field. Next, the electron currents due to this field are calculated from the linear conductivities. The resulting density perturbation is found from the continuity equation. The answer is a complicated, but general equation for  $\delta n$  (Sanuki and Schmidt, 1977):

$$\delta n(\omega, \underline{k}) = -\underline{k} \cdot \underline{\sigma}_e \cdot \left[ \frac{M^{-1}}{c^2} \cdot \underline{\sigma}_e \cdot \underline{k} \left( \frac{\omega^2}{e^2 c^2} \frac{4\pi \psi_p}{c^2} \right) + \frac{i \underline{k} \psi_p}{e^2 \omega} \right] . \quad (41)$$

$\underline{\sigma}_e$  is the low frequency electron conductivity,  $M^{-1}$  is the

TABLE 3  
SAMPLE OF MAGNETIZED WAVES AND THEIR COUPLING THROUGH  
DENSITY PERTURBATIONS WITH HIGH FREQUENCY LANGMUIR WAVES

Wave	$\omega^{\sigma}$	$\Lambda^{\sigma}$
Ion Acoustic (Partly Magnetized)	$k c_s$	1
Ion Acoustic (Fully Magnetized)	$k_{\parallel} c_s$	1
Ion Cyclotron	$\omega_{ci}$	$\left(\frac{k_{\perp} v_i}{\omega_{ci}}\right)^2$
Electron Cyclotron	$\omega_{ce} \cos\theta$	$\left(\frac{k_{\perp} v_e}{\omega_{ce}}\right)^2 \left(\frac{\omega_{ce}}{\omega_{pe}}\right)^4$
Electron Bernstein	$2\omega_{ce}$	$\frac{1}{4} \left(\frac{\omega^2 - \omega_{ce}^2}{\omega^2 - \omega_{UH}^2}\right)^2 \left(\frac{k_{\perp} v_e}{\omega_{ce}}\right)^4$
Lower Hybrid	$(\omega_{ce} \omega_{ci})^{\frac{1}{2}}$	$\left(\frac{k_{\perp} v_e}{\omega_{ce}}\right)^2$
Whistler	$\frac{k^2 c^2}{\omega_{pe}^2} \omega_{ce} \cos$	$\left(\frac{\omega_{ci}}{\omega}\right)^2 \left(\frac{c_s}{v_A}\right)^2 \sin^2\theta$
Alfven (Fast)	$k v_A$	$\left(\frac{c_s}{v_A}\right)^2 \sin^2\theta$
Magnetosonic (Partly Magnetized)	$k v_A$	$\left(\frac{c_s}{v_A}\right)^2$
Alfven (Slow)	$k_{\parallel} v_A$	$\left(\frac{k_{\perp} v_i}{\omega_{ci}}\right)^2$

inverse of the Maxwell wave matrix, and  $\psi_p$  is the Fourier transform (a convolution) of the ponderomotive potential [see Eq. (32)].

We can evaluate this expression for various normal modes by making a resonant approximation. The result is very interesting, because for each normal mode  $\omega^\sigma$ , we can write an equation for  $\delta n$  in this form:

$$(\omega^2 - \omega^\sigma)^2 \frac{\delta n}{n_0} = \omega^\sigma \Lambda^\sigma \frac{\psi_p}{T} . \quad (42)$$

On the left side of the equation is a linear wave operator on  $\delta n$ , and on the right side is the nonlinear driving term due to the ponderomotive potential. Notice that the coupling is proportional to  $\Lambda^\sigma$ . For the ion sound wave,  $\Lambda = 1$ . In every other instance,  $\Lambda^\sigma$  is a smallness parameter, such as  $c_s^2/v_A^2$  [where  $c_s$  is the sound speed and  $v_A = (B_0^2/4\pi m_i n_0)^{1/2}$  is the Alfvén speed] or  $k_\perp^2 v_e^2/\omega_{ce}^2$ . The coefficient  $\Lambda^\sigma$ , calculated for each of the normal modes in Table 3, is given in the last column. In the lower solar corona, when  $\omega_{ce}^2/\omega_{pe}^2 \sim 0.1$ , these numbers are of the order (using parameters from Bardwell and Goldman, 1976),

$$\frac{c_s^2}{v_A^2} \sim \frac{1}{40} , \quad \frac{k_\perp^2 v_e^2}{\omega_{ce}^2} \sim 10^{-3} . \quad (43)$$

These parameters have interesting physical interpretations.  $c_s^2/v_A^2$  is the ratio of the thermal to magnetic

energy,  $n_0 T / (B_0^2 / 4\pi)$ . In this case, we might deduce that more of the wave energy is in the magnetic perturbations than in the density perturbations. The other parameter  $k^2 v_e^2 / \omega_{ce}^2$  is the ratio of the thermal gyroradius to the wavelength. This factor enters because the electron motion across the magnetic field is restricted.

Without solving the complete, nonlinear equations, what conclusions can we reach regarding the intensity of the nonlinear interactions from the coupling coefficient  $\Lambda^\sigma$  in Eq. (42)? With several simplifying assumptions, we can derive an upper limit on the growth rates of parametric wave instability. We will use this as an indication of the relative significance of the various low frequency wave modes in the nonlinear theory.

First we assume a simple three-wave instability (see Figure 6) involving a large amplitude Langmuir wave at  $(\omega_0, \underline{k}_0)$ , an unstable Langmuir wave at  $(\omega_L, \underline{k}_L)$ , and a low frequency wave at  $(\omega^\sigma, \underline{k})$ . We can obtain a very simple dispersion relation (Bardwell and Goldman, 1976) by linearizing Eq. (40) (Fourier transformed in time and space) and Eq. (42) about the pump wave field,  $E_0$ :

$$(x - \Delta + i\gamma_L) (x + i\nu) + \lambda^2 = 0 , \quad (44)$$

where the frequency mismatch terms are defined

$$\Delta = \omega_0 - \omega_L - \omega^\sigma , \quad x = \omega - \omega^\sigma . \quad (45)$$

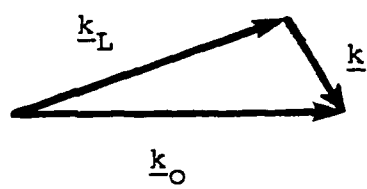


FIGURE 6. Three-wave wavenumber matching condition.

We have included the phenomenological damping of the Langmuir and the low frequency modes,  $\gamma_L$  and  $\nu$ , respectively. The term  $\lambda^2$  is defined

$$\frac{\lambda^2}{\omega_{pe}^2} = \frac{\omega^\sigma}{\omega_{pe}} \left[ \frac{u^2}{8} \left( \frac{E_0^2}{8\pi n_0 T} \right) \right] \Lambda^\sigma \quad (46)$$

In order to estimate the maximum growth rate, we now assume 1) perfect frequency matching,  $\Delta = 0$ ; 2)  $\omega$  is nearly resonant with the low frequency mode, so that  $x \sim i\text{Im}(\omega) \equiv i\Gamma^\sigma$ ; and 3) negligible Landau damping of the high frequency Langmuir wave,  $\gamma_L = 0$ . Equation (46) solved for  $\Gamma$  gives

$$\Gamma^\sigma = \frac{1}{2} ( \nu - \sqrt{\nu^2 + 4\lambda^2} ) . \quad (47)$$

For waves which are weakly damped, the condition that  $\nu \ll \lambda$  is very easy to satisfy, and the growth rate is given by

$$\Gamma^\sigma \sim -\lambda . \quad (48)$$

This may not be true for the ion-acoustic wave, which is heavily damped at equal temperatures,  $\nu \sim c_s k$ . Let us consider the consequences of damping on the growth of the ion-acoustic mode. To be specific, we choose  $k = 0.078 k_{De}$ , which is the wavenumber matching required near a few solar radii for a three-wave decay instability during a Type III burst (Bardwell and

Goldman, 1976), and a pump energy  $E_0^2/8\pi n_0 T = 10^{-4}$ . For these parameters,  $v^2/\lambda^2 = 144$ , and the growth rate given by (47) is reduced by 1/6 when compared with (48). Generally, the smallness parameters  $\Lambda^\sigma$  in Table 3 are smaller than 1/6, so that the damping of the ion-acoustic mode can be ignored in the context of this discussion.

Therefore, to the extent that our assumptions have led to the most favorable conditions for growth, (48) can be viewed as an upper limit to the growth rate. Because  $\Gamma^\sigma \propto \Lambda^\sigma$ , we can conclude that for instabilities involving two Langmuir waves and a low frequency wave in a weakly magnetized field, the growth rate will be largest if the low frequency wave is the ion-acoustic wave. Without further justification, we will extend this conclusion to wave interactions in general, and exclude the magnetic modes in the computation of  $\delta n$ .

#### Low Frequency Nonlinear Equation

The above discussion motivates the derivation of the low frequency wave equation under assumptions which, in the linear regime, give the weakly magnetized ion-acoustic mode. We will assume

$$\mathbf{E}_L = -\nabla\phi, \quad \delta n_e \sim \delta n_i = \delta n, \quad (49)$$

$$v_\perp^e/v_\parallel^e \ll 1.$$

Together with these assumptions, Eq. (31) leads to the following low frequency equation:

$$\left( \frac{\partial^2}{\partial t^2} + c_s^2 \nabla^2 \right) \delta n = \frac{n_0}{m_i} \nabla^2 \left( \frac{e^2 |E|^2}{m_e \omega^2} \right),$$

$$\frac{k_z}{k} > \left( \frac{m_e}{m_i} \right)^{\frac{1}{2}}. \quad (50)$$

#### Summary of Nonlinear Equations

The basic equations describing the behavior of intense Langmuir waves have been derived from the following equations: the electron and ion continuity equations, the electron and ion force equations, and Maxwell's equations. The treatment is general enough to include a background magnetic field. Several assumptions used during the derivation are:

- 1) All quantities are high or low frequency;
- 2) Displacement of electrons in the high frequency motion is much less than the scale length of the slow variations;
- 3) Electric field energy density is small compared to the thermal energy density;
- 4) Magnetic field is weak-- $\omega_{ce} \ll \omega_{pe}$ .

In addition, the following important assertions were found to be justified:

- 1) The high frequency field is electrostatic;
- 2) Density nonlinearities are more important than magnetic nonlinearities in the high frequency equation;
- 3) Density perturbations due to magnetic modes are negligible.

The fluid derivation of the wave equations does not include damping. Kinetic theory shows that both the Langmuir wave and the ion-acoustic wave are damped by the interaction of thermal particles with the wave electric fields (Landau damping). This effect is added to the equations in the form of phenomenological damping rates  $v_e$  and  $v_i$  for the Langmuir wave and the ion-acoustic wave, respectively.

Before writing the equations in their final form, we define the following convenient units:

$$[t] = \frac{3}{2} \frac{1}{n} \frac{m_i}{m_e} \omega_{pe}^{-1},$$

$$[x, y] = \frac{3}{2} \left( \frac{1}{n} \frac{m_i}{m_e} \right)^{\frac{1}{2}} \lambda_e,$$

$$[n] = \frac{4}{3} n \frac{m_e}{m_i} n_o,$$

$$[E] = n \left( \frac{m_e}{m_i} \right)^{\frac{1}{2}} \left( \frac{16\pi n_o T}{3} \right)^{\frac{1}{2}}, \quad (51)$$

where the electron Debye length is  $\lambda_e = k_{De}^{-1} = (T/m_e \omega_{pe}^2)^{\frac{1}{2}}$  and the dimensionless ratio  $n = (\gamma_e T_e + \gamma_i T_i)/T_e$ .

In these units, the coupled equations for  $E$  and  $n$  are:

$$\left( i \frac{\partial}{\partial t} + \frac{v_e}{2} + \nabla^2 - \Omega^2 \sin^2 \theta \right) E = n E ,$$

$$\left( \frac{\partial^2}{\partial t^2} + i v_i \frac{\partial}{\partial t} - \nabla^2 \right) n = \nabla^2 |E|^2 . \quad (52)$$

The magnetic parameter is

$$\Omega = \frac{\omega_{ce}}{\omega_{pe}} \left( \frac{3}{4} \frac{1}{n} \frac{m_i}{m_e} \right)^{\frac{1}{2}} . \quad (53)$$

These dimensionless units (Nicholson, Goldman, Hoyng, and Weatherall, 1978) will be used throughout this work except on occasion when dimensional units are used for the sake of familiar notation. These should not be confused with other units defined in the literature, e.g., Zakharov and Rubenchik (1973) or Goldman and Nicholson (1978).

In the adiabatic approximation (Goldman, Rypdal, and Hafizi, 1980) the inertia of the ions is ignored, which allows  $(\partial/\partial t)n \rightarrow 0$ . The two equations can then be combined to give a nonlinear Schroedinger equation for the scalar envelope field  $E$ :

$$i \frac{\partial}{\partial t} E + \frac{v_e}{2} E + \nabla^2 E - \Omega^2 \sin^2 \theta E + (|E|^2 - \overline{|E|^2}) E$$

$$= 0 . \quad (54)$$

## Numerical Simulation

We can solve Equation (52) numerically in time and in two spatial dimensions using a split-step Fourier method (Hardin and Tappert, 1973). The algorithm is described in detail in a paper by Nicholson (1978, unpublished). The idea is to use complimentary grids in real space and wavenumber space, where each grid consists of 64 points in each dimension (or sometimes 32 points when computer time is restricted). This allows the solution of the linear part of the equation in  $k$ -space and the evaluation of the nonlinear terms in real space.

The introduction of the magnetic field is made by two changes in the algorithm. One is to add the magnetic dispersion to the thermal dispersion of the high frequency waves in the linear part of the program. The other is to suppress the low frequency density fluctuations directly perpendicular to  $B_0$  when  $k v_e / \omega_{ce} < 1$ .

For equal electron and ion temperatures, the ion-acoustic mode is heavily damped. Nonetheless, the wave behavior is adequately described by including a phenomenological damping,  $v_i \sim 2c_s k$  (DuBois and Goldman, 1965; Bardwell, 1976; Bardwell and Goldman, 1976; and Weatherall, Nicholson, and Goldman, 1979). The damping in the high frequency equation can be set equal to zero,  $v_e = 0$ , because the wavenumbers contained in the numerical grid are small and only very weakly Landau damped.

The simulations described in later pages of this work involve two sets of parameters for the solar corona which we have summarized below:

1) 1.1 R

$$n_e = 10^8 \text{ cm}^{-3}$$

$$T_e = T_i = 140 \text{ eV}$$

$$k_o = 0.05 \lambda_{De}^{-1}$$

$$\omega_{pe} = 5.64 \times 10^8 \text{ s}^{-1}$$

$$\lambda_{De} = 0.88 \text{ cm}$$

$$\omega_{ce} = 0.1 \omega_{pe} \text{ for } B_o = 3.2 \text{ gauss}$$

2) 0.5 A.U.

$$n_e = 50 \text{ cm}^{-3}$$

$$T_e = T_i = 20 \text{ eV}$$

$$k_o = 0.011 \lambda_{De}^{-1}$$

$$\omega_{pe} = 4 \times 10^5 \text{ s}^{-1}$$

$$\lambda_{De} = 470 \text{ cm}$$

$$\omega_{ce} = 0.01 \omega_{pe} \text{ for } B_o = 2.3 \times 10^{-4} \text{ gauss}$$

## CHAPTER III

### LINEAR AND NONLINEAR LANGMUIR WAVEPACKETS

Before solving the nonlinear equations numerically for the time evolution of large amplitude Langmuir waves, we should see what can be learned from two simple examples. The first is a dispersive wavepacket of Langmuir waves. Dispersion is a completely linear effect, and can be studied numerically in the context of Equation (52) for very low amplitude fields. The second is an interesting example of a one-dimensional soliton. The soliton is an exact, localized, nonlinear solution to Equation (54). However, the soliton is unstable to two-dimensional perturbation. Below we consider these two examples, and, in addition, study the effect the magnetic field has on dispersion and soliton stability.

#### Linear Dispersion

Dispersion of waves is due to the simple fact that waves of different wavelengths have different natural frequencies. One effect of dispersion is that waves of different wavelengths travel at different phase velocities. This has an interesting consequence when the wave is

localized in space in a wavepacket. Because the wavepacket is made up of many different wave components, and these component waves do not travel at exactly the same velocity, the packet will tend to spread out or to disperse.

In order to examine this effect, we will look at coherently phased Gaussian wavepackets. Gaussian wavepackets have the convenient property that at later times, at least to the extent of the approximations we will use, they remain Gaussian shaped. Therefore we represent the wave field (in one-dimension) as the real part of

$$E(z) = A e^{ik_0 z}, \quad (55)$$

where  $k_0$  is the central wavenumber,  $z$  is the spatial dimension, and the envelope function,  $A(z)$ , is a Gaussian with width  $L$ ,

$$A(z) = A_0 \exp[-(z-z_0)^2/2L^2]. \quad (56)$$

In linear theory, any field can be represented as a superposition of plane waves. The time evolution of any of these component waves is found from the wave equation and is independent of the others. For example, the variation of the phase of a wave with wavenumber  $k$  is  $\phi = \omega(k)t$ , where  $\omega(k)$  is given by the dispersion relation. The time evolution of the wavepacket can be found by Fourier transforming the packet into  $k$ -space, shifting

the phase of each Fourier component by  $\phi(k, t)$ , and transforming back to real space again:

$$E(z, t) = \frac{1}{2\pi} \int_{-\infty}^{\infty} E(k) e^{-\phi(k, t)} e^{ikz} dk. \quad (57)$$

Absorption is ignored.

In  $k$ -space, the packet is a Gaussian centered around  $k_o$ :

$$E(k) = A_o \sqrt{2\pi} L e^{-\frac{(k-k_o)^2 L^2 / 2}{e^{-i(k-k_o)z}}}. \quad (58)$$

In the limit that  $L$  becomes infinite (no wavepacket),  $E(k)$  is a  $\delta$ -function about  $k_o$ . If  $L$  is finite, but there are many oscillations in a packet width, then the spread of wavenumbers around  $k_o$  is small.  $\phi(k, t)$  can be expanded about  $k_o$ ,

$$\begin{aligned} \phi(k, t) &= \phi(k_o) + (k-k_o) \frac{d}{dk} \phi(k_o) \\ &+ \frac{1}{2} (k-k_o)^2 \frac{d^2}{dk^2} \phi(k_o) + \dots \end{aligned} \quad (59)$$

Now we can see how each order in  $(k-k_o)$  affects  $E(z, t)$  (Ginzburg, 1970).

To zero order, each wave mode in  $k$ -space advances in phase by  $\phi = \omega_o t$ , where  $\omega_o = \omega_{pe}^2 + 3k_o^2 v_e^2$ . In this case there is no dispersion. The integral (57) is easily done to find the real space field:

$$E(z, t) = A(z) \exp(ik_o z - i\omega_o t). \quad (60)$$

Notice that the packet envelope itself does not move, although the waves inside the packet propagate with the phase velocity,  $\omega_0/k_0$ .

To the next order, the phase is linearly dependent on wavenumber. Now the integral (57) becomes

$$E(z, t) = A \left( z - \frac{d\omega_0}{dk_0} t \right) \exp(ik_0 z - i\omega_0 t) . \quad (61)$$

The packet moves without distortion with the velocity  $\Delta z / \Delta t = d\omega_0 / dk_0$ , called the group velocity. To this order, both the group and phase velocities are well defined.  $A(z)$  can be any shape, not just Gaussian.

Finally, to second order, the expression for  $E$  becomes more complicated:

$$\begin{aligned} E(z, t) &= A_0 \sqrt{\frac{1}{1+i\beta t}} \exp(ik_0 z - i\omega_0 t) \\ &\cdot \exp \left[ -\frac{(z-z_0-\alpha t)^2}{L^2(1+\beta^2 t^2)} (1-i\beta t) \right], \\ \alpha &= \frac{d\omega_0}{dk_0} = \frac{3v_e^2 k_0^2}{\omega_0} , \\ \beta &= \frac{2}{L^2} \frac{d^2 \omega_0}{dk_0^2} = \frac{3v_e^2}{L^2} \frac{\omega_p^2}{\omega_0^2} . \end{aligned} \quad (62)$$

We have used the dispersion relation for Langmuir waves (8) in solving for  $\alpha$  and  $\beta$ . The maximum of the envelope,  $|E|$ , moves with the group speed as before. But now the width of  $|E|$  is increasing with time. This is because

neither the position nor velocity of the wavepacket is precisely defined. The coordinate uncertainty in the position of the waves is  $\Delta x = L$ , and the uncertainty in velocity is due to the spread of wavenumbers,  $\Delta k = 2/L$ . In quantum mechanics the probability function of a free particle has similar behavior (Leighton, 1964).

These results can be extended to two dimensions of a wavepacket centered around  $x = x_0$  and  $z = z_0$ , with  $\underline{k}_0$  in the z-direction:

$$E(x, z) = A_0 \exp\{-[(x-x_0)^2 + (z-z_0)^2]/2L^2\} \exp(i\underline{k}_0 \cdot \underline{z}) \quad (63)$$

The time behavior is a generalization of (57):

$$E(x, z, t) = \frac{1}{(2\pi)^2} \int_{-\infty}^{\infty} \int_{-\infty}^{\infty} E(\underline{k}_x, \underline{k}_z) \cdot \exp[i(\underline{k}_z z + \underline{k}_x x)] \exp[-i\phi(\underline{k})] d\underline{k}_x d\underline{k}_z \quad (64)$$

To first order in  $(\underline{k} - \underline{k}_0)$ , the phase propagates with the velocity  $v_{ph} = \omega_0/k_0 \hat{z}$ , and the packet envelope moves with the velocity  $v_{gr} = d\omega_0/dk_0$ , as one would expect.

The expansion of  $\phi(\underline{k})$  to second order in  $(\underline{k} - \underline{k}_0)$  is

$$\begin{aligned} \phi(\underline{k}) = \phi(\underline{k}_0) + (\underline{k} - \underline{k}_0)_i \frac{\partial}{\partial k_i} \phi(\underline{k}_0) + \frac{1}{2} (\underline{k} - \underline{k}_0)_i (\underline{k} - \underline{k}_0)_j \frac{\partial}{\partial k_i} \frac{\partial}{\partial k_j} \phi(\underline{k}_0) \end{aligned} \quad (65)$$

(In the summation convention, sums over both coordinate indices are implied by repeated decay indices.) If the matrix  $(\partial/\partial k_i)(\partial/\partial k_j)[\phi(k_o)]$  is not diagonal, the integration in (64) becomes very difficult. We will choose two examples for which the matrix is diagonal: 1) an isotropic plasma with a symmetric Gaussian wavepacket; and 2) an anisotropic plasma with  $k_o$  in the direction of  $B_o$ . The equation for the envelope modulus squared has the form (in either case):

$$|E|^2 = A_o^2 \sqrt{\frac{1}{(1+\alpha^2 t^2)} \frac{1}{(1+\beta^2 t^2)}} \cdot \exp\left[-\frac{(x-x_o)^2}{L^2(1+\alpha^2 t^2)}\right] \exp\left[-\frac{(z-z_o-\gamma t)^2}{L^2(1+\beta^2 t^2)}\right]. \quad (66)$$

When there is a magnetic field (case 2), the dispersion parameters for Langmuir waves, as derived from (11), are

$$\begin{aligned} \alpha &= \frac{1}{\omega_o} \frac{1}{k_o^2} \frac{1}{L^2} (\omega_{ce}^2 + 3k^2 v_e^2) , \\ \beta &= \frac{1}{\omega_o} \frac{1}{k_o^2} \frac{1}{L^2} (3k^2 v_e^2) , \\ \gamma &= 3 \frac{v_e^2 k_o}{\omega_o} . \end{aligned} \quad (67)$$

The case with no magnetic field (case 1) is found by setting the electron cyclotron frequency,  $\omega_{ce}$ , in the above expressions to zero.

Now we will use the computer to solve for the time behavior of a wavepacket of Langmuir waves. Actually, we are solving the complete set of wave equations (52), but for small amplitudes of the fields the nonlinear behavior is not important. We can compare the numerical results with the analytic theory to verify that the code is doing the linear physics correctly.

The initial wavepacket is shown in Figure 7 at an early time. The plot shows contours of constant amplitude for the envelope field in real space on a 64x64 point grid. In physical units, the wavepacket contains waves with wavenumber  $k_o = 0.01 k_{De}$ , where  $k_o$  points in the z-direction. However, rather than belabor the physical dimensions, we will express distance in terms of grid units  $\Delta x$  ( $\Delta x$  is about  $100 \lambda_{De}$ ) and time in the dimensionless units of the equations (one unit,  $T$ , is 220 electron plasma periods). The wavelength of the wave is about  $5\Delta x$ , although this periodicity does not appear in the pictures which plot only the modulus of  $E$ . The packet widths,  $L$ , which are initially the same in both dimensions, are about  $2\Delta x$ , as seen in the picture.

With no magnetic field, the group velocity,  $\gamma$ , and the spreading rates,  $\alpha$  in the x-direction, and  $\beta$  in the z-direction are

$$\gamma = 0.4 \Delta x/T, \quad \alpha = 0.12/T, \quad \beta = 0.12/T. \quad (68)$$

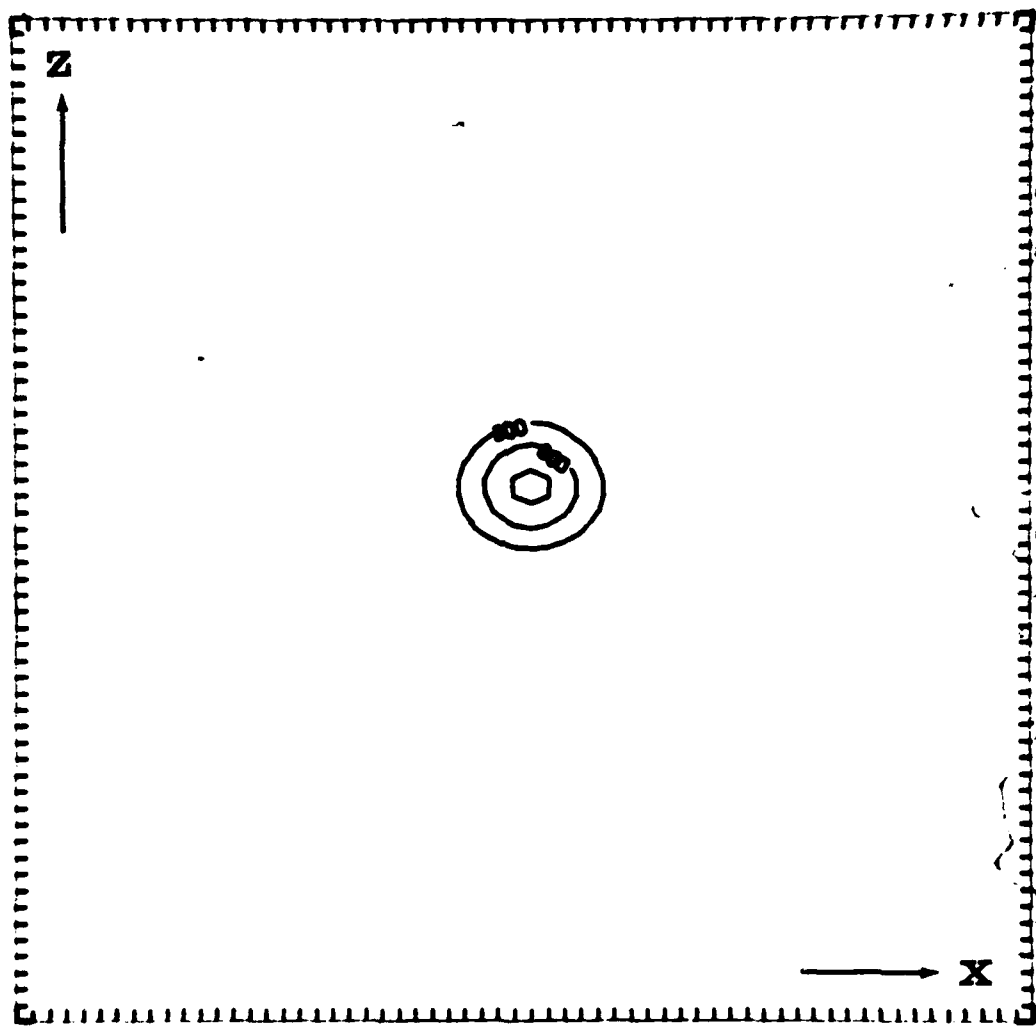


FIGURE 7. Initial linear Gaussian wavepacket in real space. The contours represent regions of equal electric field amplitude. The packet envelope contains waves with wave vectors centered about  $k_0 = 0.01 k_{De} \hat{z}$ . The labels are scaled by  $10^5$ , and the units are those of Eq. (51). The hatch-marks indicate the separation between points in the grid. There are 64 grid units on each axis.

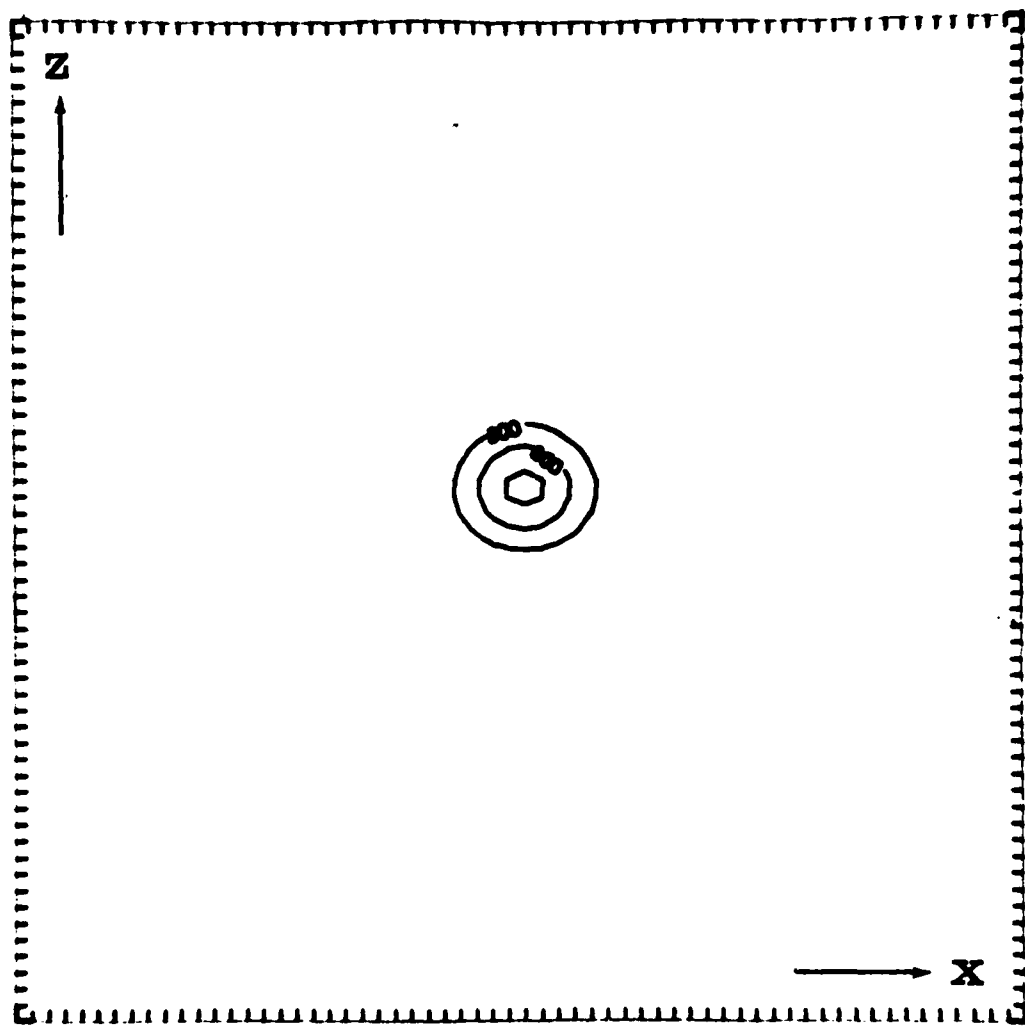


FIGURE 7. Initial linear Gaussian wavepacket in real space. The contours represent regions of equal electric field amplitude. The packet envelope contains waves with wave vectors centered about  $k_0 = 0.01 kDe^2$ . The labels are scaled by  $10^5$ , and the units are those of Eq. (51). The hatch-marks indicate the separation between points in the grid. There are 64 grid units on each axis.

At later time,  $T = 35$ , the wavepacket appears as in Figure 8. The packet motion between  $T = 0$  and  $T = 35$  is about 12 units, as expected from (68). The dispersive increase in the packet widths should only be about 5%. Most of the spreading in the direction perpendicular to  $\underline{k}_0$  is due to the angular spread in  $k$ , which is  $\Delta k_x/k_0 \sim 1/4$ . Because the component waves travel in the direction of their wave vectors, some of which are not parallel or even nearly parallel to  $\underline{k}_0$  as we previously assumed, the packet becomes distorted as it moves forward. This cannot be avoided because the angular separation of modes is inherent in the algorithm.

Nonetheless, this makes an interesting contrast to the magnetized case, when  $\omega_{ce} = 0.03 \omega_{pe}$ :

$$\gamma = 0.4 \Delta x/T, \quad \alpha = 0.40/T, \quad \beta = 0.12/T. \quad (69)$$

Now the spreading in the perpendicular direction becomes more significant. In 15 time units, the increase in wavepacket width transverse to the magnetic field is over 600%, as can be seen in Figures 9a and 9b. By comparing with the previous example, we can deduce that most of the spreading of the packet in the pictures is due to the magnetic dispersion. This is remarkable because the magnetic dispersion is only three times the thermal dispersion.

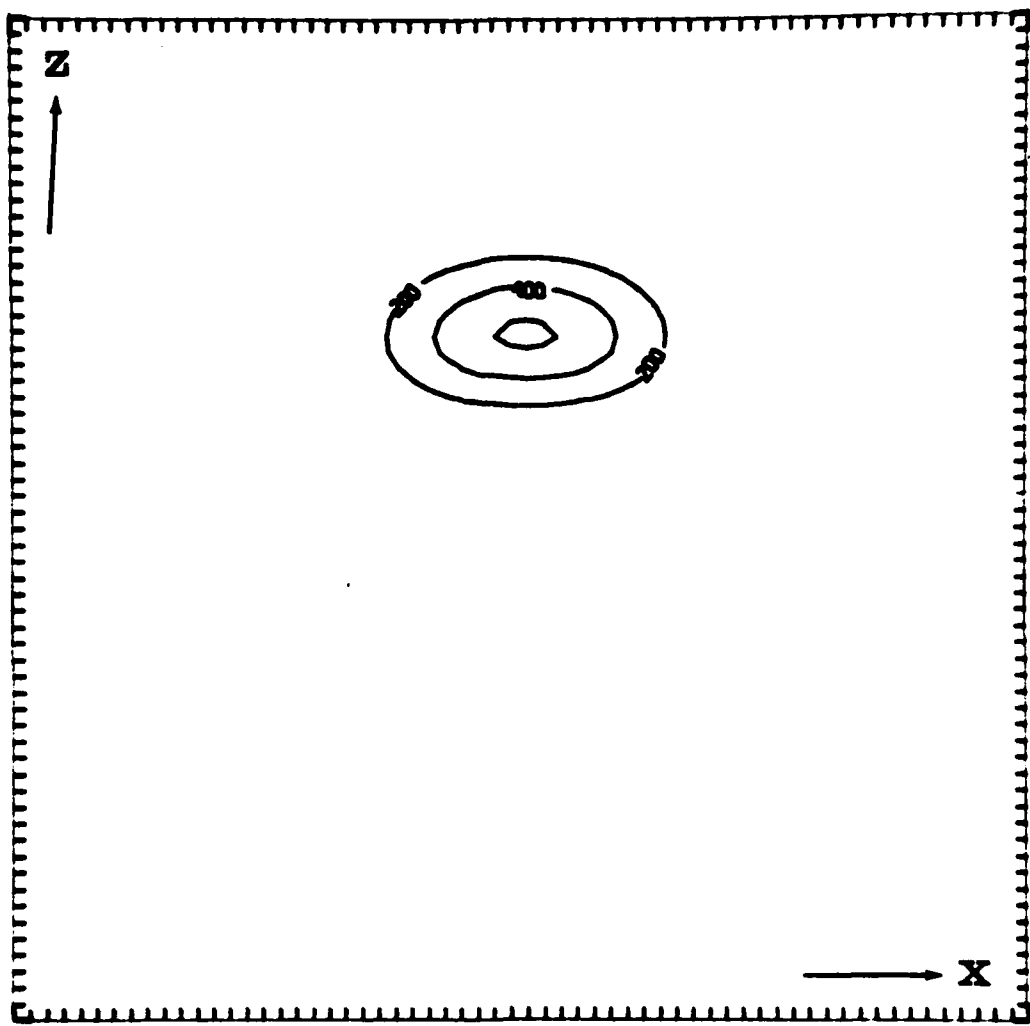


FIGURE 8. Electric field amplitude contours of the wave-packet in Fig. 7 at later time,  $T=35$  (7700 plasma periods). There is no magnetic field. The packet has moved in the  $z$ -direction at a speed determined by the Langmuir wave group velocity. The spreading is mainly due to the angular spread in wave vectors in the component waves.

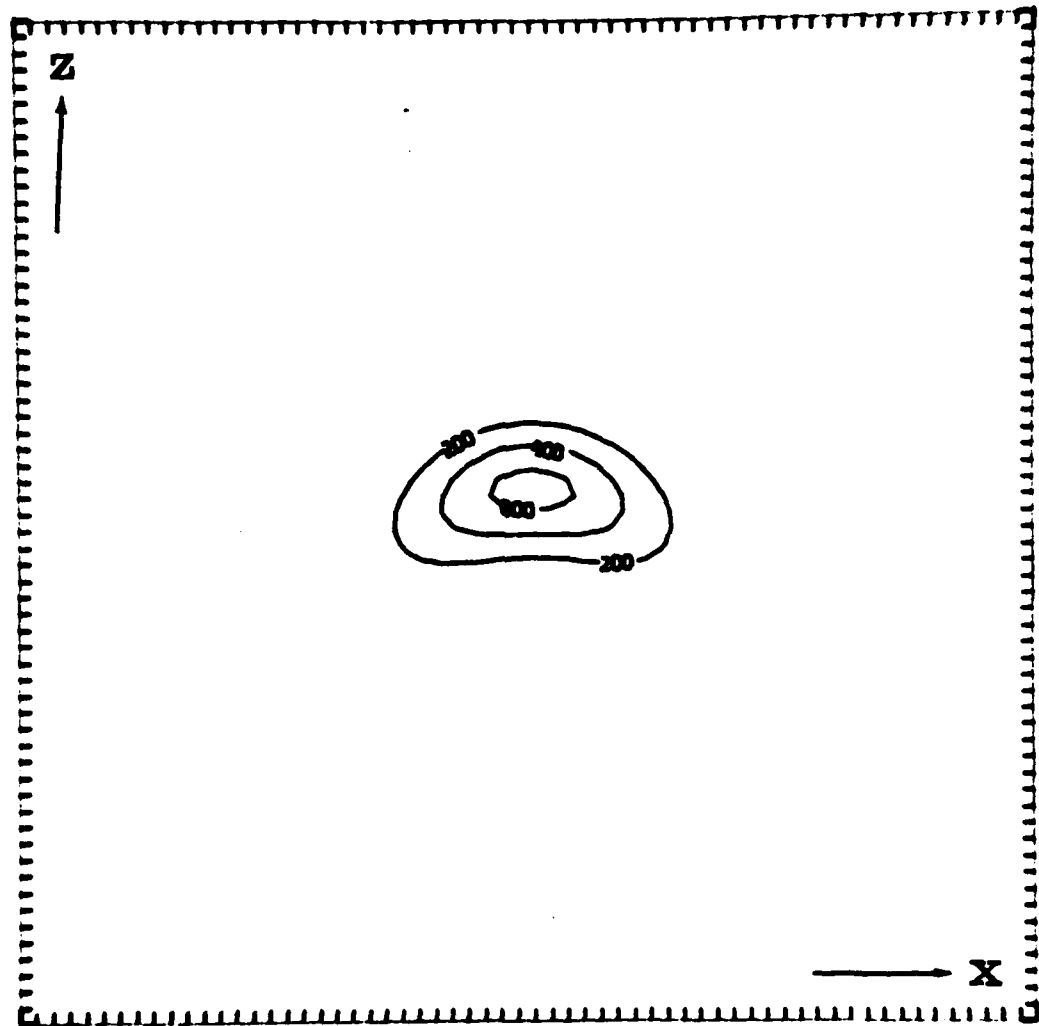


FIGURE 9a) Wavepacket of Figure 7 at a time  $T=5$  (1100 plasma periods). There is a magnetic field in the  $z$ -direction. The spreading is principally due to magnetic dispersion.

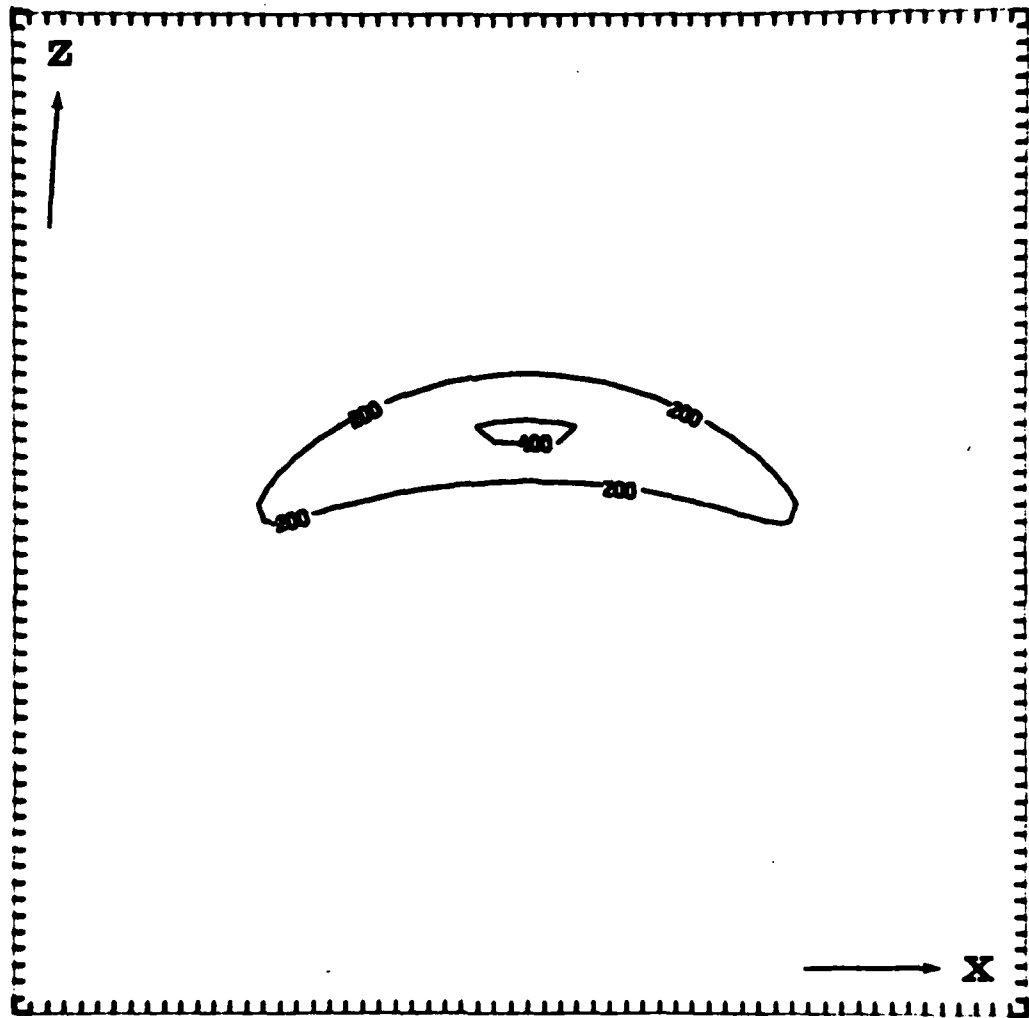


FIGURE 9b) Wavepacket at later time,  $T=15$  (3300 plasma periods). The magnetic dispersion has caused the spreading of the wave envelope in the direction transverse to the field.

In the above examples we have seen a wavepacket in real space change its shape due to dispersion. It is important to understand that in k-space there is no change in wave mode amplitude: the plot of wave mode amplitude in k-space is identical for all of the above figures. What has happened is that the relative phases of these modes (initially the same) change with time and mix in real space to produce a less localized packet. The reason that there is no change in amplitude of the wave modes is that in the linear regime, every mode is independent of the others (principle of superposition). The next example, though, is highly nonlinear. The instabilities which result from the interaction of various wave modes are evident from the behavior in k-space.

#### Nonlinear Instability

Equation (52) has the following exact one-dimensional soliton solution:

$$\underline{E}_s = \hat{x} \phi_s(\xi) \exp[i(k_o x - \omega_o t)] , \quad (70)$$

where

$$\phi_s = [(1-v^2)2]^{1/2} \sqrt{\lambda} \operatorname{sech} \sqrt{\lambda} \xi ,$$

$$n_s = -2\lambda \operatorname{sech}^2 \sqrt{\lambda} \xi ,$$

$$\xi = x - vt , \quad \lambda = (k_o^2 - \omega_o^2) , \quad v = 2k_o .$$

The nonlinear Schrödinger equation, (54), also has a soliton solution for which  $\phi_s = \sqrt{2\lambda} \operatorname{sech} \sqrt{\lambda} \xi$ . These soliton solutions can be verified by substitution. (See Scott, Chu, and McLaughlin, 1973, for a general discussion of the derivation and properties of solitons.) Although the nonlinear terms are large, they are exactly balanced by dispersion.

An interesting question arises as to whether or not this solution is stable. Several investigations of this problem have appeared in the literature (Zakharov and Rubenchik, 1973; Yajima, 1974; Schmidt, 1975; Pereira, Sudan, and Denavit, 1976). The stability is investigated by perturbing the soliton:

$$\underline{E} = (E_s + \delta E) \hat{x} ,$$

$$n = n_s + \delta n ,$$

(71)

with  $\delta E$  and  $\delta n$  such as

$$\delta E = [f(\xi) + ig(\xi)] \exp[i(k_0 x - \omega_0 t)] \cos k_{\perp} y \exp(\gamma t)$$

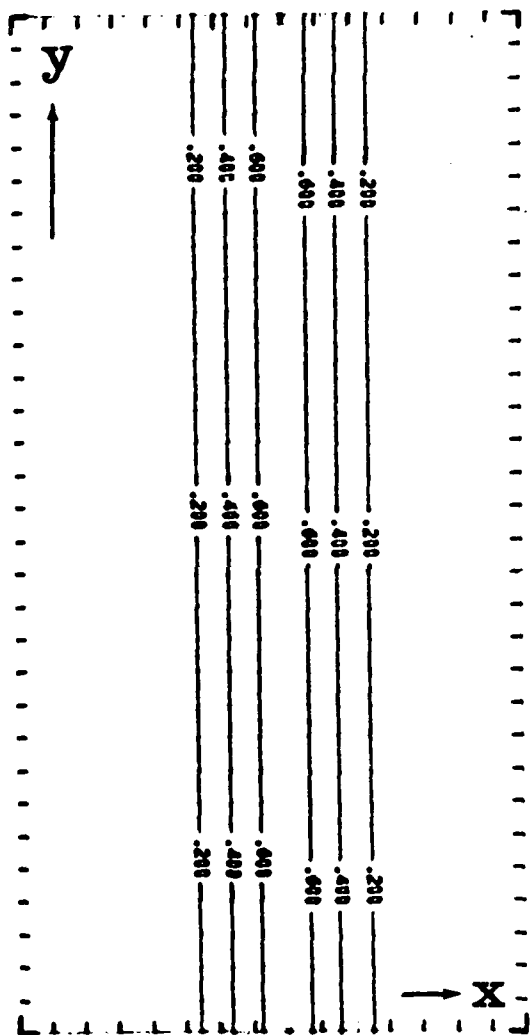
$$\delta n = n(\xi) \cos k_{\perp} y \exp(\gamma t) .$$

Schmidt shows analytically that there is no marginal stability ( $\gamma = 0$ ) for finite  $k_{\perp}$ . Zakharov and Rubenchik use the perturbation theory on the nonlinear Schrödinger equation (54), and find that for  $k^2 \ll \lambda$ , the transverse perturbations will grow at the rate  $\gamma^2 = 4k_{\perp}^2 \lambda$ . They

agree with Schmidt that the instability should peak somewhere around  $\gamma_{\max} \sim \lambda^2$  when  $k_{\perp}^2 \sim \lambda$ . Although in numerical work, Pereira et al. find a similar maximum growth rate, they do not observe any strong dependence on  $k_{\perp}$ .

We can see the instability ourselves using the two-dimensional code. First we construct the one-dimensional soliton according to the above analytic forms for the electric field envelope and density. For simplicity, we choose  $V = 0$  so the soliton remains stationary. The initial conditions are plotted in Figure 10. Each unit length,  $\Delta x$ , corresponds to  $85 \lambda_{De}$ , and each unit  $T$  is 220 plasma periods. The parameter  $\sqrt{\lambda} = 0.5$  gives the soliton a half-width of about  $\Delta x$ , and amplitude  $E = \sqrt{8\pi nT} \cdot 0.01$ . Notice that the contours are parallel to the  $y$  (transverse) direction, so that the initial conditions are truly one-dimensional. In  $k$ -space, all of the wave amplitude is on the  $k_x$ -axis. That this is a valid solution to the equations can be demonstrated by solving the equations numerically. After a significant lapse of time, at  $T = 100$ , the initial conditions have evolved unchanged, as seen in Figure 11.

Now we can test whether this is a stable solution. First, we can test for stability to perturbations in the  $x$ -direction by adding a small amplitude random noise to each  $k$ -mode on the  $k_x$ -axis. This noise adds an



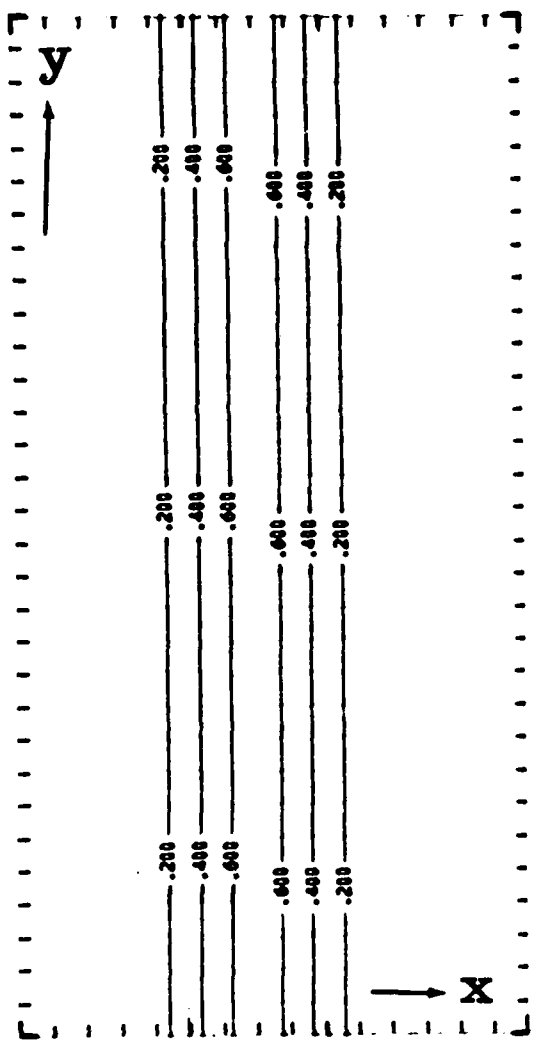


FIGURE 11. Soliton after  $T=100$  (22000 plasma periods). Since it is essentially unchanged from  $T=0$ , this demonstrates that it is an exact solution to the wave equations.

insignificant amount of energy to the system: less than  $10^{-5}$  of the total energy. The soliton is stable to these perturbations after 50 time units, as seen in Figure 12.

Next we put the small amount of random noise in all of the  $k$ -modes, including the transverse modes. Now the soliton is dramatically unstable, as seen in Figures 13a,b. But rather than becoming unstable to growing wave-like perturbations (corresponding to the fastest growing  $k_{\perp}$  of the linear perturbation theory), the soliton evolves in a very nonlinear way to "collapse" to smaller and smaller length scales. Although the perturbation theory is correct in predicting transverse instability, it is not capable of describing the collapse process. Computer simulation is sometimes the only recourse in this highly nonlinear regime.

Something very interesting happens when a small magnetic field in the  $x$ -direction is introduced. When  $\omega_{ce}/\omega_{pe} = 0.03$ , the thermal dispersion is roughly one-half the magnetic dispersion:

$$\frac{3k^2 v_e^2}{\omega_{ce}^2} \sim \frac{3\lambda/k_{De}^2}{\omega_{ce}^2/\omega_{pe}^2} \sim \frac{1}{2} . \quad (72)$$

The effect on soliton stability is seen in Figures 14a,b. The magnetic field evidently slows down the collapse, because at  $T = 40$  the soliton is still in the early instability stage. The soliton does eventually collapse, . . . later time,  $T = 50$ . Notice that the magnetized

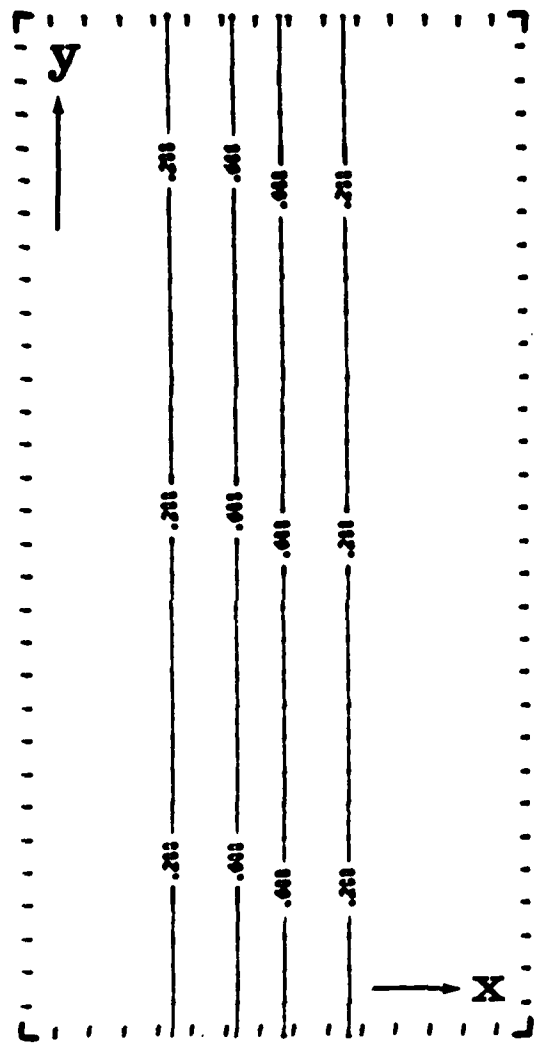


FIGURE 12. Soliton at  $T=50$  (11000 plasma periods) after being perturbed in the  $x$ -direction. This demonstrates that the soliton is stable to one-dimensional perturbations.

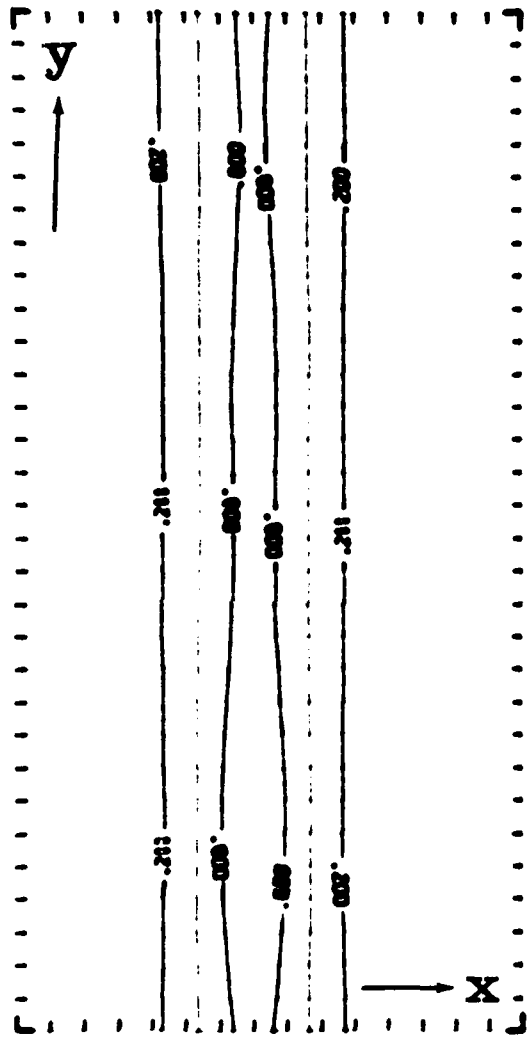


FIGURE 13a) Soliton at  $T=30$  after being slightly perturbed in the  $y$ -direction. It is clearly unstable to these perturbations.

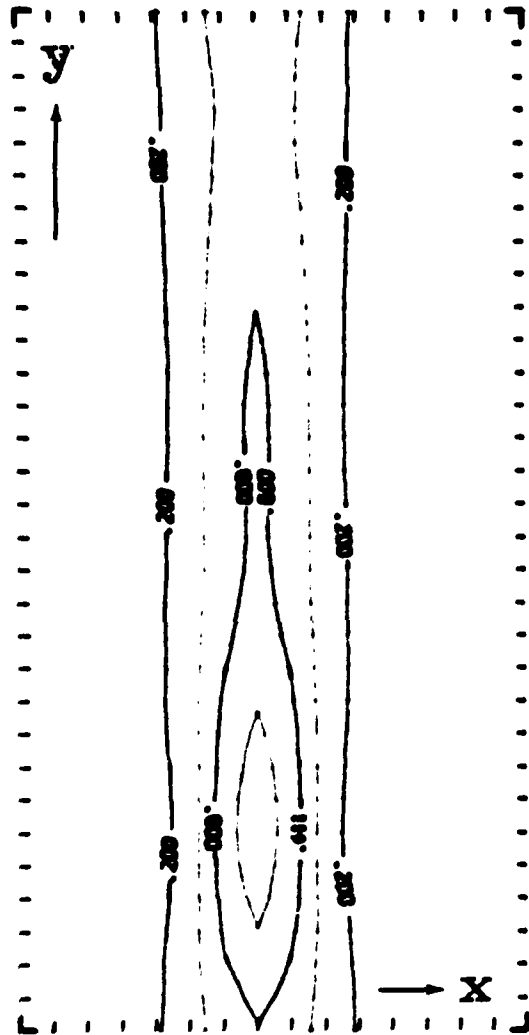


FIGURE 13b) The perturbed soliton at later time,  $T=40$ . The initial perturbation has disrupted the soliton and nonlinear processes are causing a localized region of intense fields to form.

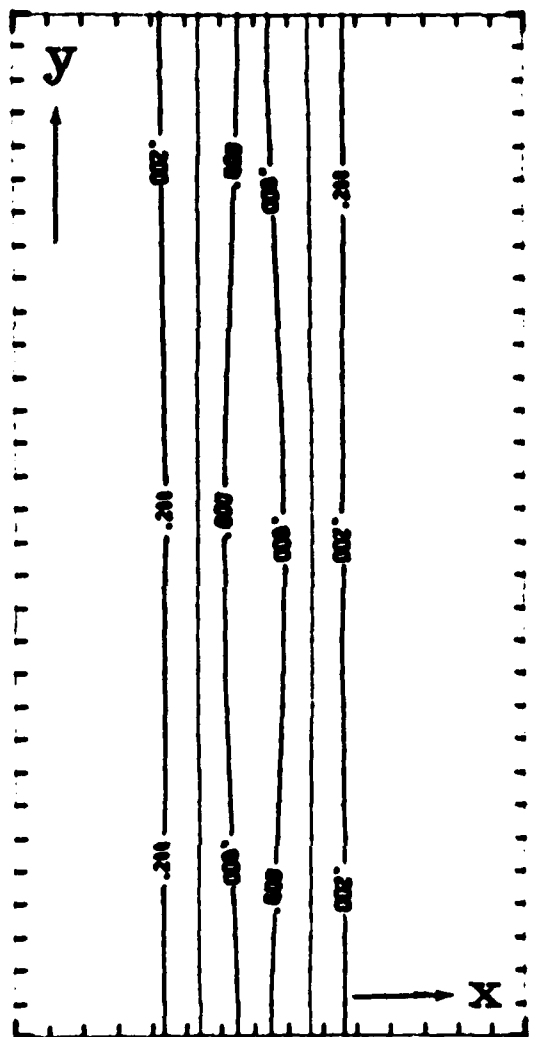


FIGURE 14a) Soliton at  $T=40$  after being slightly perturbed in the  $y$ -direction. There is a magnetic field in the  $x$ -direction. It is still unstable, but the instability is slower than with no magnetic field (compare with Figure 13).

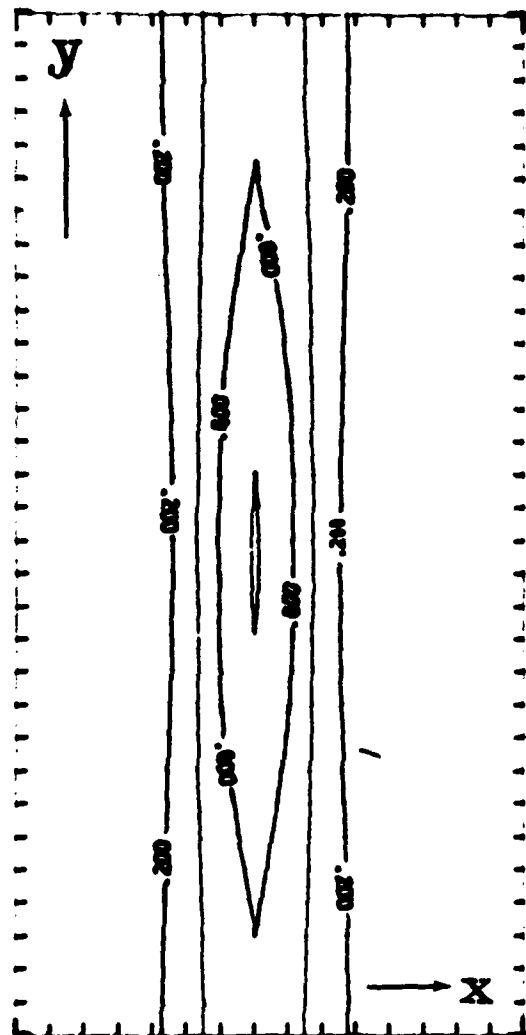


FIGURE 14b) The perturbed soliton in a magnetic field at  $T=50$ . The geometry of the collapsing core is clearly affected by the magnetic field.

collapsing soliton is more elongated transverse to the field than the unmagnetized one. The magnetic dispersion has the same effect on the linear wavepackets. However, the difference in this case seems to be due to changes in the spectra of the growing modes, not just the phase behavior.

#### Summary of Magnetic Effects

From this brief examination of linear wavepackets and soliton stability, we can make the following statements concerning the magnetic field:

1) New physical effects can occur when the magnetic dispersion term exceeds the thermal dispersion term. Let  $k$  be some inverse scale length in the problem. Then the magnetic field becomes important when

$$\omega_{ce}^2 > 3k^2 v_e^2. \quad (73)$$

This may occur when the ratio of the electron cyclotron frequency to the plasma frequency,  $\omega_{ce}/\omega_{pe}$ , is still a very small number.

2) The magnetic field tends to elongate wave structures in the direction perpendicular to the magnetic field.

3) One-dimensional solitons "collapse" when two-dimensional behavior is allowed, but this collapse takes a longer time in a magnetic field than without it.

## CHAPTER IV

### PARAMETRIC WAVE INSTABILITY

Nonlinear wave physics is of great interest in the study of Type III solar radio bursts. The production of electromagnetic radiation near the plasma frequency (fundamental) and at twice the plasma frequency (harmonic) during the bursts is due to the interaction of intense Langmuir waves with ion density perturbations and other Langmuir waves. The source of the intense Langmuir waves is a beam plasma instability caused by a high speed electron stream emitted from the sun.

The stability of the electron stream out to distances of the earth's orbit has been an interesting problem since Sturrock (1964) pointed out that quasilinear theory predicts that the stream loses its energy to Langmuir waves very close to the sun. Further calculations, taking into account the inhomogeneous nature of the stream (but ignoring wave-wave interactions) show that the stream can reabsorb Langmuir waves and continue to propagate outward (Baldwin, 1964; Zaitsev, Mityakov, and Rapoport, 1972; Zaitsev, et al., 1974; Magelssen, 1976; Grognard, 1975; Magelssen and Smith, 1977; Takakura and Shibahashi, 1976). However, since the wave levels in the inhomogeneous

quasilinear calculations are still very large, nonlinear wave phenomena might occur. But studies of induced scattering of Langmuir waves (Sturrock, 1965; Kaplan and Tsytovich, 1968) and wave instability have not indicated important roles for these kinds of wave processes in preventing the quasilinear relaxation (Zheleznyckov and Zaitsev, 1970; Smith and Fung, 1971; and Hayvaerts and de Genouillac, 1974).

Recent work on the role of nonlinear waves in the evolution of Type III Langmuir waves has centered around two different theories. Smith, Goldstein, and Papadopoulos (1979) propose the following scenario for the nonlinear wave processes:

- 1) The electron stream from the sun associated with Type III bursts causes the growth of plasma waves resonant with the beam;
- 2) Resonant "pump" waves continue to grow until the energy density reaches the threshold of the oscillating two stream instability (OTSI);
- 3) The OTSI transfers wave energy to plasma waves with lower phase velocity. The instability causes growing ion density waves as well;
- 4) The buildup of the ion density fluctuations has two effects: a) the reduction of the threshold for the instability, and b) the scattering of long wavelength

Langmuir waves to shorter wavelengths (anomalous resistivity effect);

5) Eventually, Landau damping at the shortest wavelengths balances the scattering.

Goldstein, Smith, and Papadopoulos (1979) do numerical calculations with this theory to model Type III bursts. All of this work is in one dimension.

Nicholson, Goldman, Hoyng, and Weatherall (1978) solve the nonlinear plasma wave equations numerically in two dimensions. Although ignoring quasilinear effects, the treatment includes all of the wave-wave effects contained in the equations: the decay instability, the OTSI, modulational instabilities, and nonlinear "collapse." The scenario of this theory is as follows:

1) Langmuir waves grow linearly due to the beam instability, and have a finite bandwidth in k-space both parallel to the stream direction and perpendicular to it;

2) When the waves reach a significant amplitude, wavepackets begin to "collapse," resulting in a wider spectrum in k-space, and intensifying solitons in real space;

3) A statistical steady state may be established as solitons collapse, damp out (through Landau damping), and form, leading to a saturation of electrostatic energy.

In both of the nonlinear wave calculations, the saturation of the beam instability occurs in less than

a second. Because the anomalous resistivity lowers the threshold for the OTSI, Smith, et al. (1979) conclude that quasilinear relaxation does not occur. Nicholson, et al. (1978) find that the wave levels of the nonlinear wave theory are still comparable with those given by inhomogeneous quasilinear theory. In many respects, the two theories are far apart.

One of the central issues is whether or not the nonlinear wave evolution is in one dimension, since including another spatial dimension introduces completely different physics. We saw in the last chapter that stable solitons occur in one dimension, but collapse rapidly in two dimensions. Although it may be correct to treat parametric instability as the dominant nonlinear wave process in one dimension, in more dimensions collapse can occur before the parametrically excited waves buildup to significant amplitude.

The one-dimensional treatment originally derived from the use of the dipole approximation for the beam driven Langmuir waves (Papadopoulos, Goldstein, and Smith, 1974; Smith, Goldstein, and Papadopoulos, 1976). As a result of this approximation, the OTSI figured prominently and occurred along the beam direction. However, Bardwell and Goldman (1976) showed that the OTSI will occur in a direction perpendicular to the beam as a result of finite wave-number effects. They also found a decay instability, and

a modulational instability in a forward cone around the beam direction. In later work, Smith, et al. (1979) continue to use the one-dimensional approximation and the dipole geometry of the OTSI: they argue that broadband effects suppress off-axis instability and raise the threshold for the decay instability. Furthermore, they never consider two-dimensional effects of plasma collapse because the magnetic field is presumed to prevent collapse in the direction perpendicular to the field (Papadopoulos and Freund, 1978; Smith, et al., 1979).

Below we will examine more carefully the assertions used to justify a one-dimensional treatment, and show why they are not adequate. We will find that 1) the parameter regime for which the instabilities are intrinsically one dimensional are not generally applicable in Type III theory; 2) the background magnetic field does not suppress transverse instabilities; and 3) the broadband pump does not prevent the transfer of energy into unstable modes.

#### Instability Geometries in the Type III Problem

Large amplitude Langmuir waves are unstable because perturbations in density cause modulations in the natural frequency of oscillation of the Langmuir wave and lead to parametric instability. The instability is due to the coupling together of a number of wavemodes. If an intense Langmuir wave has frequency  $\omega_0$  and wavenumber  $k_0$ , a low

frequency density wave with frequency  $\omega$  and wavenumber  $k$  will modulate the frequency of the Langmuir wave (because the frequency depends upon density) and couple to other Langmuir waves at frequency and wavenumbers  $(\omega_0 + \omega, k_0 + k)$  and  $(\omega_0 - \omega, k_0 - k)$ . The electric fields from these waves can beat with the Langmuir wave field to cause a modulation of the ponderomotive force, and the growth of the density waves. The instability results in parametric excitation.

The standard parametric theory (Nishikawa, 1968; Nishikawa and Liu, 1976) involves a number of approximations. If there exists a single large amplitude wave in the plasma, then the nonlinear terms in the wave equation may be linearized to be first order in the amplitude of this wave. This is justified only when the non-resonant waves are linear waves, and the resonant waves form a sufficiently narrow wavepacket about the central wave vector. Then the nonlinear processes can be assumed to be dominated by a single large amplitude pump wave. Second, the only Langmuir waves generated by the modulation of the pump waves are the waves at  $(\omega_0 \pm \omega, k_0 \pm k)$ . Other waves are assumed not to be resonant and have negligible amplitude. This means that waves such as  $(\omega + 2\omega_0, k + 2k_0)$  have to be well removed from the linear dispersion curve for Langmuir waves.

The coupled wave equations result in new normal modes described by the dispersion relation (Weatherall,

Nicholson, and Goldman, 1979):

$$\omega^2 + i\nu_i \omega - k^2 = k^2 |E_0|^2$$

$$\cdot \left[ \frac{\mu_+^2}{\omega + (i\nu_e/2) - 2\bar{k} \cdot \bar{k}_0 - k^2 - \Omega^2 (k_\perp^2/k^2)} \right. \\ \left. - \frac{\mu_-^2}{\omega + (i\nu_e/2) - 2\bar{k} \cdot \bar{k}_0 + k^2 + \Omega^2 (k_\perp^2/k^2)} \right] . \quad (74)$$

Notice that the left side of the equation is the Fourier transform of the linear wave operator of the ion-acoustic wave. The denominators of the terms on the right side are the Fourier transforms of the linear wave operator of the Langmuir wave envelope evaluated at  $\bar{k}_0 + \bar{k}$  and  $\bar{k}_0 - \bar{k}$  (upshifted and downshifted from  $\bar{k}_0$  of the pump wave). The angular terms are  $\mu_\pm^2 = (\bar{k}_0 \pm \bar{k})^2 / |\bar{k}_0 \pm \bar{k}|^2$ .

A dimensionless pump strength is usually defined as the ratio of the pump wave energy density to the particle thermal energy density:

$$\frac{|\tilde{E}_0|^2 / 4\pi}{nn_0 T} = \frac{|E_0|^2}{(3/4n)(m_i/m_e)} . \quad (75)$$

Because the real and envelope fields are related by  $\tilde{E} = 2\text{Re}[E \exp(-i\omega_{pe} t)]$ , this definition of pump strength will give one-quarter the strength used by Bardwell and Goldman (1976) and other work. Therefore, we define  $W$ , the dimensionless spectral energy, to be

AD-A096 560 COLORADO UNIV AT BOULDER DEPT OF ASTRO-GEOPHYSICS F/G 4/1  
PLASMA WAVE TURBULENCE AND PARTICLE HEATING CAUSED BY ELECTRON --ETC(U)  
JAN 81 M V GOLDMAN AFOSR-80-0022  
UNCLASSIFIED CU-1533143 AFOSR-TR-81-0148 NL

3 or 4

AF 4  
099-60

1  
100  
1

$$W = \frac{4 |E_0|^2}{(3/4\pi)(m_i/m_e)} . \quad (76)$$

This definition is consistent with the common usage.

The normal frequencies,  $\omega$ , which have a positive imaginary part, are growing in time and are unstable. The instabilities described by this dispersion relation with  $\omega_{ce} = 0$  have been described in great detail in Bardwell (1976) and Bardwell and Goldman (1976). We will elaborate on only one point; that is, the circumstances for which the unstable wavenumbers,  $k$ , are larger than the pump wavenumber,  $k_0$ . The premise that  $k \gg k_0$  is an important condition in the one-dimensional treatment of parametric instability. We will investigate this question by examining the behavior of the OTSI under different sets of parameters.

The geometry of the purely growing instability is determined by the values of the pump energy and wavenumber,  $W_0$  and  $k_0$ . If  $W_0 \ll 10 k_0^2$ , as is generally the case for Type III parameters, then the instability will have  $k \ll k_0$ , and have a maximum growth rate perpendicular to the pump wave vector. On the other hand, with  $W_0 \gg 10 k_0^2$ , then  $k \gg k_0$ , the maximum growth rate is in the direction of the pump wave vector, and the instability is essentially one dimensional as in Smith, et al. (1979).

In either case, the OTSI involves two Langmuir daughter waves. The instability occurs when the upshifted and downshifted waves beat with the pump wave at nearly the same frequency. The frequency mismatch, or the beat frequency,  $\delta_{\pm}$ , for the two waves is

$$\begin{aligned}\delta_{\pm} &= \omega_{pe} - \omega_L(k_o \pm k) \\ &= -\frac{3}{2} (k^2 \lambda_e^2) \omega_{pe} \mp 3(k \cdot k_o \lambda_e^2) \omega_{pe} .\end{aligned}\quad (77)$$

In the dipole limit, a)  $k \gg k_o$ , both daughter waves have nearly the same mismatch because of the smaller wavenumber of the pump wave,  $k_o$ . The threshold for instability is  $\omega_o > 3k^2/k_{De}^2$  (Smith, et al., 1979). Because  $k \gg k_o$ , this threshold condition implies  $\omega_o > 3k_o^2/k_{De}^2$ . In the other limit, b)  $k \ll k_o$ , the mismatch frequencies are made equal when  $k \perp k_o$  (Bardwell and Goldman, 1976). The fastest growing wavenumber for this instability is given by

$$k \lambda_e = (\omega_o/12)^{\frac{1}{2}} . \quad (78)$$

Since the wavenumber  $k$  is assumed to be much less than  $k_o$ , this requires  $\omega_o \ll 12 k_o^2/k_{De}^2$ .

Hence, we arrive at the important conclusion that as the pump strength  $\omega_o$  increases, the OTSI goes from case b) to case a).

We can demonstrate the validity of these conclusions by solving the wave equation (52) numerically to find the change in amplitude of the various  $k$ -modes with time. This is not exactly the same as solving the dispersion relation. No approximation has to be made in choosing the set of wave modes such as the truncation scheme used to limit the analytic treatment of four waves. The computer program treats all of the waves. We find, however, that the growth rates derived in this way are consistent with those found from three and four-wave theories.

There is a further subtle difference between this numerical simulation and the solution of the dispersion relation. Because the dispersion relation is symmetric under the transformation  $(\omega, k) \rightarrow (\omega^*, -k)$ , an anti-Stokes wave at  $\underline{k}_0 + \underline{k}$  has the same growth rate as the Stokes wave at  $\underline{k}_0 - \underline{k}$ . However, as pointed out in Bardwell and Goldman (1976), the anti-Stokes wave, if it is off-resonance, attains much less amplitude than the resonant Stokes wave. In fact, what happens in the numerical simulation, which starts with the same initial amplitude (noise) in all modes, is that the Stokes wave quickly attains steady growth rate. Because the contour pictures discussed below depict the largest amplitude growing modes at early times, the nonresonant modes, even though they may later have large growth rates, do not appear. Actually, the numerical simulation is a better representation of the physics than

the linear dispersion relation. The use of linear growth rates to model the time evolution would result in unphysical amplitude of the anti-Stokes modes.

Consider the case that the pump wavenumber is  $k_o \lambda_e = 0.01$ . This corresponds to Type III excited Langmuir waves at 1/2 A.U. A small amount of random phase noise is put into all modes except the single pump mode, which has very large amplitude. In Figures 15a-d we show the wave growth rates for different values of  $W_o$  after 15 time units (3300 plasma periods). The arrow, which is four grid units  $\Delta k$  in length, represents the wave vector of the pump wave. Table 4 summarizes the numerical data.

In Figure 15a,  $W_o$  is  $10^{-4}$ , so  $W_o \ll 10 k_o^2$ . The spectra of Langmuir waves with wavenumbers less than  $k_o$  is due to a four-wave decay, or modulational instability. The position of these modes at wavenumber  $k_o/3$  can be confirmed analytically (Bardwell and Goldman, 1976; Nicholson, et al., 1978).

As the pump energy is increased to  $W_o = 10^{-3}$  (Figure 15b), the growth rates become larger, and the region of physically significant growth begins to include previously nonresonant modes.

When  $W_o$  is  $3 \cdot 10^{-3}$  (Figure 15c) so that  $W_o \gtrsim 10 k_o^2$ , we see a change in the geometry from Figures 15a,b. The OTSI with  $\mathbf{k} \perp \mathbf{k}_o$  is evident, as well as forward and backward scattering instabilities which might also be

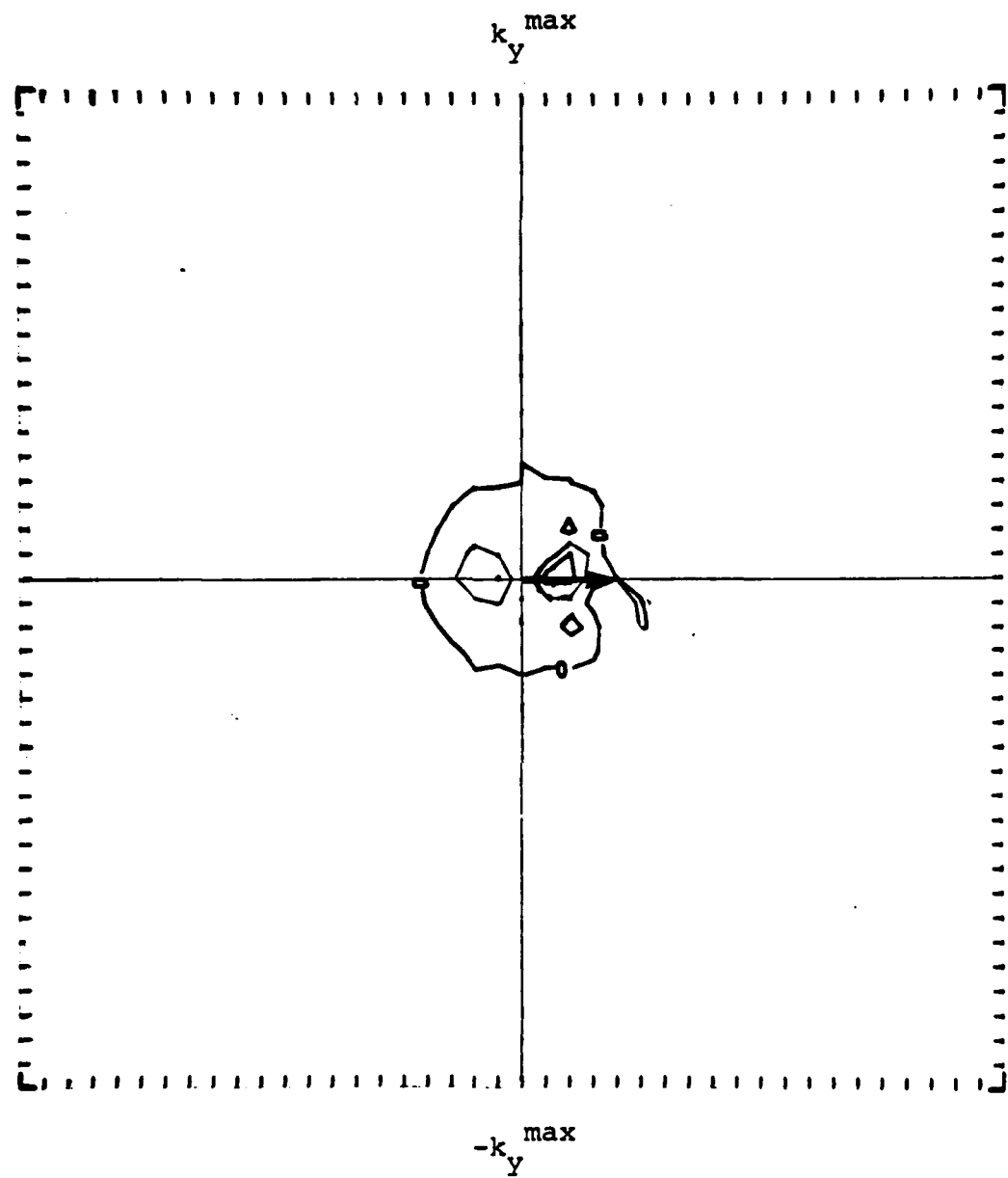


FIGURE 15a) Parametric growth rates in  $k$ -space for Langmuir wave excited by pump mode indicated by arrow.  $k_o = 0.01 k_{De}$  and  $\omega_o = 10^{-4}$ . Regions of maximum growth are due to a four-wave decay instability. The contours represent regions of constant growth rate from 0 to  $1.5 \times 10^{-5} \omega_{pe}$  at intervals of  $0.73 \times 10^{-5} \omega_{pe}$ . Maximum growth rate is  $1.8 \times 10^{-5} \omega_{pe}$ .

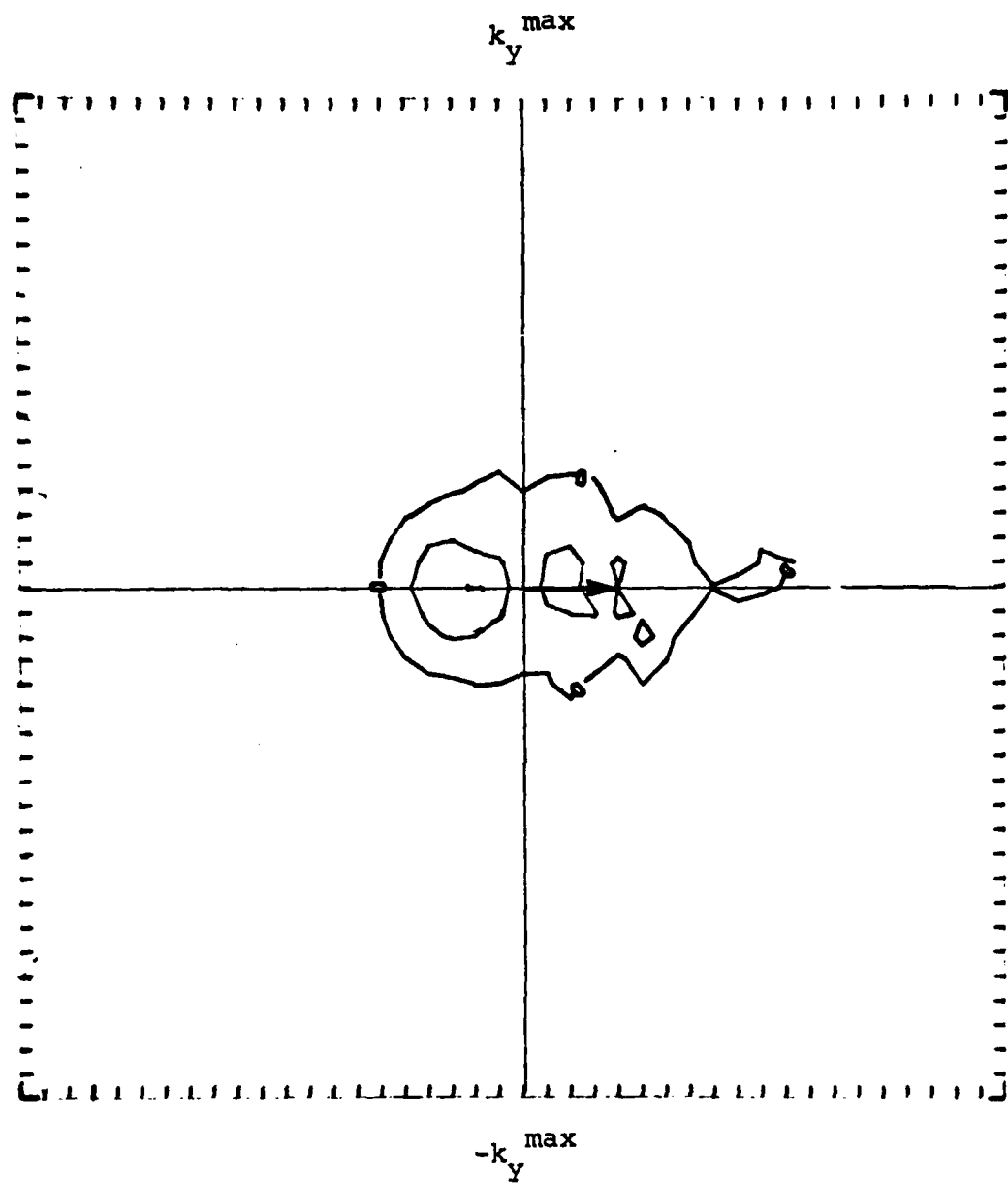


FIGURE 15b) Parametric growth rate contours in  $k$ -space for  $k_0 = 0.01 k_{De}$  and  $W_0 = 10^{-3}$ . Contours are for growth rates of 0 and  $7.3 \times 10^{-5} \omega_{pe}$ . Maximum growth rate is  $12 \times 10^{-5} \omega_{pe}$ .

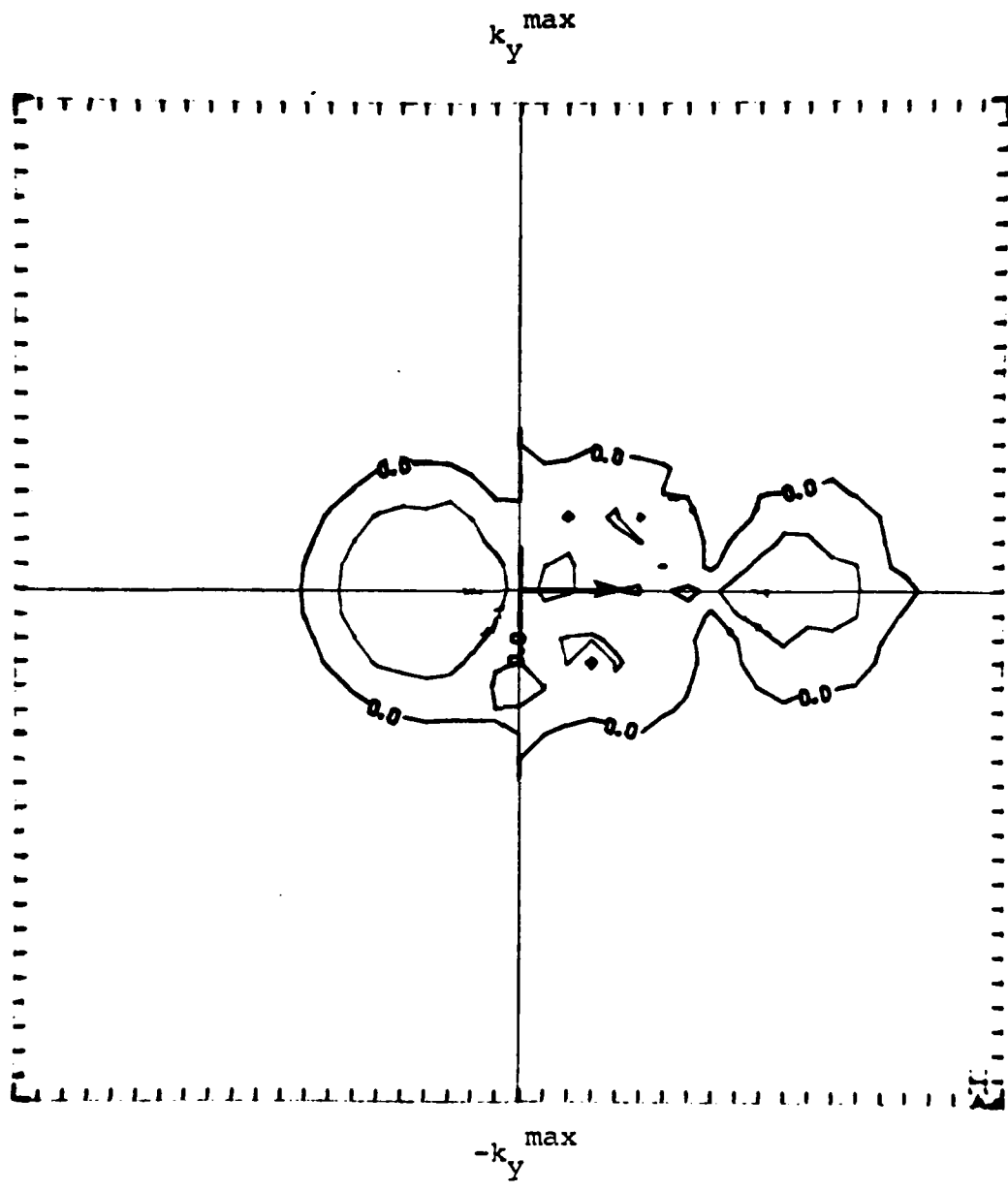


FIGURE 15c) Parametric growth rate contours in  $k$ -space for  $k_o = 0.01 k_{De}$  and  $\omega_o = 3 \times 10^{-3}$ . This is an intermediate regime for which four-wave instabilities occur both parallel to and perpendicular to the pump wave vector. Contours are for 0 and  $15 \times 10^{-5} \omega_{pe}$ . Maximum growth rate is  $30 \times 10^{-5} \omega_{pe}$ .

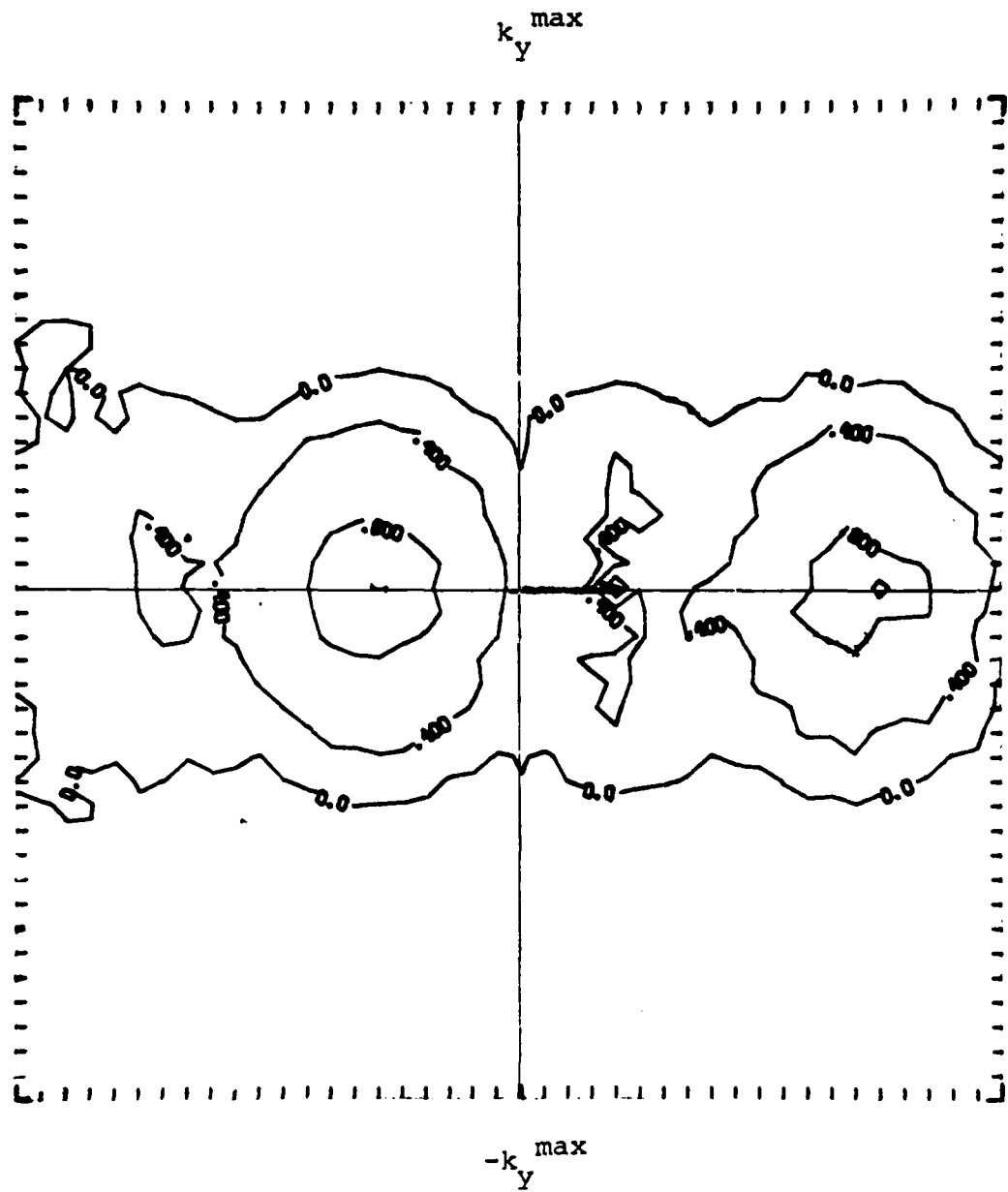


FIGURE 15d) Parametric growth rate contours in k-space for  $k_o = 0.01 k_{De}$  and  $\omega_o = 10^{-2}$ . The dipole geometry of the OTSI is prevalent in this example. Contours are for growth rates of  $0, 30 \times 10^{-5} \omega_{pe}$ , and  $60 \times 10^{-5} \omega_{pe}$ . Maximum growth rate is  $70 \times 10^{-5} \omega_{pe}$ .

TABLE 4

NUMERICALLY DETERMINED PROPERTIES OF PARAMETRIC  
 INSTABILITY FOR  $k_o = 0.01 k_{De}$  AND VARIOUS  
 VALUES OF PUMP ENERGY

$w_p$	$k_{  } \lambda_e$	$k_{\perp} \lambda_e$	$\gamma/\omega_{pe}$
$10^{-4}$	-.002	0	$0.9 \times 10^{-5}$
	+.003	0	$1.8 \times 10^{-5}$
$10^{-3}$	-.005	0	$12.0 \times 10^{-5}$
	+.003	0	$8.7 \times 10^{-5}$
$3 \times 10^{-3}$	-.010	0	$30.0 \times 10^{-5}$
	+.032	0	$23.0 \times 10^{-5}$
	.010	.007	$17.0 \times 10^{-5}$
$10^{-2}$	-.015	0	$68.0 \times 10^{-5}$
	+.032	0	$65.0 \times 10^{-5}$

associated with an OTSI instability. Because this example falls between the analytic limiting cases for the OTSI, probably neither of these instabilities is "purely growing."

Finally, in Figure 15d,  $W_o$  is  $10^{-2}$  and  $W_o \gg 10 k_o^2$ . The instabilities produce a spectrum of Langmuir waves nearly symmetric in  $k$ -space and with wave vectors parallel to and larger than the pump wave vector. This is the dipole limit of the OTSI. Notice that the energy in the pump wave is very large--over two orders of magnitude larger than the saturation level of Magelssen's inhomogeneous quasilinear model.

These results for large  $W_o$  are in good agreement with other work, such as Freund and Papadopoulos (1980), which correctly treats the finite wavenumber pump. On the other hand, the descriptions of the nonlinear wave processes given in Smith, et al. (1979) and Goldstein, et al. (1979) require instabilities which produce wave-numbers much larger than  $k_o$ , so their treatment is self-consistent only for very large  $W$ , i.e.,  $W_o \gtrsim 10^{-2}$  at 1/2 A.U. Closer to the sun the wavenumber of the beam resonant waves is larger because the temperatures are higher; then the energy density which must exist to produce a dipole geometry is even larger.

### Magnetic Effects

There is a substantial body of literature concerning parametric instabilities in a magnetized plasma; see, e.g., Kaw (1976), Porkolab and Goldman (1976), Kaufman and Stenflo (1975), Sanuki and Schmidt (1977), and Dysthe and Pcseli (1978). Nevertheless, most applications of parametric instability theory to Type III bursts have not treated magnetic field effects systematically. The first work including the magnetic field in the wave-wave interactions of Type III bursts was Weatherall, Goldman, and Nicholson (1978). The subsequent paper by Weatherall, et al. (1979), which generalizes the work of Bardwell and Goldman (1976), discusses the role of the magnetic field on the parametric instabilities in the lower solar corona. We will review the results below.

The parametric growth rates in a magnetic field are found from the dispersion relation (74) with finite  $\omega_{ce}$ . The effect on the high frequency wave is included explicitly in the denominators on the right side. The terms involving  $\omega_{ce}$  are due to magnetic dispersion. We find that the magnetic field has an important effect on the low frequency wave only when  $k_{||}/k < (m_e/m_i)^{\frac{1}{2}}$ . In order to make this effect explicit, we must rewrite the low frequency operator in terms of the kinetic susceptibilities  $\chi_e$  for electrons and  $\chi_i$  for ions (Bardwell, 1976; Kaw, 1976; Weatherall, et al., 1979). In dimensional units:

$$\omega^2 + 2iv\omega - k^2 c_s^2 \rightarrow \left[ \frac{1}{\chi_e(\omega, k)} + \frac{1}{\chi_i(\omega, k)} \right] \omega_{pi}^2 . \quad (79)$$

The magnetized kinetic susceptibilities for species s are given by Bekefi (1966):

$$\begin{aligned} \chi_s &= \frac{1}{k^2 \lambda_e^2} \left[ 1 + \zeta_s e^{-a_s} \sum_{n=-\infty}^{\infty} I_n(a_s) Z \left( \zeta_s^{-n} \frac{\omega_{cs}}{\sqrt{2} k_{||} v_s} \right) \right] \\ \zeta_s &= \frac{\omega}{\sqrt{2} k_{||} v_s} \\ a_s &= \frac{k_{\perp} v_s}{\omega_{cs}} . \end{aligned} \quad (80)$$

$I_n$  are modified Bessel functions,  $v_s$  the thermal speed of species s, and Z the plasma dispersion function (Fried and Conti, 1961) which arises because the background electron and ion distribution functions have been taken to be Maxwellian.

The ions are unmagnetized if  $kv_i \gg \omega_{ci}$  and  $\omega \gg \omega_{ci}$ . Then the ion susceptibility simplifies to (Montgomery, 1971):

$$\chi_i = \frac{1}{k^2 \lambda_i^2} [1 + \zeta_i Z(\zeta_i)] . \quad (81)$$

In the limit of "cold" ions,  $kv_i \ll \omega$ ,

$$\chi_i = -\frac{\omega_{pi}^2}{\omega} , \quad (k_{\perp} v_i \gg \omega_{ci}, \omega \gg kv_i) . \quad (82)$$

But, for equal electron and ion temperatures, the plasma dispersion function must be evaluated numerically because  $\zeta_i \sim 1$ . In that case the imaginary part of  $\chi_i$  is of the same order as the real part of  $\chi_i$ . The large imaginary part causes heavy damping.

The susceptibility for electrons has two interesting limits. First, when  $\zeta_e \gg 1$ , the electron susceptibility reduces to its unmagnetized value:

$$\chi_e = \frac{k_{De}^2}{k^2}, \quad (\omega \ll k_{||} v_e) . \quad (83)$$

In the other limit,  $\zeta_e \ll 1$ , the electrons are strongly affected by the magnetic field:

$$\chi_e = \frac{\omega_{ce}^2}{\omega_{pe}^2}, \quad (\omega \gg k_{||} v_e, k_{\perp}^2 v_e^2 \ll \omega_{ce}^2) . \quad (84)$$

This is smaller by  $k_{\perp}^2 v_e^2 / \omega_{ce}^2$ , the ratio of the thermal gyroradius to the transverse wavelength, compared with the unmagnetized value.

The transition between the two limiting cases occurs when  $\omega \sim k_{||} v_e$ . Evaluating  $\omega$  at the ion acoustic frequency, we find that this occurs when

$$\frac{k_{||}}{k} \sim \left( \frac{m_e}{m_i} \right)^{\frac{1}{2}} . \quad (85)$$

Therefore, when  $k_{||}/k$  is smaller than this value, the electron motion is affected by finite Larmor radius effects. This result shows that this mathematical

treatment of the ion-acoustic waves in a weakly magnetized plasma is consistent with the physical model discussed in the second chapter.

We have solved the dispersion relation numerically for growth rates using the following parameters for the lower solar corona, at 1.1 solar radius:

$$n_e = 10^8 \text{ cm}^{-3}, T_i = T_e = 140 \text{ eV},$$

$$\omega_{pe} = 5.64 \times 10^8 \text{ s}^{-1}, k_o = 0.05 k_{De}, w_o = 3 \cdot 10^{-4}.$$

The calculation was done for two values of the electron cyclotron frequency:  $\omega_{ce} = 0$  and  $\omega_{ce} = 0.1$ . The latter corresponds to a magnetic field of 3.2 gauss.

For the unmagnetized plasma, we can reproduce the growth rate contours of Bardwell and Goldman (1976) as seen in Figure 16. There are three distinct unstable regions. The backscattered waves are unstable to the parametric decay instability. The oscillating two-stream instability (OTSI), for small  $k$  perpendicular to  $k_o$ , has a real frequency much less than its growth rate. The remaining "rabbit ear" structure is due to the stimulated modulational instability, which connects smoothly with the OTSI. These instabilities are discussed in detail by Bardwell and Goldman (1976). With the kinetic damping used here, we find that the growth rates are slightly higher, but within a factor of two of the fluid growth rates of Bardwell and Goldman (1976). The maximum growth

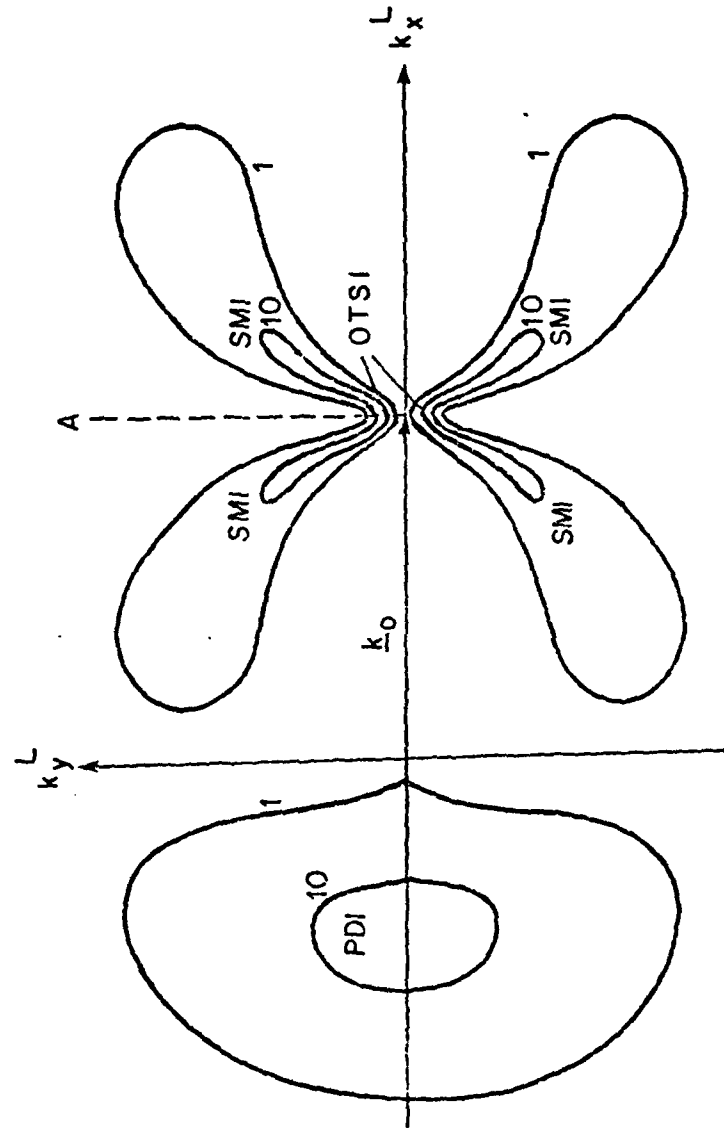


FIGURE 16. Solution of dispersion relation (74) in the unmagnetized case. The contours represent the imaginary part of the frequency (growth rate) as a function of two-dimensional Langmuir wavenumber. The contour labelled 1 represents a growth rate of  $\omega_i = 10^{-6} \omega_{pe}$ , while the contour labelled 10 represents a growth rate of  $\omega_i = 10^{-5} \omega_{pe}$ .  $\omega_o = 10^{-4} \omega_{pe}$  and  $k_o = 0.05 k_{De}$ . PDI marks the region of the parametric decay instability; SMI, the stimulated modulational instability, and OTSI the oscillating two-stream instability. Compare with Bardwell and Goldman (1976).

rate for all three instabilities is near  $\gamma = 10^{-5} \omega_{pe}$ .

For the calculation with  $\omega_{ce} = 0.1$ , we use the magnetized electron susceptibility (80). The magnetization produces some changes in the growth contours (see Figure 17). The most evident is the squeezing of the  $k$ -space contours so that they lie closer to the axis parallel to  $B_0$ , and the suppression of the OTSI. The magnitudes of the maximum growth rates for the parametric decay and stimulated modulational instabilities remain the same. There seem to be two effects of including the magnetic field. One arises from the new frequency matching of the waves which causes the shift in  $k$ -space and is responsible for the compression of the growth contours. The other is the decrease of the low frequency electron response with increasing magnetic field, in particular at angles nearly perpendicular to the background magnetic field. This causes a reduction of growth rates seen in the OTSI.

To understand the shift in wavenumber space of the growth contours, we can do an analysis for small values of  $\omega_{ce}$ , so that the shift  $\Delta k$  is small,  $\Delta k \ll k$ . When the wave-wave interaction involves a near resonant Langmuir mode, such as the anti-Stokes mode,  $k_0 - k$ , then the term on the right side of the dispersion relation associated with this mode is very sensitive to changes in frequency and wavenumber. This is because the denominator involves

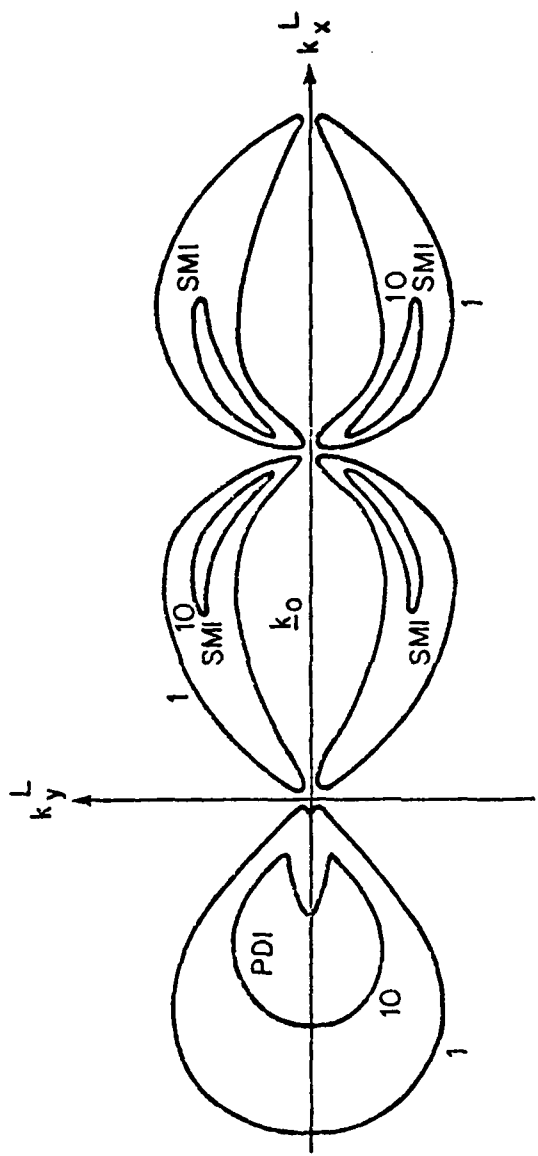


FIGURE 17. Solution of the dispersion relation (74) in the weakly magnetized case.  
 All parameters and contour labels are the same as in Figure 16.  
 $\omega_{ce} = 0.01 \omega_{pe}$ .

the near cancellation of two relatively large terms,  $\omega$  and  $\delta_-$ . Recall that  $\delta_-$  is the difference in frequency between the pump wave with frequency  $\omega_0(k_0)$  and the oblique Langmuir wave with frequency  $\omega_L(k_0 - \underline{k})$ :

$$\delta_-^{\text{mag}}(\underline{k}) = 3\underline{k} \cdot \underline{k}_0 - \frac{3}{2} \underline{k}^2 - \frac{1}{2} \omega_{ce}^2 (1 - \mu_-^2) . \quad (86)$$

With no magnetic field, the frequency mismatch is

$$\delta_-^{\text{unmag}}(\underline{k}) = 3\underline{k} \cdot \underline{k}_0 - \frac{3}{2} \underline{k}^2 . \quad (87)$$

Also, the real part of  $\omega$  can generally be assumed to be near the ion-acoustic frequency (except for instabilities which involve the anti-Stokes wave also), and the imaginary part is the growth rate. Therefore, in order to maintain a given growth rate when the magnetic field is added, a shift  $\Delta \underline{k}$  is necessary so that the difference  $\omega - \delta_-$  is not drastically changed. This means that

$$\omega_R(\underline{k}) - \delta_-^{\text{unmag}}(\underline{k}) = \omega_R(\underline{k} + \Delta \underline{k}) - \delta_-^{\text{mag}}(\underline{k} + \Delta \underline{k}) . \quad (88)$$

We can find, for small  $\Delta \underline{k}$  and  $\omega_{ce}$ , that

$$3\Delta \underline{k} \cdot (\underline{k}_0 - \underline{k}) = \frac{1}{2} \omega_{ce}^2 (1 - \mu_-^2) + c_s (|\underline{k} + \Delta \underline{k}| - |\underline{k}|) . \quad (89)$$

The last term will be small when  $|\underline{k}_0 - \underline{k}| / k_{De} \gg (m_e/m_i)^{\frac{1}{2}}$ . If we deduce that the shift  $\Delta \underline{k}$  is along the direction of the Langmuir wave vector,  $\underline{k}_0 - \underline{k}$ , then we find that the

new Langmuir wave vector is shortened by  $\Delta k$ , where

$$\frac{\Delta k}{|\underline{k}_0 - \underline{k}|} = \frac{1}{6} \frac{\omega_{ce}^2}{|\underline{k}_0 - \underline{k}|^2 v_e^2} \sin^2 \theta . \quad (90)$$

This simple result shows that the fractional change in wavenumber is just the ratio of magnetic dispersion to thermal dispersion. The magnitude of the change is proportional to  $\omega_{ce}^2$  and  $\sin^2 \theta$ , where  $\theta$  is the angle between  $\underline{B}_0$  and  $\underline{k}_0 + \underline{k}$ . This behavior is observed in the numerical calculation.

The low frequency effect is best observed for the OTSI when  $\underline{k}$  is nearly perpendicular to  $\underline{B}_0$ . If we assume the frequency is much less than the ion-acoustic frequency, we may ignore ions, and the dispersion relation, with  $\mu_+ \sim \mu_- = 1$  yields the growth rate

$$\omega = -i\omega_{oi} + i \left( \frac{\omega_0}{4} k^2 \delta \text{Re} \chi_e - \delta^2 \right)^{\frac{1}{2}} . \quad (91)$$

Unmagnetized,  $\text{Re} \chi_e = k_{De}^2 / k^2$ . Even with a magnetic field,  $\chi_e$  is approximately the same except for wavenumbers within angles  $(m_e/m_i)^{\frac{1}{2}}$  of perpendicular. For these angles  $\text{Re} \chi_e$  is much smaller, which causes the growth rates to be smaller. In the case that  $\underline{k}$  is directly perpendicular to  $\underline{B}_0$ ,

$$\frac{\text{Re} \chi_e^{\text{mag}}}{\text{Re} \chi_e^{\text{unmag}}} = \frac{k^2 v_e^2}{\omega_{ce}^2} \ll 1 . \quad (92)$$

This leads to suppression of the instability. In fact, this branch ceases to exist for magnetic fields such that  $\omega_{ce}/\omega_{pe} > 0.005$  when  $W_0 = 10^{-4}$ .

Besides the longitudinal decay waves, there also exist a number of potential electromagnetic decay products. Some specific examples were considered in the second chapter. We concluded that the longitudinal ion acoustic wave had the largest effect in modulating the high frequency wave and producing instability. Of course, in a particular region of wavenumber space, an electromagnetic instability can have the largest growth rate. For example, where the OTSI is reduced to zero growth rate by the weak magnetic field, the region of  $k$ -space which formerly contained the OTSI can now support a parametric instability involving a magnetosonic wave. However, the growth rate will be smaller than other growth rates found above for the weakly magnetized case. Thus, there is no indication that electromagnetic effects would change the overall growth rate picture.

We have studied the effects for other values of the magnetic field using numerical simulations. When  $\omega_{ce} = 0.01 \omega_{pe}$ , there is virtually no change from the unmagnetized growth rates except for the disappearance of the OTSI. This is consistent with equation (90) which predicts changes less than 1% in wavenumbers of the unstable modes. For  $\omega_{ce} = 0$  and  $\omega_{ce} = 0.1 \omega_{pe}$ ,

the numerical simulations show good agreement with the above growth rates derived analytically from the dispersion relation.

Related work by Freund and Papadopoulos (1979) examines magnetic field effects on Type III generated instabilities at 1/2 A.U., but they use questionably large values of pump energy ( $W_0 = 10^{-3}, 10^{-2}$ ). Since  $W_0 \gg k_0^2$ , this regime is different from ours as explained above. They ignore the effect of the magnetic field on the low frequency motions. Generally, this work agrees with ours in showing a shift of unstable wave vectors to smaller perpendicular wavenumbers. While they conclude that a small external magnetic field acts as a stabilizing influence for waves with finite  $k_\perp$ , we consider this to be an overstatement since, apart from the OTSI, growth rates with finite  $k_\perp$  do not decrease in amplitude.

#### Broadband Effects

If the pump energy is distributed in a number of modes centered around the principal wave mode, the unstable waves might no longer experience steady growth. This is because the frequency spread in the broadband pump disrupts the ideal resonance conditions. Analytic work which has been done for parametric instability with a broadband pump indicates that when the resonance width

of the instability is smaller than the frequency of the pump, the growth rates decrease and thresholds are increased (Thomson and Karush, 1974; Valeo and Oberman, 1973; Bardwell and Goldman, 1976; Smith, et al., 1979). We will examine these effects in a simulation of Type III wave processes.

Because of the finite velocity and angular spread in the beam, the beam excited modes will have a substantial width in  $k$ -space. For the lower corona, we will use half-widths  $\delta k_{||} = \delta k_{\perp} = 1/6 k_o$ , where  $k_o = 0.05 k_{De}$ . The initial condition for the numerical simulation is shown in Figure 18a. There is also a small amount of amplitude (noise) in all of the other  $k$ -modes. The total energy in the pump modes is  $W_o = 3 \cdot 10^{-4}$ . The  $k$ -space area of the instabilities in Figure 16 is related to its resonance width in frequency. We can deduce that the spread of frequencies in the pump wave,  $\Delta\omega = 3/2[(k_o + k)^2 - k_o^2] = 0.0014 \omega_{pe}$ , is less than the resonance widths of the decay instability, but larger than the width of the SMI. The OTSI is irrelevant because it is absorbed within the bandwidth of the beam modes. Therefore, we might expect the effect of the broadband pump on the stimulated modulational instability to be more severe than on the decay instability.

After 150 time units, the spectra in  $k$ -space is as shown in Figure 18b. There is substantial amplitude in

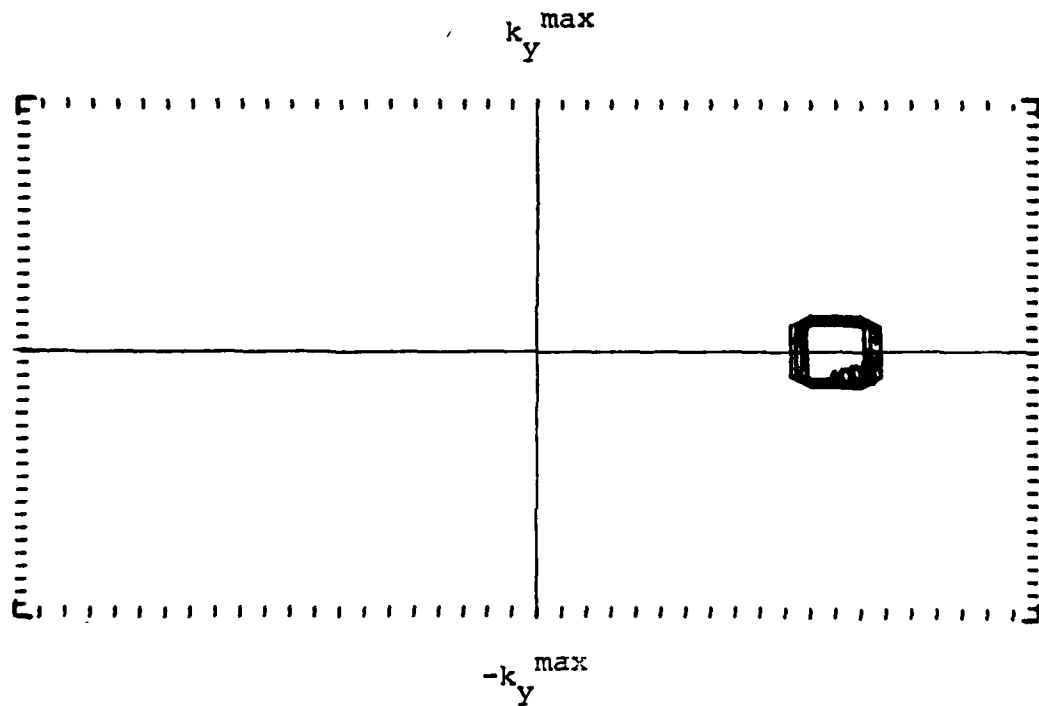


FIGURE 12a) Initial wave amplitude in wavenumber space for broadband pump centered at  $k_o = 0.5 k_{De}$ , and with energy  $w_o = 3 \times 10^{-4}$ . Contours indicate relative magnitudes. There is no magnetic field.

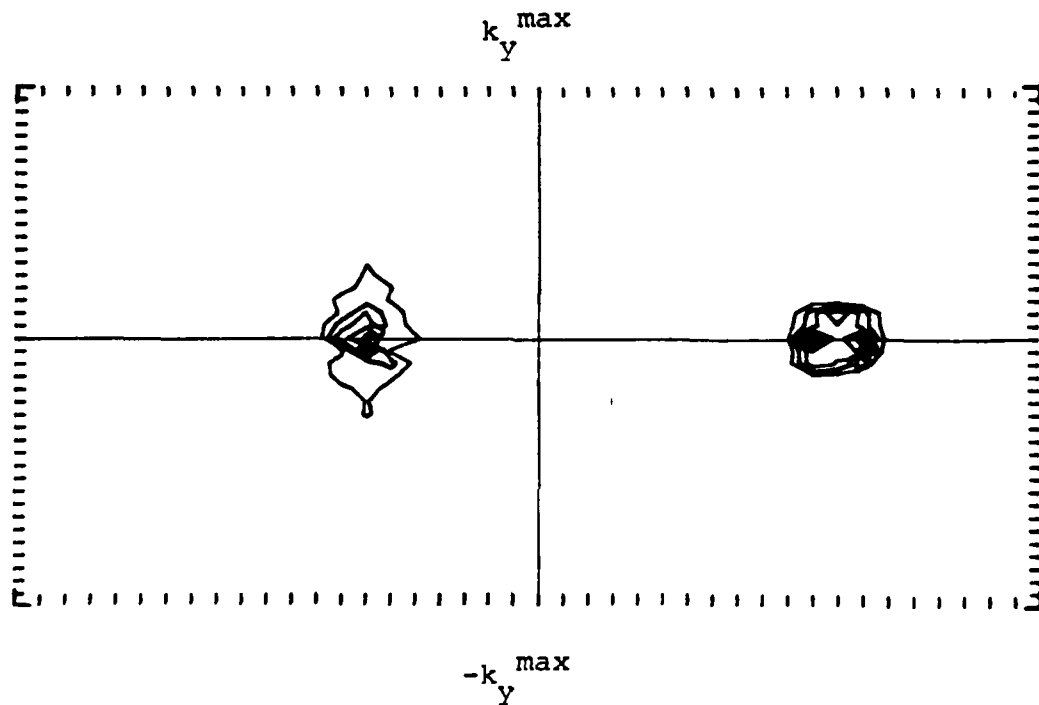


FIGURE 12b) Electric field amplitude contours in wave-number space at  $T = 150$  (33000 plasma periods). The decay instability is causing amplitude to increase in waves in the backward direction. There is no magnetic field.

the backward direction due to the decay instability. The  $k$ -mode of maximum growth is given by the three wave frequency matching condition:

$$\omega_L - \omega_o + \omega_A = \frac{3}{2} \frac{(k_o - k)^2}{k_{De}^2} \omega_{pe} + c_s k - \frac{3}{2} \frac{k_o^2}{k_{De}^2} \omega_{pe} = 0 \quad (93)$$

We find that  $k_o - k = -0.028 k_{De}$ . The numerically found decay wavenumbers agree well with the calculated value, and the numerically derived growth rate at this wavenumber,  $\gamma/\omega_{pe} = 1.74 \cdot 10^{-5}$  is within a few percent of the theoretical growth rate given by  $\gamma/\omega_{pe} = \omega_o/16$ . We conclude that the growth rate of the decay instability is not affected by the finite bandwidth for these parameters.

The growth of the modes driven by the stimulated modulational instability is about 40% less than in the monochromatic case. The numerically determined averaged growth rate (in the broadband case) is  $\gamma/\omega_{pe} = 0.69 \cdot 10^{-5}$ . Although this is not much smaller than the decay instability growth rate, after  $3 \cdot 10^4$  plasma periods ( $T = 150$ ) the decay has undergone 3.6 e-foldings, and the modulational only 1.4. This results in an order of magnitude difference in amplitude, so the modulational instability does not appear in the amplitude plots.

It is remarkable that the broadband pump does not cause a large decrease in growth rates, even though the spread in the pump frequency is two orders of magnitude larger than the growth rate. This result differs from

Thomson and Karush (1974) and Smith, et al. (1979). From Thomson and Karush we would expect a decrease in growth rate by a factor of  $\gamma/\Delta\omega$ . However, they interpret the growth rate  $\gamma$  as the resonant width of the instability. We find that the resonance widths of the instabilities are much larger than their growth rates.

Because of the importance of the resonance widths, we can speculate on a possible role of the magnetic field in reducing growth rates. We have seen that the magnetic field causes a decrease in perpendicular wavenumbers for the decay instability. For some value of the magnetic field, the transverse width will become less than the bandwidth, and a decrease in growth rates, even on the  $k_0$ -axis, could result. This has never been investigated. For Type III parameters, the width of the decay instability, even with a magnetic field, is still larger than the pump bandwidth. However, it may be an important effect in the ionosphere or in laboratory experiments.

If we continue the numerical experiment, we find that the pump modes quickly lose their energy to the decay modes. These modes themselves are large amplitude, and can drive other instabilities. In particular, they can decay into Langmuir waves in the forward direction at wavenumber  $k_L = 0.016 k_{De}$ . The  $k$ -space configuration at  $T = 240$  ( $5 \cdot 10^4$  plasma periods) is shown in Figure 18c. We can see that the second scattering is occurring in the

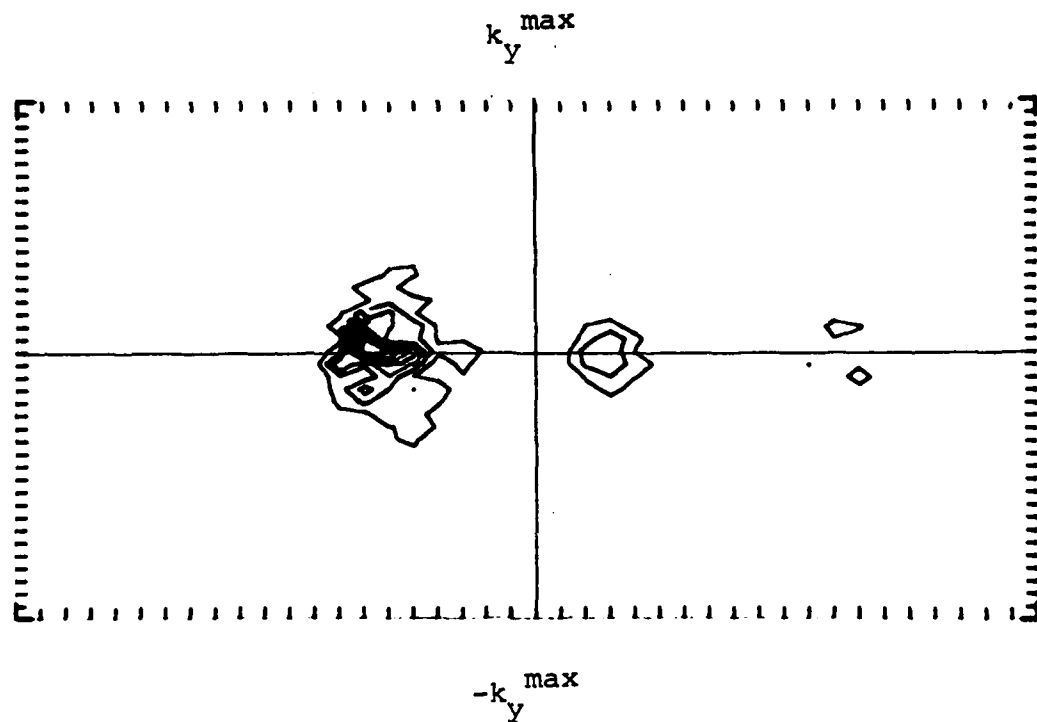


FIGURE 12c) Electric field amplitude contours in wave-number space at  $T = 240$  (52800 plasma periods). The original pump has depleted, but the decay waves are now themselves driving a decay instability. There is no magnetic field.

forward direction as predicted. This nonlinear process of successive decay is called cascade (Nicholson and Goldman, 1978). Notice that although the cascade is occurring along one dimension, the energy is going from large wavenumbers to smaller wavenumbers. The flow of energy to larger wavenumbers as postulated by Smith, et al. (1979) does not occur by parametric instability. The cascading can continue with another decay. The next decay product will also be in the forward direction, at  $k_L = 0.005 k_{De}$ . However, this  $k$  is of the order of a grid spacing, so unfortunately we must stop the simulation at this point. Solitons might be able to form at later times.

#### Summary

We have considered three subjects in the context of Type III parametric instability: the dipole approximation, the magnetic field, and finite bandwidth. We find that it is not correct to use the dipole approximation in the Type III problem, unless  $W_o \gg k_o^2$ , which implies tremendous wave energies. The magnetic field causes some new wave geometries, but does not limit growth of waves transverse to the field. Finally, we have seen that broadband effects limit the role of transverse instabilities by reducing (but not eliminating) their growth. However, the decay instability, which occurs on the

$k_o$ -axis, is not affected by the broadband nature of the pump because of its large resonance width.

There are other nonlinear processes which are enhanced by broadband effects and are intrinsically two dimensional, but do not appear in the above example. One is the constructive interference of Langmuir waves in the real space to create wavepackets which undergo a direct collapse. In the low solar corona, where  $k_o/k_{De} > (m_e/m_i)^{1/2}$ , the wavepackets have a group speed larger than the ion-acoustic speed, and collapse cannot occur without some scattering, such as the multiple cascading in the example above. For 1/2 A.U., when  $k_o = 0.01 k_{De}$ , the wavepacket can collapse directly, thus bypassing the stage of parametric instability altogether (Nicholson, et al., 1978). This is the subject of the next chapter.

## CHAPTER V

### PLASMA WAVE COLLAPSE

Besides being unstable to perturbations, wavepackets of intense Langmuir waves can experience direct spatial collapse (Zakharov, 1972). This occurs because the wavepacket creates a density cavity by ponderomotive forces and as a result becomes more compact in space and more intense in energy density. Collapse has been studied in two and three dimensions when there is no magnetic field and is found to continue until length scales become of the order of a Debye length, when particle-wave damping removes energy from the collapsing waves (Nishikawa, Lee, and Liu, 1974; Zakharov, Mastryukov, and Synakh, 1974; Degtyarev and Zakharov, 1974; Degtyarev, Zakharov, and Rudakov, 1975; Degtyarev and Zakharov, 1975; Pereira, Sudan, and Denavit, 1977; Nicholson and Goldman, 1978; Goldman and Nicholson, 1978). Langmuir collapse is expected to occur in Type III radio bursts (Nicholson, Goldman, Hoyng, and Weatherall, 1978), and may be important for other beam-plasma systems such as a radar modified ionosphere or situations in the laboratory.

In one dimension, collapse is prevented because dispersion can balance the nonlinear ponderomotive force. Other solutions, such as pulsating solitons, are possible (Goldman, Rypdal, and Hafizi, 1980). An example of a non-collapsing nonlinear solution in one dimension is the soliton discussed in the third chapter. When variation in a second dimension is allowed, the soliton "collapses."

In physical problems, a weak background magnetic field is often present. We have already presented a linear stability analysis for monochromatic Langmuir waves in the presence of a weak magnetic field in the fourth chapter. What will be the effect on collapse? Some speculation is based on the argument that the magnetic field makes the wave interactions completely one dimensional (an assumption which our work does not support). If this were the case, then collapse might be prevented. Some early work by Petviashvili (1976) seemed to show stable, pancake shaped solitons. However, other speculative arguments seem to minimize the role of the magnetic field in stopping the collapse (Nicholson, et al., 1978).

The first theory of collapse in a magnetic field was done by Zakharov (1975). Of the three high frequency plasma modes, he studied an electromagnetic slow extraordinary mode. Therefore, this work has little direct application to ours because we are studying beam-generated

Langmuir waves. However, he did suggest that collapse at the Langmuir mode frequency will be possible.

A subsequent Russian paper by Krasnosl'skikh and Sotnikov (1978) takes up the problem of the plasma wave collapse. They assume 1) a dipole pump, 2) very large amplitude waves,  $|E|^2/4\pi nT \gg m_e/m_i$ , 3) one-dimensional fields,  $E \parallel \hat{z}$ , and 4) strongly magnetized ion-acoustic modes. Their analytic work derives from linear stability analysis and the construction of self-similar solutions. First, they show that the modulational instability (OTI) produces a pancake shaped cavity because the unstable wavenumbers have  $k_{\perp} \ll k_{\parallel}$  due to the magnetic field (see also Freund and Papadopoulos, 1980). This is related to Petviashvili's solution. Then they find that the cavity collapses. As collapse occurs, the transverse dimension of the cavity changes more rapidly than the longitudinal dimension, until the latter is such that  $\Delta k_{\parallel}/k_{De} > \omega_{ce}/\omega_{pe}$ . Then the cavity becomes symmetric and the magnetic field ceases to have an effect on collapse. Numerical work by Lipatov (1977), for the same kind of geometry and field amplitude, confirms that the collapse is inevitable even with a magnetic field. He does find, however, that the magnetic field hinders the start of collapse.

Our work is fully two dimensional, treats a finite wavenumber pump, assumes unmagnetized ions, and generally involves weaker electric field energies. These are

conditions relevant to the Type III problem. We follow the collapse from early times, starting with wavepackets produced by the beam instability. These wavepackets are initially spherically symmetric. We find that collapse in the transverse direction does not proceed rapidly when there is a magnetic field, and in fact the Langmuir waves evolve in such a way as to reduce perpendicular mode energy. As a result, the wavepackets evolve into a pancake shape. At this point contact can be made with Soviet work. If we could follow collapse to the time when  $\Delta k_{||}/k_{De} \sim \omega_{ce}/\omega_{pe}$ , we would expect that the results of Krasnosele'skikh and Sotnikov would apply. However, this is not possible because of the finite numerical grid. The inability to follow the collapse to later times is a serious limitation.

Besides being applied to different parameter regimes and geometries, our work on Langmuir collapse uncovers interesting new phenomena. As we shall demonstrate numerically, even weak magnetic fields can prolong the time for collapse of a broadband Langmuir wavepacket and alter its geometry. This can have important consequences. If the collapse times are prolonged sufficiently, they will exceed characteristic times for Langmuir wave growth and higher levels of strong plasma turbulence could be produced. Also, the altered packet shapes may affect the pattern of electromagnetic emission and its polarization.

We will show from a collapse virial theorem (Goldman, Weatherall, and Nicholson, 1980) that the retardation of the collapse is due to an altered geometry of the wave-packet. In order to suggest how this new geometry can be produced, we will apply perturbation theory to the broadband initial conditions. Further arguments must rely on the evidence of the numerical simulation.

Finally, we will be able to show that the measured mean solar magnetic field can affect, but not prevent, Langmuir collapse at 1/2 A.U.

#### Simulation of Type III Wave Processes

Langmuir waves in Type III bursts are expected to grow linearly from a low level by interaction with the electron stream and to have a finite bandwidth because of the spread in velocity in the stream. As a result, a pattern of intensifying Langmuir wavepackets will be present in the solar corona whose spatial dimensions are defined by the bandwidth of the randomly phased pump modes. When these waves reach large amplitudes, they will exhibit nonlinear behavior. One possibility is that the wavepackets will undergo direct collapse. This is possible at 1/2 A.U. because the group speed of the waves is less than the sound speed, i.e.,  $k_o/k_{De} < (m_e/m_i)^{1/2}$ .

We can simulate these wave processes numerically for 1/2 A.U. parameters. In k-space, we make a broadband

pump consisting of 14 randomly phased modes centered about a wavenumber  $k_o = 0.011 k_{De}$ , and with parallel and perpendicular bandwidths of  $\delta k_{||} = 0.14 k_o$ , and  $\delta k_{\perp} = 0.2 k_o$ . These modes are caused to grow exponentially at a rate  $\gamma/\omega_{pe} = 10^{-6}$ , which is the growth rate due to the beam as inferred from quasilinear calculations (Nicholson, et al., 1978; Magelssen, 1976). Initially the pump modes have an energy  $W_p = 6 \cdot 10^{-7}$ , while the other modes have even smaller amplitudes. We do a case with no magnetic field (which was also done in Nicholson, et al., 1978), and two examples which have a magnetic field along the direction of  $k_o$  such that: 1)  $\omega_{ce} = 0.01 \omega_{pe}$ , which represents an upper limit on the mean magnetic field at 1/2 A.U. (Dulk and McLean, 1978); and 2)  $\omega_{ce} = 0.05 \omega_{pe}$ .

The time evolution of the wavepackets into collapse. is compared in Figures 19, 20, and 21. There are two noticeable differences between the unmagnetized and the magnetized cases. One is that the collapsing wavepackets are pancake-shaped in the magnetized case, with the largest dimension transverse to the field. This effect is more pronounced for the larger value of magnetic field. Also, the packets take longer to intensify in the magnetized examples. This time delay is significant for the larger magnetic field case.

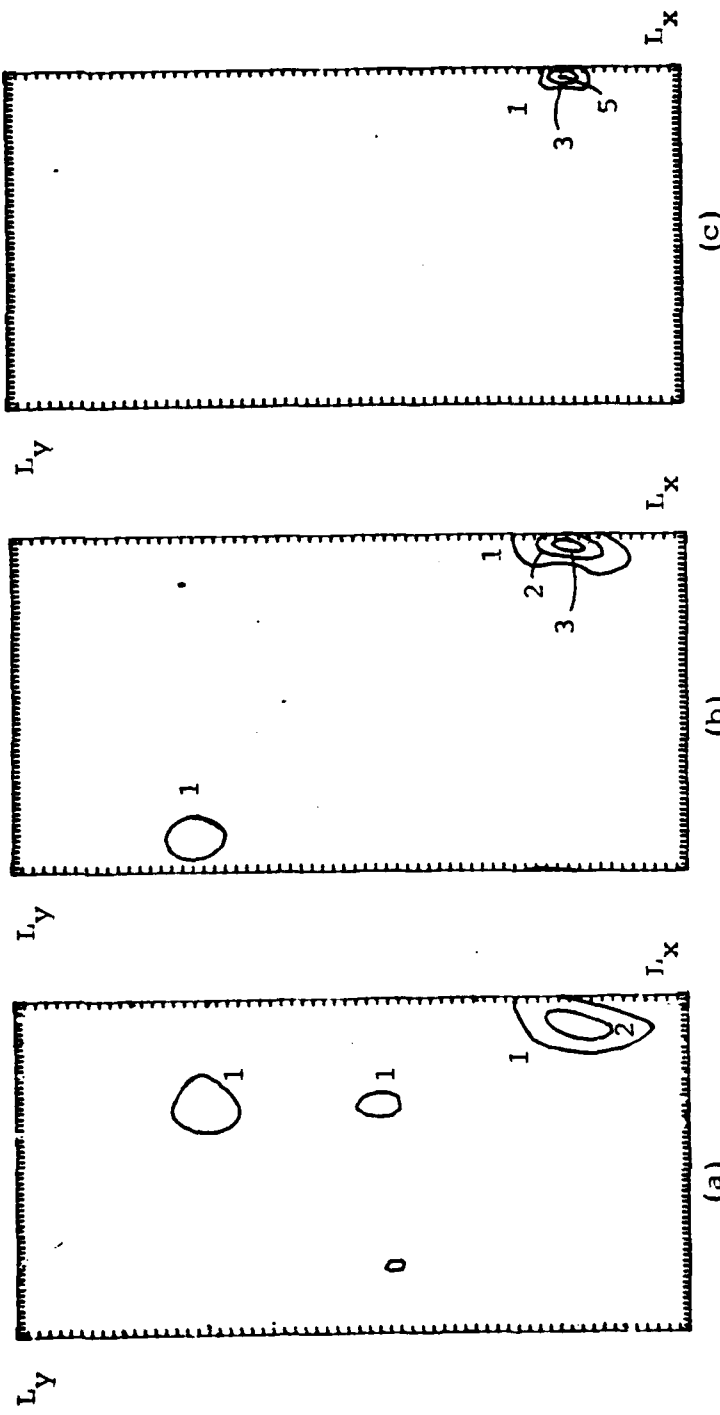


FIGURE 19. Electric field contours in real space at three times for waves being pumped by an electron stream: (a)  $T = 4.3 \times 10^5$ ; (b)  $T = 4.4 \times 10^5$ ; and (c)  $T = 4.8 \times 10^5$  plasma periods. Parameters are for 1/2 A.U. during Type III bursts. There is no magnetic field. Contour labels correspond to the following dimensionless field energies: 1 -  $2 \times 10^{-4}$ ; 2 -  $4 \times 10^{-4}$ ; 3 -  $8 \times 10^{-4}$ ; 4 -  $12 \times 10^{-4}$ ; 5 -  $18 \times 10^{-4}$ ; 6 -  $25 \times 10^{-4}$ ; 7 -  $32 \times 10^{-4}$ .  $L_y = 2 L_x = 7500 \lambda_{De}$ .

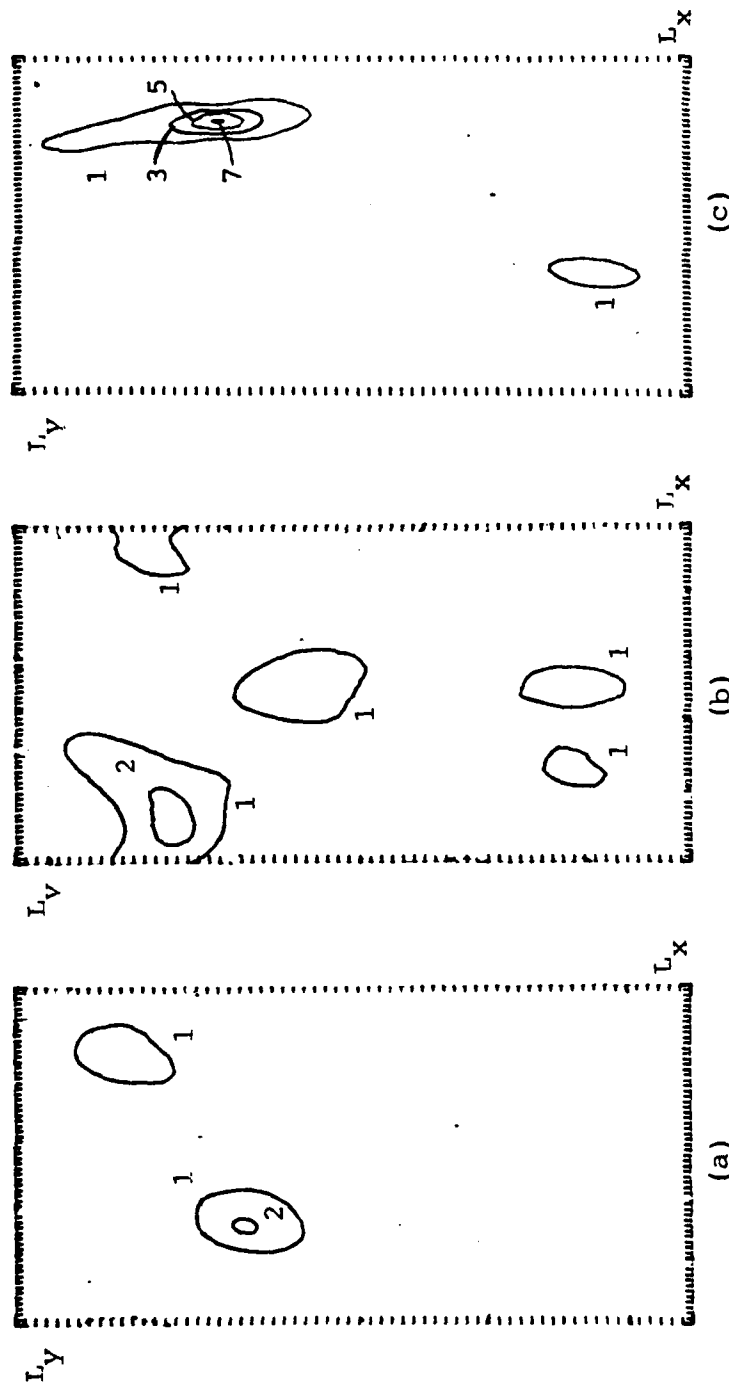


FIGURE 20. Electric field contours in real space at three times for waves being pumped at the same rate as in Figure 19, but for a magnetic field  $\omega_{ce} = 0.01 \omega_{pe}$ : (a)  $T = 4.3 \times 10^5$ ; (b)  $T = 4.4 \times 10^5$ ; (c)  $T = 4.8 \times 10^5$  plasma periods.

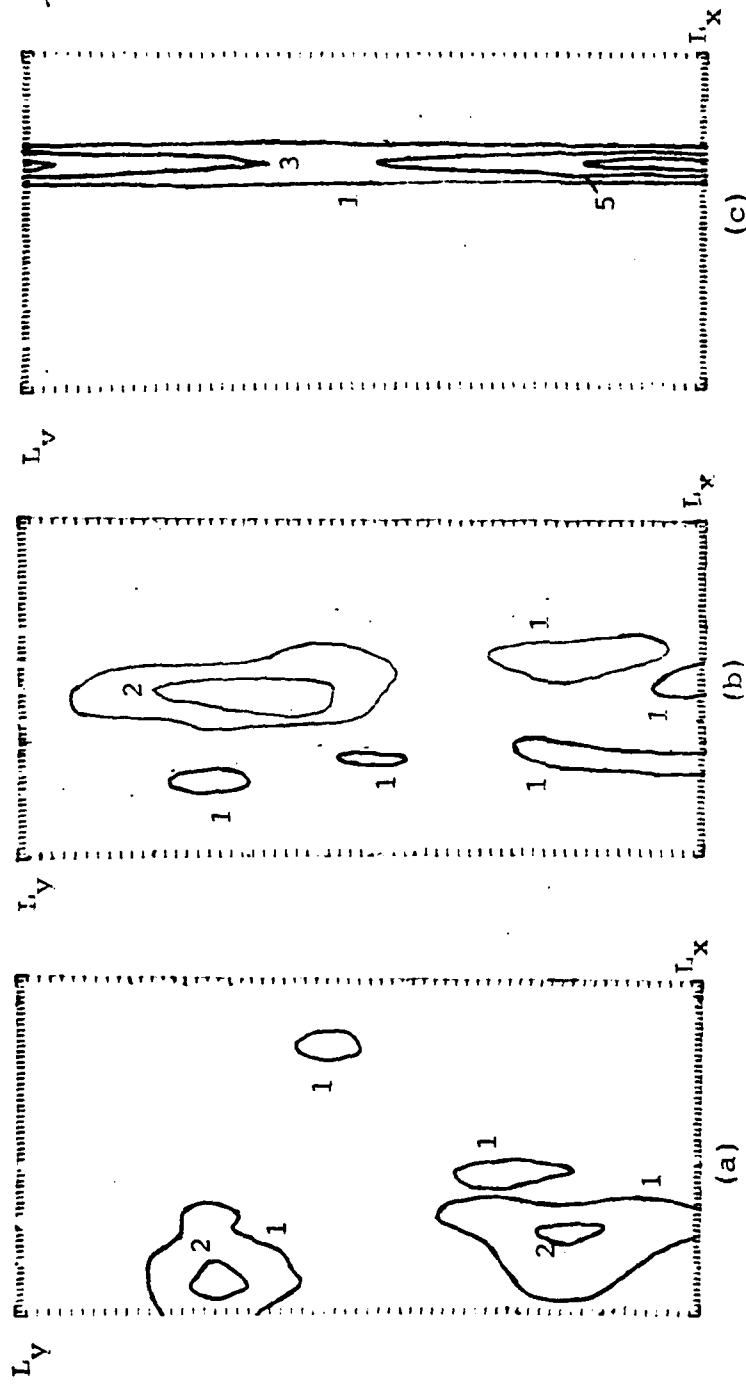


FIGURE 21. Electric field contours in real space at three times for waves being pumped at the same rate as in Figure 19 but for a magnetic field  $w_{ce} = 0.05 w_{pe}$ : (a)  $T = 4.3 \times 10^5$ ; (b)  $T = 4.4 \times 10^5$ ; (c)  $T = 4.8 \times 10^5$  plasma periods.

One consequence of the nonlinear wave interaction between the pump modes and other wave modes in the system is that wave energy can be taken out of resonance with the beam. In Figure 22 we plot the pump electrostatic energy ( $W_p$ ) as a function of time. In all three cases the pump energy saturates at a maximum value, and then rapidly depletes. Although the resonant modes are still being pumped, energy is being removed much faster than it can be absorbed by the resonant waves. Since the rate at which energy can be absorbed by the waves is proportional to  $\gamma W_p$ , where  $\gamma$  is the linear beam growth rate, this depletion can have a stabilizing effect on the beam and limits the amplitude of the Langmuir wave turbulence. Therefore, we see the total electrostatic energy approaching a steady value after the pump waves are depleted (Figure 23).

The magnetic field causes a change in the saturation level of the pump waves and the total electrostatic energy. Because the dominant nonlinear wave interactions are slower in the magnetized cases, the beam can remain resonant with the pump waves for a longer time before they deplete. This results in the higher levels of Langmuir turbulence. Further increase of the magnetic field should not cause higher levels than we see in the case  $\omega_{ce} = 0.05 \omega_{pe}$ . We deduce this from another simulation (not shown here) in which we forced the wave evolution to be one

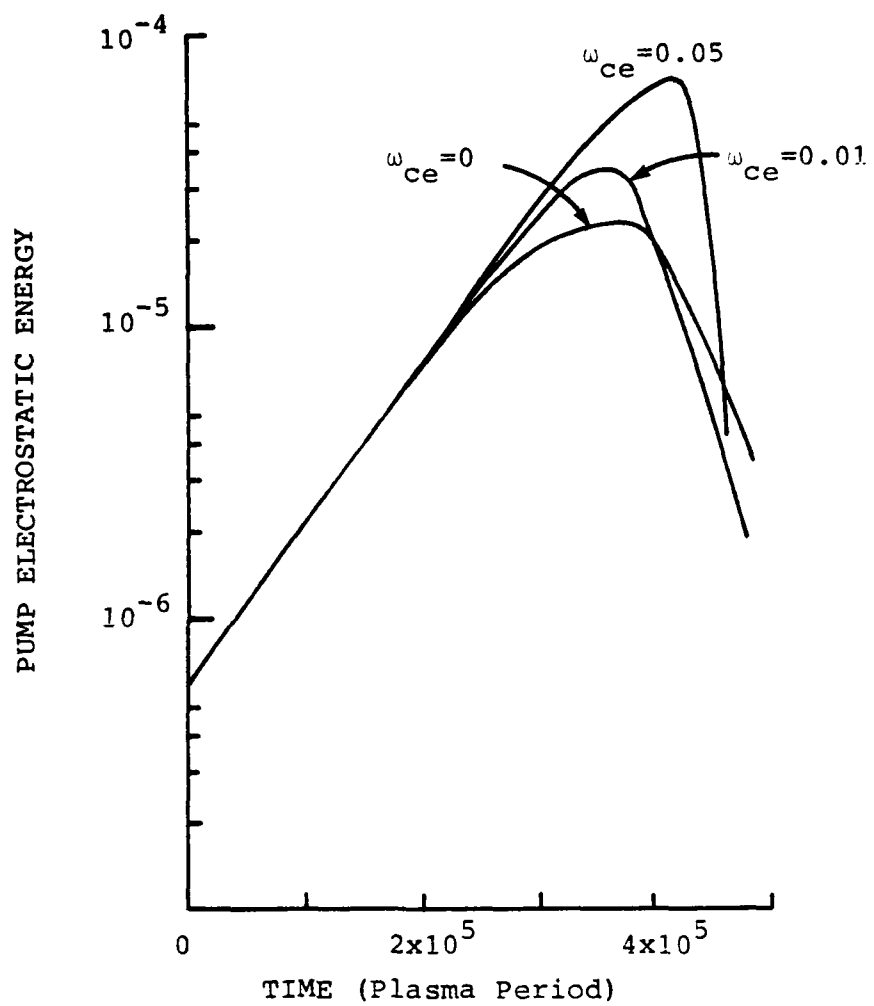


FIGURE 22. Pump electrostatic energy vs. time for waves being driven at a constant rate. The three curves correspond to three different values of the magnetic field:  $\omega_{ce} = 0, 0.01$ , and  $0.5 \omega_{pe}$ . There is steady growth until the pump waves saturate, and then deplete due to nonlinear wave effects.

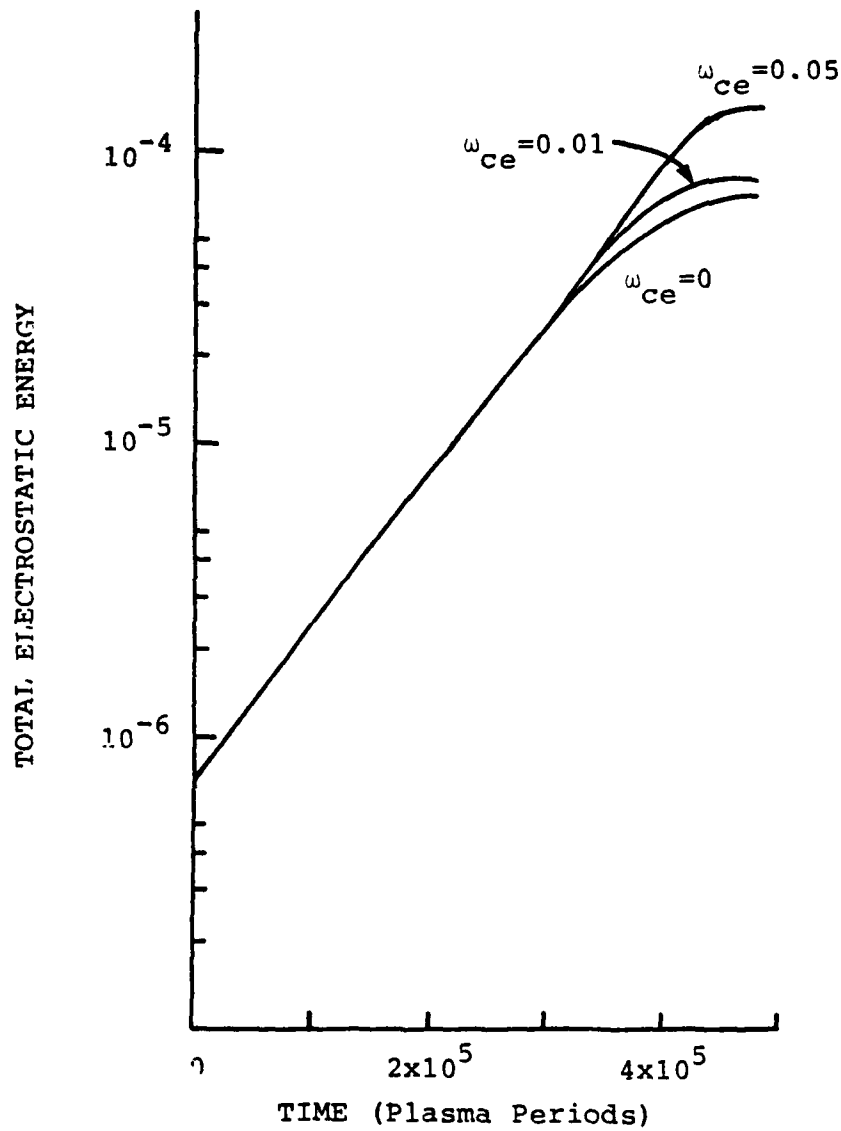
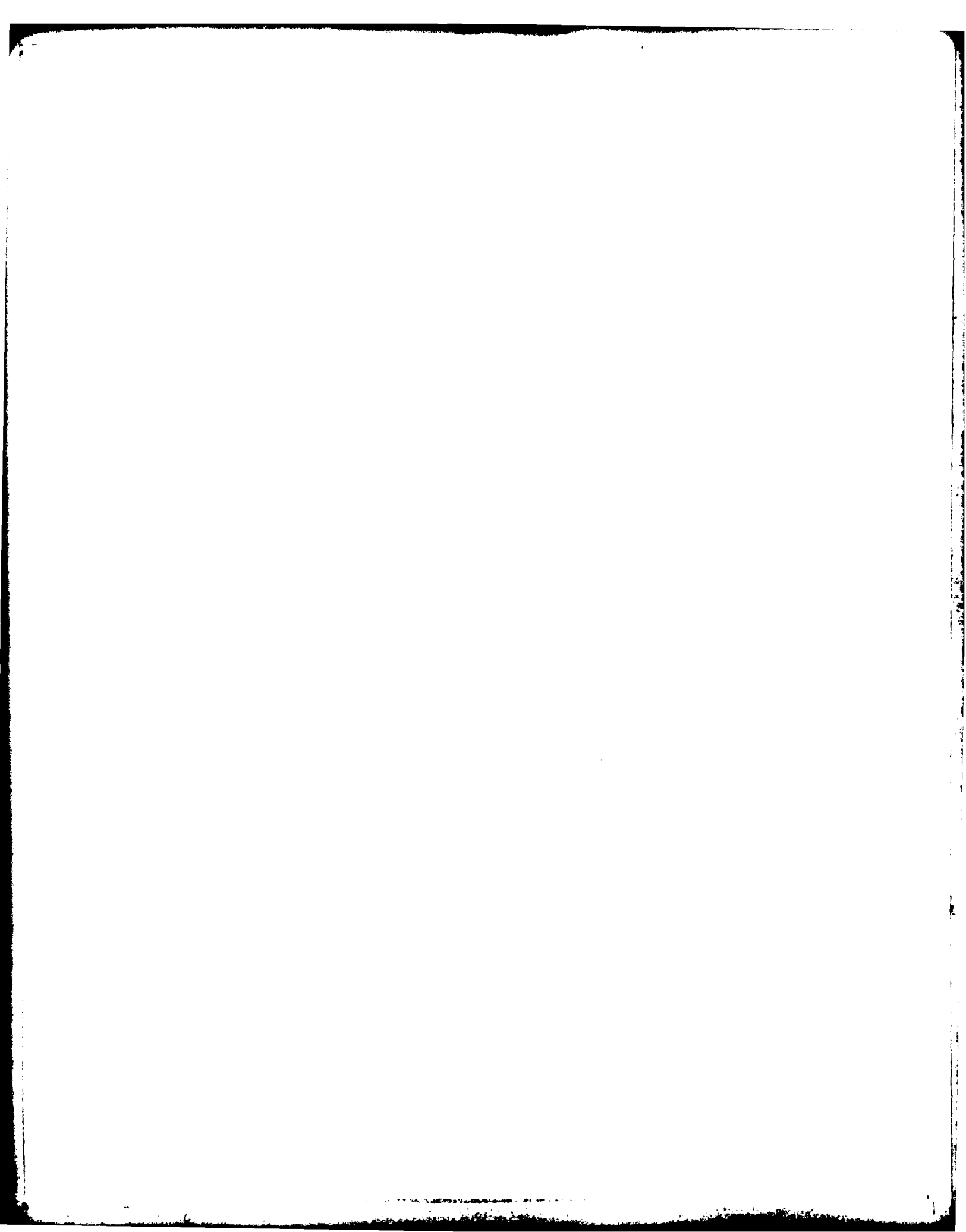


FIGURE 23. Total electrostatic energy vs. time in plasma waves for a system driven by a beam-plasma instability. The three curves correspond to three different values of the magnetic field:  $\omega_{ce} = 0, 0.01$ , and  $0.05 \omega_{pe}$ . The total energy saturates due to wave interactions.



dimensional by putting no noise in the transverse modes and using only two pump modes along the  $k_x$ -axis. The saturated values for  $W_p$  and  $W$  were the same as in the case  $\omega_{ce} = 0.05 \omega_{pe}$ . Since the wave-wave interactions seem to be increasingly limited to the longitudinal direction for larger values of the magnetic field, this puts an upper limit on how much the magnetic field can affect the depletion of the pump.

In order to appreciate the role of various wave interactions in the unmagnetized and magnetized cases, we should examine the evolution of wave amplitude in  $k$ -space. In Figures 24, 25, and 26 we can identify collapse with the transfer of energy out of the pump modes into adjacent  $k$ -space modes. In the magnetic cases, the collapse seems to be inhibited in the direction transverse to the field. The saturation of the beam instability can be associated with collapse. However, in the process of collapsing, the wavepacket acquires wave components which are parametrically unstable. This is seen in the buildup of wave amplitude in modes near  $k_0/3$ , which is the position for the four-wave decay instability at these parameters (see Figure 15a; also Nicholson, et al., 1978). It is important to note that these modes have not grown from the noise levels, which would take a longer time, but grow exponentially from the enhanced levels produced in the collapse. The subsequent

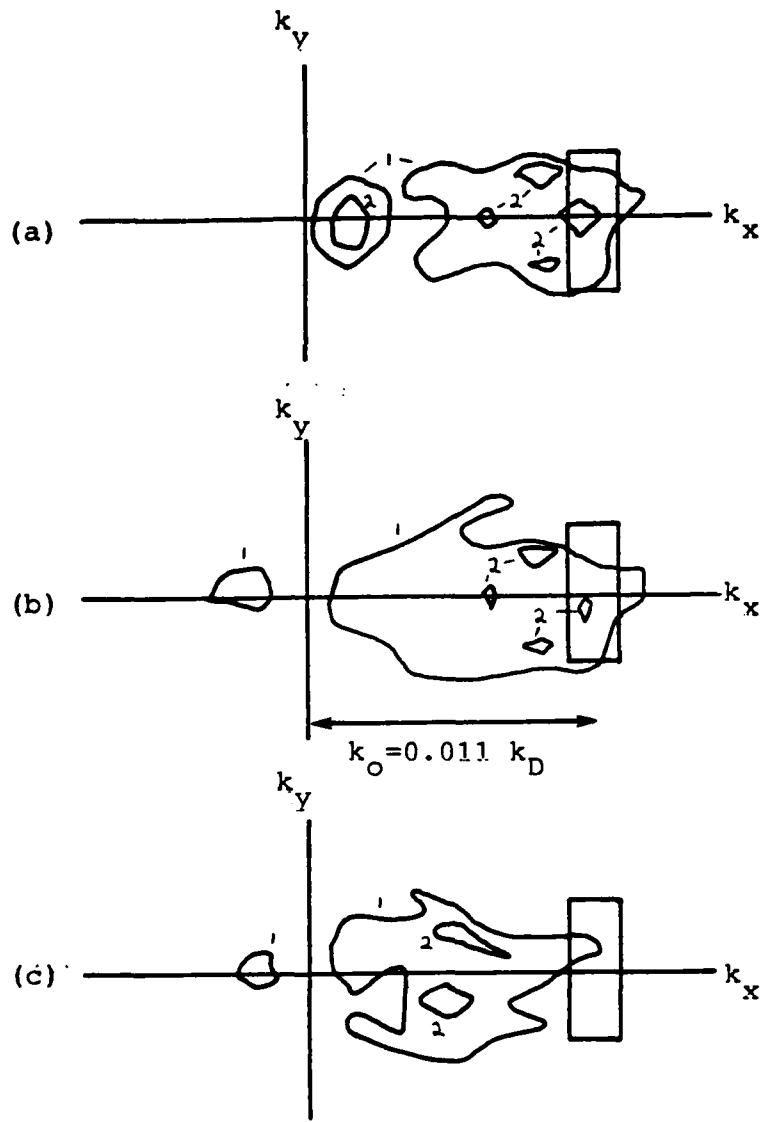


FIGURE 24. Electric field contours in wavenumber space at three times: (a)  $T = 4.3 \times 10^5$ ; (b)  $T = 4.4 \times 10^5$ , and (c)  $T = 4.8 \times 10^5$  plasma periods. The wave modes within the box centered at  $k_o = 0.01 k_{De}$  are those being driven with a constant growth rate,  $\gamma = 10^{-6} \omega_{pe}$ . The contour levels indicate relative magnitudes. There is no magnetic field.

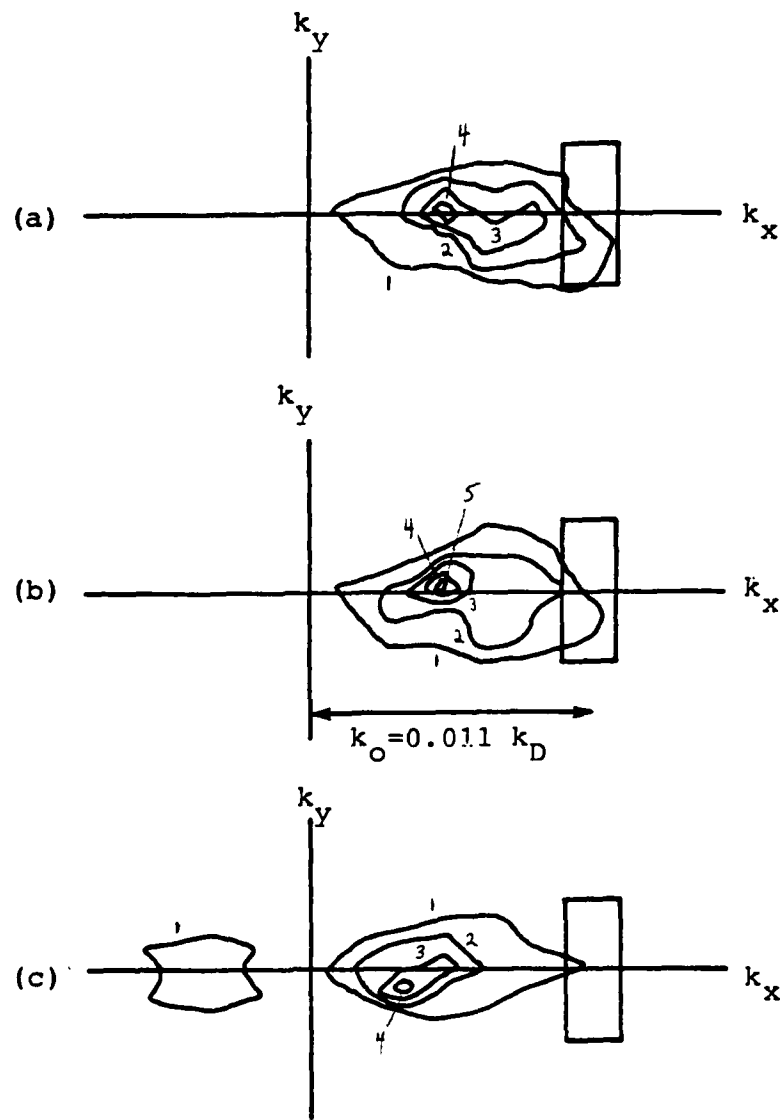


FIGURE 25. Electric field contours in wavenumber space times: (a)  $T = 4.3 \times 10^5$ ; (b)  $T = 4.4 \times 10^5$ ; and (c)  $T = 4.8 \times 10^5$  plasma periods. The wave modes within the box centered at  $k_o = 0.01 k_{De}$  are driven with a constant growth rate. There is a magnetic field  $\omega_{ce} = 0.01 \omega_{pe}$ .

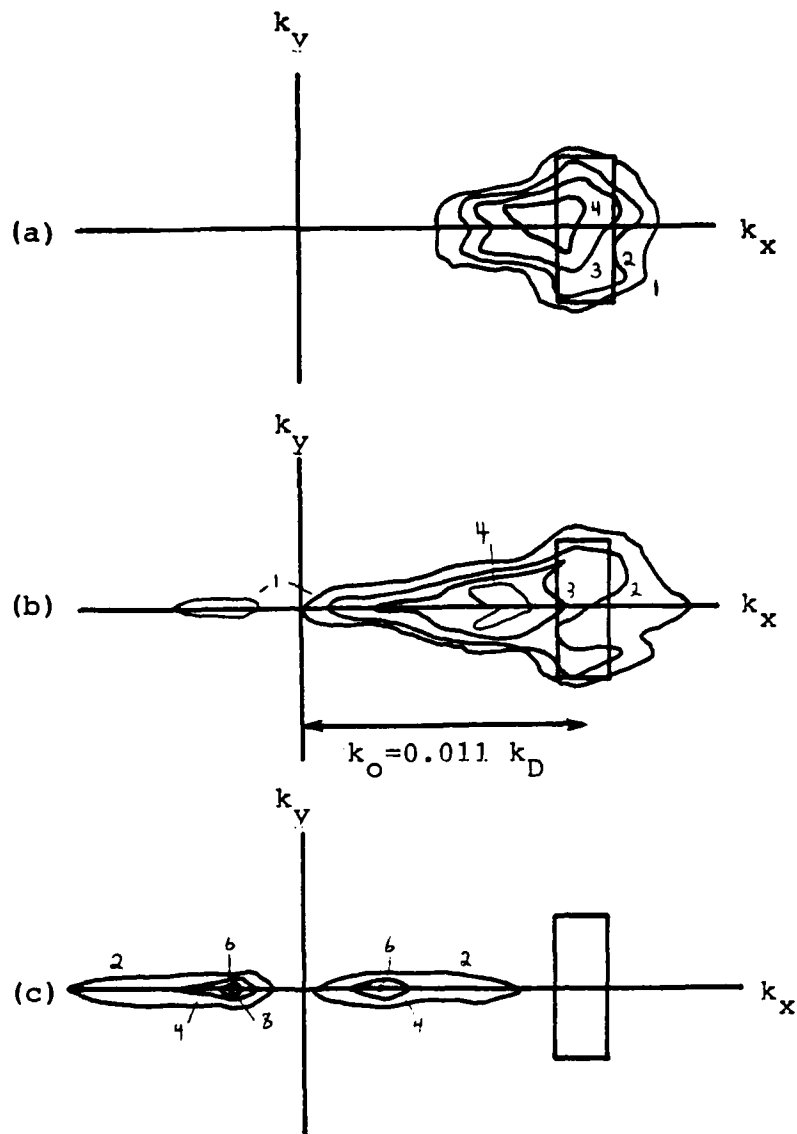


FIGURE 26. Electric field contours in wavenumber space at three times: (a)  $T = 4.3 \times 10^5$ ; (b)  $T = 4.4 \times 10^5$ ; and (c)  $T = 4.8 \times 10^5$  plasma periods. The wave modes within the box centered at  $k_o = 0.01 k_{De}$  are driven with a constant growth rate. There is a magnetic field  $\omega_{ce} = 0.05 \omega_{pe}$ .

parametric excitation results in a very sudden depletion of the pump. This does not appear to disrupt the collapse, as we see wavepackets continue to intensity. In fact, in the magnetized case, these instabilities seem to play an important role in forming the pancake-shaped wavepacket which precedes the collapse.

Therefore, it seems consistent to attribute the depletion of the pump waves to the decay instability at modes enhanced by the collapse process, rather than directly by the collapse itself, as suggested in Nicholson, et al., 1978. This behavior is most evident in the magnetized examples. It is also observed in a purely one-dimensional code (Hafizi, 1980).

#### Scenario for Magnetic Collapse

From these simulations, and other initial value computations (Goldman, Weatherall, and Nicholson, 1980), we construct the following scenario for magnetic collapse of beam generated wavepackets:

- 1) The collapse begins at the same threshold energy as in the unmagnetized case. However, unlike the unmagnetized case, the collapse transverse to the field is inhibited, and seems to be slower. In real space, the transverse dimension of the packets remain the same,

although the longitudinal dimension decreases because collapse is occurring in that direction.

2) Eventually, parametric excitation will occur to produce a new  $k$ -space configuration. These instabilities will be very intense because the background level of the unstable modes has been enhanced in the longitudinal collapse. Because the scatter is principally in the  $B_0$ -direction (as shown in the last chapter, and in Weatherall, Nicholson, and Goldman, 1980), the wavepackets are elongated in the transverse direction, as well as continuing to contract in the longitudinal direction.

3) The new configuration in real space is a pancake-shaped wavepacket which can collapse in both directions. Although our simulations do not continue beyond this point, the results of Krasnosel'skikh and Sofnikov (1978) show that as collapse proceeds to dimensions for which  $\Delta k_{||}/k_{De} \sim \omega_{ce}/\omega_{pe}$ , the wavepacket will tend to become symmetric. After this point, the magnetic field will have no further effect on collapse.

We have seen from computer simulations that at pump values of  $W_p = 2 \cdot 10^{-5}$ , even a magnetic field as small as  $\omega_{ce} = 0.01 \omega_{pe}$  at 1/2 A.U. might cause pancake-shaped wavepackets and slowdown of collapse of Type III generated Langmuir waves. Later, we will show how these effects scale with the wave energy and magnetic field. Now, by use of a collapse virial theorem, we will show that the

increased collapse time is the result of the altered k-space geometry of wave modes.

#### The Virial Theorem

In classical mechanics, an identity due to Lagrange and Jacobi relates the time behavior of the mutual distances between masses to the value of the quantity  $2T+w$ , where  $T$  is the kinetic energy of the center of mass motion of the particles and  $w$  is their potential energy (which is negative in the case of gravity). If the so-called virial quantity is positive, in an average sense the masses will tend to separate from each other; if it is negative, they will tend to get closer.

A virial theorem can also be derived in Langmuir wave mechanics to describe the stability of a wavepacket (Goldman and Nicholson, 1978; and Goldman, Weatherall, and Nicholson, 1980). In this case, the time behavior of the spatial width of a wavepacket is also related to various wave energy quantities. Relevant field quantities are defined as:

$$\begin{aligned}
 H &= \frac{1}{2} \int (4|\nabla \cdot \underline{E}|^2 - \frac{1}{4} |\underline{E}|^4 + H_B) d\underline{x} , \\
 S &= \frac{1}{2i} \int 4(\underline{E}^* \nabla \cdot \underline{E} - \underline{E} \nabla \cdot \underline{E}^*) d\underline{x} , \\
 N &= \int |\underline{E}|^2 d\underline{x} . \tag{94}
 \end{aligned}$$

All of the above integrals are conserved by the nonlinear Schrödinger equation (54). The first integral gives the total field energy  $H$ , where the first term is due to thermal dispersion and the second is from the nonlinear wave interaction. The third term,  $H_B$ , is defined as

$$H_B = \frac{\Omega^2}{2} \int 4 |\underline{E} \cdot \underline{P}|^2 d\underline{r} , \quad (95)$$

where the operator  $P_{ij} = \delta_{ij} - \hat{b}_i \hat{b}_j$ , selects vector components perpendicular to the magnetic field direction,  $\hat{b}$ . For illustration, consider a monochromatic Langmuir wave of the form  $\underline{E} = \hat{k}_0 \exp(i\hat{k}_0 \cdot \underline{x})$ . The integrand of  $H_B$  becomes  $\Omega^2/2 \sin^2 \theta$ , where  $\theta$  is the angle between  $\underline{E}$  and  $\underline{B}_0$ . This, of course, is due to magnetic dispersion. The other integrals give the wave momentum,  $\underline{S}$ , and boson number,  $N$ .

We will define the mean square width of the wavepacket,  $\langle \delta r^2 \rangle$ , by a spatial average with  $|\underline{E}|^2/N$  as a weighting function:

$$\langle \delta r^2 \rangle = \int \frac{|\underline{E}|^2 |\underline{r} - \underline{r}_0|^2 d\underline{r}}{N} . \quad (96)$$

$\underline{r}_0$  is the centroid position of the wavepacket. In two dimensions, the virial theorem shows that

$$\partial_t^2 \langle \delta r^2 \rangle = 2 \left( A - \frac{2H_B}{N} \right) . \quad (97)$$

The quantity  $A$  is invariant:

$$A = \frac{2H}{N} - \frac{s^2}{N^2} . \quad (98)$$

When there is no magnetic field, the condition for collapse is that  $A < 0$ . With a magnetic field, the rate of collapse is no longer constant because  $H_B$  is not invariant, and collapse is not assured even if initially  $A - 2H_B/N$  is negative. We can demonstrate numerically that a magnetic field can cause the wavepacket to evolve toward smaller perpendicular wavenumbers and cause  $H_B$  to decrease. As  $H_B$  gets smaller and  $A$  remains constant, the collapse rate will go from a large negative number (fast collapse) to a smaller negative number (slower collapse). If the collapse rate changes sign, which is possible if

$$\frac{2H_B}{N} > |A| , \quad (99)$$

then collapse in two dimensions may be prevented. What we find in numerical simulation is that at this point other wave interactions, such as parametric instability, take place and the virial theorem no longer applies. These interactions seem to always lead to a situation for which collapse can occur. We have seen this happen in the numerical examples in the last section.

These points are well demonstrated in initial value runs (Goldman, Weatherall, and Nicholson, 1980). For a broadband pump of 21 modes with energy  $w_p = 3 \cdot 10^{-4}$  (which

is well above the threshold found in the growing pump simulations), we find initially that<sup>1</sup>

$$A - \frac{2H_B}{N} \sim -17 \times 10^{-3} , \quad (100)$$

with or without a magnetic field, and

$$\frac{2H_B}{N} \sim 30 \times \left( \frac{\omega_{ce}}{\omega_{pe}} \right)^2 . \quad (101)$$

For  $\omega_{ce} = 0.1 \omega_{pe}$ , we find that  $2H_B/N \sim 300 \cdot 10^{-3}$ .

Therefore, a change of only 5% in  $H_B$  can inhibit collapse. In Table 5 we show the behavior for  $2H_B/N$  during adiabatic collapse for various values of the magnetic field. For some cases, there is a significant decrease in  $2H_B/N$ , enough to make  $A - 2H_B/N$  positive. Above threshold, this effect seems to occur when the magnetic energy is greater than the nonlinear energy:

$$H_B \gtrsim \frac{1}{16} \int |E|^4 dr . \quad (103)$$

The result is a slowdown, or cessation of two-dimensional collapse. In Figure 27 we plot the collapse times for the various values of magnetic field. We find that the collapse time increases with larger magnetic field strength in a way consistent with the above theory.

---

<sup>1</sup>To convert to the system of dimensionless units used in Goldman, Weatherall, and Nicholson (1980), multiply by  $(n/3)(m_e/m_i)$ .

TABLE 5

$$2H_B/N \times 10^{+3}$$
 DURING ADIABATIC COLLAPSE

T	$\omega_{ce}/\omega_{pe}$			
	0.01*	0.05*	0.075*	0.10**
10	3	74	167	229
20	3	74	162	224
30	4	72	157	220
40	6	71	145	207
50	11	73	132	220
60		77	117	197
70			106	192
80				185
⋮				⋮
150				154

\*21 mode pump.

\*\*39 mode pump.

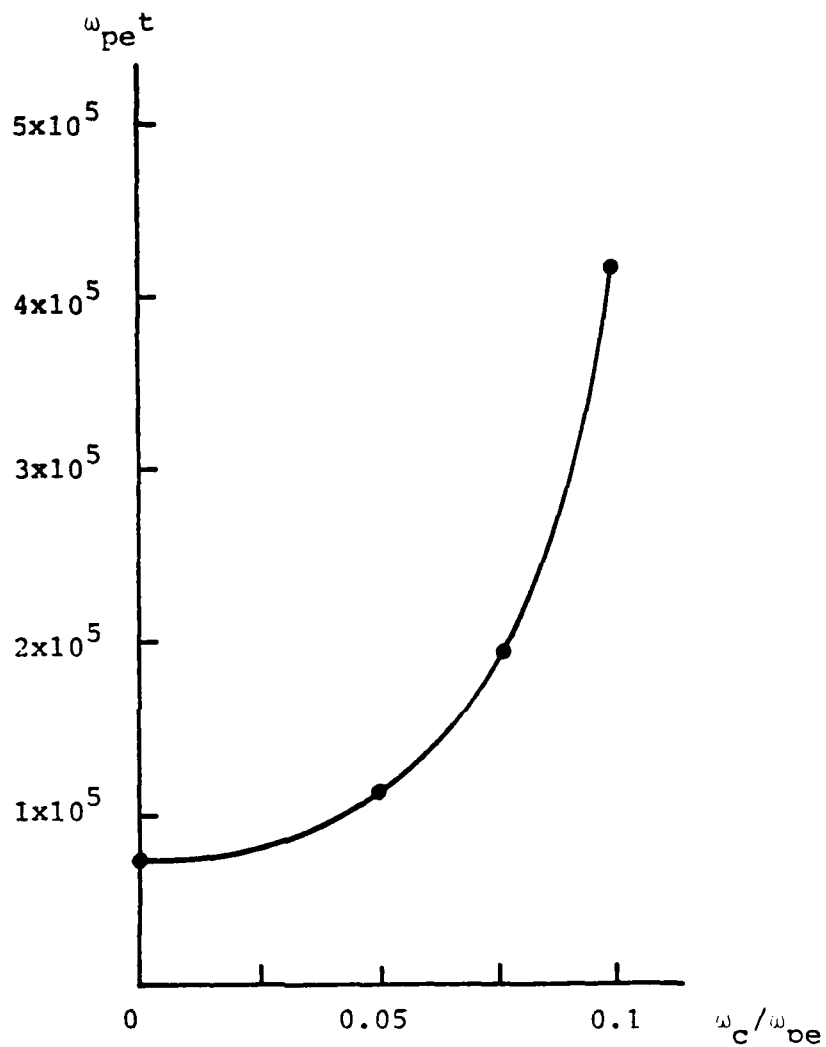


FIGURE 27. Time for central energy density in collapsing wavepacket to reach ten times its initial value for various magnetic field strengths. Initial value of the pump is  $w_0 = 3 \times 10^{-4}$ .

Magnetic collapse can take so long that wave interaction time scales will be the same as for a one-dimensional wavepacket.

For  $W_p = 3 \cdot 10^{-4}$ , magnetic effects become observable for  $\omega_{ce} \sim 0.03 \omega_{pe}$ . In the simulations of last section, the pump only reached an amplitude of  $W_p = 2 \cdot 10^{-5}$ , less by a factor of 10. In that case we found magnetic effects when  $\omega_{ce} = 0.01 \omega_{pe}$ , which means that  $(\omega_{ce}/\omega_{pe})^2$  is also smaller by 1/10. This scaling is expected from Equation (99). This is quite different from the magnetic effects on parametric instability, which did not depend on pump energy, but occurred when

$$\frac{\omega_{ce}}{\omega_{pe}} \sim \frac{k}{k_{De}} \sin\theta. \quad (103)$$

These latter effects are purely geometric (Krasnosel'skikh and Sotnikov, 1977; Weatherall, Goldman, and Nicholson, 1978; Freund and Papadopoulos, 1980). The new behavior we have just described depends upon the energy in the system.

We have seen that the decrease in  $H_B$  affects collapse in a significant way. The computer simulations showed us that  $H_B$  decreases, and the virial theorem enabled us to calculate the effect on collapse. However, neither offers any enlightenment as to why this occurs. In the next section we will use a perturbation theory to describe collapse. This will show that wave-wave

transitions perpendicular to the field become increasingly difficult for larger  $k_{\perp}$  because of the  $\sin^2\theta$  dependence in the magnetic energy term.

### Perturbative Collapse Theory

We will do a time-dependent perturbation theory on a simple broadband pump consisting of five pump modes centered on  $k = k_0$  in a rectangular grid with spacing  $\Delta k = \Delta$  (see Figure 28). We assume that the interaction is weak so that each pump mode amplitude,  $A$ , can be considered constant, and the effect on the other modes can be treated as a perturbation. The interaction is described by the nonlinear term,  $(|E|^2 - \overline{|E|^2})E$ , in the nonlinear Schrödinger Equation (54). To order  $A^2$ , the perturbation theory shows the modulational instability. The order  $A^3$  seems to be related to collapse.

We can write the linear wave equation as

$$-i\partial_t E = L_0 E, \quad (104)$$

where the linear wave operator  $L_0 = \nabla^2 - \Omega^2 \sin^2\theta$ . The vector nature of  $E$  has been ignored by assuming  $E \parallel k_0$ . This will cause small errors in the interaction amplitudes, but in this theory only the phase difference between modes seems to be critical.

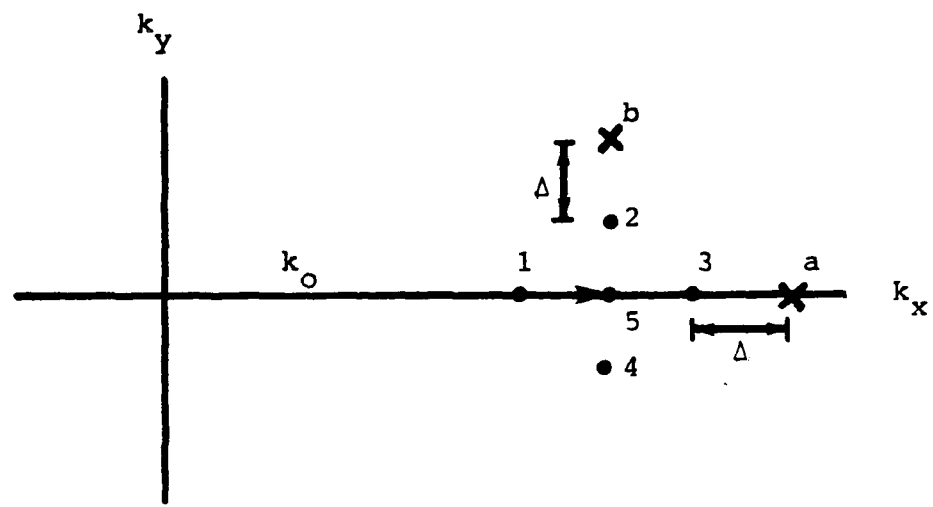


FIGURE 28. Pump modes 1-5 and test modes a, b in broadband perturbation theory.

In the absence of interactions, we can write  $E$  in terms of its independent wave functions:

$$E = \sum_{\substack{s = \\ \text{all modes}}} a_s u_s e^{-i\phi_s t}. \quad (105)$$

For the pump waves, the amplitude  $a_s = A$ ; for all other waves,  $a_s \ll A$ . The spatial functions  $u_s$  are the orthogonal wave functions

$$u_s = \exp i \underline{k}_s \cdot \underline{x}. \quad (106)$$

For a finite grid, both  $\underline{k}_s$  and  $\underline{x}$  are discrete. Finally, the phase factor,  $\phi_s$ , can be found from the linear dispersion relation,  $\omega = k^2 + \tilde{\Omega}^2 \sin^2 \theta$ . For the pump modes,

$$\phi_1 = k_o^2 - 2k_o \Delta ,$$

$$\phi_2 = k_o^2 + \Delta^2 + \tilde{\Omega}^2 ,$$

$$\phi_3 = k_o^2 + 2k_o \Delta + \Delta^2 ,$$

$$\phi_4 = k_o^2 + \Delta^2 + \tilde{\Omega}^2 ,$$

$$\phi_5 = k_o^2 ,$$

and for the test modes,

$$\phi_a = k_o^2 + 4\Delta^2 + 4\tilde{\Omega}^2 ,$$

$$\phi_b = k_o^2 + 4k_o \Delta + 4\Delta^2 .$$

When  $k_o \gg \Delta$ , the angular terms are  $\sin\theta_s \sim k_{ys}/k_o$ ; so we have defined  $\tilde{\Omega}^2 = \Omega^2(\Delta^2/k_o^2)$ .

Now let us include the nonlinear coupling due to the "potential"

$$V = |E|^2 - \overline{|E^2|} . \quad (107)$$

The time behavior is given by the nonlinear Schroedinger equation:

$$-i\partial_t E = L_o E + VE . \quad (108)$$

Because of the interaction, the nonlinear system has different eigenfunctions. We can still write  $E$  in terms of its old wave functions, but the coefficients  $a_s$  will vary with time. We find from Equations (105) and (108) that

$$i \sum_s \dot{a}_s u_s e^{-i\phi_s t} = \sum_s a_s v u_s e^{-i\phi_s t} ,$$

and the potential  $V$  is

$$V = \sum_m \sum_{\substack{n \\ m \neq n}} a_m a_n^* u_m u_n^* e^{-i(\phi_m - \phi_n)t} + a_m^* a_n u_m^* u_n e^{+i(\phi_m - \phi_n)t}$$

(the terms where  $m = n$  are subtracted out by the spatial average). The amplitude of the  $i^{\text{th}}$  mode,  $a_i$ , is given by

$$\begin{aligned}
 -ia_i = & \sum_m \sum_{\substack{n \\ m \neq n}} \sum_s \delta[(k_i - k_s) - (k_m - k_n)] a_s a_m a_n^* \\
 & \cdot e^{i(\phi_i - \phi_s)t} e^{-i(\phi_m - \phi_n)t} + \delta[(k_i - k_s) + (k_m - k_n)] \\
 & \cdot a_s a_m^* a_n e^{i(\phi_i - \phi_s)t + i(\phi_m - \phi_n)t}, \quad (109)
 \end{aligned}$$

The  $\delta$ -functions assure that the spatial dependence of the right side is the same as  $u_i$ . This requirement is essentially wavenumber matching between four waves.

We can do the perturbation theory for different orders of the pump amplitude. To zero and first order in  $A$ , the mode coupling is very small. The second order case corresponds to the usual linearization scheme when there is only one pump mode, and describes parametric instability. The third order theory describes the transfer of wave amplitude from the pump modes to adjacent modes (which is seen in the early stages of collapse). This order does not occur in parametric theory because one pump mode does not satisfy the wavenumber matching condition. Although growth is not exponential, this process can lead to large amplitudes in non-pumped modes before parametric excitation can build up from small background noise levels.

Below we examine two cases. First we will treat the five pump modes as a single pump mode with amplitude  $A = \sqrt{5} A$ , and demonstrate that the theory contains the

modulational instability. This will involve only  $o(A^2)$ . Next, we concentrate on the broadband effects by working only with  $o(A^3)$ . Thus we assume that the collapse process occurs before parametric instability. We derive an a posteriori condition for the validity of this treatment.

#### Modulational Theory, $o(A^2)$

With the one pump mode, Equation (109) gives to second order:

$$-i\dot{a}_i = 2|\tilde{A}|^2 a_i + 2 \sum_n \tilde{A}^2 a_n * \delta(k_i + k_n - 2k_o) \exp[i(\phi_i + \phi_n - 2\phi_o)t] . \quad (110)$$

This results in a set of coupled equations between  $a_i$  and  $a_n$ , where  $k_i + k_n = 2k_o$ :

$$\begin{aligned} -i\dot{a}_i &= 2|\tilde{A}|^2 a_i + 2\tilde{A}^2 a_n * e^{2iat} , \\ +i\dot{a}_n * &= 2|\tilde{A}|^2 a_n * + 2\tilde{A}^2 a_i e^{-2iat} , \end{aligned} \quad (111)$$

where  $2\alpha = \phi_n + \phi_i - 2\phi_o$  is a function of  $k_o$  and  $k_i$ . The coupled equations can be more simply written in terms of the functions  $c_1 = a_i \tilde{A} * \exp(-iat)$  and  $c_2 = a_n * \tilde{A} \exp(iat)$ :

$$-i\dot{c}_1 = (2|\tilde{A}|^2 - \alpha)c_1 + 2|\tilde{A}|^2c_2 ,$$

$$i\dot{c}_2 = (2|\tilde{A}|^2 - \alpha)c_2 + 2|\tilde{A}|^2c_1 . \quad (112)$$

If we assume that  $c_1$  and  $c_2$  have the time behavior  $\exp(-i\omega t)$ , then we find the dispersion relation:

$$\omega^2 = -4\alpha|\tilde{A}|^2 + \alpha^2 . \quad (113)$$

An exponentially growing solution is obtained when  $\alpha < 4|\tilde{A}|^2$ . This describes the modulational instability (Nishikawa, 1976). The maximum growth rate is given by

$$\omega_i = 2|\tilde{A}|^2 . \quad (114)$$

### Collapse Theory, $\propto (A^3)$

The third order terms in the wave interaction give

$$i\dot{a}_i = |A|^2 A \sum_m \sum_n \sum_s 2\delta(k_i + k_n - k_s - k_m) \\ m \neq n \\ \exp[i(\phi_i + \phi_n - \phi_s - \phi_m)t] . \quad (115)$$

If we consider  $(s, m)$  the "initial state," and  $(a, n)$  the "final state" when  $i = b$ , there are two allowed transitions which preserve wavenumber matching (see Table 6). The rate of change of  $a_b$  is given by

TABLE 6  
WAVENUMBER MATCHED CONDITIONS

Initial	Final	$\phi_f - \phi_i$	Degeneracy
2,5	b,4	$4\Delta^2$	4
2,2	b,5	$2\Delta^2$	2

$$-ia_b = |A|^2 A (4e^{i4\Delta^2 t} + 2e^{i2\Delta^2 t}) . \quad (116)$$

This can be integrated to solve for  $a_b$ . The modulus squared of the amplitude is

$$|a_b|^2 = |A|^6 \left[ 32 \left( \frac{\sin 2\Delta^2 t}{2\Delta^2} \right) + 4 \left( \frac{\sin \Delta^2 t}{\Delta^2} \right) \right] . \quad (117)$$

This formula is similar to Fermi's golden rule for quantum mechanical transitions in perturbed systems (Leighton, 1959, or Bahm, 1951). By analogy,  $|a_b|^2$  is the probability that the system will be found in state b after time t,  $A|A|^2$  is the matrix element for a transition from an initial state i to the final state f, and  $\phi_f - \phi_i$  is the difference in energy between the final and initial states. As in quantum mechanics, only "transitions" for which the phase difference  $\phi_f - \phi_i$  is small will occur. This has interesting implications for the mode a, which is located perpendicular to the magnetic field relative to the pump, because its phase contains an additional magnetic term which will cause a larger mismatch in  $\phi_f - \phi_i$ . The calculation for  $|a_a|^2$  gives

$$|a_a|^2 = |A|^6 \left\{ 32 \left[ \frac{\sin 2(\Delta^2 + \tilde{\Omega}^2) t}{2(\Delta^2 + \tilde{\Omega}^2)} \right] + 4 \left[ \frac{\sin^2(\Delta^2 + \tilde{\Omega}^2) t}{(\Delta^2 + \tilde{\Omega}^2)} \right] \right\} \quad (118)$$

The new phase term in the equation can explain the inhibition of collapse across the magnetic field that we observed in the numerical simulations.

The theory also describes other features of the collapse well, such as the time scale, and the fact that collapse occurs as a "broadening" in  $k$ -space and is independent of the initial background noise.

We can compare this theory with a numerical example (Goldman, Weatherall, and Nicholson, 1980) for which the grid spacing  $\Delta$  was  $0.00125 k_{De}$ , the central wavenumber,  $k_0 = 0.01 k_{De}$ , and the magnetic field  $\omega_{ce} = 0.1 \omega_{pe}$ . In dimensionless units,

$$\Delta^2 = 0.2 \times 10^{-2}, \quad \tilde{\Omega}^2 = 4.8 \times 10^{-2}. \quad (119)$$

The initial amplitude for each pump mode was

$$A = 0.03. \quad (120)$$

In this case there were 39 pump modes, so the total amplitude was  $\tilde{A} = 0.185$ , corresponding to a pump strength  $W = 3 \times 10^{-4}$ . According to the above discussion, we can expect the time behavior of  $a_a$  and  $a_b$  to be given by

$$|a_a| \sim |\tilde{A}|^3 \left| \frac{\sin(\Delta^2 + \tilde{\Omega}^2)t}{(\Delta^2 + \tilde{\Omega}^2)} \right|$$

$$|a_b| \sim |\tilde{A}|^3 \left| \frac{\sin \Delta^2 t}{\Delta^2} \right|. \quad (121)$$

In Table 7, we show that the magnetic field has an important effect in inhibiting transitions perpendicular to the field. At  $T = 30$ , when collapse is observed to begin when there is no magnetic field,  $|a_b|$  has reached

TABLE 7

 EFFECT OF FREQUENCY MISMATCH ON AMPLITUDE  
 GROWTH OF COLLAPSE MODES

T	$\left  \frac{\sin \Delta^2 t}{\Delta^2} \right $	$\left  \frac{\sin (\Delta^2 + \tilde{\Omega}^2) t}{(\Delta^2 + \tilde{\Omega}^2)} \right $
10	10	10
20	20	17
30	30	21
40	40	20
50	50	14
:	:	:
1000	625	12

significant amplitude compared with the pump modes. However, in the magnetized case, the collapse transverse to the field cannot sustain itself beyond this time. We can interpret this to mean that the nonlinear interaction is not strong enough to drive this higher energy state. If similar interactions among the pump modes cause the waves to populate the lowest energy modes (near the  $k_z$  axis), then we can deduce that not only will collapse be inhibited transverse to the field, but that  $H_B$  will decrease with time as well. This, according to the virial theorem, will slow down collapse.

Now we must see when the above treatment of four-wave interactions, which ignores interactions of  $\mathcal{O}(A^2)$ , is consistent. The third order process can proceed vigorously as long as

$$\Delta^2 t \ll 1. \quad (122)$$

This means that the argument of  $\sin$  is small, and the amplitude will be steadily increasing with time;  $a \sim |A|^3 t$ . In this case, the amplitude,  $a$ , will be the order of the pump amplitude within times

$$t \sim 1 / |\tilde{A}|^2. \quad (123)$$

This time interval allows only one e-folding for the modulational instability, so these unstable modes will still be near the background level. Therefore the

collapse will occur sooner than the modulational instability as long as the time is short enough that  $\Delta^2 t$  is still small. This requires

$$|\tilde{A}|^2 \gg \Delta^2. \quad (124)$$

If we interpret  $\tilde{A}$  as the total pump amplitude and  $\Delta$  as the bandwidth of the pump, then, in physical units, this inequality gives

$$W > 12 \frac{(\Delta k)^2}{k_{De}^2}. \quad (125)$$

This is approximately the collapse threshold condition given by the virial theorem (Goldman and Nicholson, 1979).

#### Summary

In numerical simulations of collapse, we have identified two effects due to the magnetic field: a change in shape of the collapsing wavepacket and a slowing in the collapse rate. These effects seem to be related. The virial theorem shows that the rate of collapse is slowed because of a decrease in magnetic energy,  $H_B$ , which is brought about by a decrease in amplitude of perpendicular wavenumbers.

The explanation for the decrease in  $k_{\perp}$  is suggested by a perturbation theory which shows that higher order wave interactions are inhibited between waves when the

frequency mismatch is large relative to the rate of nonlinear amplitude growth. By analogy to quantum mechanics, we interpret this to mean that the probability of a transition to various wave states becomes small if the energy difference between these states and the initial state is larger than the interaction energy. The magnetic energy of a state (analogous to the wave dispersion) is proportional to  $\Omega^2 \sin^2 \theta$ , and increases for larger angles  $\theta$  between the wave vector and the magnetic field. Therefore, the lower energy states will correspond to waves with smaller  $k_{\perp}$ . When the magnetic energy is large compared with the interaction energy wave transitions will favor these lower energy states. This will result in a net decrease of  $k_{\perp}$ . Thus,  $H_B$  will become smaller, and magnetic effects will become evident.

When our theory is applied to growing beam problems, the slowdown results in an overshoot of the beam saturation levels and extra electrostatic energy is introduced into the system. In the Type III problem, we find that this effect increases wave energy by a factor of two in two-dimensional calculations. At 1/2 A.U., a magnetic field strength of  $\omega_{ce} = 0.01 \omega_{pe}$  does not seem to produce a significant overshoot, but does alter the geometry of the collapsing wavepacket. However,  $\omega_{ce} = 0.05 \omega_{pe}$  seems to be a very strong magnetic field for wave energy levels near  $2 \cdot 10^{-5}$ .

## CHAPTER VI

### CONCLUSION

What can this work tell us about the magnitude of the magnetic field needed to affect nonlinear Langmuir wave processes?

For parametric instability, we found that the magnetic field caused a change in the wave vectors of unstable waves. This shift enables the waves to maintain frequency matching in the multiple wave interaction. In this sense, the effect of the magnetic field is on the "geometry" of the instability. Such a shift is required when the magnetic field introduces a significant change in the frequency mismatch between the pump wave and the unstable wave, or equivalently, when the magnetic dispersion is comparable with the thermal dispersion,

$$\frac{k_{\perp}}{k} \frac{\omega_{ce}}{\omega_{pe}} > \sqrt{3} \frac{k}{k_{De}} . \quad (126)$$

This effect does not reduce the growth rates of instabilities, but only causes them to have smaller perpendicular wavenumbers.

Instabilities which are nearly perpendicular to the magnetic field [ $k_{\perp}/k_{\parallel} \ll (m_e/m_i)^{1/2}$ ] are suppressed by small magnetic fields. This is due to a change in the nature of the low frequency electron motion for oscillations directly across the magnetic field when  $\omega_{ce} \gtrsim kv_e$ .

We observe two effects of the magnetic field on collapse. The collapsing wavepackets become "pancakes" with their largest dimensions transverse to the magnetic field. The other effect is a slowing in the timescale of the collapse.

Let us consider a two-dimensional Gaussian wavepacket,

$$E = i \frac{E_0}{k_0} \nabla \exp \left[ ik_0 z - \frac{\Delta k_{\parallel}^2 z^2}{2} - \frac{\Delta k_{\perp}^2 x^2}{2} \right]. \quad (127)$$

For this shape, the virial theorem gives us the following condition for collapse to be affected [see Eq. (99)]

$$\frac{\Delta k_{\perp}^2 \omega_{ce}^2}{3k_0^2 \omega_{pe}^2} > \left| \frac{\Delta k_{\parallel}^2}{k_{De}^2} + \frac{\Delta k_{\perp}^2}{k_{De}^2} - \frac{W}{24} \right|. \quad (128)$$

This is not a very useful condition, because close to collapse threshold, the right side of Eq. (128) will be near zero. This implies that an infinitesimal magnetic field can alter collapse. However, while this is necessary, it is not a sufficient condition for magnetized collapse. A sufficient condition [see Eq. (102)] is discovered empirically to require

$$\frac{\Delta k_{\perp}^2}{3k_o^2} \frac{\omega_{ce}^2}{\omega_{pe}^2} > \frac{w}{24} . \quad (129)$$

This condition is consistent with, but not proven by, a broadband perturbation theory. At collapse threshold, we can write the condition for the magnetic field to affect collapse as

$$\frac{\omega_{ce}}{\omega_{pe}} > \frac{3k_o^2}{k_{De}^2} . \quad (130)$$

This assures that the magnetic dispersion in the wavepacket exceeds the thermal dispersion. This condition is independent of the packet width  $\Delta k_{\perp}$ .

For Type III parameters at 0.5 A.U.,  $k_o = 0.01 k_{De}$  and  $\omega_{ce} = 0.01 \omega_{pe}$ , so that the terms in Equation (130) are roughly equal. Our numerical simulation with these parameters showed some change due to the magnetic field. The effects for a slightly stronger field,  $\omega_{ce} = 0.05 \omega_{pe}$ , were more dramatic. We conclude that magnetic effects in Type III bursts are possible.

In all of the examples we have seen, the magnetic field does not prevent the collapse of Langmuir waves. Even in cases where the initial wavepacket does not itself collapse, wave interactions seem to eventually create a pancake-shaped wavepacket which does.

## BIBLIOGRAPHY

Allen, C. W., 1976, Astrophysical Quantities (London: William Clowes and Sons, Limited).

Appleton, E. V., and J. S. Hey, 1946, Solar Radio Noise, Phil. Mag. 37, 73.

Baldwin, D. E., 1964, Electron Overtaking as a Cause of Instability in Type III Solar Radio Bursts, Phys. Letters 12, 202.

Bardwell, S., 1976, Pump Wavenumber Dependent Effects in the Parametric Instabilities of a Plasma, Ph.D. Thesis, University of Colorado at Boulder.

Bardwell, S., and M. V. Goldman, 1976, Three-Dimensional Langmuir Wave Instability in Type III Radio Bursts, Ap. J. 209, 912.

Bekefi, G., 1966, Radiation Processes in Plasmas (New York: Wiley).

Brejzman, B. N., and L. S. Pekker, 1978, Electromagnetic Radiation from a Localized Langmuir Perturbation, Phys. Lett. 65A, 121.

Benford, G., 1979, private communication.

Billings, D. E., 1966, A Guide to the Solar Corona (New York: Academic Press).

Bohm, D., 1951, Quantum Theory (New York: Prentice-Hall).

Chen, F., 1977, Introduction to Plasma Physics (New York: Plenum Press).

Cox, J. L., and W. Bennett, 1970, Reverse Current Induced by Injection of a Relativistic Beam into a Pinched Plasma, Phys. Fluids 13, 182.

Degtyarev, L. M., and V. E. Zakharov, 1974, Dipole Character of the Collapse of Langmuir Waves, Zh. Exp. Teoret. Fiz. Pis'ma 20, 365 (JETP Letters 20, 164).

Degtyarev, L. M., and V. E. Zakharov, 1975, Supersonic Collapse of Langmuir Waves. Zh. Exp. Teor. Fiz. Pis'ma 21, 9 (JETP Letters 21, 4).

Degtyarev, L. M., V. E. Zakharov, and L. I. Rudakov, 1975, Two Examples of Langmuir Wave Collapse, *Zh. Exp. Teoret. Fiz.* 68, 115 (Sov. Phys. *JETP* 41, 57).

DuBois, D. F., and M. V. Goldman, 1965, Radiation-Induced Instability of Electron Plasma Oscillations, *Phys. Rev. Lett.* 14, 544.

Dulk, G., and D. J. McLean, 1978, Coronal Magnetic Fields, *Solar Phys.* 57, 279.

Dulk, G. A., and S. Suzuki, 1980, The Position and Polarization of Type III Solar Bursts, *Astron. Astrophys.* 88, 203.

Dysthe, K. B., E. Mjolhys, H. L. Pcseli, and L. Stenflo, Langmuir Solitons in Magnetized Plasmas, *Plasma Phys.* 20, 1087.

Dysthe, K. B., and H. L. Pcseli, 1978, Wave Modulation in Weakly Magnetized Plasmas, *Plasma Phys.* 20, 971.

Fitzenreiter, R. J., L. G. Evans, R. P. Lin, 1976, Quantitative Comparisons of Type III Radio Burst Intensity and Fast Electron Flux at 1 A.U., *Solar Phys.* 46, 437.

Fried, B. D., and S. D. Conti, 1961, The Plasma Dispersion Function (New York: Wiley).

Freund, H. P., and K. Papadopoulos, 1980, Oscillating Two-Stream and Parametric Decay Instability in a Weakly Magnetized Plasma, *Phys. Fluids* 23, 139.

Galeev, A. A., R. Z. Sagdeev, Y. S. Sigov, V. D. Shapiro, and V. I. Shevchenko, 1975, Nonlinear Theory for the Modulational Instability of Plasma Waves, *Fiz. Plazmy* 1, 10 (Sov. J. Plasma Phys. 1, 5).

Ginzburg, V., 1970, The Propagation of Electromagnetic Waves in Plasmas (Oxford: Pergamon Press).

Ginzburg, V., and V. V. Zheleznyakov, 1958, On the Possible Mechanisms of Sporadic Solar Radio Emission, *Sov. A. J.* 2, 653.

Goldman, M. V., and D. R. Nicholson, 1978, Virial Theorem of Direct Langmuir Collapse, *Phys. Rev. Lett.* 41, 406.

Goldman, M. V., G. F. Reiter, and D. R. Nicholson, 1980, Radiation from a Strongly Turbulent Plasma: Applications to Electron Beam-Excited Solar Emission, *Phys. Fluids* 23, 308.

Goldman, M. V., K. Rypdal, and B. Hafizi, 1980, Dimensionality and Dissipation in Langmuir Collapse, *Phys. Fluids* 23, 945.

Goldman, M. V. J. Weatherall, and D. R. Nicholson, 1980, Langmuir Collapse in a Weak Magnetic Field, submitted to *Physics of Fluids*.

Goldstein, M. L., R. A. Smith, and K. Papadopoulos, 1979, Nonlinear Stability of Solar Type III Radio Bursts: II. Application to Observations Near 1 A.U., *Ap. J.* 234, 683.

Grognard, R. J.-M., 1975, Quasilinear Dynamics of a Hot Maxwellian Electron Distribution Released from a Localized Region in a Homogeneous Plasma, *Aust. J. Phys.* 28, 731.

Gurnett, D. A., and R. R. Anderson, 1976, Electron Plasma Oscillations Associated with Type III Bursts, *Science* 194, 1159.

Gurnett, D. A., and R. A. Anderson, 1977, Plasma Wave Electric Fields in the Solar Wind: Initial Results from Helios 1, 2. *Geophys. Res.* 82, 632.

Hafizi, B., 1980, private communication.

Hammer, D. A., and N. Rostoker, 1970, Propagation of High Current Relativistic Electron Beams, *Phys. Fluids* 13, 1831.

Hardin, R., and F. Tappert, 1973, Applications of the Split Step Fourier Method to the Numerical Solution of Nonlinear and Variable Coefficient Wave Equations, *SIAM Rev.* 15, 423.

Hayvaerts, J., and C. V. deGenoullac, 1974, Effects of Turbulence Anisotropy on Propagation and Electromagnetic Radiation of Particle Streams in the Solar Corona, *Astr. Ap.* 30, 211.

Hubbard, R. F., and G. Joyce, 1976, Parametric Instabilities Generated by an Energetic Electron Beam, *Plasma Phys.* 18, 681.

Jackson, J., 1962, Classical Electrodynamics (New York: Wiley).

Kai, K., 1970, The Structure, Polarization and Spatial Relationship of Solar Radio Sources of Spectral Types I and III, *Solar Phys.* 11, 456.

Kaplan, S. A., and V. N. Tsytovich, 1968, Radio Emission from Beams of Fast Particles Under Cosmic Conditions, *Soviet Astr.-A.J.* 11, 956.

Kaufman, A. N., and L. Stenflo, 1975, *Phys. Scr.* 11, 269.

Kaw, P. K., 1976, Parametric Excitation of Electrostatic Waves in a Magnetized Plasma, in Advances in Plasma Physics, Vol. 6 (New York: Wiley).

Krall, W., and A. Trivelpiece, 1973, Principles of Plasma Physics (New York: McGraw-Hill).

Krasnosl'skikh, V. V., and V. I. Sotnikov, 1977, Plasma-Wave Collapse in a Magnetic Field, *Fiz. Plazmy* 3, 872 (Sov. J. Plasma Phys. 3, 491).

Kundu, M. R., 1965, Solar Radio Astronomy (New York: Interscience Publishers).

Lawson, J. D., 1977, The Physics of Charged Particle Beams (Oxford: Clarendon Press).

Leighton, R., 1964, Principles of Modern Physics (New York: McGraw-Hill).

Levine, L. S., I. M. Vitkovitsky, D. A. Hammer, M. L. Andrews, 1971, Propagation of an Intense Relativistic Electron Beam Through a Plasma Background, *J. Appl. Phys.* 42, 1863.

Lin, R., 1979, private communication.

Lin, R. P., L. G. Evans, and J. Fainberg, 1973, Simultaneous Observations of Fast Solar Electrons and Type III Radio Burst Emission Near 1 A.U., *Astrophys. Lett.* 14, 191.

Lipatov, A. S., 1977, Numerical Investigation of the Collapse of Langmuir Waves in a Magnetic Field, *Pis'ma Zh. Exp. Teor. Fiz.* 26, 516 (JETP Lett. 26, 377).

Magelssen, G. R., 1976, Nonrelativistic Electron Stream Propagation in the Solar Atmosphere and Solar Wind in Type III Bursts, Ph.D. Thesis, University of Colorado at Boulder.

Magelssen, G. R., and D. F. Smith, 1977, Nonrelativistic Electron Stream Propagation in the Solar Atmosphere and Type III Radio Bursts, *Solar Phys.* 55, 211.

Melrose, D. R., 1974, On the Propagation of the Electron Stream Generating Type III Bursts, *Solar Phys.* 38, 205.

Melrose, D. R., 1977, Plasma Astrophysics (in press).

Mikhailovskii, A. R., 1974, Theory of Plasma Instabilities, Vol. I (New York: Consultant's Bureau).

Montgomery, D., 1971, Theory of the Unmagnetized Plasmas (New York: Gordon and Breach).

Newkirk, G., 1967, Structure of the Solar Corona, *Ann. Rev. Astron. Ap.* 5, 213.

Nicholson, D. R., 1978, private communication.

Nicholson, D. R., and M. V. Goldman, 1978, Cascade and Collapse of Langmuir Waves in Two Dimensions, *Phys. Fluids* 21, 1766.

Nicholson, D. R., M. V. Goldman, P. Hoyng, and J. Weatherall, 1978, Nonlinear Langmuir Waves During Type III Solar Radio Bursts, *Ap. J.* 223, 605.

Nishikawa, K., 1968, Parametric Excitation of Coupled Waves, *J. Phys. Soc. Japan* 24, 916, 1152.

Nishikawa, K., Y. C. Lee, and C. S. Liu, 1976, Langmuir Wave Turbulence--Condensation and Collapse, *Comm. Plasma Phys.* 2, 63.

Nishikawa, K., and C. S. Liu, General Formalism of Parametric Excitation, in Advances in Plasma Physics, Vol. 6 (New York: Wiley).

Papadopoulos, K., and H. P. Freuni, 1978, Solitons and Second Harmonic Radiation in Type III Bursts, *Geophys. Res. Lett.* 5, 881.

Papadopoulos, K., M. L. Goldstein, and R. A. Smith, 1974, Stabilization of Electron Streams in Type III Solar Radio Bursts, *Ap. J.* 190, 175.

Pasachoff, J., 1977, Contemporary Astronomy (Philadelphia: W. B. Saunders Company).

Pereira, N., R. Sudan, and J. Denavit, 1977, Numerical Study of Two-Dimensional Generation and Collapse of Langmuir Solitons, *Phys. Fluids* 20, 936.

Petviashvili, V. I., 1975, Three-Dimensional Solitons of Extraordinary and Plasma Waves, *Fiz. Plazmy* 1, 28 (Sov. J. Plasma Phys. 1, 15).

Porkolab, M., and M. V. Goldman, 1976, Upper-Hybrid Solitons and Oscillating Two-Stream Instabilities, *Phys. Fluids* 19, 872.

Rowland, H. L., and K. Papadopoulos, 1977, Simulations of Nonlinearly Stabilized Beam Plasma Interactions, *Phys. Rev. Lett.* 39, 1276.

Ryutov, D. D., and R. Z. Sagdeev, 1970, Quasi-gasdynamical Description of a Hot Electron Cloud in a Cold Plasma, *Zh. Eksp. Teor. Fiz.* 48, 739 (Sov. Phys. JETP 31, 396).

Sanuki, H., and G. Schmidt, 1977, Parametric Instabilities in Magnetized Plasmas, *J. Phys. Soc. Japan* 42, 664.

Schmidt, G., 1975, Stability of Envelope Solitons, *Phys. Rev. Lett.* 34, 724, 1975.

Scott, A. C., F. Chu, and D. McLoughlin, 1973, The Soliton: A New Concept in Applied Science, *Proc. IEEE* 61, 1443.

Smith, D. F., 1974, Type III Radio Bursts and Their Interpretation, *Space Sci. Rev.* 16, 91.

Smith, D. F., 1970, Type III Solar Radio Bursts, *Adv. Astron. Astrophys.* 1, 147.

Smith, D. F., 1977, Second Harmonic Radiation and Related Nonlinear Phenomena in Type III Solar Radio Bursts, *Astrophys. J.* 216, L53.

Smith, D. F., and P. C. W. Fung, 1971, A Weak Turbulence Analysis of the Two-Stream Instability, *J. Plasma Phys.* 5, 1.

Smith, D. F., and D. R. Nicholson, 1979, in Wave Instabilities in Space Plasmas (Dordrecht: D. Reidel Publishing Company), p. 225.

Smith, R. A., M. L. Goldstein, and K. Papadopoulos, 1979, Nonlinear Stability of Solar Type III Radio Bursts: I. Theory, *Ap. J.* 234, 348.

Stix, T., 1962, The Theory of Plasma Waves (New York: McGraw-Hill).

Sturrock, P. A., 1964, in AAS-NASA Symposium on the Physics of Solar Flares, ed. W. N. Hess (NASA SP-50), p. 357.

Sturrock, P. A., 1965, Scattering of Electrostatic Waves by Inhomogeneities in a Plasma, Phys. Fluids 8, 281.

Takakura, T., 1977, Dynamics of a Cloud of Fast Electrons Travelling Through the Plasma, Solar Phys. 52, 429.

Takakura, T., and H. Shibahashi, 1976, Dynamics of a Cloud of Fast Electrons Travelling through the Plasma, Solar Phys. 46, 323.

Thomson, J. J., and J. I. Karush, 1974, Effects of Finite-Bandwidth Drivers on the Parametric Instability, Phys. Fluids 17, 1608.

Tsytovich, V. N., 1970, Nonlinear Effects in a Plasma (New York: Plenum Press).

Valeo, E., and C. Oberman, 1973, Model of Parametric Excitation by an Imperfect Pump, Phys. Rev. Lett. 30, 1035.

Weatherall, J., M. V. Goldman, and D. R. Nicholson, 1978, Bull. Am. Phys. Soc. 23, 787.

Weatherall, J., D. R. Nicholson, M. V. Goldman, 1979, Parametric Instabilities in Weakly Magnetized Plasma, Astrophys. J., in press.

Wild, J. P., S. F. Smerd, and A. A. Weiss, 1963, Radio Bursts from the Solar Corona, Ann. Rev. Astron. Ap. 10, 159.

Wild, J. P., and S. F. Smerd, 1972, Radio Bursts from the Solar Corona, Ann. Rev. Astron. Ap. 10, 159.

Yajima, N., 1974, Stability of Envelope Solitons, Prog. Theor. Phys. 52, 1066.

Zaitsev, V. V., M. V. Kunilov, N. A. Mityakov, and V. O. Rapoport, 1974, Generation of Type III Radio Bursts by Electron Fluxes Having Large Injection Times, Soviet Astr. 18, 147.

Zaitsev, V. V., N. A. Mityakov, and V. O. Rapoport, 1972, A Dynamic Theory of Type III Solar Radio Bursts, Solar Physics 24, 444.

Zakharov, V. E., 1972, Collapse of Langmuir Waves, *Zh. Exp. Teor. Fiz.* 62, 1745 (Sov. Phys. *JETP* 35, 908).

Zakharov, V. E., 1975, Plasma Collapse in a Magnetic Field, *Zh. Exp. Teor. Fiz.* 62, 1745 (Sov. J. *Plasma Phys.* 3, 491).

Zakharov, V. E., A. F. Mastryukov, and V. S. Synakh, 1974, Two-Dimensional Collapse of Langmuir Waves, *Zh. Exp. Teor. Fiz. Pis'ma*, 20, 7 (JETP Lett. 20, 3).

Zakharov, V. E., and A. M. Rubenchik, 1973, Instability of Wave-guides and Solitons in Nonlinear Media, *Zh. Eksp. Teor. Fiz.* 65, 997 (Sov. Phys. *JETP* 38, 494).

Zheleznyakov, V. V., and V. V. Zaitsev, 1970, Contribution to the Theory of Type III Solar Radio Bursts, *Soviet Astr.-A.J.* 14, 47.

## APPENDIX F

F. "Breakup and Reconstitution of Langmuir Wavepackets"  
T. Tajima, M. V. Goldman, J. N. Leboeuf, and J. M. Dawson  
Physics of Fluids, January 1981, in press

## Breakup and reconstitution of Langmuir wavepackets

T. Tajima, M. V. Goldman,<sup>a)</sup> J. N. Leboeuf, and J. M. Dawson

Physics Department, University of California,  
Los Angeles, California 90024

(Received 23 January 1980)

#### Abstract

Recursive behavior has been observed in a two-dimensional electrostatic particle simulation of a coherent intense Langmuir wavepacket. The recursion may be associated with the fact that the plasma frequency has a spatial variation in the density depression created by the ponderomotive force.

a) Permanent address: Department of Astro-Geophysics, University of Colorado, Boulder, Colorado 80309.

The behavior of intense Langmuir waves involves many possible processes; solitons,<sup>1</sup> wavepacket collapse,<sup>2</sup> cascading,<sup>3</sup> stimulated scattering, nonlinear Landau damping, explosive instabilities,<sup>4</sup> and modulational instabilities,<sup>5</sup> are only a few. Competition between some of these effects is only just beginning to be studied. Effects seen in a two-dimensional electrostatic particle simulation including ion and electron dynamics are reported here: an initial wavepacket undergoes virtually complete reconstitution following its initial break-up.

Use is made of a standard finite-sized particle code. The initial condition consists of a Langmuir wavepacket which has a Gaussian intensity profile in wavenumber space with average wavenumber  $k_o = k_o \hat{x}$  and half-width  $\Delta k_x = \Delta k_y < k_o$ . The Langmuir waves are turned on in an initially uniform unmagnetized plasma over the time interval  $t = 0$  to  $t = \omega_p^{-1}$ . The waves have approximately constant energy after the initial transients subside. Typical parameters in our study are: number of electrons (ions)  $N_e (N_i) = 32768$ , number of grids in the  $x$  ( $y$ ) direction  $L_x = 128$  ( $L_y = 32$ ) in this doubly periodic system, electron (ion) Debye length  $\lambda_{De} (\lambda_{Di}) = 1\Delta$ ,  $k_o = 12\pi / 128\Delta$  (in the  $x$  direction),  $\Delta k_x = \Delta k_y = 2\pi / 32\Delta$ , the mass ratio  $M/m = 5$ , and particle size  $a_x = a_y = \Delta$ , where  $\Delta$  is the grid spacing in both the  $x$  and  $y$  directions. In such a system, the electron collision frequency is  $5 \times 10^{-4} \omega_p$  and the electron Landau damping decrement for the  $k_o$  mode is  $3 \times 10^{-2} \omega_p$ . The plasma is therefore fairly dissipationless over the period of  $10 \omega_p^{-1}$ .

Figure 1 shows three snapshots of equi-energy contours of the electrostatic wave energy density for a case with the initial wave amplitude for the  $k = k_o$  mode of  $\tilde{E}_{k_o} = eE_{k_o} / m\omega_p^2 \Delta = 0.6$  and the average wave energy  $W = \langle E_e^2 \rangle / 2\pi n T_e \approx 0.5$  over the period of  $t = (5,100)\omega_p^{-1}$ . Here, the angular brackets denote

spatial averaging. The peak of the wavepacket is located at  $x = 64\Delta$  at  $t = 0$ . It travels in the positive  $x$  direction with the group velocity  $v_g \approx 0.6 \Delta\omega_p$  until  $t = 10 \omega_p^{-1}$ . Linear theory predicts  $v_g \approx 0.7 \Delta\omega_p$ . Figure 1(b) illustrates a slightly later stage,  $t = 20 \omega_p^{-1}$ . The coherent wavepacket has broken into many seemingly random subpackets all over the space. The break-up occurs not only in the  $x$  direction, but also in the  $y$  direction. The behavior of the wave intensity in wave vector space (not shown here) indicates that the peak of the wave energy has shifted from  $k = k_0$  to roughly  $k = \frac{1}{2}k_0$  at  $t = 20 \omega_p^{-1}$ . The assemblage of subpackets continues to change its structure until  $t \sim 50 \omega_p^{-1}$ , when a somewhat more organized structure begins to emerge. Figure 1(c) at  $t = 70 \omega_p^{-1}$  shows that the process of reconstitution of the subpacket has been completed and the wavepacket profile is close to the one at  $t = 0$ , although at a somewhat shifted position. Also in  $k$  space we see that the energy has oscillated back to around  $k = k_0$  in the  $k$  space. When we made  $L_x = 256$ , the packet first propagated forward, then backward, and became many subpackets; it eventually came back to the original shape at the same place in about the same time. The size of the plasma does not appear to be a factor in the results. The density depression associated with the packet became shallower and wider as time elapsed. Although Fermi, et al.<sup>6</sup> found nonlinear recursion in a computer simulation of the vibrations of a nonlinear string some two decades ago, there are few works in fluid or plasma physics dealing with the recursive process until the recent work of Yuen et al.<sup>7</sup> who solved a model nonlinear Schrödinger equation in one dimension numerically.

To determine the physical process responsible for the wavepacket recursion, we have made runs with several different wavepacket energy densities. Figure 2 shows the recursion time vs the average wavepacket energy density. All the cases shown in Fig. 2 produced recursion. All parameters except for the

packet energy density are fixed at the same values as for the case  $W = 0.5$ . With  $W$  ranging from 0.25 to 0.75, the recursion time,  $\tau_r$ , was found to be approximately inversely proportional to the wave energy density,  $W$ , as shown in Fig. 2. There were only minor differences in the wavepacket evolution during the various recursions.

The observed behavior of  $\tau_r$  as a function of  $W$  is consistent with theoretical observations made by Kaw et al.<sup>8</sup> who studied the effect of fixed, spatially periodic ion density fluctuations on Langmuir wave evolutions. The break-up and recursion of an original Langmuir plane wave is due to the density dependence of the plasma frequency, which causes the oscillations in different spatial regions of the plasma to go in and out of phase with each other. In Fourier space the wave vectors  $\mathbf{k}_i$  of the ion density fluctuation mix in with  $\mathbf{k}_o$ , producing sidebands at  $\mathbf{k}_o \pm \mathbf{k}_i$ . The original mode at  $\mathbf{k}_o$  gets smaller in amplitude at first, but then returns at the time when the Bessel function,  $J_o$ , has its next extremum. This gives an approximate recursion time of

$$\tau_r = \frac{7.7 \omega_p^{-1}}{|\delta n_{\max}/n_o|} \quad , \quad (1)$$

where  $\delta n_{\max}$  is the maximum of the density ripple.

In our problem the density perturbation is self-consistently generated by the ponderomotive force of the Langmuir wavepacket. If the ions are roughly adiabatic, then balancing the plasma pressure against the ponderomotive force gives the relation between the density perturbation and the Langmuir field:  $\delta n_{\max}/n_o \approx -W/4$ . This predicts a scaling

$$\tau_r = 31/W \quad , \quad (2)$$

which shows good agreement with the results of simulation, as given in Fig. 2.

[Also, the numerically obtained  $\delta n_{\max}$  measurements were in good agreement with Eq. (1).]

The argument in Ref. 8 predicts a temporally periodic migration to both higher and lower wavenumbers in the Fourier-space evolution of the packet. We do not observe the generation of higher Fourier modes. Their absence is probably due to Landau damping, so we see only oscillation in the direction of lower wavenumbers and back.

Note. Since the submission of this manuscript we have found some recent theoretical results which appear relevant to our numerical studies. A. Thyagaraja<sup>9</sup> has shown that recurrence can be expected in one-dimensional wave phenomena describable by a cubic Schrödinger equation, and has pointed out (private communication, 1980) that, in two dimensions, such systems will either collapse or recur. The wavepackets we have studied should be roughly adiabatic, and therefore be describable by a simple cubic Schrödinger equation<sup>2</sup> to the extent that damping is negligible.

This work was supported by National Science Foundation Grants PHY79-01319 at the University of California and ATM76-14275 at the University of Colorado, and by Air Force Office of Scientific Research Contract No. F49620-76-C-0005. Two of us (T.T. and M.V.G.) appreciate the hospitality of the Aspen Center for Physics where a part of this work was done. One of us (M.V.G.) would like to thank the Guggenheim Foundation for a fellowship held during part of this research.

References

1. V. E. Zakharov, *Zh. Eksp. Teor. Fiz.* 62, 1745 (1972) [*Sov. Phys.-JETP* 35, 908 (1972)].
2. M. V. Goldman and D. R. Nicholson, *Phys. Rev. Lett.* 41, 406 (1978).
3. D. R. Nicholson and M. V. Goldman, *Phys. Fluids* 21, 1766 (1978).
4. M. Jones and J. Fukai, *Phys. Fluids* 22, 132 (1979).
5. A. A. Vedenov and L. I. Rudakov, *Dokl. Akad. Nauk SSSR* 159, 767 (1964) [*Sov. Phys.-Dokl.* 9, 1073 (1965)].
6. E. Fermi, J. Pasta, and S. Ulam, Collected Papers of Enrico Fermi (University of Chicago Press, Chicago, 1965), Vol. II, p. 977.
7. H. C. Yuen and W. E. Furguson, *Phys. Fluids* 21, 1275 (1978).
8. P. Kaw, A. T. Lin, and J. M. Dawson, *Phys. Fluids* 16, 1967 (1973).
9. A. Thyagaraja, *Phys. Fluids* 22, 2093 (1979).

Figure Captions

Fig. 1 Time sequence of contours of electric field energy density  $E^2/4\pi$  in x-y space. (a) at  $t = 10 \omega_p^{-1}$ , (b) at  $t = 20 \omega_p^{-1}$ , and (c) at  $t = 70 \omega_p^{-1}$ . Real lines represent high energy contours and dotted ones low contours.

Fig. 2 Inverse of the wavepacket recursion time vs the normalized wave energy density  $W$ , obtained by simulations.

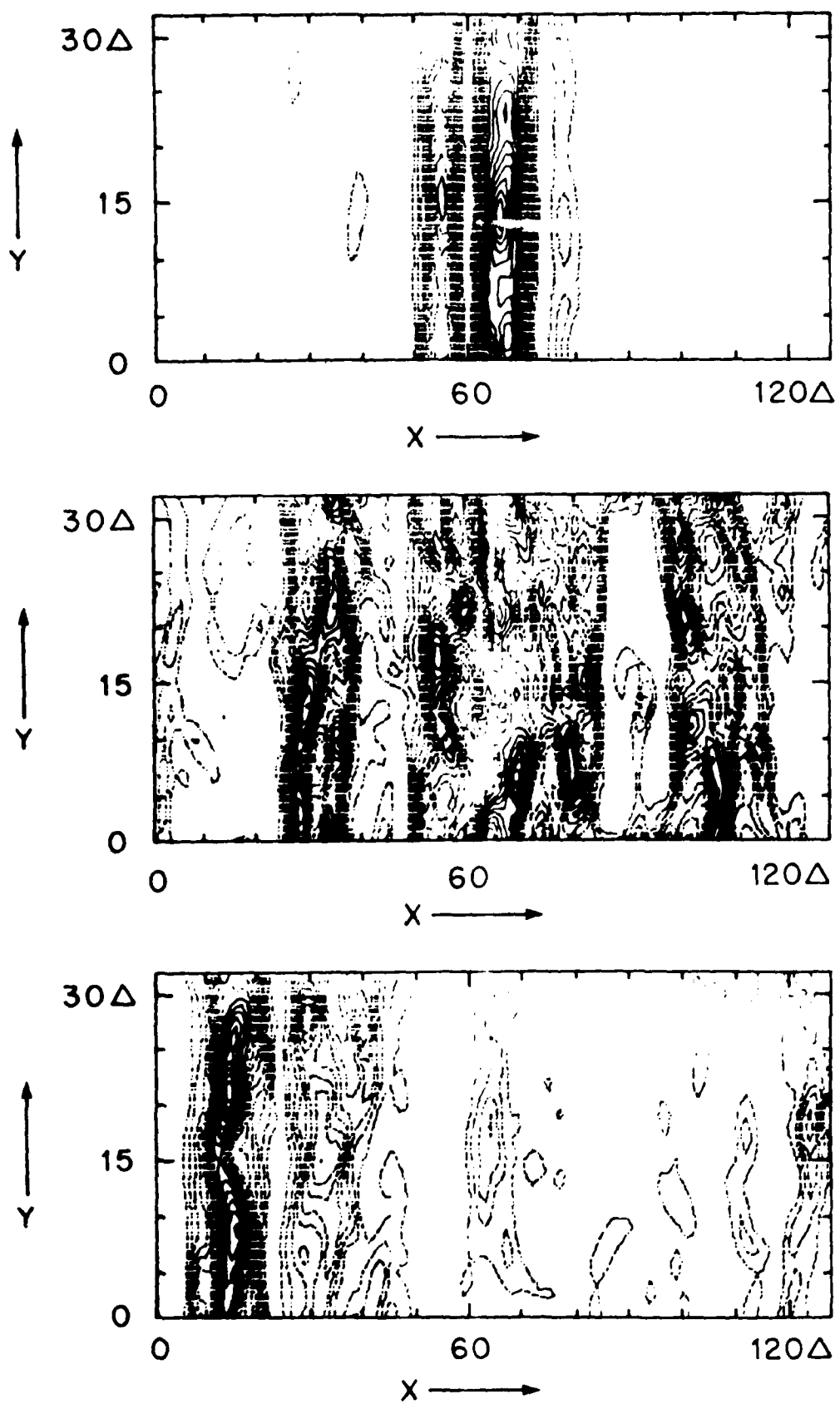


FIGURE 1

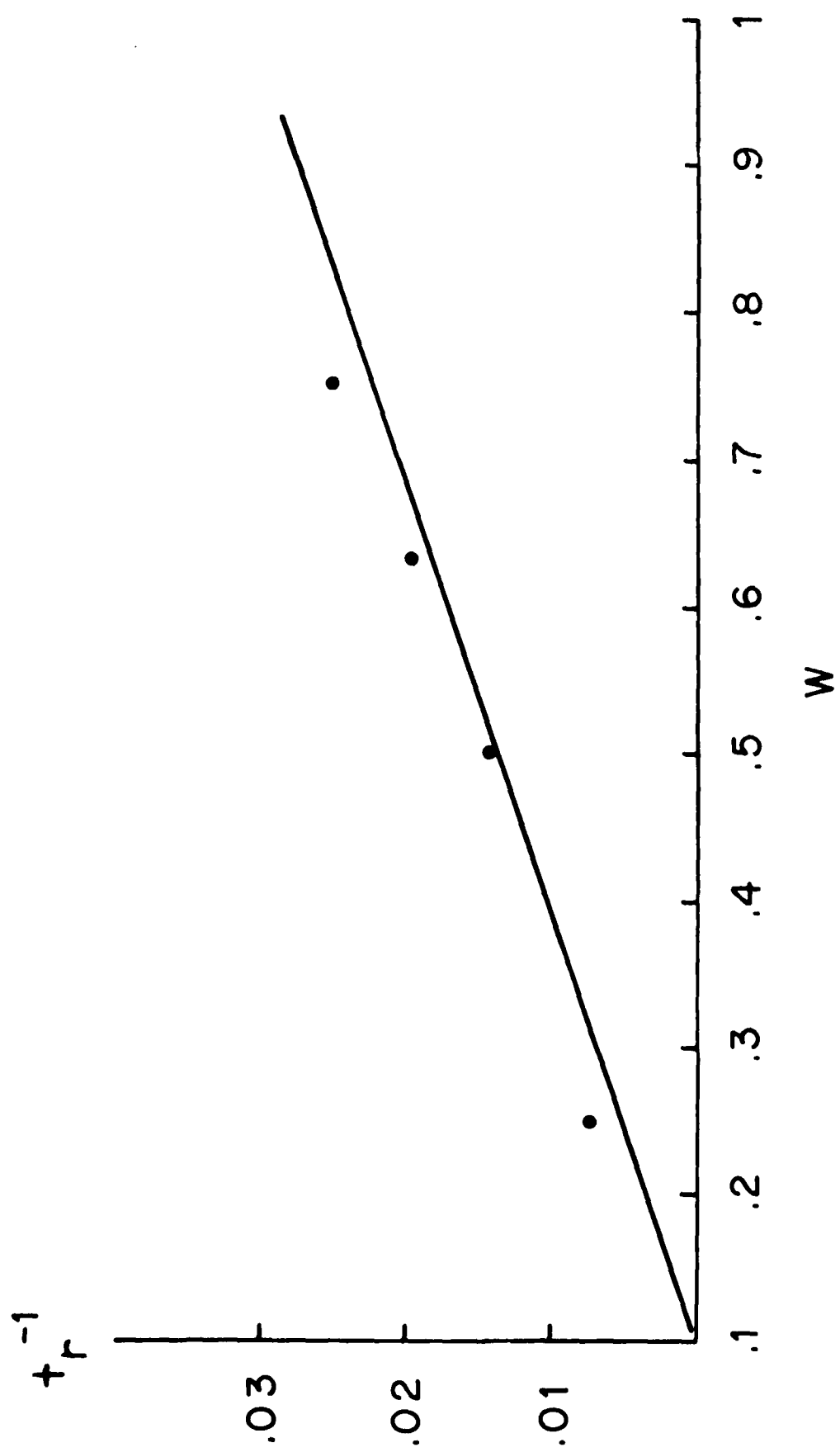


FIGURE 2

## APPENDIX G

G. "Self-Focusing of Radio Waves in an Underdense Ionosphere"  
F. W. Perkins and M. V. Goldman  
Astrophysical Journal, in press

Submitted to JGR  
April 1980

1

CU #1038

## Self-Focusing of Radio Waves in an Underdense Ionosphere

F. W. Perkins

Plasma Physics Laboratory, Princeton University, P.O. Box 451,  
Princeton, New Jersey 08544

and

M. V. Goldman

Department of Astro-Geophysics, Campus Box 391, University of Colorado,  
Boulder, Colorado 80309

### ABSTRACT

The theory of self-focusing instabilities in the ionosphere is developed emphasizing the critical parameters required to obtain sufficiently fast temporal and spatial growth rates so that the instability may be observed. It is shown that self-focusing will not occur unless  $2cf/\pi f_p^2 l < 1$ , where  $f$  is the radio wave frequency,  $f_p$  a typical ionospheric plasma frequency, and  $l$  the spatial growth length. (In the F-region,  $l \approx 25$  km is used, while in the E-region  $l \approx 1$  km.) In the F-region, the threshold power flux  $P_c$  is  $P_{c,F} \approx (1.5 \mu\text{watts}/\text{m}^2)(f/15 \text{ MHz})^3 (T_e/1000^\circ\text{K})^4 \times (10^6 \text{ cm}^{-3}/n_e)^3 C_F$ , where  $n_e$  and  $T_e$  are typical electron densities and temperatures, and  $C_F \approx 1$  depends on spatial and temporal

growth rates. In the E-region, the result is

$P_{c,E} \approx (1 \text{ milliwatt/m}^2)(f/15 \text{ MHz})^3 (10^5 \text{ cm}^{-3}/n_e) C_E$ , where  $C_E \approx 1$  again depends on growth rates. Dimensional analysis indicates nonlinear saturation will set in when variations of order unity occur in the radio wave intensity. The corresponding relative electron density fluctuations are given by  $\delta n/n \sim \pi c f / f_p^2 l$ . Applications to planned ionospheric heating experiments and ionospheric modification by the microwave beam from a satellite power station are discussed.

## 1. INTRODUCTION

Self-focusing of radio waves in the F-region of the ionosphere has occurred in many overdense ionospheric modification experiments [Thome and Perkins, 1974; Duncan and Behnke, 1978] and its principles are well understood in terms of theory [Vas'kov and Gurevich, 1976; Cragin and Fejer, 1974; Gurevich, 1978; Perkins and Valeo, 1974]. These theories all indicate that self-focusing should occur in underdense ionospheric conditions as well, and recent observations [Novozhilov and Savel'yev, 1978] are qualitatively in accord with this prediction. The improved ionospheric heating facilities now nearing completion at Arecibo and Tromsø will permit scientific investigation of underdense self-focusing both in the E- and F-regions. Furthermore, there is current interest in what effect the 2.4 GHz microwave beam from a proposed Satellite Power Station (SPS) [Brown, 1973; Glaser, 1977; Vanke et al., 1978] would have on the ionosphere. It will be shown that self-focusing of the SPS microwave beam may well occur, but not under all ionospheric conditions.

It is important to state clearly what the word underdense means. We take it to mean that the radiowave frequency  $f$  exceeds the maximum ionospheric plasma frequency  $f_{p,\max}$  so that resonant interactions, such as parametric decay instabilities [Fejer and Kuo, 1973; Das and Fejer, 1980; Perkins et al., 1974; DuBois and Goldman, 1972; Vas'kov and Gurevich, 1977], which require the frequency matching condition  $f = f_p$  to be satisfied somewhere in the ionosphere, cannot occur. With this definition, a radiowave

with frequency up to several times the maximum ionospheric plasma frequency can be reflected obliquely from the ionosphere and still be considered as underdense, as indeed was the case for the diagnostic wave in the Novozhilov and Savel'yev [1978] experiment. We will consider only cases with  $f > f_{p,\max}$  so that just the self-focusing instability operates and parametric decay processes are not allowed.

The book by Gurevich [1978] provides an excellent summary of the physics governing the F-region self-focusing instability. In particular, the instability exhibits exponential growth both in time and in space, along the direction of the radiowave beam. The goal of this work is to use this understanding to calculate the threshold radiowave power flux  $P_c$  required to induce the self-focusing instability in cases of practical interest. The key considerations beyond the basic physical principles derive from the finite extent of the ionosphere (which means that the spatial amplification must be sufficiently rapid) and the finite width of the radiowave beam. In particular, the temporal growth time must be a small fraction of the time it takes the ambient  $\bar{E} \times \bar{B}$  drift to convect the ionospheric plasma through the beam. These two conditions set the practical threshold power flux. In contrast, according to Equation (6.31) of Guervich [1978], there is no threshold power flux for the self-focusing instability!

There are some interesting new physics points as well. First, we shall show that there is an upper limit to the radiowave frequency above which self-focusing will not occur for a medium of finite extent. Secondly, in the E-region, the ion-neutral

collision frequency  $\nu_{in}$  exceeds the ion gyrofrequency  $\Omega_i$ ,  $\nu_{in} \gg \Omega_i$ , which means the ion motion across the magnetic field line is allowed. As a consequence, ion motion can be sufficiently rapid so that recombination does not suppress the self-focusing instability as predicted by Gurevich.

The question of whether the SPS microwave beam will introduce structure into the ionosphere via the self-focusing instability is best addressed by a combination of theory and experiment. As is the case with Ohmic heating [Perkins and Roble, 1978], experiments done at a frequency of 15 MHz using the improved Arecibo heating facility will both simulate the geometry of the SPS beam-ionosphere and be clearly in the underdense regime. Results of these experiments can be utilized to validate and refine the theory developed below, before it is extrapolated to the SPS parameters. But this extrapolation involves very large factors--160 in frequency,  $4 \times 10^6$  in threshold power flux--and should be taken as indicative rather than quantitative.

Section 2 of this paper sets forth the model. Section 3 derives the expressions for the critical power flux in the F- and E-regions. Section 4 applies these formulas to planned ionospheric heating experiments and to the SPS microwave beam. The paper concludes with a discussion and summary. Certain aspects of the eigenvalue problem associated with the finite beam width are discussed in the Appendix.

## 2. MODEL AND EQUATIONS

The basis for our model is the recognition that the transverse dimensions of ionospheric modification are small

AD-A096 560

COLORADO UNIV AT BOULDER DEPT OF ASTRO-GEOPHYSICS  
PLASMA WAVE TURBULENCE AND PARTICLE HEATING CAUSED BY ELECTRON --ETC(U)  
JAN 81 M V GOLDMAN AFOSR-80-0022

F/6 4/1

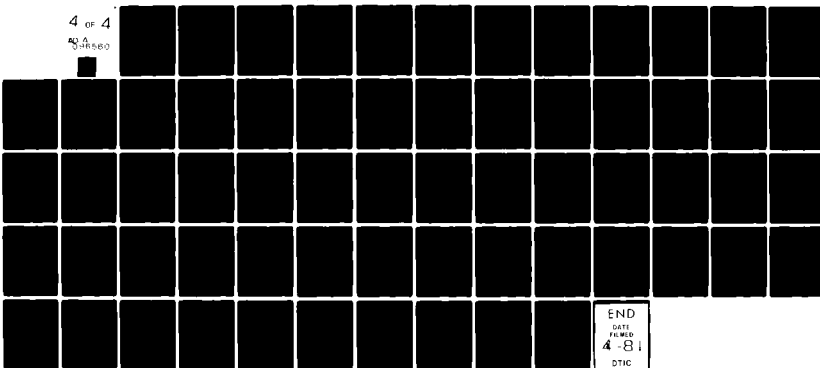
UNCLASSIFIED

CU-1533143

AFOSR-TR-81-0148

NL

4 OF 4  
AFOSR-80-0022



END  
4 8 i  
DTIC

substantially smaller than the characteristic lengths associated with the ionospheric plasma. We shall therefore adopt the model of a plasma with spatially uniform properties but containing a radiowave beam of finite transverse dimensions,  $2a$ , propagating in the  $\underline{z}$ -direction. The plasma contains a uniform magnetic field  $B$  in the  $\underline{b}$ -direction which we take to lie in the  $\underline{x}$ - $\underline{z}$  plane. The principle spatial variation of the striations associated with the self-focusing instability can then be shown to be in the  $\underline{z} \times \underline{b}$  direction (i.e., the  $\hat{\underline{y}}$ -direction). Figure 1 portrays the geometry.

The actual orientation of the  $\underline{z}$ -direction in space depends on the application: For most ionospheric modification experiments  $\underline{z}$  is vertically upward; for SPS beams,  $\underline{z}$  is inclined downward, for powerful HF transmissions,  $\underline{z}$  is almost horizontal [Novozhilov and Savel'yev, 1978].

The previous work [Perkins and Valeo, 1974; Gurevich, 1978] has shown that self-focusing striations do not propagate relative to the plasma. But the ambient  $\underline{E} \times \underline{B}$  drifts will convect the plasma through the radiowave beam which is stationary. Typical convection velocities  $v_D$  range from  $20-60 \text{ m sec}^{-1}$  [Blanc and Amayenc, 1979], yielding interaction times  $T$  given by

$$T \approx \frac{2a}{v_D} = (300 \text{ sec}) \left( \frac{a}{5 \text{ km}} \right) \left( \frac{30 \text{ m sec}^{-1}}{v_D} \right). \quad (1)$$

In order for an instability to fully develop, we require that the growth rate  $\gamma$  satisfy

$$\gamma T \gtrsim 10. \quad (2)$$

In practical units, (1) and (2) combine to give

$$\gamma > \left( \frac{1}{30 \text{ sec}} \right) \left( \frac{5 \text{ km}}{a} \right) \left( \frac{v_D}{30 \text{ m/sec}} \right) . \quad (3)$$

Our model takes into account the finite size of the microwave beam by requiring that the growth rate be sufficiently fast.

Apart from this, it is a good approximation to assume that the initial microwave beam intensity is independent of the  $y$ -coordinate, so that in a linear stability analysis one can employ plane wave structures in the  $y$ -direction. Quantitatively, this approximation requires that the beam intensity change by a negligible amount over the scale size of a striation. One can easily check a posteriori that this approximation is well satisfied.

In the F-region, a plane wave approximation is not appropriate in the  $x$ -direction because electron thermal conduction and plasma ambipolar diffusion along the magnetic field play an important role in determining the threshold power flux. Following the previous work, we shall assume that the perturbations grow exponentially along the center of the beam as  $e^{z/\ell}$ . Hence, the self-focusing instability is a spatial amplifier, requiring seed perturbations to get it started. The growth length  $\ell$  must be sufficiently short so that the total spatial amplification  $e^A$  is large ( $A \approx 7$ ). For the F-region, we shall adopt a nominal value of  $\ell = 25 \text{ km}$  while for the E-region  $\ell = 1 \text{ km}$ . It is important to keep in mind that  $\ell$  represents the exponentiation distance along the radiowave beam. Beams propagating obliquely through the ionosphere clearly have a longer path length available for amplification than do vertically incident beams.

The calculations below constitute linear stability analysis which yields a generalized dispersion relation, i.e., a function which relates the temporal growth and the spatial amplification lengths to the power flux in the beam and the wavenumber in the y-direction. This dispersion relation will form the basis of our application discussions.

Our model incorporates the following physics: (1) Radio-wave propagation is adequately described by an isotropic, parabolic approximation to the wave equation [Fock, 1965]. An isotropic index of refraction is a valid assumption because the radiowave frequency is large compared to the electron gyrofrequency  $\omega \gg \Omega_e$ . (2) The calculations are done in a frame in which the ambient electron drifts vanish. (3) Ion motion is controlled by ambipolar diffusion through the neutral gas. In the E-region, the ions have an ambient drift relative to the electrons in the range  $20-100 \text{ m s}^{-1}$  [Harper et al., 1976]. (4) Electron motion and thermal conductivity is along the magnetic field and controlled by diffusion through ions and neutrals. The E $\times$ B velocity does not generate density fluctuations because it represents incompressible motion. (5) Recombination takes place in the E-region. (It will be shown to be of moderate importance.) (6) No ion temperature perturbations occur because of their good thermal contact with neutrals. (7) Ohmic heating by the beam provides a heat source in the electron equation. Electrons lose energy by exchange with ions (in the F-region) or with neutral molecules (in the E-region).

Let us first turn to the equation governing radiowave propagation in a medium with weak density fluctuations. Since we can safely assume that the ionosphere is an isotropic medium, the equation governing linearized wave propagation is

$$\left( \nabla^2 + \frac{\omega_0^2 - \omega_p^2(\underline{x})}{c^2} \right) \underline{E} = 0 \quad (4)$$

which is solved by

$$\begin{aligned} \underline{E}(\underline{x}, t) = & \left[ \underline{E}_0 + \underline{E}_1(\underline{x}, z) e^{\gamma t} \cos(ky - \omega t) \right] e^{i(k_0 z - \omega_0 t)} \\ & + \left[ \underline{E}_0^* + \underline{E}_1^*(\underline{x}, z) e^{\gamma t} \cos(ky - \omega t) \right] e^{-i(k_0 z - \omega_0 t)}, \end{aligned} \quad (5)$$

The justification for steady state in Eq. (4) is the condition  $\gamma \ell \omega_0 / c^2 k_0 \ll 1$ , where  $\ell$  is the scale length,  $|\underline{E}_1 / \partial_z \underline{E}_1|$ . The plasma frequency  $\omega_p^2(\underline{x})$  is given by

$$\omega_p^2(\underline{x}) = \omega_p^2(1 + \delta n / n_0) \quad (6)$$

in terms of the relative density fluctuations

$$\delta n / n_0 = \Delta(\underline{x}, z) e^{\gamma t} \cos(ky - \omega t). \quad (7)$$

Our notation is straightforward:  $k$  is the wavenumber of the plasma density striation in the  $y$ -direction,  $\omega$  and  $\gamma$  denote the frequency and growth rate of these striations,  $\omega_0$  and  $k_0 = (\omega_0^2 - \omega_p^2)^{1/2} c^{-1}$  the frequency and wavenumber of the intense radiowave in the absence of striations. The Poynting flux  $P_0$  of this wave is

$$P_0 = \frac{E_0^2 c}{2\pi} \left( \frac{c k_0}{\omega_0} \right) ,$$

where the last factor is effectively unity because the plasma is underdense:  $\omega^2 \gg \omega_p^2$ . Let us substitute (5) into (4), retain only terms linear in  $\delta n$  and  $\underline{E}_1$ , and make the assumption

$$k_o \frac{\partial}{\partial z} \gg \frac{\partial^2}{\partial z^2}$$

which leads to the linearized parabolic wave equations

$$\begin{aligned} 2ik_o \frac{\partial}{\partial z} E_1 + \left( \frac{\partial^2}{\partial x^2} - k^2 \right) E_1 - \frac{\omega_p^2}{c^2} \Delta E_o &= 0, \\ -2ik_o \frac{\partial}{\partial z} E_1^* + \left( \frac{\partial^2}{\partial x^2} - k^2 \right) E_1^* - \frac{\omega_p^2}{c^2} \Delta E_o &= 0. \end{aligned} \quad (8)$$

The overall lensing effect associated with  $\Delta E_1$  have been ignored. Since the first order field,  $\underline{E}_1$  propagates almost parallel to  $\underline{E}_o$  (i.e.,  $k \ll k_o$ ), we have taken their polarizations to be parallel and used scalar fields  $E_1$  and  $E_o$  in Eq. (8). A further simplification results by noting that the plasma density striations will vary much more rapidly in the  $y$ -direction than the  $x$ -direction, so that the  $x$ -derivatives can be ignored in (8). This simplification is based on the recognition that variations in the  $x$ -direction imply variations along the magnetic field (see Fig. 1). The high electron thermal conductivity combined with rapid  $x$ -variations suppresses instabilities. Hence, equations (8) become

$$\begin{aligned} 2ik_o \frac{\partial}{\partial z} E_1 - k^2 E_1 &= \frac{\omega_p^2}{c^2} \Delta E_o, \\ -2ik_o \frac{\partial}{\partial z} E_1^* - k^2 E_1^* &= \frac{\omega_p^2}{c^2} \Delta E_o. \end{aligned} \quad (9)$$

The self-focusing instability is driven by spatially dependent ohmic heating  $Q$  which enters through the steady-state electron

heat equation

$$0 = \frac{\partial}{\partial \xi} K \frac{\partial}{\partial \xi} T_e + Q - v_R n (T_e - T_o) , \quad (10)$$

where

$$Q = \frac{\omega_p^2 v}{\omega_o^2 2\pi} [E_o^2 + E_o (E_1 + E_1^*) + \dots] . \quad (11)$$

and  $\xi$  is a coordinate parallel to the magnetic field (see Fig. 1a). Here,  $v_R$  denotes the electron energy relaxation frequency,  $v$  the electron momentum collision frequency, and  $K$  the electron thermal conductivity. One can easily check a posteriori that the temporal growth rate for self-focusing instabilities is small compared to the faster of two rates: (1) the rate of electron heat diffusion across the radio beam (F-region) or (2) the electron thermal relaxation frequency  $v_R$  (E-region). Hence the steady-state heat equation is appropriate.

The electron heat equation is best discussed separately for the E- and F-regions. Let us first consider the F-region where electron-ion collisions dominate the physics. The appropriate collision frequencies and thermal conductivity are [Braginskii, 1965]

$$K = \frac{3.16 T_e n}{v m} , \quad v_R = 3 \left( \frac{m}{M} \right) v ,$$

$$v = \frac{4\sqrt{2\pi}}{3} \frac{n e^4}{m^{1/2} T_e^{3/2}} \ln \Lambda , \quad (12)$$

where  $m$  and  $M$  denote the electron and ion (taken to be  $O^+$ ) mass, respectively. Both a zero-order and a first order solution to

(10) and (11) are required. Let us write this as

$$T_e = \delta T_e^{(0)} + \delta T_e^{(1)} + T_o$$

where  $T_o$  is the ambient temperature,  $\delta T_e^{(0)}$  is the heating correction produced by  $E_o^2$  and  $\delta T_e^{(1)}$  is due to  $E_o E_1$ . We assume that departures from the ambient electron temperature  $T_o$  are small:

$$\delta T_e^{(0)} \ll T_o, \quad \delta T_e^{(1)} \ll \delta T_e^{(0)}.$$

The electron heat conductivity equation can then be written as

$$0 = \frac{2}{7} C_1 \frac{\partial^2}{\partial \xi^2} \theta + \frac{C_2 (n/n_o)^2}{\theta^{3/7}} [E_o^2 + E_o (E_1 + E_1^*)] - C_3 \frac{(n/n_o)^2}{\theta^{3/7}} (\theta^{2/7} - 1), \quad (13)$$

where

$$\theta = \left( \frac{T_e}{T_o} \right)^{7/2}, \quad (14)$$

and

$$C_1 = \frac{3.16 T_o^2 n_o}{m v_o},$$

$$C_2 = \omega_{po}^2 v_o / 2\pi \omega_o^2,$$

$$C_3 = 3 T_o n_o v_o (m/M). \quad (15)$$

Let us expand  $\theta$  as

$$\theta = 1 + \delta \theta^{(0)} + \delta \theta^{(1)}, \quad (16)$$

where  $\delta\theta^{(0)}$  satisfies the linearized equilibrium equation with constant density

$$0 = \frac{2}{7} C_1 \frac{\partial^2}{\partial \xi^2} \delta\theta^{(0)} + C_2 E_0^2 - C_3 \frac{2}{7} \delta\theta^{(0)} . \quad (17)$$

The equation governing the linearized response to the self-focusing ohmic heating term is

$$0 = \frac{2}{7} C_1 \frac{\partial^2}{\partial \xi^2} \delta\theta^{(1)} + C_2 E_0^2 \left[ \frac{2\delta n}{n_0} - \frac{3}{7} \delta\theta^{(1)} + \frac{E_1 + E_1^*}{E_0} \right] - C_3 \frac{2}{7} \delta\theta^{(1)} , \quad (18)$$

where we have neglected the small cross terms  $\delta\theta^{(0)}\delta\theta^{(1)}$ , etc.

Let the temperature perturbation associated with the self-focusing instability be denoted by

$$\frac{\delta T_e^{(1)}}{T} = \frac{2}{7} \delta\theta^{(1)} \equiv \tau(x, z) e^{\gamma t} \cos(ky - \omega t) . \quad (19)$$

Then, in terms of the power flux  $P_0$ , the equation governing  $\tau$  reads

$$\frac{\partial^2}{\partial \xi^2} \tau - \frac{\tau}{L_F^2} \left( 1 + \frac{3}{2} \frac{P_0}{P_1} \right) + \frac{1}{L_F^2} \frac{P_0}{P_1} \left( 2\Delta + \frac{E_1 + E_1^*}{E_0} \right) = 0 , \quad (20)$$

where

$$L_F^2 = \frac{C_1}{C_3} = \frac{1.05 T_0}{m v_0^2} \left( \frac{M}{m} \right) , \quad (21)$$

$$P_1 = \frac{c C_3}{2\pi C_2} = \frac{3c T_0 \omega_0^2 m^2}{4\pi e^2 M} , \quad (22)$$

and  $\Delta$  is defined in Eq. (7). In practical units, the formulas for  $P_1$  and  $L_F$  are

$$P_1 = \left(600 \frac{\mu\text{watts}}{\text{m}^2}\right) \left(\frac{T_0}{1000^\circ\text{K}}\right) \left(\frac{v}{15 \text{ MHz}}\right)^2, \quad (23)$$

$$L_F = (13 \text{ km}) \left(\frac{T_0}{1000^\circ\text{K}}\right)^2 \left(\frac{10^6 \text{ cm}^{-3}}{n}\right). \quad (24)$$

The last term on the left-hand side of (20) brings out the competition between the stabilizing effects of density fluctuations (caused by the density dependence of the collision frequency) and the destabilizing contribution from self-focusing.

In the E-region, electron-neutral collisions play the principal role. Furthermore, the ohmic heating may be sufficiently intense so that the electron temperature in the radiowave beam considerably exceeds the ambient electron temperature [Perkins and Roble, 1978]. The principal electron temperature dependence of electron-neutral collision processes is adequately represented by considering only electron- $N_2$  collisions. Thus, in (10) and (11), we can see [Banks and Kockarts, 1973]

$$v = v_{en} = 2.3 \times 10^{-8} \left(\frac{T_e}{1000^\circ\text{K}}\right) n_n, \\ K = \frac{8}{\pi} \frac{n_o T_e}{m v_{en}} = C_4 \frac{n_o}{n_n}. \quad (25)$$

The electron-neutral energy relaxation frequency  $v_R$  is generally much smaller than the momentum collision frequency  $v_{en}$  but has important variations with temperature. For energy loss by excitation of rotational levels, one can take [Banks and Kockarts, 1973]

$$v_R = 1.1 \times 10^{-11} \left(\frac{1000^\circ\text{K}}{T_e}\right)^{1/2} n_n, \quad (26)$$

while for excitation of vibrational levels of  $N_2$  the appropriate formula is

$$v_R = 8.6 \times 10^{-11} \left( \frac{1000^\circ K}{T_e} \right) e^{-3353^\circ K/T_e} n_n . \quad (27)$$

According to (26) and (27), the transition between rotational and vibrational cooling occurs near  $T_e = 1500^\circ K$ . A lower transition temperature would result had vibrational excitations of  $O_2$  been included, but this will not be important to our arguments.

The next question to answer is: Will thermal conduction or local cooling control the electron temperature perturbations in the E-region? Let us introduce a characteristic length  $L_E$  which makes the rate of cooling by thermal conduction [estimated by  $(K/n_O)(L_E^{-2})$ ] equal to the local cooling rate. The formula for  $L_E$  reads

$$L_E = \left( \frac{K}{n_O v_R} \right)^{1/2} = (1 \text{ km}) \left( \frac{3.9 \times 10^{11}}{n_n} \right) \left( \frac{T_e}{1000^\circ K} \right)^{1/4} , \quad (28)$$

where we used the rotational cooling rate (26). The CIRA 1972 atmosphere [Committee on Space Research, 1972] gives  $n_n \approx 5 \times 10^{11}$  at 120 km. Hence throughout the E-region, electron thermal conduction will not play a major role, provided the self-focusing striations have a parallel wavenumber satisfying  $k_{||E} L_E < 1$ . On the other hand, the characteristic scale sizes for radiowave beams and typical variations in E-region parameters are at least several kilometers. It follows that in the E-region a plane wave model with  $k_{||E} L_E \lesssim 1$  can be used in the direction along the magnetic field.

To reiterate, our arguments show the importance of thermal conductivity is different in the E- and F-regions. Because  $L_F$  is comparable to or larger in the F-region than the size of the radiowave beam, in the F-region we must treat a nonlocal thermal diffusion problem. In the E-region, the radiowave intensity does not vary over the characteristic scale  $L_E$ , permitting a plane wave approximation.

As was the case in the F-region, the solution to the electron temperature equation in the E-region is composed of an equilibrium part  $T_{eo}$  which can be taken as spatially uniform and a perturbed part. The equilibrium part is the solution of

$$\frac{\omega_p^2 E_o^2}{2\pi\omega_o^2 n_o} = \frac{v_R}{v_{en}} (T_{eo} - T_o) , \quad (28)$$

where the right-hand side is just a function of  $T_{eo}$ . The perturbed part satisfies the equation

$$0 = L_{eo}^2 \frac{\partial^2}{\partial \xi^2} \tau + \frac{\omega_p^2 v_o E_o^2}{\omega_o^2 2\pi n_o T_{eo} v_{Ro}} \left( \frac{E_1 + E_1^*}{E_o} \right) - \beta \tau , \quad (29)$$

where

$$\beta = 1 + \frac{\omega_p^2 v_o E_o^2}{2\pi\omega_o^2 n_o v_{Ro} T_{eo}} \left[ \left( \frac{T}{v_R} \frac{\partial v_R}{\partial T} \right)_{T_{eo}} - 1 \right] , \quad (30a)$$

$$\beta = 1 + \left( 1 - \frac{T_o}{T_{eo}} \right) \left[ \left( \frac{T}{v_R} \frac{\partial v_R}{\partial T} \right)_{T_{eo}} - 1 \right] . \quad (30b)$$

Here  $\tau = \delta T_e / T_{eo}$  and the subscript o on collision frequencies and temperatures denotes evaluation at the equilibrium electron temperature  $T_{eo}$ . In Eq. (29) we have retained the thermal

conduction term. For a thermally stable equilibrium solution to exist, one must have  $\beta > 0$ .

In the case of HF ionospheric modification experiments, the second term in  $\beta$  will be small near threshold and  $T_{eo}$  will be close to  $T_o$ . Under conditions where the equilibrium electron temperature is well above the ambient temperature  $T_{eo} \gg T_o$  [Perkins and Roble, 1978], Eq. (30b) shows that

$\beta \approx (T/v_R) (\partial v_R / \partial T) \approx 4$  because of the rapid increase of vibrational cooling with electron temperature.

### 3. SELF-FOCUSING INSTABILITIES

The equations governing plasma motion also differ in the E- and F-regions, because in the F-region the ion-neutral collision frequency  $v_{in}$  is much less than ion gyrofrequency  $\omega_i$  and plasma motion can proceed only along magnetic field lines. In the E-region,  $v_{in} \gg \omega_i$  and ion motion across the field is important.

Let us turn first to the F-region, where the formula for  $v_{in}$  is [Banks and Kockarts, 1973]

$$v_{in} \approx 7 \times 10^{-10} n_n . \quad (31)$$

At an altitude of 300 km, the CIRA 1972 [Committee on Space Research, 1972] atmosphere yields  $v_{in} \approx 1$  Hz.

Upon elimination of the ambipolar electric field, the momentum and continuity equations governing plasma motion yield

$$0 = -2T_o \frac{\partial \Delta}{\partial \xi} - T_o \frac{\partial \tau}{\partial \xi} - Mv_{in}v_{||} , \quad (32a)$$

$$\frac{\partial \Delta}{\partial t} + \frac{\partial}{\partial \xi} v_{||} = 0 , \quad (32b)$$

where  $\Delta$  and  $v_{||}$  are the relative electron density and temperature fluctuations defined in (7) and (19) respectively. Equations (9), (20), (31) and (32) form a closed set which govern the linear stability of self-focusing striations.

These equations are most easily solved in the  $(\xi, \eta)$  coordinate system of Fig. 1. It is clear that the dependent variables should depend on the distance along the magnetic field from beam center,  $\xi - \xi_0$ , where  $\xi_0 = -(\sin \phi_D / \cos \phi_D)$ , and should show spatial exponential growth along the direction of the beam. In other words the functional dependence will be

$$\Delta(\xi, \eta) = \Delta(\xi - \xi_0) \exp(\eta / \ell \cos \phi_D) , \quad (33a)$$

$$\Delta(\xi, \eta) = \Delta \left( \xi + \frac{\eta \sin \phi_D}{\cos \phi_D} \right) \exp \left( \frac{\eta}{\ell \cos \phi_D} \right) , \quad (33b)$$

where  $\ell$  is the real spatial growth length along the direction of the beam, and  $\phi_D$  is the magnetic dip angle (see Fig. 1a). All other dependent variables will have the same functional form. A standard coordinate rotation yields

$$\frac{\partial}{\partial z} = \cos \phi_D \frac{\partial}{\partial \eta} - \sin \phi_D \frac{\partial}{\partial \xi} , \quad (34)$$

with the consequence that

$$\frac{\partial}{\partial z} (\xi - \xi_0) = \frac{\partial}{\partial z} \left( \xi + \frac{\eta \sin \phi_D}{\cos \phi_D} \right) = 0 . \quad (35)$$

Using the functional form (33b) for  $E_1, E_1^*$  and  $\Delta$  and (34), we

can solve Eqs. (9) to obtain

$$\frac{E_1 + E_1^*}{E_0} = - \Delta \frac{\omega_p^2 \ell}{2k_0 c^2} \left( \frac{2\alpha}{\alpha^2 + 1} \right), \quad (36)$$

where

$$\alpha = k^2 \ell / 2k_0. \quad (37)$$

The dependence of Eq. (36) on  $\alpha$  is characteristic of modulational instabilities [Bardwell and Goldman, 1976]. Two interesting observations can be made at this point. First, the term evaluated in (36) is the destabilizing term in (20). The most unstable modes will occur when (36) has its maximally negative value. Since  $\ell$  is fixed by the requirement of a particular rate of spatial growth, the most unstable mode will occur when the function  $2\alpha/(\alpha^2+1)$  has its maximum value. This occurs when

$$\alpha = k^2 \ell / 2k_0 = 1. \quad (38)$$

In practical units, the perpendicular wavelength  $\lambda_{\perp}$  of this mode is

$$\lambda_{\perp} = \frac{2\pi}{k} = \left( \frac{\pi \ell c}{f} \right)^{1/2} = (1.2 \text{ km}) \left( \frac{\ell}{25 \text{ km}} \right)^{1/2} \left( \frac{15 \text{ MHz}}{f} \right)^{1/2}, \quad (39)$$

where  $f$  is the radiowave frequency.

The second observation concerns the competition between the destabilizing (36) and stabilizing terms ( $2\Delta$ ) in (20). Thus for a self-focusing instability to occur, in the F-region, the inequality

$$\frac{\omega_p^2 \ell}{4k_0 c^2} \equiv \frac{1}{\varepsilon} = 700 \left( \frac{n_0}{10^6 \text{ cm}^{-3}} \right) \left( \frac{\ell}{25 \text{ km}} \right) \left( \frac{15 \text{ MHz}}{f} \right) > 1, \quad (40)$$

must be satisfied. Clearly, there is no question that this inequality will be strongly satisfied for HF ionospheric modification experiments. But the SPS application is a close call. We can recast inequality (40) into the form

$$4.4 \left( \frac{n_o}{10^6 \text{ cm}^{-3}} \right) \left( \frac{\ell}{25 \text{ km}} \right) \left( \frac{2.4 \text{ GHz}}{f} \right) > 1 , \quad (41)$$

which shows the ionosphere is ordinarily just dense enough to permit self-focusing at the SPS frequency. Inequality (40) has physical significance: it says that a 100% density modulation should produce a phase shift of at least  $2\pi$  between two ray paths in a distance  $\ell$ . It is evident that unless the ionosphere is sufficiently dense to produce significant phase shifts, self-focusing could not take place.

Let us return to the calculation of the threshold value for F-region self-focusing. It will turn out that the threshold flux is substantially less than  $P_1$ . Thus, combining (20), (36) and (40), we obtain the equation

$$\frac{\partial^2}{\partial \xi^2} \tau - \frac{\tau}{L_F^2} = \frac{P_o (\xi - \xi_o)}{L_F^2 P_2} \Delta \left( \frac{2\alpha}{\alpha^2 + 1} - \tau \right) , \quad (42)$$

where

$$P_2 = n_o T_o c \left( \frac{6m\omega_o^3 c}{4 \mu_p} \right) , \quad (43)$$

and we have explicitly indicated that the power flux in the radio-wave beam varies as a function of  $\xi - \xi_o$ . Combining (32a) and (32b), one obtains the plasma ambipolar diffusion equation

$$\frac{\partial \Delta}{\partial t} = 2D \frac{\partial^2}{\partial \xi^2} \Delta + D \frac{\partial^2}{\partial \xi^2} \gamma \quad . \quad (43)$$

where

$$D = T_0 / M v_{in} \quad . \quad (44)$$

Substitution of forms (7) and (19) into (43) shows that  $\gamma = 0$  and

$$\gamma \Delta = 2D \frac{\partial^2}{\partial \xi^2} \Delta + D \frac{\partial^2}{\partial \xi^2} \gamma \quad . \quad (45)$$

The coupled set (42), (45) can be simplified when the variation of  $P_0(\xi - \xi_0)$  occurs on a much faster spatial scale than  $L_F$ . Indeed, this is our basic approximation. Hence in regions where  $P_0$  is appreciable, we can ignore the term involving  $L_F^2$  on the left-hand side of (42). This permits an elimination of  $\partial^2 \gamma / \partial \xi^2$  and the eigenvalue equation becomes

$$\frac{\gamma}{D} \Delta - 2 \frac{\partial^2 \Delta}{\partial \xi^2} = \frac{P_0(\xi - \xi_0)}{L_F^2 P_2} \Delta \left( \frac{2\alpha}{\alpha^2 + 1} - \varepsilon \right) \quad , \quad (46)$$

and the boundary conditions are

$$\Delta \sim \Delta_0 \exp \left[ -|\xi - \xi_0| \left( \frac{\gamma}{2D} \right)^{\frac{1}{2}} \right] \quad , \quad (47)$$

as  $|\xi - \xi_0| \rightarrow \infty$ . For definiteness, we shall assume that the radio wave beam has a Gaussian dependence in the  $x$ -direction

$$P_0(\xi - \xi_0) = P_0 e^{-x^2/a^2} = P_0 e^{-[(\xi - \xi_0)^2 \cos^2 \phi_D / a^2]} \quad , \quad (48)$$

where  $\phi_D$  is the magnetic dip angle (see Fig. 1a). We make the change of variable

$$u = (\xi - \xi_0) / L_\gamma , \quad (49)$$

$$L_\gamma = \left( \frac{2D}{\gamma} \right)^{\frac{1}{2}} = (3.3 \text{ km}) \left( \frac{T_0}{1000^\circ \text{K}} \right)^{\frac{1}{2}} \left( \frac{1 \text{ Hz}}{v_{\text{in}}} \right)^{\frac{1}{2}} \left( \frac{10^{-1} \text{ sec}}{\gamma} \right)^{\frac{1}{2}} \quad (50)$$

[The neglect of the  $L_F^{-2}$  term on the left side of Eq. (42) is justified by the inequality  $L_\gamma^2 \ll L_F^2$ .] This change of variables leads to the nondimensional eigenvalue equation

$$\Delta - \frac{\partial^2}{\partial u^2} \Delta = \Lambda e^{-u^2/u_0^2} \Delta , \quad (51)$$

where

$$u_0 = (a/L_\gamma \cos \phi_D) , \quad (52)$$

$$\Lambda = \frac{D P_0}{\gamma L_F^2 P_2} \left( \frac{2\alpha}{\alpha^2 + 1} - \varepsilon \right) . \quad (53)$$

The next step is to find the eigenvalue  $\Lambda$  in terms of the parameter  $u_0$ . In general an analytic solution of (51) is not possible. However, we can obtain solutions when  $u_0 \gg 1$  and when  $u_0 \ll 1$ . For the case  $u_0 \gg 1$ , we expand the exponential and obtain the harmonic oscillator equation of quantum mechanics

$$\frac{\partial^2}{\partial u^2} \Delta + \left[ (\Lambda - 1) - \frac{\Lambda u^2}{u_0^2} \right] \Delta = 0 , \quad (54)$$

whose fundamental solution is accurately given by

$$\Delta = \exp \left[ - \frac{u^2}{2u_0} \left( 1 + \frac{1}{u_0} \right)^{\frac{1}{2}} \right] , \quad (55)$$

$$\Lambda \approx 1 + \frac{1}{u_0} . \quad (56)$$

When  $u_o$  is large,  $\Delta$  becomes small before  $|u/u_o|$  reaches unity, justifying our expansion.

When  $u_o \ll 1$ , the exponential term varies rapidly compared to  $\Delta$  and we can integrate (51) assuming  $\Delta$  is constant (but  $\partial\Delta/\partial u$  varies) to obtain the eigenvalue equation

$$\frac{1}{\Delta} \frac{\partial\Delta}{\partial u} = -1 = -\Lambda \int_0^\infty e^{-u^2/u_o^2} du = -\frac{\Lambda\sqrt{\pi}}{2} u_o . \quad (57)$$

An adequate interpolation formula which combines (56) and (57) is

$$\Lambda = 1 + \frac{2}{\sqrt{\pi}u_o} . \quad (58)$$

Most self-focusing experiments have  $u_o > 1$ . In the Appendix it is shown by a variational principle that the interpolation formula (58) is likely to be accurate in the vicinity of  $u_o \approx 1$ .

Our key result, the generalized dispersion relation, is

$$P_o = P_{C,F} \frac{\left(1 + \frac{2}{\sqrt{\pi}u_o}\right)}{\left(\frac{2\alpha}{1+\alpha^2} - \frac{\epsilon}{2}\right)} , \quad (59)$$

where

$$P_{C,F} = \frac{\gamma L_F^2 P_2}{2D} = 3.15 (n_o T_o c) \left(\frac{c_{n_o}}{4}\right) \left(\frac{\gamma v_{in}}{2}\right) \left(\frac{M}{m}\right) , \quad (60)$$

In practical units, the formula for  $P_{C,F}$  is

$$P_{C,F} = \left(1.5 \frac{\mu\text{watts}}{m^2}\right) \left(\frac{10^6 \text{ cm}^{-3}}{n}\right)^3 \left(\frac{T_o}{1000^\circ\text{K}}\right)^4 \left(\frac{f}{15 \text{ MHz}}\right)^3 C_F \quad (61)$$

with the definition

$$C_F \equiv \left(\frac{\gamma}{10^{-1} \text{ sec}^{-1}}\right) \left(\frac{25 \text{ km}}{\ell}\right) \left(\frac{v_{in}}{1 \text{ Hz}}\right) . \quad (62)$$

We note that the critical power flux is quite sensitive to temperature and density, principally because of the density and temperature dependence of the electron-ion collision frequency  $\nu_{oi}$ . The requirement for a rapid growth rate limits the self-focusing perturbation to the center of the radiowave beam, because otherwise plasma ambipolar diffusion would not be fast enough. This is in contrast to the results of Gurevich [1978] and Vas'kov and Gurevich [1977], who ignore the fact that ambipolar diffusion proceeds at a finite rate and that only a limited interaction time is available because of ambient  $E \times B$  drifts [see (1)].

The plasma dynamics of the E-region requires separate consideration of ions and electrons. The ion motion is governed by the E-region ion-neutral collision frequency [Banks and Kockarts, 1973]

$$\nu_{in} = 7.5 \times 10^{-10} n_r . \quad (63)$$

Using the CIRA 1972 atmosphere [Committee on Space Research, 1972], we find  $\nu_{in} = 1.4 \times 10^3$  at 110 km. Since  $\nu_{in} \gg \nu_i$ , the ion motion is unmagnetized ambipolar diffusion and governed by

$$\left( \frac{\partial}{\partial t} + \underline{v}_D \cdot \underline{\nabla} \right) \Delta + \underline{\nabla} \cdot \underline{v}_i = - \nabla A, \quad (64)$$

$$\underline{v}_i = - \frac{T_{eo}}{M \nu_{in}} \underline{\nabla} \left( \psi + \frac{T_o}{T_{eo}} \Delta \right) , \quad (65)$$

$$\psi = e\phi/T_{eo} , \quad \Gamma = 2\alpha n_o , \quad (66)$$

where  $\phi$  is the electrostatic potential, and  $\alpha = 3 \times 10^{-7} \text{ cm}^3 \text{ sec}^{-1}$  is a typical E-region recombination coefficient. Equation (64) takes account of the relative electron-ion drift  $v_D$ . The corresponding electron equations are

$$\frac{\partial}{\partial t} \Delta + \nabla \cdot v_e = -\Gamma \Delta , \quad (67)$$

$$v_{e\perp} = \frac{-T_{eo} c}{eB_0} \nabla \psi \times \hat{b} , \quad (68)$$

$$v_{e\parallel} = \frac{-T_{eo}}{mv_0} \nabla_{\parallel} (\Delta - \psi + \tau) , \quad (69)$$

where  $v_0$  denotes the electron-neutral collision frequency (25) evaluated at temperature  $T_{eo}$ .

The appropriate form for the dependent variables is

$$\left. \begin{array}{l} \Delta \\ \psi \\ \tau \end{array} \right\} \propto g(t, \xi, n) \text{ Re} \left\{ \begin{pmatrix} \Delta_0 \\ \psi_0 \\ \tau_0 \end{pmatrix} e^{i(ky - \omega t)} \right\} , \quad (70)$$

where

$$g(t, \xi, n) = e^{\gamma t} \cos[k_{\parallel}(\xi - \xi_0)] \exp[n/\lambda \cos \phi_D] , \quad (71)$$

and  $\Delta_0$  is real. Hence  $\Delta$  has exactly the same form (7), (33) as the F-region calculations. It follows that we can use (36) in (29) to obtain

$$0 = L_E^2 \frac{\partial^2}{\partial \xi^2} \tau - \alpha \tau - \frac{\omega_p^2 \lambda E_0^2}{4 \pi \omega_0^3 c v_{Ro} n_0 T_{eo}} \Delta \left( \frac{2\alpha}{\alpha^2 + 1} \right) , \quad (72)$$

Equation (72) can be recast into

$$\tau_o = \frac{-\Delta_o P_o}{F_3} , \quad (73)$$

where

$$P_3 = (n_o T_{eo} c) \frac{\frac{2c_o}{4} \frac{3v_{ro}}{v_o} \left(\frac{\alpha^2 + 1}{2\alpha}\right)}{p_o} (1 + k_{||}^2 L_E^2) , \quad (74)$$

Next, we make use of (73) and of the fact that the most rapid spatial variation comes from the  $\exp[i(ky - \omega t)]$  dependence to evaluate (64)-(69):

$$\left[ \gamma + \Gamma + i(k \cdot v_D - \omega) + \frac{k^2 T_{eo}}{Mv_{in}} \right] \Delta_o = - \frac{k^2 T_{eo}}{Mv_{in}} \psi_o , \quad (75)$$

$$\left[ \gamma + \Gamma - i\omega + \frac{k_{||}^2 T_{eo}}{Mv_o} \left( 1 - \frac{P_o}{P_3} \right) \right] \Delta_o = \frac{k_{||}^2 T_{eo}}{Mv_o} \psi_o . \quad (76)$$

The solution of (75), (76) is

$$\omega = \frac{k v_D \cdot \vec{y}}{1 + \frac{k^2 M v_o}{k_{||}^2 M v_{in}}} , \quad (77)$$

$$P_o = P_3 \left[ 1 + \frac{T_{eo}}{T_{eo}} + \frac{(\gamma + \Gamma) M v_{in}}{k^2 T_{eo}} \left( 1 + \frac{k^2 M v_o}{k_{||}^2 M v_{in}} \right) \right] . \quad (78)$$

Let us discuss the result of Eq. (78). First, for nominal E-region densities  $n_o \sim 10^5 \text{ cm}^{-3}$ , the recombination rate  $\Gamma = 2n_o \alpha \sim 6 \times 10^{-2} \text{ sec}^{-1}$  is comparable to the growth rates we envision. Second, for values of  $\alpha = k^2 l / 2k_o$  near unity, the ion diffusion rate  $\gamma_{Di}$  is

$$\gamma_{Di} = \frac{k^2(T_{eo} + T_o)}{Mv_{in}} = \alpha \frac{2k_o(T_{eo} + T_o)}{\ell Mv_{in}} = (0.1 \text{ sec}^{-1}) \alpha \left( \frac{1 \text{ km}}{\ell} \right) \left( \frac{1500 \text{ sec}^{-1}}{v_{in}} \right) \left( \frac{T_{eo} + T_o}{1000 \text{ }^{\circ}\text{K}} \right) \left( \frac{f}{15 \text{ MHz}} \right), \quad (79)$$

which is also comparable to growth rates. We can, however, satisfy the double inequality

$$\frac{1}{L_E^2} \gg k_{\parallel}^2 \gg k^2 \frac{m v_o}{M v_{in}} \quad (80)$$

because

$$k^2 L_E^2 \frac{m v_o}{M v_{in}} = \frac{8}{\pi} \frac{\gamma_{Di}}{v_{Ro}} \ll 1. \quad (81)$$

The first part of the inequality (80) justifies our assertion that thermal conduction is small relative to local cooling in the E-region. As a result, we can choose  $k_{\parallel}^2$  so that terms involving  $k_{\parallel}^2$  in (74), (77) and (78) are ignorable. This choice minimizes the threshold flux and leads to the generalized dispersion relation

$$P_o = P_{c,E} \left( \frac{\alpha^2 + 1}{2\alpha} \right) \left[ 1 + \frac{(\gamma + \alpha)}{\alpha \gamma_{Di}} \right], \quad (82)$$

where

$$P_{c,E} = n_o (T_{eo} + T_o) c \left( \frac{2c_o^3 v_{Ro}}{\ell \omega_p^4 v_o} \right). \quad (83)$$

In practical units, the formula for  $P_{c,E}$  is

$$P_{c,E} = \left( 1 \frac{\text{milliwatt}}{\text{m}^2} \right) \left( \frac{f}{15 \text{ MHz}} \right)^3 \left( \frac{10^5 \text{ cm}^{-3}}{n_o} \right) c_E, \quad (84)$$

where

$$c_E = \left( \frac{T_{eo} + T_o}{T_{eo}} \right) \left( \frac{1000 \text{ }^{\circ}\text{K}}{T_{eo}} \right)^{\frac{1}{2}} \left( \frac{1 \text{ km}}{\ell} \right). \quad (85)$$

The temperature and density dependence are not so strong in the E-region because neutral rather than charged particle collisions are involved. The strong dependence on radiowave frequency remains. Formula (39) shows that the perpendicular wavelength of the striations will be close to 300 m for E-region self-focusing. The next generation of ionospheric modification experiments will easily exceed this threshold value for self-focusing, especially if the frequency is near  $f = 5$  MHz.

#### 4. APPLICATIONS AND DISCUSSION

Our central results are the threshold power fluxes for the onset of self-focusing instabilities: Equation (61) for the F-region and Equation (84) for the E-region. For comparison, the European ionospheric heating facility nearing completion at Tromsø, will have an effective radiated power of 360 MW, yielding an E-region flux at 2 milliwatts/m<sup>2</sup> and an F-region flux of 300  $\mu$ watts/m<sup>2</sup>. These fluxes will exceed the respective threshold fluxes, even when  $f = 15$  MHz. The question then arises, what are the consequences of self-focusing instabilities and how do we detect them?

Dimensional analysis of linear theory provides estimates for the nonlinear consequences. We can interpret Equation (36) as giving the fluctuations  $\delta P$  in the power flux

$$\frac{\delta P}{P_0} = -2 \frac{\delta n}{n} \left( \frac{\omega_p^2}{4k_0 c^2} \right) \left( \frac{2\alpha}{\alpha^2 + 1} \right), \quad (86)$$

while (40) shows that the coefficient of  $\delta n/n$  is very large. Consequently, nonlinearities will develop first in the wave propagation equation and the self-focusing instability will cause intensity fluctuations of order unity to develop. Equation (86) provides an estimate of the magnitude of the concomitant density fluctuations when  $\delta P/P_0 \approx 1$ . The expected wavelength of the density fluctuations is given by (39) and Fig. 1 portrays their geometry. Vas'kov and Gurevich [1977] discuss a mathematical model for the nonlinear saturation.

It is important to recognize that the self-focusing instability generates density fluctuations with just the correct magnitude and orientation to produce intensity scintillations in the driving beam. Hence, in order for these fluctuations to produce significant intensity scintillations in a diagnostic wave, that wave should be propagating parallel (or antiparallel) to the driving wave and should have a frequency which differs from the driving frequency by no more than a factor of 3. In particular, the diagnostic wave should not have a component of its wave vector in the  $\hat{z} \times \hat{b}$  direction, which would result in its propagating across the density maxima and minima, thereby averaging out their effect. The geometry of Novozhilov and Savel'yev [1978] was ideal from this point of view with the diagnostic wave propagating antiparallel to the driving wave and closely matched in frequency. Radio-stars are another possible source of diagnostic waves. In this case, the driving wave would be launched in the direction of the radio-star, and scintillations

of the radio-star signal should be observed up to frequencies several times the driving frequency. As (86) and (40) show, the density fluctuations associated with HF-driven self-focusing instabilities have a magnitude  $\delta n/n \sim 10^{-3}$  and are probably not directly observable. The characteristic exponentiation times of roughly 10 sec imply delay times of roughly a minute after transmitter turn-on before scintillations become observable. The Novozhilov and Savel'yev [1978] experiment agrees with this prediction. Although high-peak-power radars can exceed the threshold power flux, the long growth times show that the self-focusing instability is driven by the average, not peak, power of a radar system.

There is a distinct possibility that the 2.4 GHz microwave beam from a proposed Satellite Power Station could produce self-focusing. Recasting (61) into a form appropriate to the SPS, we find

$$P_{c,F} = \left( 6 \frac{\text{watts}}{\text{m}^2} \right) \left( \frac{10^6}{n} \right)^3 \left( \frac{T_0}{1000^\circ\text{K}} \right)^4 \left( \frac{f}{2.4 \text{ GHz}} \right)^3 C_F ,$$

where  $C_F$  is given by (62) and is roughly unity. Although planned power fluxes for the SPS are in the range 250 watts  $\text{m}^{-2}$ , natural variations in ionospheric density and temperature can raise the threshold flux to this value. Furthermore, the ohmic heating of the ionosphere by the SPS microwave beam itself [Perkins and Roble, 1978] can raise the electron temperature above  $2000^\circ\text{K}$ , which works toward stabilizing the instability. Hence one cannot make an unequivocal prediction regarding whether the SPS beam

will generate self-focusing. Our best estimate is that at times the ionosphere could be sufficiently cold and dense so that self-focusing would occur. According to (39), the wavelength of striations created by SPS self-focusing will be  $\lambda_{\perp} \approx 100$  meters. By (86) and (41), the density fluctuations would be quite large:  $\delta n/n \sim 10^{-1}$ . A scaled HF test of self-focusing at  $f = 15$  MHz could validate predictions for the threshold flux, but would have a much smaller effect on telecommunications than SPS self-focusing because of the much weaker density fluctuations at HF combined with the larger scale-size. Ten percent density fluctuations with scale-sizes of 100 meters can seriously effect ionospherically propagated short-wave broadcast signals. If the striations were steepened by  $E \times B$  drifts as in the case with artificial plasma clouds [Scannapieco et al., 1976], then higher frequency telecommunications systems could be affected as well. A quantitative investigation of this question awaits future work. It is also evident that if the SPS generates self-focusing, then intensity fluctuations of order unity could be expected on the rectenna.

In closing, we can remark that thermal self-focusing is under investigation in the laboratory (J. Drummond and W. B. Thompson, private communication) and in laser-fusion applications [Langdon, 1979]. The details differ from the ionospheric theory.

Acknowledgements. Discussions with Drs. Gerald Meltz and Charles Rush contributed substantially to this work. Financial support came from the U.S. Department of Energy Contract DE-AT03-76ER10100 with SRI International, and from the U.S. Air Force Office of Scientific Research Contract 80-0022 with the University of Colorado, and from the U.S. Air Force Office of Science Research Contract 80-00656 with Princeton University.

## APPENDIX

## VARIATIONAL PRINCIPLE APPROXIMATION TO EIGENVALUE PROBLEM

In the eigenvalue problem of Equation (51), namely,

$$(\partial_u^2 - 1)\Delta = -\Lambda e^{-u^2/u_0^2} \Delta , \quad (A-1)$$

the lowest eigenvalue  $\Lambda$  may be found approximately by the following variational principle [Morse and Feshbach, 1953, pg. 1108]:

$$\Lambda = \int_{-\infty}^{+\infty} du [\Delta_u^2 + \Delta^2] \left/ \int_{-\infty}^{+\infty} du \Delta^2 e^{-u^2/u_0^2} \right. . \quad (A-2)$$

The eigenvalues are not terribly sensitive to the precise shape of the trial function. We use the trial function,

$$\Delta = e^{-\alpha u^2/2} , \quad (A-3)$$

to find

$$\Lambda = (1 + 1/\alpha u_0^2)^{1/2} (1 + \alpha/2) . \quad (A-4)$$

Differentiating with respect to  $\alpha$  gives the minimum eigenvalue,  $\Lambda_{\min}$ , at

$$\alpha = [(1 + 16 u_0^2)^{1/2} - 1]/4u_0^2 . \quad (A-5)$$

From (A-4) and (A-5), we find the asymptotic behavior

$$\begin{aligned} \lim_{u_0 \rightarrow 0} \Lambda_{\min} &= \frac{\sqrt{2}}{u_0} , \\ \lim_{u_0 \rightarrow \infty} \Lambda_{\min} &= 1 + \frac{1}{u_0} . \end{aligned} \quad (A-6)$$

These agree quite well with the exact asymptotic solutions (56) and (57). (Note, the exact coefficient  $2/\sqrt{\pi} = 1.13$  is slightly smaller than  $\sqrt{2}$ .) Moreover, when  $u_0 = 1$ , (A-4) and (A-5) yield  $\Lambda_{\min} = 2.10$ , whereas the interpolation formula (58) gives  $\Lambda = 2.13$ .

## REFERENCES

Banks, P. M., and G. Kockarts, Aeronomy, Academic Press, New York, 1973.

Bardwell, S., and M. V. Goldman, Three-dimensional Langmuir wave instabilities in type III solar radio bursts, Astrophys. J. 209, 912-926, 1976.

Blanc, M., and P. Amayenc, Seasonal variations of the ionosphere ExB drifts above Saint-Saintin on quiet days, J. Geophys. Res., 84, 2691-2704, 1979.

Braginskii, S. I., Transport processes in a plasma, p. 205 in Reviews of Plasma Physics, Vol. 1, M. A. Leontovich, Ed., Consultants Bureau, New York, 1965.

Brown, W. C., Satellite power stations: a new source of energy?, IEEE Spectrum, 10, 38-47, 1973.

Committee on Space Research, CIRA 1972, COSPAR International Reference Atmosphere, Akademie-Verlag, Berlin, 1972.

Cragin, B. L., and J. A. Fejer, Generation of large-scale field-aligned irregularities in ionospheric modification experiments, Radio Science, 9, 1071-1075, 1974.

Das, A. C., and J. A. Fejer, Generation of small-scale field-aligned irregularities in heating experiments, J. Geophys. Res. (in press), 1980.

DuBois, D. F., and M. V. Goldman, Spectrum and anomalous resistivity for the saturated parametric instability, Phys. Rev. Letters, 28, 218-221, 1972.

Duncan, L. M., and R. A. Behnke, Observations of self-focusing electromagnetic waves in the ionosphere, Phys. Rev. Letters, 41, 998-1001, 1978.

Fejer, J. A., and Y. Y. Kuo, Structure in the nonlinear saturation spectrum of parametric instabilities, Phys. Fluids, 16, 1490, 1973.

Fock, V. A., Electromagnetic Diffraction and Propagation Problems, p. 213, Pergamon, New York, 1965.

Glaser, P. E., Solar power from satellites, Physics Today, p. 30, February 1977.

Gurevich, A. V., Nonlinear Phenomena in the Ionosphere, pp. 282-298, Springer-Verlag, New York, 1978.

Harper, R. M., R. H. Ward, C. J. Zamlatti, and D. T. Farley, E region ion drifts and winds from incoherent scatter measurements at Arecibo, J. Geophys. Res., 81, 25-35, 1976.

Langdon, A. B., Filamentation in collisional ICF plasmas, Bull. Am. Phys. Soc., 24, 1105, 1979.

Morse, P. M., and H. Feshbach, Methods of Theoretical Physics, McGraw-Hill, New York, 1953.

Novozhilov, V. I., and S. M. Savel'yev, Geomagnetism and Aeronomy, 18, 145-147, 1978.

Perkins, F. W., C. Oberman, and E. J. Valeo, Parametric instabilities and ionospheric modification, J. Geophys. Res., 79, 1478-1496, 1974.

Perkins, F. W., and R. G. Roble, Ionospheric heating by radiowaves: predictions for Arecibo and the satellite power station, J. Geophys. Res., 83, 1611-1624, 1978.

Perkins, F. W., and E. J. Valeo, Thermal self-focusing of electromagnetic waves in plasmas, Phys. Rev. Letters, 32, 1234-1237, 1974.

Scannapieco, A. J., S. L. Ossakov, S. R. Goldman, and J. M. Pierre, Plasma cloud late time spectra, J. Geophys. Res., 81, 6037, 1976.

Thome, G. D., and F. W. Perkins, Production of ionospheric striations by self-focusing of intense radiowaves, Phys. Rev. Letters, 32, 1238-1240, 1974.

Vanke, V. A., V. M. Lopukhim, and V. L. Savin, Satellite solar power stations, Usp. Fiz. Nauk, 123, 633-655, 1977 [Sov. Phys. Usp., 20, 989-1001, 1977].

Vas'kov, V. V., and A. V. Gurevich, Modulational instability of radiowaves in upper ionosphere, Geomagnetism i Aeronomiya, 16, 239, 1976 [Geomag. Aeronomy, 16, 141-144, 1976].

Vas'kov, V. V., and A. V. Gurevich, Resonance instability of small-scale plasma perturbations, Zh. Eksp. Teor. Fiz., 73, 923, 1977 [Sov. Phys. JETP, 46, 487, 1977].

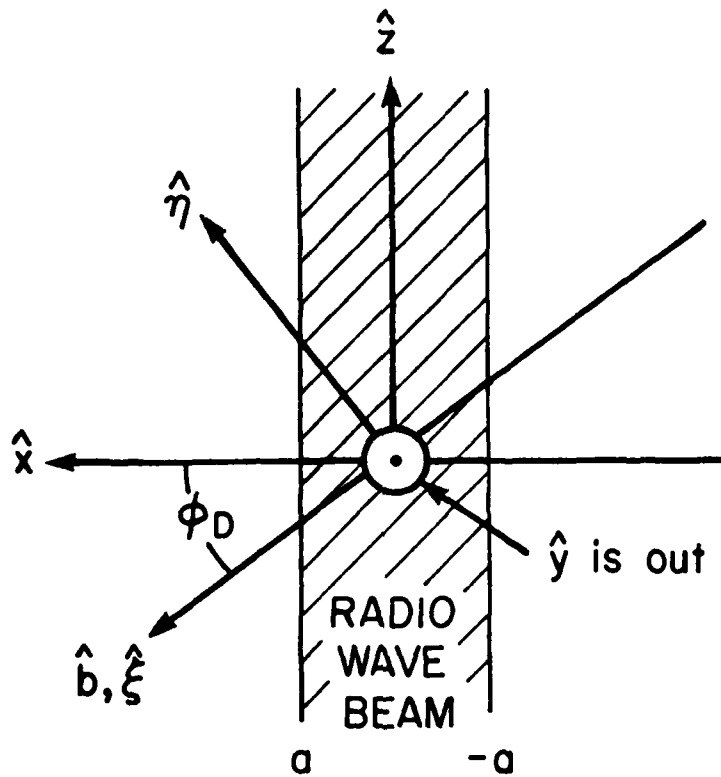
Vas'kov, V. V., and A. V. Gurevich, Saturation of the modulation instability of narrow radiobeams in a magnetized plasma, Fiz. Plazmy, 3, 329-377, 1977 [Soviet J. Plasma Phys., 3, 185-190, 1977].

## FIGURE CAPTION

Fig. 1. Geometry of the self-focusing instability.

(a) The radiowave beam is propagating in the z direction. The actual orientation of z in space depends on the application (see text). The magnetic field lies in the b direction which is taken to be in the x-z plane. The finite dimensions of the radiowave beam in the x-z plane are indicated. (b) Geometry of the self-focusing striations as viewed along the radiowave beam. The striations are elongated along the magnetic field and grow slowly in the direction of the radiowave beam, but they have a rapid spatial variation the zxb-direction (i.e., the  $\hat{y}$ -direction).

a)



b)

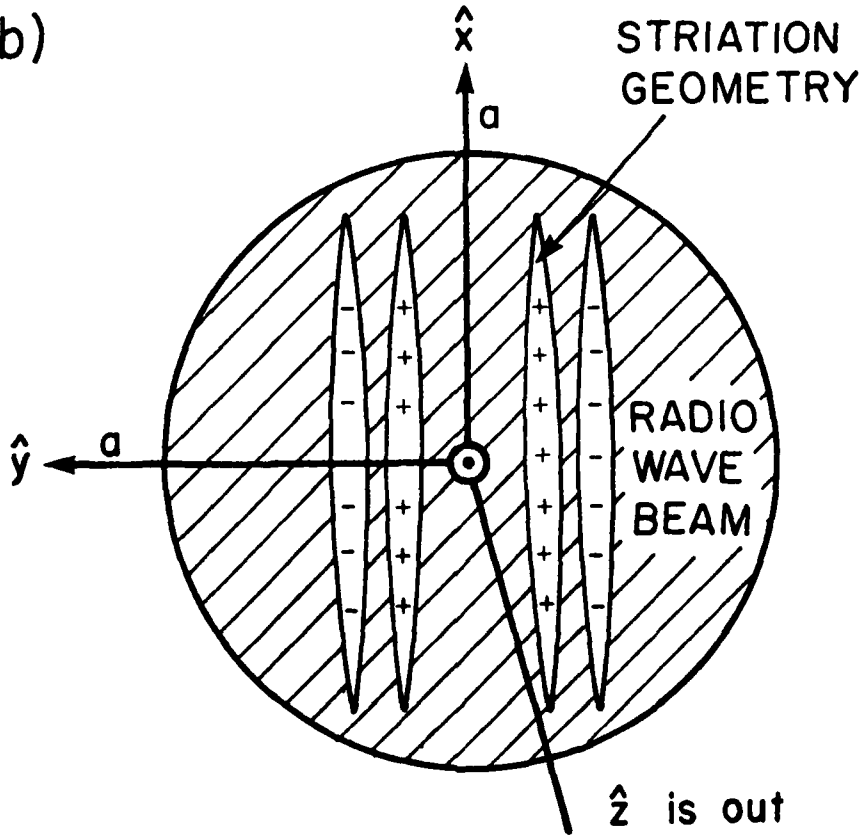


FIGURE 1

## APPENDIX H

H. "Inhomogeneous Effects in RIKE and Other Coherent  
Diagnostics"

M. V. Goldman

Research Memorandum, August 1980

M E M O R A N D U M

TO: N. Peacock and R. Kirk

FROM: M. Goldman

DATE: 19 August 1980

SUBJECT:

Inhomogeneous Effects in RIKE  
and Other Coherent Diagnostics

I. INTRODUCTION

The purpose of this memo is to consider the effects of density and temperature space and time dependence on coherent-scattering diagnostics of plasma-collective responses, such as those at Langmuir and ion-acoustic frequencies.

The problem may be thought of in two parts. First, how are electron density fluctuations driven coherently by the beat-ponderomotive-force between two lasers? Second, how does an "incident" laser beam (which may or may not be identical to one of the "beating lasers") scatter from the coherent electron density response? The answer to the second question is trivial. Let  $I_{inc}$  be the incident beam at frequency  $\omega_i$ . Then the power scattered into the solid angle  $\Delta\Omega$  at the detector in the frequency interval  $\Delta\omega_s$  about  $\omega_s$  is

$$P = I_{inc} \sigma_T \Delta\Omega N \frac{\Delta\omega_s}{2\pi} S(\underline{k}_s - \underline{k}_{inc}, \omega_s - \omega_{inc}), \quad (1)$$

Here,  $\sigma_T$  is the Thompson scattering cross-section,

$$\sigma_T \equiv \frac{e^4}{m^2 c^4} \left[ 1 - (\hat{k}_s \cdot \hat{e}_{inc})^2 \right] \quad (2)$$

$N$  is the total number of electrons contributing to the scatter,

$$N = n_o V \quad (3)$$

$V$  is the effective scattering volume,  $n_o$  is the mean\* electron density, and  $S(q, w)$  is the density correlation function,

$$S(q, w) = \frac{1}{n_o} \frac{|n_L^e(q, w)|^2}{VT} \quad . \quad (4)$$

In this expression for  $S$ ,  $n_L^e$  is the electron density response at the (low) beat-ponderomotive-force frequency, and  $T$  is the interaction time available (e.g., the pulse duration or inverse bandwidth).

The first problem, therefore, is to calculate  $S(q, w)$ , taking inhomogeneity (and possibly time-dependence) into account.

\*It is assumed that the density doesn't vary significantly over the effective scattering volume.

## II. RESPONSE TO THE PONDEROMOTIVE "BEAT" FORCE

We assume the driving laser fields consist of a monochromatic "pump" field,  $E_0 \cos(\omega_0 t - \underline{k}_0 \cdot \underline{r})$ , and a broadband field of form

$$E_1(\underline{r}, t) = E_1 \eta(t) \cos(\omega_1 t - \underline{k}_1 \cdot \underline{r}), \quad (5a)$$

where

$$\eta(t) = \begin{cases} 1, & 0 \leq t \leq T \\ 0, & t < 0 \text{ or } t > T \end{cases} \quad (5b)$$

Hence, this field has a bandwidth determined by the pulse duration, T. (Other sources of shorter bandwidth must be considered individually, but will generally lead to the same kind of frequency shapes, with different normalization.)

The Fourier transform of the beat-ponderomotive-force between the two fields may be written as<sup>(1)</sup>:

$$F_p(\underline{k}, \omega) = -\frac{ik\epsilon^2}{2m\omega_0\omega_1} E_0 \cdot E_1(\underline{k}_0 - \underline{k}, \omega_0 - \omega)^* \quad (6)$$

The spatial Fourier transforms are taken over the scattering volume, V, to be discussed later. The time Fourier transforms are one-sided. Combining (6) with the transform of (5) gives:

$$F_p(\underline{k}, \omega) = - \frac{ik e^2}{2m\omega_0 \omega_1} \underline{E}_0 \cdot \underline{E}_1^* V \delta_{\underline{k}_0 - \underline{k}, \underline{k}_1} \frac{T}{2} f(\omega_0 - \omega_1 - \omega). \quad (7)$$

The line shape factor is  $f(\omega_0 - \omega_1 - \omega)$ , where,

$$f(\Omega) = e^{i\Omega T/2} \frac{\sin \Omega T/2}{\Omega T/2}, \quad (8a)$$

which has a maximum of one at  $\Omega = 0$  and a half-width of  $\Delta_1$ , where

$$\Delta_1 \approx \frac{3.8}{T} \quad (8b)$$

For other sources of bandwidth in  $\omega_1$ ,  $|f(\Omega)|$  will always have a maximum of order unity at  $\Omega = 0$  and a half-width  $\approx \Delta_1$ .

For a homogeneous stationary plasma, the relation between the driven electron density,  $n_L^e$ , the electrostatic field,  $\underline{\mathcal{E}}$ , and the ponderomotive-beat-force of Equation (7) is

$$-en_L^e = - \frac{ik}{4\pi} \chi_L^e \left[ \underline{\mathcal{E}} - \frac{F_p}{e} \right]. \quad (9)$$

Combining with Poisson's Equation and the linear constitutive relation for the ion density, we obtain the equation for  $\underline{\mathcal{E}}$ :

$$L(\underline{k}, \omega) \underline{\mathcal{E}}(\underline{k}, \omega) = F_p(\underline{k}, \omega)/e, \quad (10)$$

where,

$$L(\underline{k}, \omega) \equiv \frac{\epsilon(\underline{k}, \omega)}{\chi_L^e(\underline{k}, \omega)} , \quad (11)$$

$\epsilon = 1 + \chi_L^e + \chi_L^i$  is the dielectric function, and  $\chi_L^e$  and  $\chi_L^i$  are the electrostatic electron and ion susceptibilities. To obtain the spatial wave equation for the inhomogeneous (but stationary) problem, we simply replace  $\underline{k} \rightarrow -i\nabla$  in  $L$ , so that it becomes an operator,  $\hat{L}$ , and the wave equation becomes,

$$\hat{L}(-i\nabla, \omega) \mathcal{E}(\underline{r}, \omega) = F_p(\underline{r}, \omega)/\epsilon . \quad (12)$$

The procedure for finding the density response  $n_L^e(\underline{q}, \omega)$  which must enter into  $\epsilon$  [Equation (4)] is then as follows: We first solve Equation (12) for  $\mathcal{E}(\underline{r}, \omega)$ . Then  $n_L^e(\underline{r}, \omega)$  is found from the inverse of Equation (9), and, finally,  $n_L^e(\underline{r}, \omega)$  is Fourier transformed and  $n_L^e(\underline{q}, \omega)$  is evaluated. We first show how this is accomplished for Langmuir waves.

### III. DRIVEN LANGMUIR WAVES

For Langmuir waves, the ion susceptibility may be ignored, and the electron susceptibility is

$$\chi_L^e = -\frac{\omega_p^2}{\omega^2} - \frac{3k^2 v_e^2}{\omega^2} + \frac{i\gamma}{\omega} \quad (13)$$

Here, it is assumed  $\omega^2$  is close to  $\omega_p^2$  and that  $3k^2 v_e^2/\omega^2$  and  $\gamma/\omega$  are both much less than one, so that  $\chi_L^e \approx -1$  at resonance.

Also,  $\gamma$  is the temporal damping rate of the wave. Hence, we may write

$$L(\underline{k}, \omega) \approx \frac{3k^2 v_e^2}{\omega^2} - 1 + \frac{\omega_p^2}{\omega^2} - \frac{i\gamma}{\omega} \quad (14)$$

The driven Langmuir wave, Equation (12), then becomes

$$\nabla^2 \mathcal{E} + \frac{\omega^2}{3v_e^2} \left( 1 - \frac{\omega_p^2}{\omega^2} + \frac{i\gamma}{\omega} \right) \mathcal{E} = - \frac{\omega^2}{3v_e^2} \frac{F_p(\underline{r}, \omega)}{e} = s_\omega e^{i\underline{q} \cdot \underline{r}} \quad (15)$$

where,

$$s_\omega \approx \frac{i q e \omega^2}{12 m v_e^2 \omega_0 \omega_1} \underline{E}_0 \cdot \underline{E}_1^* T f(\omega_0 - \omega_1 - \omega), \quad (16)$$

and,

$$\underline{q} \equiv \underline{k}_0 - \underline{k}_1 \quad (17)$$

We now adopt the following geometry:

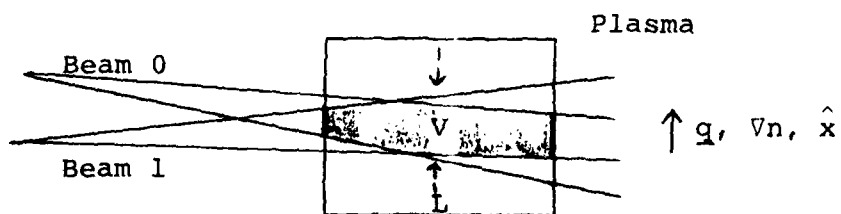


Fig. 1

That is, we assume the angle between  $\underline{k}_0$  and  $\underline{k}_1$  is small, and the length  $L$  is determined by the intersection volume. Also, the density gradient is assumed to lie in the  $q$  direction, so we need only deal with inhomogeneity in  $x$ .

The wave equation may now be written in the form

$$\partial_x^2 \mathcal{E} + k_c(x)^2 \mathcal{E} = s_\omega e^{iqx}, \quad (18)$$

where,

$$k_c(x) \equiv k(x) + iK(x), \quad (19)$$

$$k(x) \equiv \frac{1}{3v_e^2} \left[ \omega^2 - \omega_p(x)^2 \right] \quad (20)$$

$$K(x) \equiv \frac{\gamma}{v_g} = \gamma(k) \frac{\omega}{3v_e^2 k(x)} \quad (21)$$

Here, the density depends on  $x$  through  $\omega_p(x)^2 = 4\pi e^2 n(x)/m$ ,  $k(x)$  is the WKB wave-number of the homogeneous wave equation, and  $K \ll k$  is the spatial damping decrement. ( $v_g$  is the group velocity.) It is also implicit here that  $s_\omega$  falls to zero, unless  $x$  is in the range  $-L/2 \leq x \leq +L/2$ , where the beams intersect (Figure 1).

The solution to the driven wave Equation (18) may be written down in terms of the exact solutions to the homogeneous (undriven) version of (18) through the use of the following Green's function<sup>(2)</sup>:

$$G(x, x') = \frac{1}{W} \left[ \theta(x - \bar{x}) \mathcal{E}_+(x) \mathcal{E}_-(\bar{x}) + \theta(\bar{x} - x) \mathcal{E}_-(x) \mathcal{E}_+(\bar{x}) \right] \quad (22)$$

Here,  $W$  is the Wronskian,

$$W \equiv \mathcal{E}_- \mathcal{E}'_+ - \mathcal{E}_+ \mathcal{E}'_-, \quad (23)$$

which is independent of space, and  $\theta(x)$  is the usual step function, equal to zero for  $x < 0$  and one for  $x > 0$ ;  $\mathcal{E}_+$  is the solution to the homogeneous equation which obeys the proper boundary condition as  $x \rightarrow \infty$ , and  $\mathcal{E}_-$  is the solution which obeys the proper boundary condition as  $x \rightarrow -\infty$ . The proper boundary conditions depend on the shape of the profile, and, in particular, on whether or not there are reflection points  $k(x) = 0$  for the driven waves. The solution to the wave Equation (18) may be written in terms of the Green's function,  $G$ , as

$$\mathcal{E}(\omega, x) = \frac{s_\omega}{W} \left[ \mathcal{E}_+(x) \int_{-L/2}^x d\bar{x} \mathcal{E}_-(\bar{x}) e^{iq\bar{x}} + \mathcal{E}_-(x) \int_x^{+L/2} d\bar{x} \mathcal{E}_+(\bar{x}) e^{iq\bar{x}} \right] \quad (24)$$

In the applications we shall consider, the second integral can be ignored, since it tends to phase mix, whereas the first integral can have a resonant point. We next consider a specific form for the density profile,  $\omega_p(x)^2$ .

## V. PARABOLIC DENSITY PROFILE

We choose the specific shape,

$$\omega_p(x)^2 = \omega_{p0}^2 \left[ 1 - \frac{x^2}{2\ell^2} \right] \quad (25)$$

The advantage of this profile is that reflection points can be avoided, and the homogeneous limit is  $\ell \rightarrow \infty$ . Measurements can be performed near  $x = 0$ , where the profile has zero slope.

The disadvantage of this profile is that the focus-device plasma profile may be such that  $\omega_{pmax}$  is changing too rapidly to yield much of a scattered signal. (A plasma jet would seem superior here.) The more normal situation might occur when a Langmuir wave reflection point exists somewhere, and the density profile is taken as linear about the reflection point.

In this case, WKB methods cannot be used as freely as in the case where Langmuir wave reflection does not occur.

The wavenumber  $k(x)$  in Equation (20) may be expressed as,

$$k(x) = \left[ p_\omega^2 + \frac{x^2}{6\ell^2} k_D^2 \right]^{1/2} \quad (26a)$$

$$p_\omega^2 = \frac{1}{3v_e^2} \left[ \omega^2 - \omega_{p0}^2 \right] \quad (26b)$$

We shall assume that  $x^2/\ell^2 \ll 1$ , and show, a posteriori, that this condition is satisfied for all  $x$ -values which contribute significantly to the relevant integrals. The Debye wave-number is defined by  $k_D^2 = \omega_{p0}^2/v_e^2$ .

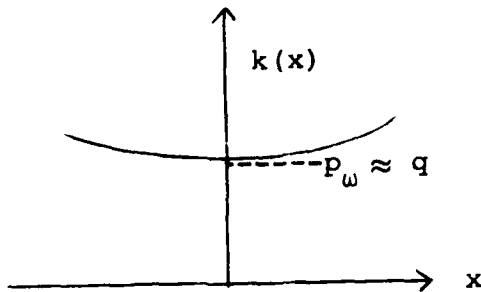


Fig. 2

The frequency,  $\omega = \omega_{\text{inc}} - \omega_s$  is a free parameter which can be tuned as we look over the spectrum of the signal,  $\omega_s$ . The line shape of the observed signal is controlled by two factors: the shape of the probe [present in  $s_\omega \propto f(\omega_0 - \omega_1 - \omega)$ ], and the shape of the plasma wave spectrum. The probe spectrum peaks at  $\omega = \omega_0 - \omega_1$ , and has a half-width at  $\omega_\pm$ , where,

$$\omega_\pm \equiv \omega_0 - \omega_1 \pm \Delta_1 \quad (27)$$

One of our objects in this section will be to see how the half-width and shape of the plasma wave spectrum depends on  $l$  and  $\gamma$ , and how it compares with the shape of the probe spectrum.

Another free parameter is  $q = k_0 - k_1$ , which is controlled by the angle between the two beams. We shall choose  $q$  so that Landau damping is suppressed. A good choice will turn out to be  $q/k_D = 0.1$ . Let us suppose that the difference frequency,  $\omega_0 - \omega_1$ , between the pump and the center of the probe is adjusted so that

$$p_{\omega_0 - \omega_1}^2 = q^2 \quad (28)$$

Hence, making reference to Equation (26), the ponderomotive force will drive the wavenumber  $k(o)$  at  $x = 0$  most effectively. For each different frequency within the bandwidth of the probe, there will be a "matched" wavenumber which occurs at a frequency-dependent position,  $x_{\omega}$ , defined by

$$k(x_{\omega}) = q \quad (29)$$

Let us ask what is the matched point at the edges of the probe bandwidth [Equation (27)]. No matching can occur at  $\omega_+$  because  $p_{\omega_+}^2 > q^2$ , and  $x^2$  is positive in Equation (26a). In fact, no matching can occur for  $\omega > \omega_0 - \omega_1$ . However, a matched point will occur for each  $\omega < \omega_0 - \omega_1$ , down to the edge of the probe bandwidth at  $\omega_-$ . It is easy to show that

$$\frac{|x_{\omega_-}|}{\ell} = 2 \sqrt{\frac{\Delta_1}{\omega_p}} \quad (30)$$

This is the largest significant  $x$ -position we shall deal with, and it will be assumed that  $\Delta_1$  is sufficiently small that  $x_{\omega_-}/\ell \ll 1$ . It can also be shown that  $p_{\omega_-} = q - \Delta p_{\omega}$ , where  $\Delta p_{\omega} \equiv k_D^2 \Delta_1 / 3q\omega_p$ . As long as  $\Delta p_{\omega} \ll q$ , there can be no reflection points (which would require  $p_{\omega} = 0$ ). We shall take this to be the case by requiring,

$$\frac{\Delta_1}{\omega p} \ll \frac{3q^2}{k_D^2} \quad (31)$$

Hence,  $p_\omega$  will always be in the vicinity of  $q$  and can be approximated by  $q$ , where appropriate. In particular,  $k(x)$  in Equation (26a) can now be expanded as

$$k(x) \approx p_\omega + \frac{x^2}{12\ell^2} \frac{k_D^2}{q} , \quad (32)$$

for all significant  $x$ .

We can now solve the wave equation by using WKB solutions for  $\mathcal{E}_\pm$ :

$$\mathcal{E}_\pm(x) = \frac{1}{k_C(x)^{1/2}} \exp(\pm i \int dx k_C(x)) \quad (33)$$

Since there are no reflection points, the boundary conditions have been taken as outgoing waves at  $x \rightarrow \infty$  (right-going waves at  $x = +\infty$ , left-going waves at  $x = -\infty$ ). The condition for validity of WKB is  $|k(x)^2 \partial k / \partial x| \ll 1$ . Using  $x_{\omega_-}$  as the maximum value of  $x$ , this gives

$$2 \sqrt{\frac{\Delta_1}{\omega p}} \ll k_D \ell \frac{q^3}{k_D^3} , \quad (34)$$

as the condition for the validity of WKB everywhere.

We note the following example:

$$\begin{aligned}
 \theta_e &= 300 \text{eV} , & n_{\max} &= 10^{19} \text{cm}^{-3} \\
 k_D &= 2.5 \times 10^5 \text{cm}^{-1} , & \omega_p &= 1.8 \times 10^{14} \\
 \frac{\gamma_{\text{coll.}}}{\omega_p} &\approx 2.5 \times 10^{-4} , & l &= 0.2 \text{cm} \\
 \frac{q}{k_D} &= 0.1
 \end{aligned} \tag{35}$$

For these parameters, a choice of

$$\frac{\Delta_1}{\omega_p} = 2 \times 10^{-3} \tag{36}$$

would easily satisfy both (34) and (31), and also guarantee  $\Delta_1 \gg \gamma_{\text{coll.}}$ , where  $\gamma_{\text{coll.}}$  is the collision-damping rate for Langmuir waves.

Using the formal solution (24), to the wave equation, but ignoring the second integral because it possesses no matched points and, therefore, phase mixes to zero, we find

$$\mathcal{E}(\omega, x) = -\frac{i}{z} \text{ s} \frac{e^{+i\int dx k_c(x)}}{k(x)^{1/2}} \int_{-L/2}^x d\bar{x} \frac{e^{-i\int d\bar{x} k_c(\bar{x})}}{k(\bar{x})^{1/2}} e^{iq\bar{x}}. \tag{37}$$

The Wronskian  $W$ , has been evaluated as  $2i$ . We have also ignored the damping  $K \ll k(x)$  in the swelling factors (denominators).

For Langmuir waves, the relationship between  $\mathcal{E}(x)$ , and the electron density,  $n_L^e(x)$ , is particularly simple. Poisson's equation gives  $n_L^e(x) \propto \delta_x \mathcal{E}(x)$ . Hence, we shall

take the Fourier transform of  $\mathcal{E}(x)$ , in order to evaluate  $n_L^e(q')$ , for insertion into equation (4). For the Raman-induced Kerr effect, the probed wave vector  $q'$  is always identical to the driven wave vector  $q$ . This is because the "incident" field is identical with the pump for RIKE. In other coherent scatter measurements, such as that of Nodwell, et al.,<sup>3</sup> this need not be the case. We are thus led to consider for RIKE, the Fourier transform field  $\mathcal{E}(\omega, q)$ :

$$\mathcal{E}(\omega, q) = -\frac{i}{2} s_\omega A \int_{-L/2}^{+L/2} dx \frac{e^{-i \int dx [q - k_c(x)]}}{k(x)^{1/2}} \times \int_{-L/2}^x d\bar{x} e^{+i \int d\bar{x} [q - k_c(\bar{x})]} . \quad (37)$$

Here,  $A$  is the beam-intersection cross-section in Figure 1 in the  $y$ - $z$  plane, transverse to the density gradient. We now consider three limits, which we shall refer to as the globally homogeneous (gh) limit, the locally homogeneous (lh) limit, and the inhomogeneous (i) limit.

### 1. Homogeneous Limit (global and local)

To facilitate an understanding of the conditions which must be satisfied in this limit, we integrate equation (37) by parts, to obtain

$$\begin{aligned}
 \mathcal{E}(\omega, q) = & -\frac{A}{2} s_{\omega} \int_{-L/2}^{+L/2} dx \frac{1}{k(x) \{ [q-k(x)] + iK(x) \}} \\
 & + \frac{A}{2} s_{\omega} \int_{-L/2}^{+L/2} \frac{[-k'(x)] e^{-i \int dx [q-k_c(x)]}}{\{ [q-k(x)] + iK(x) \}^2 k(x)^{1/2}} \int_{-L/2}^x d\bar{x} \frac{e^{+i \int d\bar{x} [q-k_c(\bar{x})]}}{k(\bar{x})^{1/2}} . \quad (38)
 \end{aligned}$$

In this expression, we have neglected the boundary terms (they are far from resonance and also heavily damped if condition  $KL \gg 1$  is satisfied). In addition, we have neglected the action of the derivation on  $k^{-1/2}$  because this yields a term which is less resonant than the second term on the right of (38). We now show the conditions for neglect of the second term on the right of (38). This term will be negligible provided the factor  $k'(x)/[q-k(x)+iK(x)]^2$  is small over the range of  $x$ -values which contribute most to  $\mathcal{E}(q)$ . Evidently, this is the range of  $x$ -values near resonance, for which  $|q-k(x)| < K(x)$ . However, the matched point\*  $x_{\omega}$  satisfies  $k(x_{\omega}) = q$ , so the criterion for keeping only the first, simple integral in (38) is

$$k'(x_{\omega}) \ll k^2 . \quad (39)$$

---

\*The significance of the matched point in the homogeneous limit is therefore that it is a resonance point at which the WKB wave vector,  $k(x)$ , equals the driving wave vector,  $q$ . In the inhomogeneous limit, it will turn out to be a point of stationary phase.

This is the condition for the homogeneous limit. We must now ask, what is the range of points  $\Delta x$  about a given  $x_{\omega}$  (for a given frequency) which contribute significantly to the first integral in (38). Let us define this range by the condition

$$k(x_{\omega} + \Delta x) - q = K(q) , \quad (40)$$

so that  $x_{\omega} + \Delta x$  is at the edge of the plasma resonance. It is easy to show from the defining equations that

$$\lim_{x_{\omega} \ll 2\ell} \frac{\Delta x}{\ell} = 2 \left( \frac{\gamma}{\omega_p} \right)^{1/2} \quad (41a)$$

$$\lim_{x_{\omega} \gg (2\gamma/\omega_p)^{1/2}} \frac{\Delta x}{\ell} = \frac{2\gamma}{\omega_p} \frac{\ell}{x_{\omega}} \ll 2 \left( \frac{\gamma}{\omega_p} \right)^{1/2} . \quad (41b)$$

Note  $\Delta x$  gets much smaller, as  $x_{\omega}$  exceeds the critical value,

$$x_{\omega}^{cr} = (2\gamma/\omega_p)^{1/2} . \quad (42)$$

For values of  $\omega$  such that  $x_{\omega} \gg x_{\omega}^{cr}$ ,  $\mathcal{E}(\omega, q)$  is greatly reduced because the domain over which the integrand is large is greatly reduced. Hence, (42) defines the boundaries of the frequency spectrum associated with the plasmon line, for Eq. (42) is satisfied at

$$\omega = \omega_0 - \omega_1 - \gamma/2 , \quad (43)$$

which gives  $\gamma/2$  as the usual half-frequency width of the plasma line in the homogeneous limit. For the parameters of

Equations (35) and (36) this shift is much less than the line width  $\Delta_1$  of the probe. We may now sharpen the condition (39) for the homogeneous limit to be valid, by using (42). The result is the condition

$$d(\gamma/\omega_p)^{3/2} \ll 1, \quad (44)$$

where  $d$  is the following dimensionless measure of the profile scale length,  $\ell$ :

$$d \equiv k_D^2 \ell / q. \quad (45)$$

When (44) is satisfied, we obtain from (38),

$$\mathcal{E}(\omega, q) \approx - \frac{A s_\omega}{2q} I_\omega, \quad (46a)$$

$$I_\omega \approx \int_{-L/2}^{+L/2} dx \frac{1}{q - k(x) + iK} . \quad (46b)$$

If the plasma were totally homogeneous, with  $k(x) \equiv q$  for all  $x$ , then we would have the result

$$I_\omega \approx \frac{L}{iK}, \quad (47a)$$

which is independent of frequency, and which contains the intersection length  $L$  (see Fig. 1). In order for this limit to hold, we would have to require that

$$\frac{L}{2} \ll x_\omega^{cr} = \ell \sqrt{2\gamma/\omega_p} . \quad (47b)$$

[Note, if  $\Delta_1$  were much less than  $\gamma/\omega_p$ , so that  $x_\omega \ll x_\omega^{cr}$ , then  $L$  in (47a) would be replaced by  $x_\omega$ . This would be

analogous to the typical situation in narrow-band spectroscopy of ordinary incoherent scattering from a weakly inhomogeneous plasma, in which the band-width of the detector sets the range of spatial points which contribute to the scatter.]

We refer to Eq. (47b) as the condition for the globally homogeneous limit. When the inequality is reversed, but (44) is still satisfied, we have the locally homogeneous limit, in which

$$I_{\omega} \approx \frac{2\Delta x}{iK} = \frac{12}{i} \frac{1}{d(\gamma/\omega_p)^{1/2}} , \quad (48a)$$

$$\frac{L}{2} \gg x_{\omega}^{cr} = \ell \sqrt{2\gamma/\omega_p} . \quad (48b)$$

Here,  $\Delta x = 2\ell(\gamma/\omega_p)^{1/2} = O(x_{\omega}^{cr})$  is the contributing range at small  $x_{\omega}$  (near the center of the spectrum) defined by (41a). Note,  $\Delta x$  is here the effective scattering length, rather than  $L$ .

We may actually do better in the evaluation of the integral  $I_{\omega}$  in (46), although the preceding heuristic arguments are quite useful. By using the expansion (32), the integral (46b) may be done exactly, to yield,

$$I_{\omega} = \frac{6q\ell}{k_D^2} \frac{1}{g(\omega)} \ell \ln \left[ \frac{4\ell}{4\ell - L} \frac{g(\omega)}{g(\omega) + L} \right] , \quad (49)$$

where

$$g(\omega) = \left[ \frac{3q}{k_D^2} (q - p_{\omega} + iK) \right]^{1/2} . \quad (50a)$$

By using the definitions of  $K$ ,  $p_{\omega}$ , and  $x_{\omega}$  [Eqs. (21) and (26)],

we arrive at two alternate forms for  $g(\omega)$ :

$$g(\omega) = \left[ \left( \frac{x_\omega}{2\ell} \right)^2 + \frac{i\gamma}{\omega_p} \right]^{1/2}, \quad (50b)$$

$$g(\omega) = \left[ \left( \frac{\delta\omega}{\omega_p} \right)^2 + \frac{i\gamma}{\omega_p} \right]^{1/2}, \quad (50c)$$

where  $\delta\omega \equiv (\omega_0 - \omega_1) - \omega$ . The analytical result (49) may now be used to corroborate and refine the estimates (47) and (48). First, consider the globally homogeneous limit, in which  $4\ell g(\omega)/L \gg 1$ . Then (49) yields,

$$\lim_{4\ell |g| \gg L} I_\omega = \frac{3q}{k_D^2} \frac{L}{g(\omega)^2}, \quad (51)$$

which is identical with (47) in the resonant limit  $\delta\omega = 0$ .

Next, consider the locally homogeneous limit, in which  $4\ell g(\omega)/L \ll 1$ . Then  $\ln(-1) = i\pi$ , and

$$\lim_{4\ell |g| \ll L} I_\omega = \frac{6i\pi q\ell}{k_D^2} \frac{1}{g(\omega)}. \quad (52)$$

At resonance,  $x_\omega \ll x_\omega^{cr}$ , this becomes  $I_\omega = 6\pi e^{i\pi/4} (\ell^2 / \sqrt{\gamma/\omega_p})$ , which is in rough agreement with the estimate of (48) for the locally homogeneous limit.

Using the two limits (51) and (52), we may estimate the frequency integrated signal. From Equations (1)-(4) and Poisson's equation,

$$\int \frac{d\omega}{2\pi} P = I_{\text{inc}} \sigma_T \Delta\Omega \frac{1}{T} J, \quad (53a)$$

$$J \equiv \int \frac{d\omega}{2\pi} |n_L e(q, \omega)|^2 = \frac{q^2}{(4\pi e)^2} \int \frac{d\omega}{2\pi} |\mathcal{E}(\omega, q)|^2 . \quad (53b)$$

Assuming  $\gamma \ll \Delta_1$ , and using (46a), the integral  $J$  becomes

$$J = \frac{A^2 s_{\omega_0 - \omega_1}^2}{2e^2 (4\pi)^3} \int_{-\infty}^{+\infty} d\omega |I_\omega|^2 . \quad (54)$$

Performing the integral in the limits of Eq. (51) and (52) yields the following: For the globally homogeneous limit,

$$J_{gh} = \frac{9}{8} (ALn_0)^2 \frac{\omega_p}{\gamma} \frac{q^2}{k_D^2} \left| \frac{e}{mk_D} s_{\omega_0 - \omega_1} \right|^2 \frac{1}{\omega_p^3} . \quad (55)$$

We note the factor  $(ALn_0)^2 = N^2$ , where  $N$  is the total number of electrons in the scattering volume (appearing squared because of the coherence of RIKE). The scattering volume in this limit is identical with the radiation beam intersection volume. We also note the usual factor  $q^2/k_D^2$  from integration over the plasma line. The factor  $\omega_p/\gamma$  appears because the density fluctuations are driven by ponderomotive force, rather than by spontaneous emission. The final factor may be rewritten, using the definition (16) of the beat-ponderomotive force driving factor as

$$\left| \frac{e}{mk_D} s_{\omega_0 - \omega_1} \right|^2 = \frac{q^2/k_D^2}{144} \frac{|\mathbf{v}_0 \cdot \mathbf{v}_1^*|^2}{v_e^4} \omega_p^2 T^2 , \quad (56)$$

where  $\mathbf{v}_0 \equiv eE_{0,1}/m\omega_{0,1}$  is the driven velocity in the radiation

field  $\underline{E}_0$  or  $\underline{E}_1$ .

In the locally homogeneous limit we perform the integral over  $|I_\omega|^2$  by using the spectral function  $f(\Omega)$  (cf 8a) to provide logarithmic cut-offs at  $|\delta\omega| = \Delta_1 \gg \gamma$ . Hence,

$$J_{lh} \approx 9\pi (Al n_0)^2 \ln \left( \frac{2\Delta_1}{\gamma} \right) \left( \frac{q^2}{k_D^2} \right) \left| \frac{e}{mk_D} s\omega_0 - \omega_1 \right|^2 \frac{1}{\omega_p^3}. \quad (57)$$

Note,  $J_{lh}/J_{gh} = 8\pi(\ell/L)^2(\gamma/\omega_p)^2 \ln(2\Delta_1/\gamma)$ , and  $16(\gamma/\omega_p)(\ell/L)^2 \ll 1$  in the locally homogeneous limit, by the condition  $4\ell|g| \ll L$  in (52), so, unless  $\Delta_1/\gamma$  is extremely large, we have  $J_{lh}/J_{gh} \ll 1$ . Note, also, that  $J_{lh}$  is now only weakly dependent on  $\gamma$ . This is because  $|I_\omega|^2 \propto \omega_p/\gamma$  by (48a), but the frequency width is still proportional to  $\gamma/\omega_p$ . Another way to look at this is also provided by (48a), namely, that  $2\Delta x$  [times  $\frac{\pi}{2} \ln(2\Delta_1/\gamma)$ ] replaces  $L$  as the effective scattering length in determining the number of contributing electrons.

In the next limit we shall study, the dependence of  $J$  on  $\gamma$  disappears altogether.

## 2. Inhomogeneous Limit

When the scale length  $\ell$ , and/or the damping  $\gamma$  is sufficiently small that the inequality (44) is reversed, we obtain the inhomogeneous limit. To treat this limit, we return to the form of Eq. (47) for  $\hat{\epsilon}(\omega, q)$ . We shall evaluate the integrals by the generalized method of stationary phase.

It is clear that  $x_\omega$  will be the point of stationary phase of  $qx - \int k(x)$ , so the denominators  $k^{\frac{1}{2}}$  may be approximated as  $q^{\frac{1}{2}}$ , and (37) may be rewritten as

$$E(\omega, q) = -\frac{is_\omega A}{2q} \ell^2 \left(\frac{36}{d}\right)^{2/3} \int_{-\infty}^{+\infty} dy e^{-if(y)} \int_{-\infty}^y d\bar{y} e^{+if(\bar{y})}, \quad (58)$$

where,

$$f(y) = 3y_0^2 y - y^3, \quad (59a)$$

$$y_0 \equiv \frac{x_\omega}{\ell} \left(\frac{d}{36}\right)^{1/3}, \quad (59b)$$

and  $d$  was defined as  $k_D^2 \ell / q$  in Eq. (44). We have used Eq. (32) to expand  $k(x)$ , and we have ignored the exponential damping factors  $\exp \mp \int dx K(x)$  for reasons to be discussed shortly. The shape of  $f(y)$  depends on the size of  $y_0$ . The extrema of  $f(y)$  (stationary phase points) occur at  $y = \pm y_0$ . These extremum points merge as  $y_0 \rightarrow 0$ . There are two distinct cases to be considered, depicted below in Figs. 3a,b:

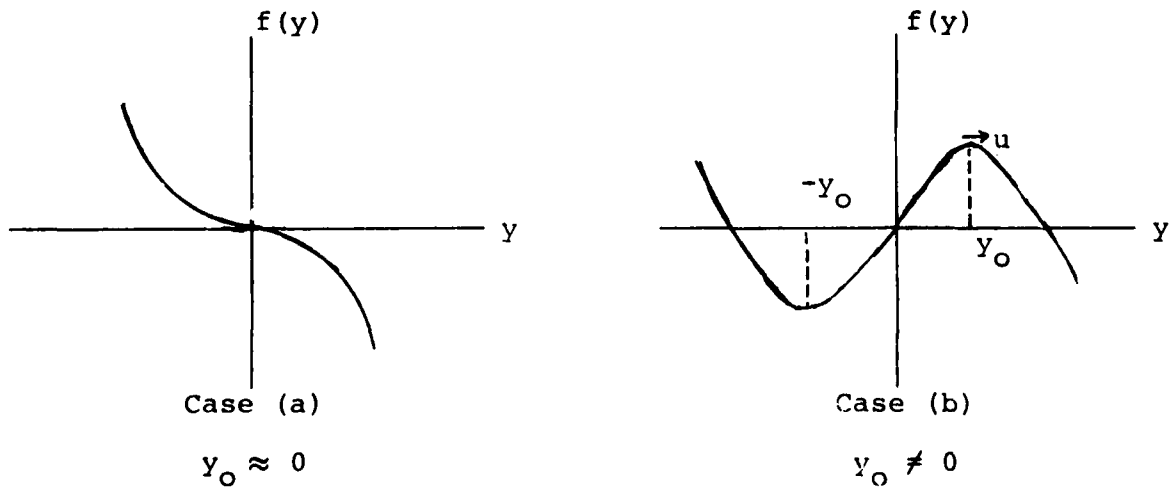


Fig. 3

When  $y_0 = 0$ , the extremum is at the origin, and  $f(y) \approx -y^3$ .

The integrals over  $y$  then have a width of order  $\Delta y = 1$ .

Hence, the linear terms in  $f(y)$  may be ignored as long as

$3y_0^2 \ll 1$ . This gives the condition on how small  $y_0$  must be for case (a) to apply. Summarizing

$$\lim_{3y_0^2 \ll 1} f(y) = -y^3, \quad \Delta y = O(1), \quad (60a)$$

In the complementary limit of case (b), the approximation about the points of stationary phase  $\pm y_0$  take a quadratic form.

If  $u_{\pm} = y \pm y_0$ , then

$$f(y) = -u^3 \pm 3y_0 u^2 \mp 2y_0^3,$$

and the condition for neglect of the cubic term is

$(\Delta u)^3 \ll 3y_0(\Delta u)^2$ , where the range  $\Delta u = (3y_0)^{-\frac{1}{2}}$ . Hence in case (b),

$$\lim_{3y_0 \gg 1} f(y) = \pm 3y_0 u^2 \mp 2y_0^3, \quad \Delta u = (3y_0)^{-\frac{1}{2}} \ll 1, \quad (60b)$$

The important thing to notice here is that the range  $\Delta u$  in case (b) is much smaller than the range in case (a), so the integrals for  $\mathcal{E}(\omega, q)$  will become smaller as  $\omega$  gets sufficiently far from  $\omega_0 - \omega_1$  that  $y_0$ , as defined in (59b) becomes equal to  $1/3$ . Hence, the frequency width is determined by the condition

$$\frac{x_{\omega}}{\ell} = \frac{(36)^{1/3}}{3} d^{-1/3} \approx d^{-1/3}, \quad (61a)$$

or, using  $x_{\omega}/\ell = (2\delta\omega/\omega_p)^{\frac{1}{2}}$ , we find

$$\frac{\delta\omega}{\omega_p} = \frac{1}{2} d^{-2/3} . \quad (61b)$$

Note that this bandwidth is independent of the damping  $\gamma$ .

We are now in a position to write down the condition for ignoring the damping factors  $\exp \pm \int dx K(x)$  in (58). Since case (a) is the case where  $\mathcal{E}(q, \omega)$  is largest, we specialize to this case. At the point  $x = 0$  of stationary phase, the damping factors are  $\exp \pm Kx$ . The range of significant  $x$  values for this case is given by (60a), or  $\Delta x = \ell(36/d)^{1/3}$ . Hence, neglect of the damping factor requires  $K\ell(36/d)^{1/3} \ll 1$ , or, using (21),

$$\left(\frac{\gamma}{\omega_p}\right)^{3/2} d \ll 1 . \quad (62)$$

It is important to note that this is precisely the opposite limit from inequality (44), which was the condition for the homogeneous limit. Inequality (62) is therefore the principal condition for the inhomogeneous limit we are now studying.

Using (62) we now see that  $\delta\omega$ , as determined by (61b) is  $\gg \gamma$ , so the plasma line is broadened by the inhomogeneity.

It remains to evaluate  $\mathcal{E}(\omega, q)$  and the frequency integrated spectral function  $J$ . Using (60a), and taking  $y = y_0 \approx 0$  in the second integral of (58), we may write

$$\mathcal{E}(\omega_0 - \omega_1, q) = -i \frac{s \omega A \ell^2}{q} \left(\frac{36}{d}\right)^{2/3} B \operatorname{Re} B , \quad (63)$$

where

$$B \equiv \int_0^\infty dy e^{iy^3} .$$

To evaluate this integral (which is standard in this generalized method of stationary phase), we consider it in the complex  $y$ -plane, rotate the path from 0 to  $\infty$  by  $30^\circ$ , and change to the new real variable,  $w$ , defined by  $y = e^{i\pi/6} w^{1/3}$ . We immediately find the result

$$B = e^{i\pi/6} \Gamma(1/3)/3 , \quad (64)$$

where the gamma function is evaluated at  $1/3$  to be 2.68. The frequency integrated spectrum,  $J_i$ , is obtained by multiplying  $|\mathcal{E}(\omega_0 - \omega_1, q)|^2$  by  $\delta\omega = (\omega_p/2)d^{-2/3}$ , as defined in (61b):

$$J_i \approx (36)^{4/3} \left(\frac{\Gamma(1/3)}{3}\right)^4 \frac{3}{8} (A \ln \omega_0)^2 \left(\frac{q^2}{k_D^2}\right) \left| \frac{e^{i\pi/6} \omega_0 - \omega_1}{mk_D} \right|^2 \frac{1}{\omega_p^{1/3}} , \quad (65a)$$

Here we have explicitly assumed that the probe bandwidth is larger than the bandwidth  $\delta\omega$ , or

$$\Delta_1/\omega_p \gg d^{-2/3} . \quad (65b)$$

The numerical factor in (65a) is  $(36)^{4/3} [\Gamma(1/3)/3]^4 (3/8) \approx 28.4 \approx 9\pi$ . Let us compare  $J_i$  for the inhomogeneous case, with the result of (57) for the locally homogeneous  $J_{1h}$ . Essentially  $J_i/J_{1h} = 1/\ln(2\Delta_1/\gamma)$ , so there is only a slight reduction (unless  $2\Delta_1 \gg \gamma$ ). In effect, the inhomogeneous spectrum is lower but broader, and so integrates to almost as large a value of  $J$ . We may view the progression from  $J_{gh}$  to  $J_{1h}$  to  $J_i$  as containing progressively weaker dependence on the damping,  $\gamma$ .

In Table 1 we have exhibited the properties of the signal spectrum in each of the various limits. We can use the parameters of (35) and (36) to get a rough idea of the experimental significance of these limits. For that case, with  $\ell = 0.2 \text{ cm}$ ,  $d = 5 \times 10^5$ ,  $\gamma_{\text{coll.}}/\omega_p = 2.5 \times 10^{-4}$ , so  $(\gamma/\omega_p)^{3/2}d = 2$ , and we are marginally in the homogeneous regime. (This could be improved by increasing  $\ell$ .) The regime will be locally homogeneous, as long as the dimension,  $L$ , of the laser intersection volume (see Fig. 1) is greater than  $0.063\ell$ , which is likely to be the case. If we assume that  $L = \ell$ , and  $2\Delta_1/\gamma = 16$ , then  $J$  is reduced by a factor  $10^{-2}$  from the globally homogeneous limit. Observability still might be good, depending on the effects of the time-dependence of the density profile, which may hinder observation by limiting the time over which Eq. (28) is satisfied.

Some general conclusions may be drawn. In all three limits the frequency-integrated signal is proportional to  $q^2/k_D^2$ , so it is of some advantage to work at high values of  $q/k_D$ , even though Landau damping may be incurred. The increased damping may even be advantageous in increasing the signal strength by moving from the inhomogeneous to the locally homogeneous or globally homogeneous limit. This seems consistent with the parameters of Nodwell's experiment<sup>3</sup>, for which  $q/k_D = 0.25$ .

TABLE 1: COMPARISON OF LIMITS FOR A PARABOLIC PROFILE,  
 $\omega_p(x)^2 = \omega_{p0}^2 (1-x^2/2\ell^2)$

	Globaly Homogeneous	Locally Homogeneous	Inhomogeneous
Condition for Validity ( $d \equiv k_D^2 \ell / q$ )	$(\gamma/\omega_p)^{3/2} d \gg 1$	$(\gamma/\omega_p)^{3/2} d \ll 1$	
	$(\gamma/\omega_p)^2 \gg 1$	$(\gamma/\omega_p)^2 \ll 1$	
Integrated Spectrum $J/A n_0^2 (q^2/k_D^2)   (e s_{\omega_0} - \omega_1 / m k_D)  ^2 \omega_p^3$	$\frac{9}{8} \ell^2 \frac{\omega_p}{\gamma}$	$9\pi\ell^2 \ln(\Delta_1/\gamma)$	$\sim 9\pi\ell^2$
Spectral Width ( $\Delta\omega \ll \Delta_1$ )	$\gamma$	$\gamma$	$\frac{\omega_p}{2d^{2/3}} (\gg \gamma)$

## SECTIONS TO BE WRITTEN

- V. Linear Profile with Reflection
- VI. Ion-Acoustic Modes and Quasimodes
- VII. Time-Dependent Density
- VIII. Magnetic Effects
- IX. Applications to the Ionosphere and to Fusion Devices

## REFERENCES

1. M.V. Goldman, "Notes on Advanced Plasma Physics."
2. M.N. Rosenbluth and C.S. Liu, Phys. Rev. Lett. 29, 701 (1972).
3. B. Stanfield, R. Nodwell, and J. Meyer, Phys. Rev. Lett. 26, 149 (1971).

